UNIVERSITY OF CAPE TOWN
IYUNIVESITHI YASEKAPA • UNIVERSITEIT VAN KAAPSTAD

CHEMICAL ENGINEERING

Assessment of Disparate Strategies for Octane Prediction

Author :
Carl Viljoen

Supervisors :
Professor Klaus Möller
Professor Andrew Yates

August 2009

Assessment of Disparate Strategies for Octane Prediction

Carl Viljoen

Thesis Presented for the Degree of

DOCTOR OF PHILOSOPHY

in the Department of Chemical Engineering

UNIVERSITY OF CAPE TOWN

August 2009

Abstract

Octane quality is a key factor in determining the profitability in a modern refinery. The final commercial product is defined by the combined blend of various gasoline component streams which are produced from different units within the refinery. The accurate prediction of the octane numbers of these blends enables the economic optimization of the production process. Currently, empirical octane models are used exclusively for this purpose.

Octane is a measure of the spontaneous autoignition propensity of a fuel-air mixture and it is quantified using a specific engine-based test method. This research project was founded on the premise that an improved octane prediction model could be harvested from building blocks that included a fundamental understanding of autoignition, appropriate choices of autoignition models and an engine model. This objective was pursued in this work by investigating detailed and reduced kinetic mechanisms for the oxidation of selected fuel molecules using various modeling techniques. Empirical octane models and semi-chemical models of autoignition were also investigated. All of these methodologies were assessed as possible strategies towards octane prediction.

In this study it was observed that both detailed and highly reduced kinetic models could describe the oxidation behaviour of pure fuel components and predict their subsequent ignition delays. Binary blends were used to further evaluate the two modeling strategies. It was found that the reduced kinetic models were limited in the scope of their autoignition prediction capability. Density functional theory (DFT) was used to probe the reasons for these limitations, which were ascribed to the exclusion of important mechanist steps and incorrect selection of the mechanistic pathways. Detailed kinetic modeling, on the other hand, was shown to be accurate in predicting ignition delay, but its commercial implementation for complex blends was blocked by the general unavailability of detailed mechanisms for a wide variety of fuel molecules and the high computational cost of these simulations.

Because of these limitations, empirical semi-chemical models were also evaluated. The application of these models is constrained by their requirement to be fitted against experimental ignition delay data. It was concluded that these models may find niche applications in computational fluid dynamics (CFD) simulations if such experimental data is available.

Throughout the course of this research, the negative temperature coefficient (NTC) characteristics of different fuel molecules emerged as the most distinctive parameter determining its autoignition behaviour and associated octane number value. Not all molecules exhibit NTC character and this provided a classification system for molecules with single-stage ignition and those having two-stage ignition behaviour. An important implication of this research finding was that surrogate fuels should contain an example of each group for each chemical class (paraffinic, olefinic aromatics, oxygenates, etc). The “strength” of the NTC behaviour in regard to octane number influence was also defined in this work.

When these insights regarding the fundamental nature of a quantified NTC description for every molecule were applied to an empirical octane model from the literature, a significant improvement in the accuracy of the octane prediction was achieved. This enhanced model has potential for practical application in oil refineries. From this work, an octane-prediction landscape was constructed which the disparate strategies identified and assessed. This will enable the appropriate roadmap to be chosen for different research and/or commercial objectives.

Acknowledgements

I wish to acknowledge and thank the following people:

- The past management of Sasol Technology Fuels Research, in particular Dr. Johan Botha and Dr. Hein Strauss for giving me the opportunity and support to pursue this research.
- The present management, in particular Mr. Paul Morgan and Dr. Johan Coetzee for allowing me to spend an extended period at the Sasol Advanced Fuels Laboratory in order to complete this thesis.
- My supervisors, Prof. Klaus Möller and Prof. Andy Yates for their guidance, constant encouragement and numerous inputs throughout the pursuit of this research. The many hours and weekends that they have devoted to this study is gratefully acknowledged.
- My colleague, Dr. Andre Swarts, for allowing me the use of some of his PRF pressure traces recorded in the CFR engine, and for his patient explanations to numerous questions about engine thermodynamics.
- Dr Roelof Coetzer, for his contributions to this work and his willingness to share his statistical expertise with us.
- My senior colleagues in Sasolburg, Ernst van Tonder, Dirk Cross and Piet Roets, who taught me everything I know about synthetic fuels.
- A special vote of thanks to Prof. Andy Yates and my fellow students at SAFL, for creating a vibrant, stimulating environment and for allowing a fuels chemist an intimate exposure to engines and their mechanical intricacies.
- This thesis is dedicated to my wife, Elvera, for her love, encouragement and unwavering support, without which I would not have been able to conclude this work.

SOLI DEO GLORIA

Table of Contents

List of Figures

List of Tables

Acronyms

API	American Petroleum Institute
ASTM	American Society for Testing Materials
BTDC	Before Top Dead Centre
CAD	Crank Angle Degrees
CARS	Coherent Anti-Stokes Raman Spectroscopy
CFD	Computational Fluid Dynamics
CFR	Cooperative Fuels Research
CI	Compression Ignition
CR	Compression Ratio
CRC	Coordinating Research Council
CSP	Computational Single Perturbation
CSTR	Continuously Stirred Tank Reactor
DFT	Density Functional Theory
FBR	Full Boiling Range
GGA	Generalised Gradient Approximations
HCCI	Homogeneous Charge Compression Ignition
ID	Ignition Delay
IFP	Institut Français du Pétrole
ILDM	Intrinsic Low Dimensional Manifold
IQT^{TM}	Ignition Quality Tester
IVC	Inlet Valve Closure
JSR	Jet-Stirred Reactor
LBV	Linear by Volume
LCAO	Linear Combination of Atomic Orbitals
LDA	Local Density Approximation
LLNL	Lawrence Livermore National Laboratory
MON	Motor Octane Number
NTC	Negative Temperature Coefficient
ON	Octane Number
OI	Octane Index
PFR	Pressurized Flow Reactor
PRF	Primary Reference Fuel
PSR	Perfectly Stirred Reactor
RAM	Random Access Memory
RCM	Rapid Compression Machine
RON	Research Octane Number
SCF	Self-consistent Field
SE	Standard Error
SI	Spark-Ignition
SKI	Standard Knock Intensity
TDC	Top Dead Centre
TEL	Tetra-ethyl Lead
TS	Transition State

Chapter 1 : Introduction

1.1 General introduction

With the proliferation of automobiles during the early part of the 20th century, there was a requirement to standardise on the performance characteristics of automotive fuels. One of the more challenging of these performance parameters was the autoignition characteristics of gasoline fuels. Autoignition or knock can be described as the rapid, explosive consumption of the end-gas (or unburned fraction) in the cylinder of a spark ignition engine, ahead of the propagating flame front, leading to poor performance, possibly engine damage and eventually failure (if the knock is left unabated for long periods). The methodology that was subsequently developed and adopted in order to prevent this phenomenon, was to select the appropriate gasoline components such that the final blended fuel had an adequate octane number (equivalent to anti-knock quality) for the specific application. Even today, more than 120 years since the first spark-ignition fuels were developed, the simulation and prediction of the octane numbers of blended petrol components remain a non-trivial matter, mainly due to their non-linear blending behaviour. This aspect is at the heart of the current study. Some of the key concepts that play a role in defining the problem are described below.

1.2 Brief overview of autoignition and engine knock

Throughout the history of the spark-ignition (SI) engine, the phenomenon of knock has imposed an upper limit on the maximum allowable compression ratio and, by implication, the maximum achievable thermodynamic efficiency (Sutton, 1984). Knock is an unwanted form of combustion in the SI engine that differs from the normal spark-ignited flame propagation. The difference lies in the rate at which the combustion takes place. In the case of knock, a significant portion of the pre-mixed air-fuel mixture autoignites almost instantaneously and this creates a localised high-pressure region within the combustion chamber (Miller and Fisk, 1987). This is shown schematically in Figure 1.1, below.

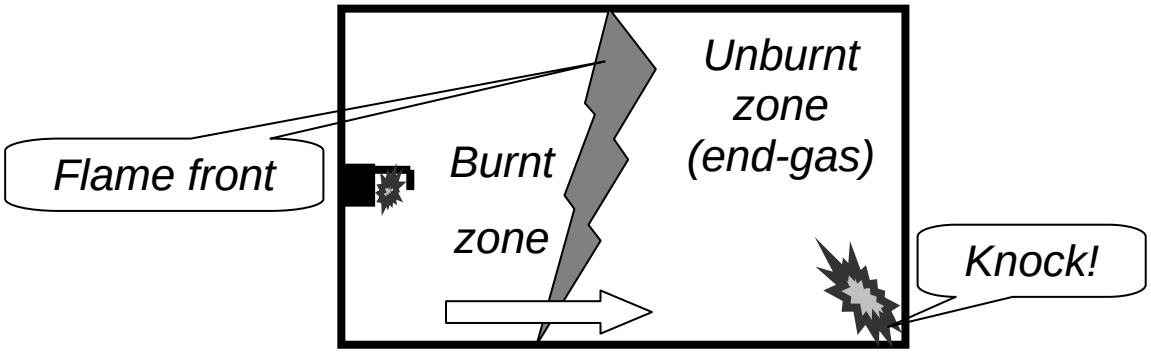

Figure 1.1: Schematic representation of an engine cylinder at maximum compression, showing the race between transport-limited flame propagation on the left and autoignition reactions on the right

The relaxation of this pressure discontinuity involves shock-waves that disturb the normal thermal boundary layer and expose the piston and cylinder walls to excessively high gas temperatures. This in turn can lead to localised overheating and resultant engine damage (Nates and Yates, 1994).

In simplistic terms, the autoignition of a homogeneous mixture of air and fuel may be regarded as the condition where the rate at which the energy being liberated by the chemical oxidation reactions exceeds the rate at which the energy is dissipated by heat loss and/or work done by expansion (Heywood, 1988). The excess energy being liberated will cause the temperature of the fuel-air mixture to increase and, as a general rule, the rate of the chemical oxidation reactions will increase exponentially with temperature. This creates a positive-feedback situation where the increased temperature leads to increased reaction rates and vice-versa, with the net result that the combustion is extremely rapid and this condition occurs simultaneously throughout the entire unburned mixture. Experiments have revealed that the oxidation reaction processes take a small but finite time interval to reach the exponential run-away stage and this time interval has been termed the ignition delay (Warnatz et al., 1996).

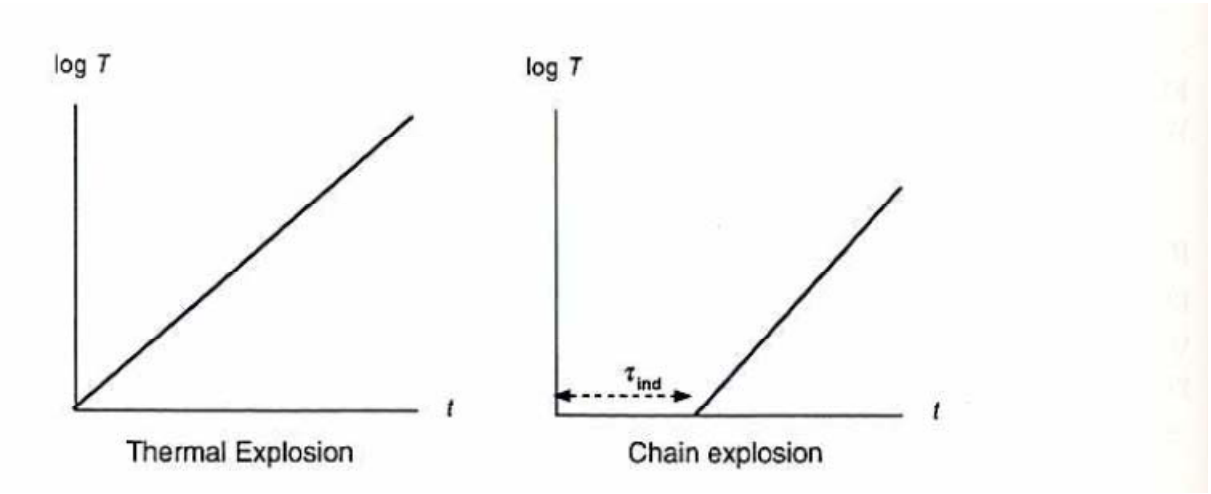

Figure 1.2: Simplified time - temperature behaviour of thermal and chain-branching explosion in an adiabatic system. τ_{ind} refers to the ignition delay (or induction period). Figure reproduced from Warnatz et al. (1996)

Figure 1.2 indicates that, contrary to thermal explosions that occur instantaneously, the chemical reactions which are progressing in the end-gas are governed by a radical chain-branching mechanism, leading to a time delay (τ_{ind}) during which the radical-pool population is increasing at an accelerating rate. Yet the amount of fuel consumed, and hence the amount of energy liberated, is still almost too small to be detected. This time of negligible temperature (and pressure) rise is also known as the induction time. Finally, the radical pool becomes large enough (reaching the critical concentration needed to consume a significant fraction of the fuel) and rapid ignition will then take place.

This ignition delay provides a window of opportunity for engine designers to extend the performance boundaries. In modern, high-compression, spark-ignition engines, the temperature attained by the unburned mixture prior to normal combustion exceeds the minimum temperatures required for auto-ignition by several hundred degrees and it is only the just-in-time consumption of the unburned mixture by the propagating normal flame that circumvents the autoignition event. From this discussion it may be appreciated that it is not only the chemistry associated with the ignition delay that is relevant, but also the pressure and temperature history associated with the whole combustion chamber environment (Gluckstein and Wallcut, 1961). For this reason, in knock research the chemical reaction kinetics cannot be divorced from the thermodynamics of the whole engine.

It follows that the occurrence or non-occurrence of knock in a spark-ignition engine will be determined by the combined influence of virtually all the operating parameters. Primary variables such as the inlet air pressure and temperature, the compression ratio, the engine speed and the ignition timing impose a direct influence on the pressure - temperature history that will be experienced by the end-gas, which is the last portion of the unburned mixture to be consumed by the normal flame propagation and which is the portion that is most likely to autoignite (Heywood, 1988). The cylinder size does not materially affect the core gas properties (although relative heat loss increases with decreasing sizes), but it impacts on the autoignition likelihood by way of the flame propagation duration. There are a number of important secondary variables such as the coolant temperature, the combustion chamber shape, the inlet swirl and turbulence which all influence the pressure and temperature history of the end-gas, both directly as well as indirectly by their impact on the speed of the normal flame propagation. The air-fuel ratio, and by extension Φ (the equivalence ratio), is an important and complex variable because it affects both the speed of the normal flame propagation and the ignition delay of the unburned mixture itself (Swarts, 2006). Associated very closely with the air-fuel ratio is the evaporative cooling which can also influence the overall temperature history (Moran and Taylor, 1995). In a similar vein, the residual exhaust fraction, which is always present from the previous cycle, will affect the reactivity of the end-gas as well as the mixture temperature and the rate of normal flame propagation.

1.3 The octane rating scale

At an early stage in the development of spark-ignition engines it became apparent that knock was a very significant factor which was hindering further advances in efficiency and increased power output. At the same time it was also discovered that not all fuels were alike in terms of their propensity for knocking. Thus, in addition to all the physical variables affecting the pressure and temperature history of the end-gas which were listed in the previous section, there is also a further variable associated with the fuel's intrinsic chemistry. In the early days of SI engine development, another abnormal ignition phenomenon, pre-ignition, was frequently confused with autoignition, and vice-versa. Pre-ignition is a surface ignition phenomenon, where the fuel-air mixture is ignited by a hot spot on the combustion chamber walls, such as an overheated valve or spark plug, or glowing combustion chamber deposits (Heywood, 1988). Some of the earliest research into knock,

conducted by Hopkinson at Cambridge University, revealed conclusively that knock was not a pre-ignition phenomenon, but in fact a pressure disturbance that occurred only after ignition by the spark plug discharge.

The establishment of the octane rating scale by Graham Edgar in 1926 (these developments were only published a couple of months later at the beginning of 1927, the date cited by most authors for Edgar's breakthrough) (for example, Boyd, 1950) as a measure of knock propensity was a remarkably insightful development. Earlier work by Ricardo (Taylor, 1985) had identified the compression ratio as an appropriate engine parameter whose effect on knock was directionally consistent, i.e., increased compression ratio always caused increased knocking severity. However, as an absolute scale for the measurement of knock propensity, the compression ratio would have required total consistency between different laboratories in terms of the engine set-up and operating conditions. The perceptive step of defining the knock-limited compression ratio in relation to a simple blend proportion of two reference fuels (plus added tetra-ethyl lead if the scale was extended beyond 100 Octane Number (ON)), provided a much more robust measurement method. It meant that the engine and associated equipment could be easily checked and minor variations could be tolerated and 'calibrated out' by means of inlet temperature tuning without compromising the accuracy of the method. In the context of octane modelling, however, it is self evident that the relationship between autoignition (knocking) and compression ratio should be regarded as the primary correlation (as was proposed by Downs and Wheeler, 1952) and that the octane number is merely a measurement definition.

The selection of the two reference fuels (n-heptane and iso-octane (the latter being a specific C8 isomer: 2,2,4-trimethyl pentane) was a clever choice. Whilst they are both saturated paraffins having almost identical boiling points, the two molecules exhibit widely divergent autoignition propensities. n-Heptane (n-C_7H_{16}) was selected as having a strong predisposition to autoignite and it was arbitrarily assigned an octane rating of zero. Iso-octane (iso-C_8H_{18}), which represents the opposite pole and is slow to autoignite, was defined as 100 on this octane scale. These two substances were designated as Primary Reference Fuels (PRFs). Intermediate octane values were obtained by volumetric blending and octane values higher than 100 were arbitrarily

defined by the addition of a specified quantity of tetra-ethyl lead (TEL) which is a very effective anti-knock additive. TEL was the most common octane booster in wide-spread use in leaded petrol internationally, until its phase-out around the globe in the last decade.

With time, it gradually became apparent that there was more to the chemistry of autoignition than a simple octane number. It was found that certain fuels would exhibit a different octane rating depending on the engine operating conditions, i.e., a particular test fuel might exhibit a certain octane rating when tested at 600 r/min but the apparent octane value would change significantly if the test fuel was rated at 900 r/min. This phenomenon led to the specification of different variants of the octane test method, which were given names such as the Research, Motor, Distribution, and Aviation methods (Waukesha, 1946). They were introduced to accommodate the various user requirements and were intended to represent a particular application. The Research and the Motor methods remain entrenched in today's automotive fuel specifications. The measurement of Research and Motor Octane Numbers (RON and MON respectively) is performed in the single cylinder, variable compression engine that became the universally accepted test equipment. It is known as the Cooperative Fuel Research (CFR) engine and the methods are standardised according to ASTM Methods D2699 (ASTM, 2007) and D2700 (ASTM, 2007), respectively. Conditions for the two tests are given in the table below.

Table 1.1 Physical conditions of the RON and MON tests

Parameter	**RON test**	**MON test**
Engine Speed	600 rpm	900 rpm
Spark Timing	13 °BTDC *	19 ° to 26 ° BTDC (varied according to compression ratio)
Inlet air temperature	51.7 °C	38 °C
Inlet mixture temperature	Not controlled	149 °C

* Before Top Dead Centre

It is clear that the conditions shown in Table 1.1 bear little similarity to those a modern spark-ignition engine is subjected to. Although there have been several attempts to re-visit the conditions of the tests (e.g. Douaud and Eyzat, 1978, Millo et al., 1995, and recently, Mittal and Heywood, 2008) as the benchmark to certify spark-ignition engine fuels. Today, a full boiling range (FBR) gasoline with a RON of 95 and a MON of 85 is generally considered to be adequate for modern fuel-efficient spark-ignition engines.

1.4 Research objective

The main aim of this study was to attain a fundamental understanding of the autoignition properties of fuel components, and especially synthetic fuel components, based only on detailed knowledge of the blend's chemical composition. When combined with an understanding of the elusive relationship between autoignition and octane rating (which necessitates coupling of ignition delay information with an accurate engine model of the CFR engine), it should enable the accurate prediction of octane numbers. In the rest of this thesis, any allusion to octane numbers incorporates both RON and MON, the two numbers used in all modern SI fuel specifications to denote the anti-knock tendency of the fuel.

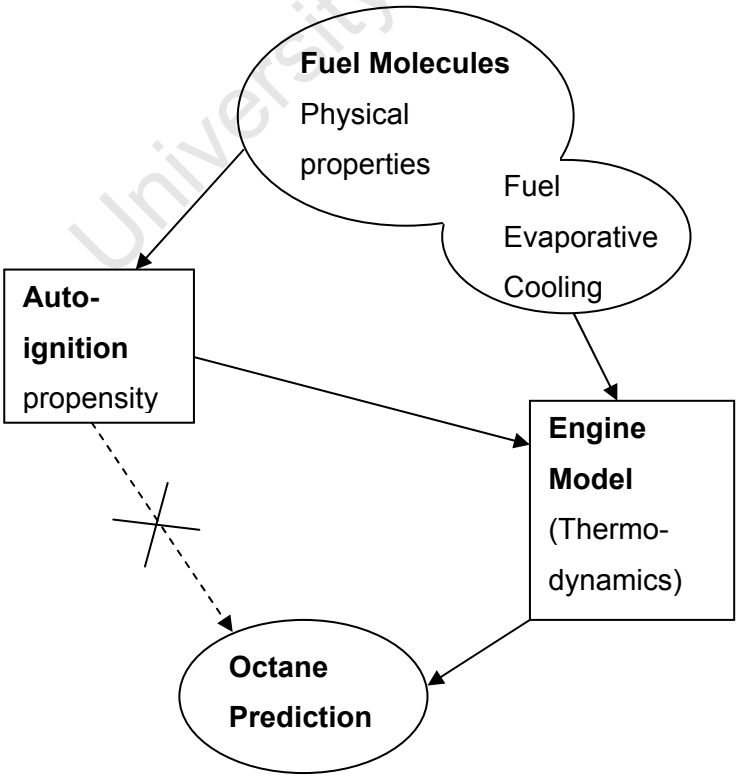

Figure 1.3: Graphical representation of the objective of this work, showing the requirement to transform ignition delays via an engine model to octane numbers

This octane prediction capability will potentially enable optimization opportunities within the Sasol refineries without compromising the quality of the synthetic (coal to liquid (CTL)) as well as crude oil-derived gasoline pools. These economic incentives associated with a fundamental understanding of octane blending in commercial streams, provided the impetus for the research project of which this thesis forms an integral part.

As is illustrated in Figure 1.3, the original notion that the prediction of autoignition delays could perhaps lead directly to octane prediction was discarded early on in the course of the project, since it is obvious that physical attributes such as evaporative cooling and burn speed of the charge, and the unique pressure and temperature history that the end-gas experiences in the CFR engine, play a role as well. Only when the molecular (purely chemical) ignition delay is transformed by application of the engine model including the physical phenomena, does it become possible to predict the CFR engine octane number (either RON or MON) of the fuel system (Swarts, 2006).

1.5 Central hypotheses of the study

The first hypothesis of this research project was that it should be possible to represent the autoignition characteristics, i.e. τ_{ind} vs. (T, P) of any commercial gasoline blend by an appropriate selection of a small number of "model" gasoline molecules. These would typically consist of molecules that would represent the chemical groupings commonly found in gasoline, e.g. a straight-chain paraffin, a highly branched paraffin, an aromatic molecule that displays single-stage ignition, and one that displays negative temperature coefficient (NTC) behaviour. (NTC is a regime where any incremental increase in temperature causes a decrease in reactivity, leading to longer ignition delays, rather than the increased reactivity which is normally associated with an increase in temperature). Similarly, all olefins may be represented by at least two members; one with single-stage ignition and one displaying two-stage ignition with strong NTC character. It must be noted that this approach (by realizing at the outset the inadequacy of the common procedure of representing all aromatics, for example, by only one single-stage molecule such as toluene) already deviated from most other research groups who also endeavoured to construct surrogate fuel mechanisms from a selected set of model compounds

(examples are discussed by Gauthier et al. (2004), Lenhert et al. (2003), Vasu et al. (2008), and Andrae (2008)).

The second hypothesis is that the classification of all gasoline molecules based on their uniquely quantified NTC character, spanning the range from pure single-stage ignition character (0% NTC) to pronounced two-stage ignition and NTC character (100% NTC), will enable an accurate description of the non-linear blending behaviour of the Octane Numbers of blends of these molecules. It must be understood that the NTC character that is being referred to here, is the behaviour of the specific molecule under the physical conditions prevalent in the CFR engine under both RON or MON test conditions, as these determine the temperature history, pressure history and air/fuel ratio of relevance to the end-gas. The hypothesis is thus that using % NTC, rather than chemical structural groupings (olefins, aromatics etc.), will provide better empirical models with which RON and MON can be predicted.

1.6 Assessment of various strategies for octane prediction

During the course of this study, the focus was put squarely on the methodologies that exist for the prediction of ignition delay for a system of known chemical composition in a predetermined physical environment. The engine model development was part of a separate PhD study by Andre Swarts (Swarts, 2006) and falls outside the scope of this thesis. The underlying assumption about the engine model application was as follows: Assuming that the autoignition characterizations for PRFs are known accurately, and that the ignition delay data for an unknown fuel is available for a range of CFR engine-relevant temperatures and pressures, then it would be possible to predict the Octane Number for the fuel to a level of precision as good as the underlying ignition delay data. Thus the problem is reduced somewhat (at least for the purposes of this study) to a prediction of ignition delay (or autoignition propensity, as it is referred to in Figure 1.4).

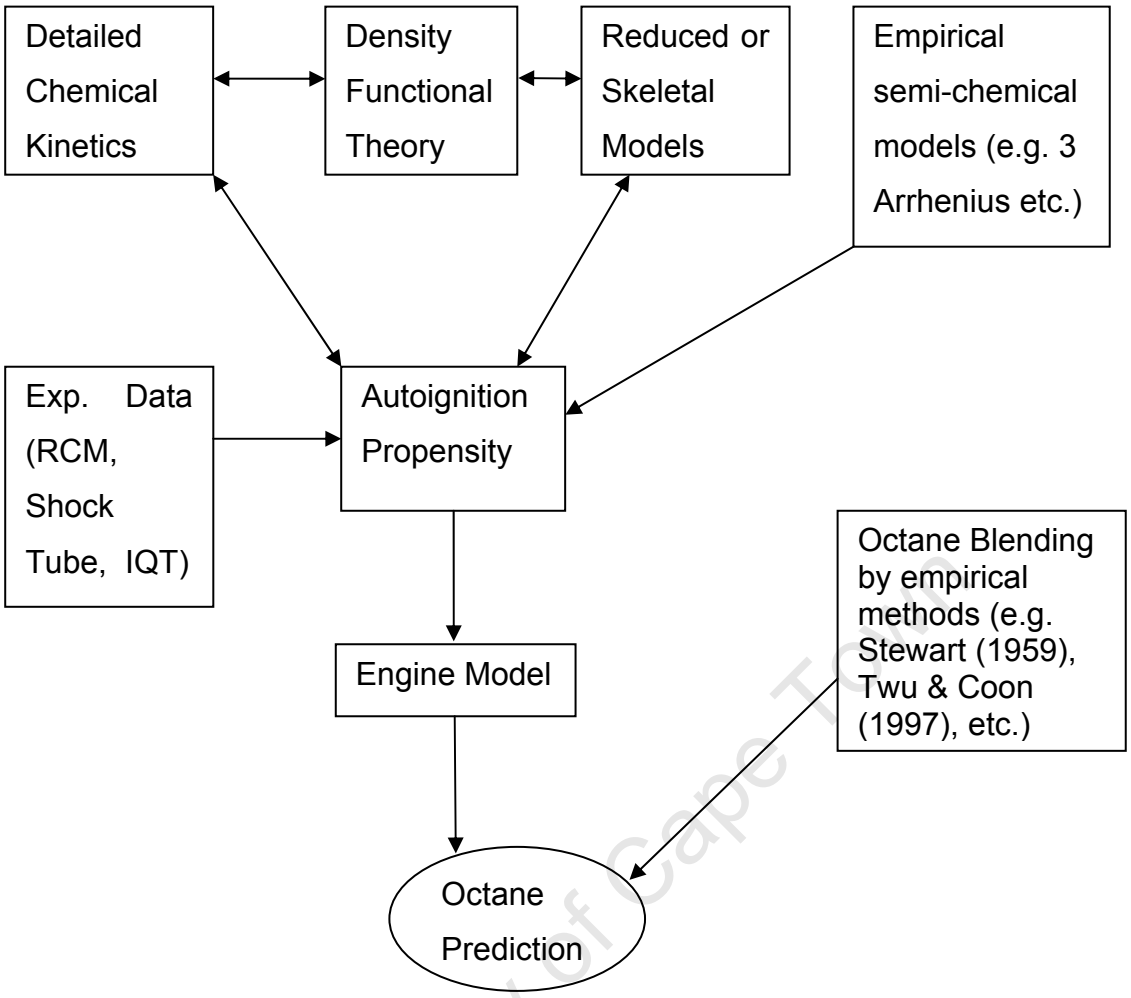

Figure 1.4: An overview of the aspects of octane prediction, as assessed in this thesis

Various strategies with which to obtain information on the ignition propensity of a fuel are shown in Figure 1.4, with the experimental techniques shown in the left-hand block. These would include data obtained in rapid compression machines, shock tubes, continuously stirred reactors (including jet stirred reactors), plug flow reactors, combustion bombs (of which the Ignition Quality Tester (IQT^{TM}) is an example), motored engines, and perhaps laminar flame speed measurement rigs. Kinetic simulations of the reactions leading up to autoignition can be explored by considering the detailed kinetic mechanisms, or by considering reduced or skeletal kinetic models.

Quantum mechanical modelling through Density Functional Theory (DFT) does not provide direct information about ignition delays, but was used in this study to glean more insight on specific aspects of either the detailed kinetic or skeletal kinetic

mechanisms. The empirical semi-chemical models may consist of those developed by Douaud and Eyzat (1978), based on the earlier work of Livengood and Wu (1955) where they proposed the "conservation of ignition delay" model, or the more recent "3-Arrhenius" model proposed by Yates et al. (2004) and Yates et al. (2005). A further development of this empirical model, with semi-chemical attributes through the formal consideration of the cool flame temperature rise (Yates and Viljoen, 2008), will also fall into this group shown in the top right-hand block of Figure 1.4. Finally, the traditional octane blending models which predict the octane number of the blend (often based on measured octane values for the components, thereby negating the necessity of considering ignition delays) are also considered. These models, such as the ones proposed by Stewart (1959), Healy et al. (1959), Morris et al. (1975) and Twu and Coon (1996, 1997) are shown in the lower right-hand block in Figure 1.4.

1.7 Research approach and thesis overview

A number of detailed oxidation mechanisms were available in the literature, characterizing the selection of model gasoline molecules that could be studied. These mechanisms were used to model the autoignition behaviour of a physical system that represents the last mass element of end-gas in a CFR engine. The modelling was performed by means of a software package, Chemkin Collection™, Release 3.7 (Reaction Design, Inc.), which was implemented on a high-end PC (Pentium 3.2 GHz, 4 GB RAM). Special emphasis was placed on constant volume combustion bomb simulations. An Ignition Quality Tester™ (IQT™), was used to measure ignition delays for a selection of these fuel components. Appendix A provides an example of the Chemkin input file used for the simulation of the IQT™.

Thus the study focussed primarily on the theoretical modelling of ignition delays, which was investigated both by detailed chemical kinetic simulations and also by reduced or skeletal kinetics, as is discussed in Chapter 3 of this thesis. This is preceded by the general introduction presented in Chapter 1, followed by a review of the relevant literature in Chapter 2. The theoretical modelling of ignition delay also branched out to molecular modelling by application of Density Functional Theory (DFT) to specific reaction sequences. This relatively novel application of DFT is discussed in more detail in Chapter 4.

In a parallel leg of the study, the empirical approach to the prediction of non-linear octane blending behaviour was also investigated, based mainly on the Stewart (1959), and Twu and Coon (1997) approaches. It was envisaged that these should be improved by incorporation of the novel approach of characterising all fuel molecules in terms of the extent of their NTC character exhibited in the engine environment, together with their clear octane values. Published experimental octane data for approximately 155 molecules from API Project 45 (American Petroleum Institute, 1957; and ASTM, 1959), formed the back-bone of this endeavour. This approach, which yielded an octane prediction tool that could be implemented in the real world, is discussed in Chapter 5. Although still empirical, it has attributes based on the fundamental understanding that was gained during this study.

In Chapter 6 an assessment is made of the different strategies for octane prediction that were evaluated, with special reference to their relative usefulness and limitations.

Finally, Chapter 7 contains the overall conclusions that were reached, as well as certain recommendations for further research to be done.

Chapter 2 : Literature Review

2.1 Introduction

This chapter provides an overview of the literature relevant to research into the measurement and modeling of the autoignition phenomenon that is associated with knock in spark ignition engines, and which could serve to trigger or enable the development of useful strategies for octane prediction.

2.2 Modelling approaches

The absolute octane numbers of gasoline mixtures (or blends of different gasoline component streams) is of great economic importance to an oil refinery; often octane quality is a key factor in determining the profit margin of a refinery (Van Gulick, 1975). Thus there has always been great interest in the development of empirical equations with which the octane numbers of gasoline blends could be accurately predicted. It is now generally accepted that a simple linear-by-volume (LBV) calculation is not accurate enough when either RON or MON values for actual full boiling range (FBR) gasoline mixtures have to be predicted, even though this linear behaviour is defined for mixtures of primary reference fuels (PRFs).

2.2.1 Fundamental approaches to the prediction of autoignition

Various approaches to the modelling of autoignition characteristics of both spark ignition and compression ignition fuels are possible, based on end-gas conditions of temperature, pressure, and lifetime (before normal consumption by the flame front in SI engines). These approaches can range from a completely global, single-step description (Warnatz, 2000), to a reduced kinetics treatment (Kirsch and Quinn, 1976; Halstead et al., 1977; Cox and Cole, 1985; Schreiber et al., 1994), or a comprehensive, detailed chemical kinetic simulation (Westbrook et al., 1988, Battin-Leclerc et al., 2000).

2.2.1.1 Global (Single Step) Reactions

Historically, the first attempts to describe autoignition were based on a single, global reaction. This was assumed to represent the combined effect of all the hydrocarbon

oxidation reactions leading to autoignition (Warnatz, 2000). An Arrhenius equation was chosen as an appropriate form for the mathematical expression describing the essential character of the global reaction. This reaction has a rate constant, k_G, of:

$$k_G = A_G \, e^{(\frac{-Ea}{RT})} \qquad ..(2.1)$$

where the subscript, *G*, refers to the global reaction, A_G is the pre-exponential constant of proportionality and E_a is the activation energy for the global reaction. The rate constant typically has units of s^{-1} (for first order reactions). For first order reactions,

$$\tau_G = \frac{Const}{k_G} \qquad ..(2.2)$$

where τ_G is the mean lifetime of all the reactant molecules, in units of seconds (s) (or milliseconds, ms). For first order reactions, the constant is unity (Logan, 1996). This implies that the mean lifetime of all the fuel molecules, before their consumption in the autoignition event, can be taken as the inverse of the global rate constant (Viljoen et al., 2005). If the hypothetical global reaction is indeed a first order reaction, then the half-life of the fuel molecules would be independent of their initial concentration, with the half-life being equal to *ln*(2) divided by the rate constant (Logan, 1996). This expression has been shown to be very successful in representing experimental autoignition data, for example from shock tubes, where the final attained temperatures are typically in excess of 1000 K and span a small range that does not extend downward towards lower temperatures. It has also been used frequently in experiments which encompassed only a small variation in the initial temperature of the system, in many instances adding [Fuel] and [Oxygen] concentration terms in order to reflect variation in ignition delay as a function of stoichiometry (as represented by the equivalence ratio, Φ).

$$\Phi = \frac{\left(\frac{Fuel_{mass}}{Air_{mass}}\right)_{Actual}}{\left(\frac{Fuel_{mass}}{Air_{mass}}\right)_{Stoichiometric}} \qquad ..(2.3)$$

If one makes allowance for possible pressure dependence in the global reaction, as indicated by early experiments from Fish et al. (1969), the well known ignition delay

relationship which was used to good effect by Livengood and Wu (1955) and Douaud et al. (1978), is obtained:

$$\tau_G = A_G \quad p^{-n_G} e^{(\frac{B_G}{T})} \qquad .. (2.4)$$

Here, the constant A_G is equal to the reciprocal of the pre-exponential factor of the Arrhenius expression shown earlier in Equation (2.1). The single event ignition delay that is predicted by this equation, refers only to the final high temperature ignition event and is therefore already a severe simplification of the actual phenomena. From the earliest experimental results obtained by rapidly compressing fuel-air mixtures and studying the cool flame evolvement, it was clear that the ignition delay involved two sequential steps and that the reactions should perhaps be better described as the sum of two Arrhenius equations. These were required to account for the data in the low and intermediate temperature regions where the measurements had been made (Lewis and von Elbe, 1961).

Edwards et al. (1992) identified three distinct temperature ranges: < 700 K as “low”, 700 - 1100 K as “intermediate”, and > 1100 K as the “high” temperature regime. Wilk et al. (1989) was even more specific when defining the temperature regimes for low pressure (≤1 atm) oxidations. They specified the temperature boundaries separating each of the reaction regimes as follows: T< 670 K (Low), 670 K < T < 900 K (Intermediate), and T > 900 K (High). It was acknowledged that these boundaries will shift to higher temperatures with increasing pressure (Wilk et al., 1989). More recently, however, most workers studying hydrocarbon oxidation under engine-relevant conditions, prefer not to distinguish a separate low temperature regime, but rather to identify the range from 600 - 900 K as the low-to-intermediate-temperature regime (Tao and Chomiak, 2002). The high temperature region is then mostly defined as > 1000 K (Viljoen et al., 2005).

In some instances, such as in CFD modelling of diesel sprays, the single global reaction suffices to describe the autoignition behaviour of the system, but from a molecular octane modelling point of view it is inadequate. It is important to note, however, that the single Arrhenius equation is sufficient to describe the ignition delay vs. 1/T behaviour of many molecules when only the high temperature region (>1000 K) is of interest.

In this combustion regime (for hydrocarbon flames) the single most important reaction is the chain-branching step (Miller and Fisk, 1987; Westbrook, 1992):

$$\cdot H + O_2 \rightarrow \cdot OH + \cdot O \qquad ..(2.5)$$

This important reaction consumes one hydrogen radical and produces two free radicals, leading to the rapid multiplication and exponential growth of the radical pool during high temperature ignition. The second most important reaction in combustion is the conversion of CO to CO_2, via the elementary reaction:

$$CO + \cdot OH \rightarrow CO_2 + \cdot H \qquad ..(2.6)$$

It is of great significance that these two most important reactions in combustion are totally independent of the hydrocarbon fuel molecules (Miller and Fisk, 1987). The implication is that the differences between various fuel molecules do not lie in the final combustion reactions, but rather in the sequences of oxidation reactions leading up to the ignition event. Thus the low- and intermediate temperature oxidation reaction sequences of fuel molecules predominantly determine their relative autoignition propensities (and thus their octane qualities).

2.2.1.2 Detailed Chemical Kinetics

The complex low-temperature oxidation chemistry of most hydrocarbon fuels was first explained by Nikolai Semenov (Glassman, 1977), through a free radical chain mechanism, where R• indicates any free radical species, as follows:

$RH + O_2 \rightarrow R\cdot + HO_2\cdot$	(1)	- chain initiation
$R\cdot + O_2 \leftrightarrow RO_2\cdot$	(2)	chain propagation
$R\cdot + O_2 \rightarrow$ olefin $+ HO_2\cdot$	(3)	
$RO_2\cdot + RH \rightarrow ROOH + R\cdot$	(4)	
$RO_2\cdot \rightarrow R'CHO + R''O\cdot$	(5)	
$HO_2\cdot + RH \rightarrow H_2O_2 + R\cdot$	(6)	
$ROOH \rightarrow RO\cdot + \cdot OH$	(7)	degenerate branching
$R'CHO + O_2 \rightarrow R'CO\cdot + HO_2\cdot$	(8)	
$RO_2\cdot \rightarrow$ destruction	(9)	- chain termination

Hydrocarbon autoignition proceeds via sets of degenerately branched chain reactions (reactions (7) and (8) shown above), the rate of which depends on the accumulation of branching agents and therefore on the history of the reaction as well as on the instantaneous state of the system. The term “degenerate chain branching” refers to the fact that the active chain carriers (RO• + •OH in this example), are formed from an intermediate stable (or meta-stable) product, rather than directly from the reactants themselves (Miller and Fisk, 1987). Also, the development of these reactions is critically dependent on the coupling between the chemical and physical systems since the heat released by the pre-flame reactions modifies the end-gas conditions during the induction (or ignition delay) period. These factors can only be taken into account by integrating the chemical rate equations with the thermodynamic relationships as a set of coupled differential equations. These can be solved at every relevant time-step by software such as the Chemkin package (Kee et al., 2002) from Reaction Design, Inc. (which was used in this study) that was originally developed at Sandia National Laboratory (Kee et al., 1989).

Since the 1980’s, the complex low- and intermediate temperature oxidation reaction mechanisms of hydrocarbon fuels have been elucidated to a large extent by the combined efforts of many international research groups, so that there is now largely consensus on the main features. These are indicated in Figure 2.1, where n-heptane is taken as a representative hydrocarbon fuel molecule. This graphical representation, which highlights the different temperature regimes, is adapted from a reaction scheme presented by Saylam et al. (2007). The same basic scheme has been presented by many authors over the last decade (for example, Westbrook et al., (2009); Faravelli et al. (1998); Curran et al. (1998); Biet et al. (2008) and Huang et al. (2008)).

In the low-intermediate temperature region (< 900 K), the most important reactions for alkyl radicals R• are combination with molecular oxygen: $R\bullet + O_2 \leftrightarrow RO_2\bullet$ (where $RO_2\bullet$ is an alkylperoxy species). The activation energy for the addition reaction is taken to be zero, but in the reverse (dissociation) direction it is relatively large at ≈ 30 kcal/mol (Curran et al., 1998). Thus the equilibrium constant for this reaction is very strongly temperature dependent. At low temperatures, this reaction

proceeds rapidly to alkylperoxy species, whilst at high temperatures RO_2• dissociates back to its reactants and the concentration of RO_2• becomes very small, effectively shutting off the low temperature branching reaction paths at approximately 800 to 850 K. This has the effect of lowering the overall rate of reaction and accompanied heat release (Westbrook et al., 1998). The literature frequently contains contradictions regarding the typical ceiling temperatures of relevance in an engine environment, and ceiling temperatures for PRFs of ~850 K (Westbrook et al., 1998) to almost 1000 K (Cavaliere and De Joannon, 2004) have been reported. These apparent contradictions can be understood by means of the comprehensive explanation offered by Cavaliere and De Joannon (2004), outlining the opposing effects of increasing pressure and decreasing oxygen concentration on the ceiling temperature.

The larger concentration of R• radicals (as the RO_2• dissociates at the increased temperature) increases the rate of the strongly inhibiting oxidation reaction:

$R\bullet + O_2 \rightarrow \bullet HO_2 +$ olefin (Reaction 2" in Figure 2.1)

This reaction is equivalent to a termination step since $\bullet HO_2$ radicals react mostly by the disproportionation reaction: $2\ \bullet HO_2 \rightarrow H_2O_2 + O_2$, leading to a further decrease in the reactivity of the system at this point. Furthermore, unimolecular reaction channels from •QOOH radicals, which have high activation energies and involve fragmentation into various products, become faster, and compete with O_2 addition. •QOOH radicals can decompose into cyclic ethers (Reaction 5 in Figure 2.1) or ketones and •OH radicals (Reaction 6) or by β-scission into $\bullet HO_2$ radicals and conjugated olefins (Reaction 4) or smaller species which do not lead generally to branching agents. Because of the decrease in the production of peroxides, the reactivity of the alkanes drops off in the 700 to 800 K temperature range. This temperature region is consequently called the negative temperature coefficient (NTC) region (Biet et al., 2008).

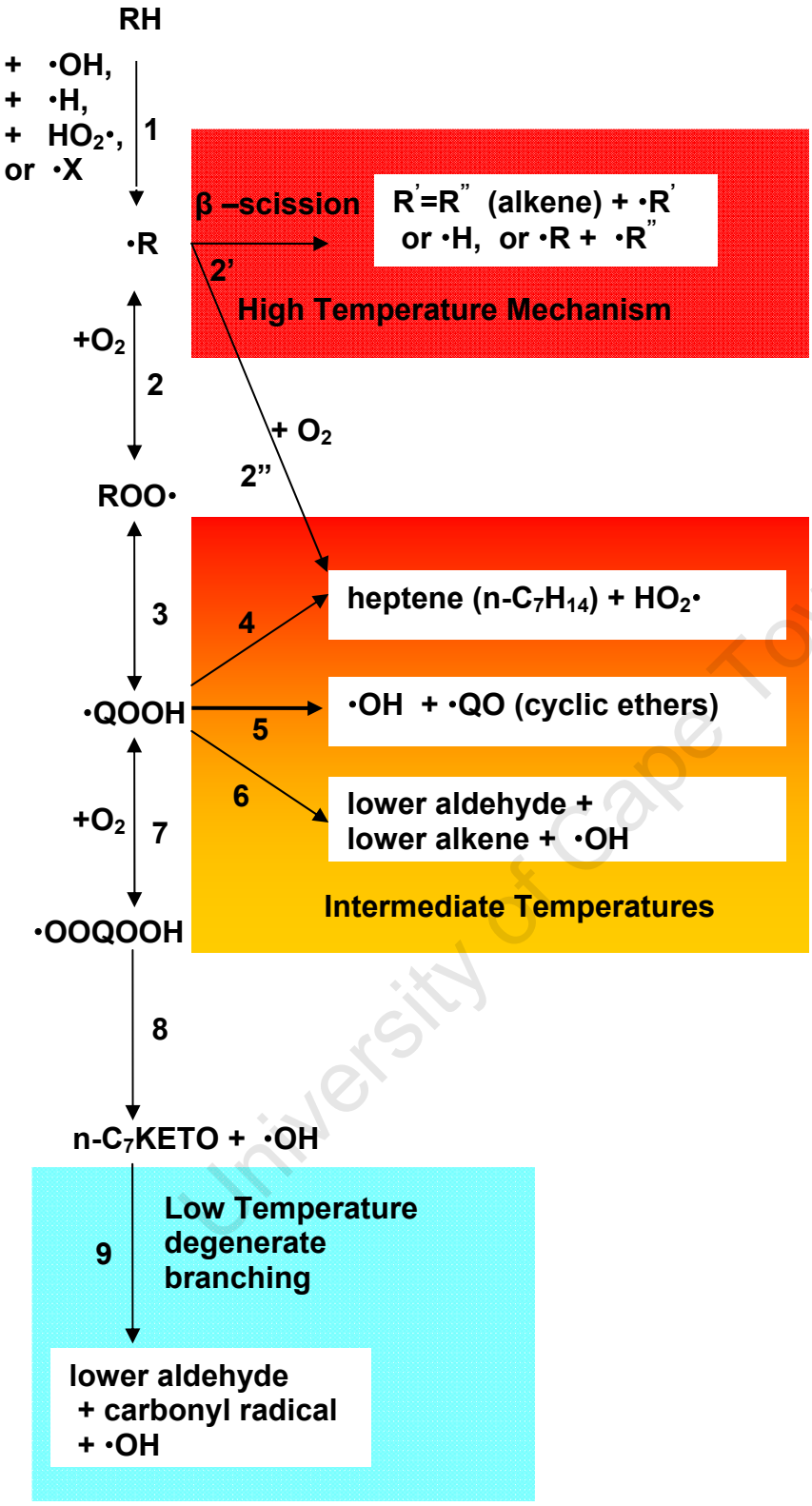

Figure 2.1: Reaction scheme of the primary oxidation mechanism of *n*-heptane involving C_7 species. RH is for *n*-heptane, •R for heptyl radicals, Q for C_7H_{14} structures, Q' for C_7H_{13} structures, QO for O-heterocycles, n-C_7KETO for ketohydroperoxides or aldohydroperoxides and •X for •OH, •CH_3, CH_3O•, CH_3O_2•, HO_2•, or •H

Pressure also influences the $R\bullet + O_2 \leftrightarrow RO_2\bullet$ equilibrium through the well known Le Chatelier principle. At elevated pressures, the $RO_2\bullet$ submechanisms continue to be more important at higher temperatures than would have been the case for a system at atmospheric pressure (Curran et al., 2002). During rapid compression machine (RCM) studies of n-pentane, Westbrook et al. (1998) observed that a pressure increase by a factor 2 increased the temperature where decomposition begins to control the reaction by approximately 50°C. The region of minimum heat release (referred to as the NTC region earlier) also shifted 50°C towards a higher temperature. Thus the complex NTC behaviour is predominantly determined by the $R\bullet + O_2 \leftrightarrow RO_2\bullet$ equilibrium, which represents the various alkyl radicals' addition equilibria with oxygen. It must also be appreciated that the second oxygen addition (reaction 7 in Figure 2.1), is also in a dynamic equilibrium as described above (for Reaction 2), therefore the preceding discussion is of equal relevance to both oxygen addition reactions (2 and 7 in Figure 2.1).

The cool flame ignition delay (which is associated with the blue block in Figure 2.1), is now widely attributed to the decomposition of ketohydroperoxide species at a temperature between 800 K and 850 K, again this temperature range will vary with pressure. These meta-stable molecules are gradually built up in the system, before their dissociation lead to rapid chain branching and sudden heat release (as indicated by reaction 9 in the scheme shown above). This heat release in the cool flame temperature regime, typically from 500 K to 800K, will raise the temperature of the system by only 100 K to maximum 200 K (Miller and Fisk, 1987). In contrast to this notion of a somewhat muted cool flame temperature rise, Yates and Viljoen (2008) presented detailed kinetic modeling results showing cool flame temperature jumps of ~350 K are quite common for a stoichiometric n-heptane system at initial temperatures < 700 K, under adiabatic conditions.

If the adiabatic flame temperatures of fuel molecules (typically in the range of 2500 to 3000 K under stoichiometric conditions in SI engines) are considered, it is clear that less than ~10% of the available heat is released by the cool flame. This is in agreement with Bood et al. (1997), who have determined by Rotational CARS (Coherent Anti-Stokes Raman Spectroscopy) measurements in an engine that more than 90% of the heat is released during the fast second stage ignition of the end-gas.

Finally, the high temperature ignition at temperatures above 1000 K is driven primarily by the decomposition of hydrogen peroxide (Westbrook, 2000; Griffiths et al., 2005). If the temperature of the system has advanced beyond the region of negative temperature coefficient behaviour, then a positive temperature dependence of ignition delay on temperature is again observed. The activation energy for H_2O_2 decomposition is large enough (≈ 45 kcal/mol) (Westbrook et al., 1998) so that its decomposition is still quite slow in the range from 800 K to 1000 K. Above about 1000 K, however, rapid decomposition of H_2O_2 is observed, leading to rapid branching causing exponential radical multiplication, and the associated high temperature ignition event. An analysis by Westbrook (2000) has shown that "*autoignition in engines is dominated by only one elementary reaction, H_2O_2 decomposition. Low temperature reactions or cool flames, including the highly chain branched alkylperoxy radical isomerization kinetic system, simply advance the time at which H_2O_2 decomposition is observed.*"

With detailed kinetic models of the autoignition kinetics, all the molecules in the fuel, as well as all the hundreds of intermediates, radicals and products must be described in absolute detail. As with normal combustion reactions, it is a daunting task to try to identify all the species and reactions, let alone their respective reaction rates. In rare cases (such as for PRFs) this task has been accomplished by large teams led by Westbrook, Battin-Leclerc, Warnatz, and Ranzi, amongst others.

In principle, the detailed kinetic approach could be a description of reality (no longer only a model), if all the reactions undergone by all the species, and the true rate constants of these reactions, were known accurately. In practice, this is unfortunately not the case and the detailed kinetic mechanisms with their optimised rate data, remain elaborate *models* of the autoignition system.

2.2.1.3 Reduced (or Skeletal) Chemical Kinetics

When a sensitivity analysis of such a detailed reaction mechanism reveals that only a fraction of the number of different reactions are necessary to describe experimental data adequately, then we enter into the realm of reduced kinetic mechanisms. These can either be constructed from the simplest set of kinetic equations consistent with the experimental data, as have been done by Schreiber et al. (1994) and the Shell Thornton researchers who developed the Shell model (Halstead et al.,1975, and later

Sazhin et al., 1999), or it can be reduced from a detailed chemical kinetic mechanism. An example of the latter is for n-heptane, where Curran, Pitz and Westbrook's detailed mechanism containing 561 species taking part in 2539 different reactions, had been reduced at Chalmers University to 65 species and 273 reactions, with negligible effect on the accuracy of the model when used to simulate experimental ignition delay data (Tao et al., 2000; Ogink and Golovitchev, 2001).

This is also in broad agreement with the results shown by Shell's Halstead et al. (1977), based on their reduced chemical kinetic model of autoignition that incorporated only 8 generalised chemical species in 5 reactions. This model is perhaps the most well-known reduced model and has found application in many CFD – and engine simulation packages. The distinction between this model – later known as the Shell BTI model, referring to Branching, Termination and Initiation – and the Chalmers reduced model referred to in the previous paragraph, is that the Shell model makes use of pseudo-species, while the Chalmers mechanism still maintains actual chemical species with atom conservation across the whole mechanism.

In an important further development of the Shell model, Cox and Cole (1985) made the reaction scheme more explicit and extended it to 10 species in 15 generalised reactions. Their reaction mechanism made provision for the formation of O-heterocyclic products, as well as for the formation of olefins and carbonyl compounds by the important β-scission mechanism of a β-hydroperoxyalkyl radical.

Subsequently, Hu and Keck (1987) further refined the reduced reaction scheme of Cox and Cole to incorporate 13 active species in 18 reactions. Of these 18 reactions, 7 are considered to be reversible, so that separate rate constants are presented for the forward and reverse reactions. Hu and Keck calibrated their model against experimental results obtained in a combustion bomb and in earlier rapid compression machine studies. It should be realised that these calibrations really represent the finding of the most suitable averages of the rates of many elementary reactions that have been replaced by a single skeletal step in the reduced model. A serious limitation of the reduced models discussed in the preceding paragraph, is that they often address only the low and intermediate temperature region, and do not allow for complete conversion of fuel to CO_2 and H_2O.

Li et al. (1996) improved the predictive capabilities of the Hu and Keck model by adding additional generic reactions and species to it, and by carefully tailoring the rate coefficients of the various reactions. The Li et al. model consisted of 29 reactions with 20 active species, and it reproduced experimentally measured ignition delay and cool flame heat release to within 15%, but was less successful in describing the high temperature oxidation mechanism (Zheng et al., 2001). Attempting to improve the overall model, for application specifically to HCCI combustion simulations, Zheng et al. (2002) incorporated the high temperature chemistry from the Griffiths model (Griffiths et al., 1994) into the Li model to describe the low, intermediate, and high temperature chemistry. This model consisted of 69 reactions and 45 species and was generally in good agreement with experimental data for pre-ignition behaviour, ignition delays and heat release rates for a PRF20 fuel in HCCI engines (Zheng et al., 2002). The improvement of these computational efficient, skeletal mechanisms is continuing at Drexel University under Nicholas Cernansky's guidance, again with a strong emphasis on HCCI simulations. It must be noted that prior to Zheng et al. (2002), most authors described the same mechanisms as being "reduced", whereas the definition as "skeletal mechanisms" is now more commonly accepted. According to this usage of the terms, the original Shell model and its successors (Cox and Cole, Hu and Keck, etc.) are now all being referred to as skeletal mechanisms (Huang et al., 2008).

2.2.1.4 Reduced versus Detailed Kinetics

In the initial approach to this study, much emphasis was placed on the investigation of the reduced kinetic approach, as this was seen as a promising avenue in developing more fundamental relationships with which octane can be predicted, while still remaining simple enough computationally to be useful in a blending model. What was probably not so obvious at the start, is the requirement alluded to earlier; that reduced models need extensive sets of experimental autoignition data with which they can be calibrated. This is problematic if access to experimental measurements is so limited. Without these sets of autoignition data for all relevant molecules, reduced kinetic models do not provide a better means to achieve the objective of octane prediction compared to empirical models. The reduced kinetic models have, however, provided deeper insights into autoignition phenomena and also with respect to the blending rules that govern the autoignition behaviour of blends.

The most convincing reason for developing skeletal (or reduced) mechanisms is the excessive computational requirements of detailed kinetic mechanisms when these are coupled to CFD codes in order to simulate physical combustion systems (Griffiths et al., 1992). Computational times in the order of months, as indicated in Figure 2.2 (taken from Aceves et al., 2005), is not realistically useful in current hardware systems. Full integration of a fluid mechanics code with a chemical kinetics code may be the method of choice for autoignition analysis in the future, as fast parallel computers may be able to surmount the very high computational intensity of this problem. However, for now, fully integrated calculations are limited to small chemical kinetic mechanisms (~100 species) and coarse grids (~1000 cells). For chemical kinetics, the computational time is proportional to the number of cells, and for fluid mechanics the computational time is proportional to the square of the number of cells (Aceves et al., 2005).

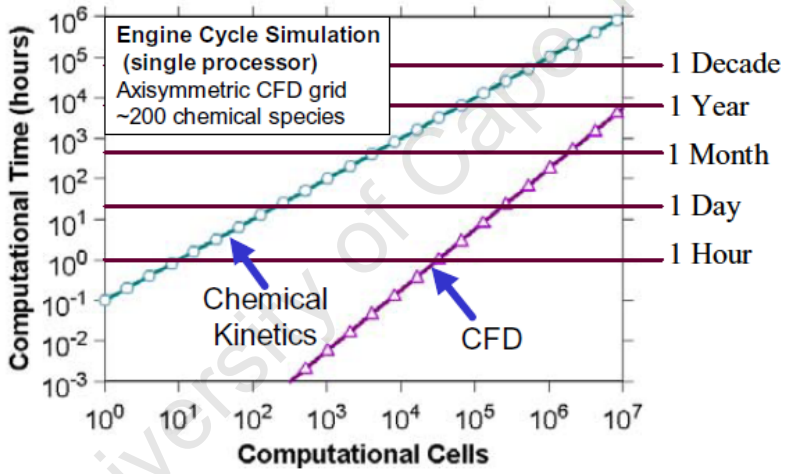

Figure 2.2: Computational time in a single processor of a 2 GHz LINUX computer as a function of the number of computational cells for a computational fluid mechanics (CFD) calculation and a chemical kinetics calculation (taken from Aceves et al., 2005)

Although no detailed kinetics model of a real commercial FBR fuel, containing aromatics, naphthenes and olefins as well as paraffins, has to date been published, work continues to elucidate the reaction mechanisms that are rate determining for the various classes of molecules and to merge them into a single mechanism. The Italian group of Ranzi and Faravelli in Milan has perhaps made the most progress in this regard (Mehl et al., 2006). As computer hardware and software continue to rapidly develop further, the goal of successful simulation of the detailed kinetics of autoignition in a real-world gasoline (or diesel) is becoming more and more within reach.

On the other hand, the detailed kinetic reaction schemes that have been developed up to the present moment to model fuel combustion, are in many instances not significantly more accurate than their reduced kinetic counterparts, for example in the prediction of the onset of knock. Thus the added computational cost of using the detailed mechanisms in 3-dimensional CFD engine models are not always warranted, even if it is technically feasible. This is argued by many authors, most of whom are working on strategies for the reduction of detailed mechanisms (examples are Elliott et al., 2006; Pepiot-Desjardins and Pitsch, 2008; Huang et al., 2008; and Kazakov et al., 2006). A graphical representation of the relative success of the LLNL detailed mechanism for n-heptane, consisting of 561 species participating in 2539 elementary reactions (Curran et al.,1998), compared to a skeletal mechanism of Peters et al. (2002), which consists of only 35 species participating in 56 reactions, is shown in Figure 2.3.

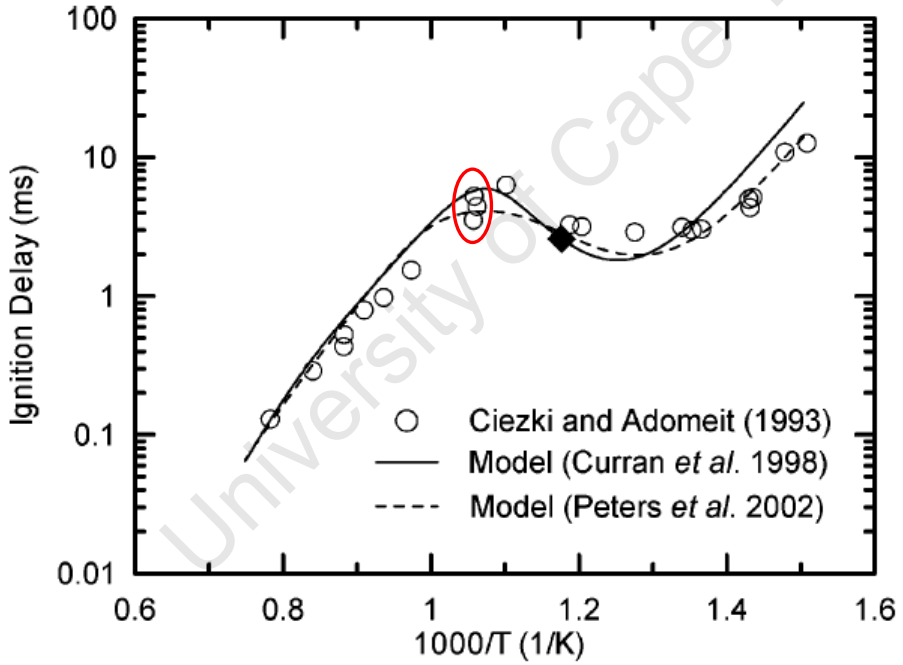

Figure 2.3: Ignition delay times as a function of temperature for a stoichiometric *n*-heptane/air mixture at 13.5 bar. The shock tube experiments of Ciezki and Adomeit (1993) are compared against results obtained from detailed (Curran et al., 1998) and skeletal (Peters et al., 2002) models. (Reproduced from Kazakov et al., 2006)

It is clear that the experimental error [see for example the 3 measurements at a temperature of 943 K (1.06 on the x-axis, in the red oval), displaying an error of ± 16%, or 4.5 ± 0.7 ms] in the underlying data are of similar magnitude as the differences between the predictions based on the detailed kinetic scheme, and those based on the highly reduced skeletal scheme. On the low temperature side, the

skeletal mechanism appears to be a better representation of the experimental data than the detailed mechanism, thus there would be even less incentive to use the computationally expensive detailed kinetics in favour of the skeletal mechanism.

Similar conclusions may be reached when the n-heptane mechanism reduction of Seiser et al. (2000) is considered. This is shown in Figure 2.4, where the original n-heptane oxidation mechanism of LLNL (Curran et al., 1998) has been reduced to only 160 species (from the original 557 species). Calculated ignition delays based on these mechanisms, and an intermediate-sized reduced mechanism of 282 species, are compared to RCM results (Minetti et al., 1995) and to shock tube results obtained by Ciezki and Adomeit (1993). It is clear that the differences between the detailed kinetic scheme and the two reduced kinetic mechanisms are small compared to the relatively large uncertainty in the underlying experimental data.

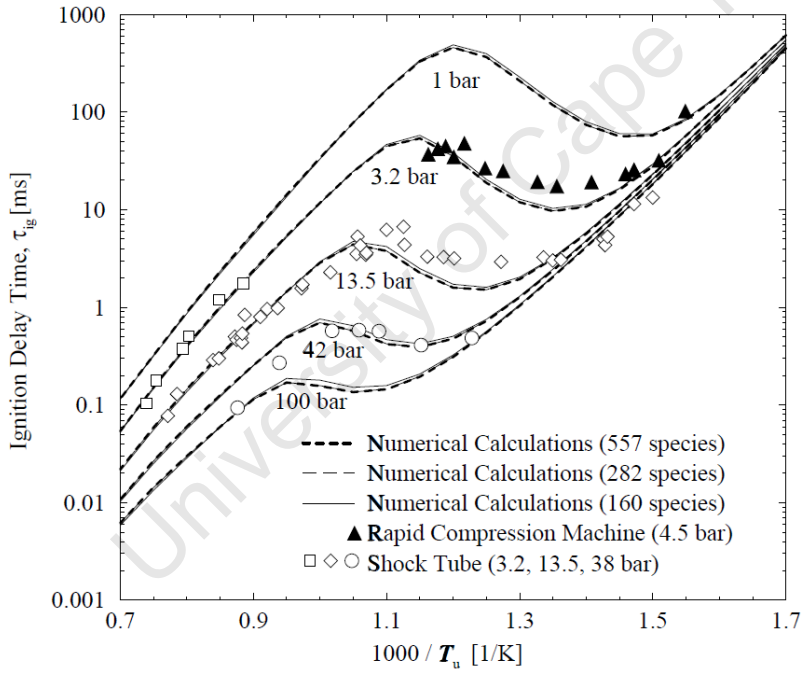

Figure 2.4: Ignition delays for stoichiometric mixtures of n-heptane vapour and air as a function of the reciprocal initial temperature for various pressures, taken from Seiser et al. (2000). The short-dashed line represents the prediction based on the detailed LLNL mechanism. The solid line represents the prediction based on the final reduced mechanism (160 species), with an intermediate reduction also shown. The symbols represent experimental data from shock tubes (Ciezki and Adomeit, 1993) and rapid compression machines (Minetti et al., 1995).

The experimental data shown in Figure 2.4 are again indicating the complexity of the autoignition phenomenon, even if it is for a single fuel molecule such as n-heptane. Since the 11.6 m total length of Ciezki and Adomeit's shock tube limited measurable

ignition delays to less than 10 ms, only high temperature ignition can be obtained at lower pressures, whereas the RCM experiments are more appropriate at longer ignition delays, in the low and intermediate temperature regimes. Unfortunately the RCM experiments at 4.5 bar cannot to be compared directly to the shock tube measurements at 3.2 bar, but the general trends seem to match relatively well.

2.2.2 Semi-chemical ignition delay relationships

In their seminal paper, Livengood and Wu (1955) proposed that an equivalent aggregate reaction may describe the concentration, x, of pertinent reaction products and that the change in the concentration is a function of pressure, temperature, time, air-fuel ratio and fuel composition. Livengood and Wu further suggested that there is a critical concentration, x_c, where the reaction proceeds to completion, signified by the ignition delay time, τ. The results of their mathematical manipulation revealed the "ignition delay integral" which reaches unity at a critical time, t_c:

$$\frac{x}{x_c} = \int_{t=0}^{t=t_c} \frac{1}{\tau} dt = 1.0 \qquad ..(2.7)$$

This concept of the conservation of ignition delay became a powerful basis for many commercial models of autoignition delay in reciprocating engines. The ignition delay model was subsequently parameterised for iso-octane by Rifkin and Walcutt (1957) and Gluckstein and Walcutt (1961).

Further research conducted by Douaud and Eyzat (1978) at IFP (Institut Français du Pétrole) on the thermodynamic analysis of combustion with knock has led to a better understanding of this phenomenon and particularly to a practical knock model based upon the autoignition delay concept. Whereas this method gives satisfactory results for predicting engine fuel behaviour, the handling of the somewhat complex experimental and calculation procedure has made it more suitable for research studies than for industrial applications. In order to fill in this gap the development of a method whose utilization would be compatible with standard industrial techniques was initiated by Douaud and Eyzat (1978). The concept of autoignition delay relies on the integration of the rate equation (for a so-called equivalent aggregate reaction, representing all the reactions preceding the autoignition event) which describes the

production rate of chain carriers as a function of their concentration α and of the pressure and temperature of the end-gas:

$$\frac{\partial \alpha}{\partial t} = \alpha A^{l} p^{n} \exp\left(\frac{-B}{T}\right) \quad ..(2.8)$$

where p = pressure, T = temperature, α = concentration of chain carriers, A^{l} = pre-exponential constant, n = pressure coefficient, B = temperature coefficient. Thus, for constant p and T,

$$\tau_{ind} = A \cdot p^{-n} \exp(\frac{B}{T}) \quad ..(2.9)$$

where τ_{ind} is the autoignition delay. From Equation 2.9 it is assumed that the ultimate consequence of the global reaction of the chain carriers is a sudden transition to a process which then proceeds to complete the combustion reaction within a time interval which is orders of magnitude smaller than the preceding delay period. This concept of a critical concentration provides a limit for an integration process during which the concentration of the chain carriers builds up. This delay time is of course a measure of the resistance against autoignition or knock. Douaud realised very early on that, since any simplification of the kinetic scheme is going to be riddled with empirical constants, the autoignition description must be as simple as possible. Since the relation shown above has only three degrees of freedom, the chances for a successful fitting of the empirical constants are greatly increased. Douaud was able to obtain representative values from the analysis of pressure diagrams of a knocking engine and proposed the following relationship to describe primary reference fuels (valid only for the range of octane numbers between 80 and 100):

$$\tau_{\text{ind}} = 0.01869\left(ON/100\right)^{3.4017} p^{-1.7} e^{3800/T} \quad ..(2.10)$$

where ON is the octane number of the fuel. It is evident that Equation 2.10 cannot describe two-stage ignition or cool flame thermal effects, as it describes a single straight line (as shown in Figure 2.5). An additional semi-chemical ignition delay relationship that has been developed during the course of this study, is the so-called “Three-Arrhenius” ignition delay expression, as described in Yates et al. (2004) and Yates et al. (2005). The objective of the three-Arrhenius approach was to describe the complex kinetic chemistry of hydrocarbon autoignition in the simplest

mathematical formulation that could be shown to be consistent with the available experimental and literature data. Thus, the proposed model (Yates et al., 2004) involved two distinct regimes; a two-stage, low-temperature regime and a single stage high temperature regime. The ignition delays for each stage were described by a general Arrhenius function:

$$\tau_i = A_i p^{n_i} e^{\frac{B_i}{T}} \qquad ..(2.11)$$

Since the two stages of the low-temperature regime were sequential, they were expressed as the arithmetic sum of the individual ignition delays, $\tau_1 + \tau_2$. Since the high temperature delay, τ_3 represented an alternative, competing pathway, the overall ignition delay for the full temperature range was described by the sum of the individual rates, i.e., the inverse sum of the two delays:

$$\tau_{overall} = \left\{ \frac{1}{\tau_1 + \tau_2} + \frac{1}{\tau_3} \right\}^{-1} \qquad ..(2.12)$$

where each of the ignition delays τ_1, τ_2, τ_3 takes the form of Equation (2.11). This empirical correlation was subsequently developed further to attain a stronger chemical kinetic relevance, based on the cool flame ignition delay and consideration of the temperature increase due to the cool flame (Yates and Viljoen, 2008).

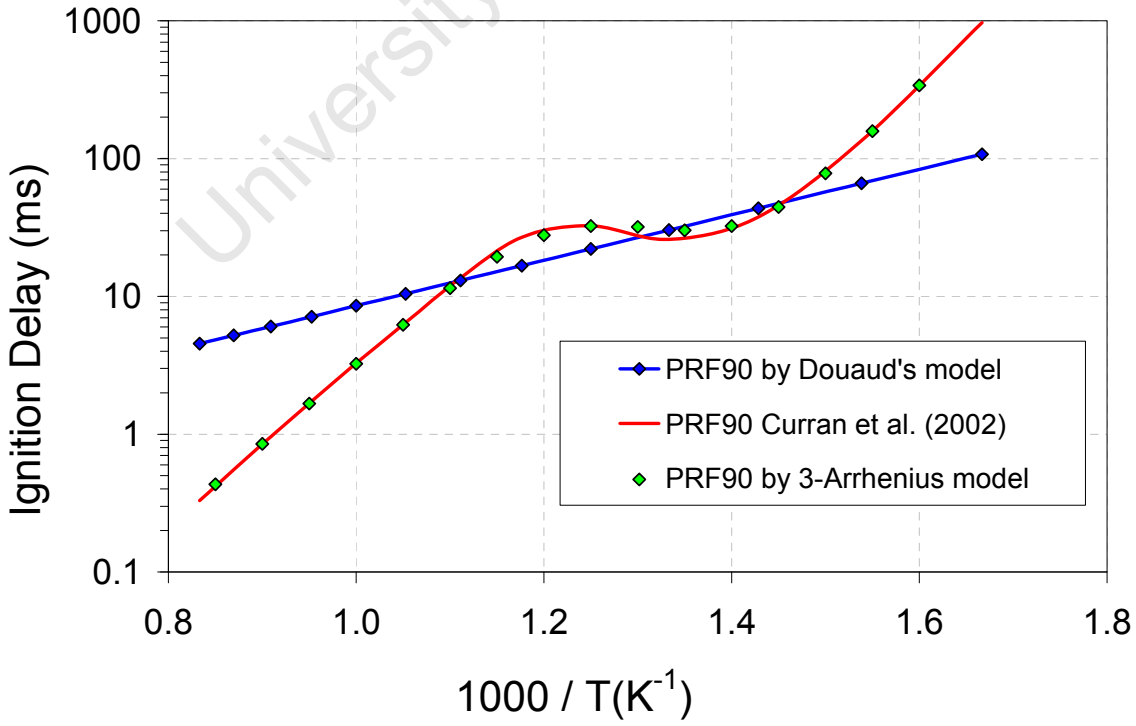

Figure 2.5: Comparison of ignition delay versus reciprocal temperature for a PRF90 at 12 atm under stoichiometric conditions. The Douaud model was implemented directly

from Eq. 2.10, while the constant volume simulation was performed using the PRF detailed kinetics mechanism from Curran et al. (2002)

From the ignition delay data shown in Figure 2.5, it is fairly obvious that the complex low and intermediate temperature ignition behaviour of a PRF blend cannot be adequately described by a single Arrhenius equation (as contained in Douaud's model). The detailed kinetics description, which is discussed in more detail in Chapter 3, can be represented very effectively by a simple ignition delay relationship based on Equation 2.12. The least squares regression coefficients for PRF90 in this representation are given in Appendix B.

2.2.3 Empirical approaches to octane number prediction

These purely empirical approaches refer to the traditional octane blending models that have been developed over many years for practical use in the refining industry. Such empirical models, as the ones proposed by Stewart (1959), Healy et al. (1959), Morris et al. (1975) and Twu and Coon (1996, 1997), can predict the octane numbers of blends and are most often based on measured octane values for the components, thereby negating the necessity of considering ignition delays. These models are critically evaluated and discussed in more detail later in this thesis, in Chapter 5.

The significant theoretical and practical contributions to the understanding of RON and MON relationships of real gasolines, made by Kalghatgi and co-workers (see, for example Cracknell et al. (2009), and Andrae et al. (2007)), must also be mentioned here. Kalghatgi (2005) found that RON or MON values on their own cannot describe the autoignition quality of gasoline-like fuels in HCCI combustion at all conditions. The reason is that the reactivities of fuels of different chemistries have different temperature and pressure dependencies. Even in cases when RON or MON cannot adequately describe the autoignition quality of gasoline fuels, it is possible to combine RON and MON into an Octane Index, OI, that describes the autoignition quality relatively well at most conditions. The octane numbers are combined into the OI with the variable K according to the following equation:

$$OI = (1-K)RON + K\,MON = RON - K\,S \quad ..(2.13)$$

where S is the sensitivity (RON – MON) of the fuel.

The OI of a sensitive fuel is the equivalent of the octane number of a primary reference fuel with the same resistance to auto-ignition in the tested condition. The

K-value is dependent on the engine condition. At RON conditions the K value is by definition zero and the K-value equals one at MON conditions. The K-value can, however, also be either above one or below zero (Kalghatgi, 2005).

2.3 Experimental techniques for the study of autoignition

In Figure 1.4, a diagrammatical outline of this research project, brief reference was made to the different experimental techniques that can be used to obtain information about the autoignition propensity of the fuel molecules under study. In the following section, which is not intended to be a critical review of these various techniques, a cursory introduction is provided to the most important experimental equipment.

Experiments in combustion kinetics normally utilize one of the following four types of devices (Miller and Fisk, 1987):

1. Static (often adiabatic) reactors
2. Plug-flow reactors
3. Continuously stirred tank reactor (CSTR) (or well-stirred reactors)
4. Laminar flames of various geometries

2.3.1 Static reactors

A large number of constant volume combustion bombs of different designs may occur in the first group. Examples are the combustion bombs of Edwards et al. (1992) and the more recent IQT^{TM}, as described by Yates et al. (2004) and Yates et al. (2007). The main challenge with static reactors is the complications due to surface effects, which are difficult to control in a consistent manner for reproducible quantitative analysis.

2.3.2 Plug-flow reactors

The concept behind the plug-flow reactor (PFR) is to replace the temporal history of a multi-step reaction (such as hydrocarbon oxidation) by a spatial distribution. Perhaps the best known examples of this kind are the Princeton Flow Reactor (Vermeersch et al., 1991) and the pressurized flow reactor developed at Drexel University (Wang et al., 1999).

2.3.3 Well-stirred reactors

In a CSTR, the rate of mixing of the reactants with products is intended to be very fast compared to the rate of the chemical reaction, thus rendering the contents of the reactor uniform. The assumption of perfect, instantaneous mixing results in sampled compositions that are purely kinetically controlled, and allows the effect of transport properties to be removed from the system under investigation (Miller and Fisk, 1987). The most important examples of this type of perfectly stirred reactors are the so-called Jet-Stirred Reactor (JSR) that are commonly used in France at CNRS-INPL, Nancy by Battin-Leclerc's group and at CNRS, Orleans. Some of these quartz reactors in high-pressure steel vessels can be used at up to 10 bar and at temperatures up to 1200 K (Dagaut et al., 1986).

2.3.4 Laminar flames

The laminar premixed flame is perhaps the most commonly used macroscopic reactor system in chemical kinetics investigations where the emphasis is purely on the high temperature ignition. Laminar flame speeds are usually measured and calculated at ambient conditions and include the effects of transport phenomena in the propagating flame front. The temperature in the reaction zone of a typical laminar flame is usually in the range between 1400 K and 1900 K. A sensitivity study of the rate coefficients of a kinetic model, performed by Warnatz (2000), revealed that only two reactions (those between atomic hydrogen and molecular oxygen (as shown by equation 2.5) on the one hand and carbon monoxide and the OH radical (see equation 2.6), on the other) govern the rate of reaction. This explains the rather similar flame velocities for a variety of alkanes and a wide range of other hydrocarbons. As the local environment in the combustion chamber of a spark-ignition engine, in the short time intervals during which the end-gas may autoignite (or alternatively, be consumed by the normal combustion) is quite turbulent, it follows that laminar flame speeds are of little direct relevance in providing information about the relative anti-knock quality of fuels.

Most of the experimental data that is of relevance to autoignition research in internal combustion engines, have therefore been provided by shock tubes, rapid

compression machines and motored engine experiments. A few of the benefits and challenges associated with the use of these devices are highlighted below:

2.3.5 Shock tubes

Shock tube experiments are excellent tests of the high temperature reaction mechanisms for hydrocarbon oxidation (Westbrook, 2000). The nearly instantaneous attainment of high temperatures (>1200 K) and fairly high pressure (i.e. >3 atm) means that the results are completely independent of the low and intermediate temperature regime reaction subsets (Westbrook and Pitz, 1987).

The reaction can be studied either the first time the shock wave passes through the test gas (incident shock), or after it has been reflected from an end wall (reflected shock). In optimised situations, the gas flow behind the incident shock approaches ideal plug-flow conditions, whereas the gas behind the reflected shock may be nearly static. Very high temperatures (> 5000 K) become accessible in the latter situation (Miller and Fisk, 1987). Various optical and laser measurement techniques have also been integrated with shock tubes of many different designs. More recently, Fikri et al. (2008) have reported shock tube measurements of gasoline surrogates under engine-relevant conditions of temperature and pressure. These ignition delay results, measured in the high pressure shock tube at the University of Duisburg-Essen, were reported for pressures from 10 bar up to 52 bar (Fikri et al., 2008). Furthermore, the high pressure single pulse shock tube at the University of Illinois (Chicago), has been used in the study of toluene oxidation at pressures as high as 550 bar and 610 bar (Sivaramakrishnan et al., 2004). These extreme pressures fall outside the domain of engine-relevant pressures, although the objective of this work was related more to the validation of oxidation mechanisms for toluene.

Shock tube methods often suffer from a lack of selectivity and are not commonly used to measure species concentration variations with time; usually only the ignition delay period is measured in these experiments. Maximum ignition delay times are also limited by the available length of the tube, most frequently to < 10 ms (Ciezki and Adomeit, 1993). This means most shock tubes (other than special high pressure ones such as the one at Duisburg-Essen) are commonly used to investigate high

temperature kinetic mechanisms, and cannot provide useful data about the low to intermediate temperature regimes.

2.3.6 Rapid compression machines

Rapid compression machines (RCMs) have long provided a fertile environment for the study of hydrocarbon oxidation in the low- to intermediate temperature regimes (Westbrook et al., 1996; Griffiths et al., 1992; Litzinger, 1990, Griffiths et al., 2001). The apparatus provides a combustion chamber with a single, very rapid piston stroke, leaving the compressed gases at temperatures from 550 K to 950 K, depending on the compression ratio of the RCM and the specific heats of the reactant and diluent gases. Compressed gases can undergo a single-stage or two-stage ignition, or the reactants may sometimes not ignite at all while heat transfer cools the mixture to room temperature (Westbrook, 2000).

RCMs have been very effective in generating ignition delay data in the NTC region as displayed by many hydrocarbon fuels, under conditions much closer to those encountered in knocking engines. However, there remains concern over the extent of reactions that may proceed during the compression stroke, as well as the exact magnitude of the temperature (typically being calculated) at the points where autoignition first occurs (Griffiths et al., 1997).

2.3.7 Motored engines

Experimental and modelling investigations into both motored and fired actual engines have allowed researchers to address the entire temperature history of the end-gas from 400 K to burnt gas temperatures. Both temperature and species concentration histories in the end gas can be measured, sometimes in engines which allow full optical access (Westbrook and Pitz, 1987). Rapid sampling valves that were integrated with some of these research engines allowed quantitative measurements of species concentration profiles in the end-gas (Litzinger, 1990). In the last decade, motored engines were again used extensively in the prolific research on HCCI fuels and control strategies for HCCI engines.

Although it is obvious that motored engines provide experimental access to the exact conditions of relevance to autoignition research on real fuels in actual engines, their use also introduce some additional uncertainties about the composition of the system and its precise temperature. For example, Bood et al. (1997), using rotational CARS in a single-cylinder Hydra engine, could not determine the temperature at -42 CAD to a better standard deviation than ±2.5% (or 577 K ±14.6 K). For the same 100 measurements, the cyclic variation in pressure showed a standard deviation of only 0.58 %, which translated (assuming adiabatic conditions) to a standard deviation in the calculated temperature of only 0.13%. Since the residual gases from the previous cycle, including blow-by gases, are never known exactly, the actual error in calculated temperature may be significantly larger. Nevertheless, the use of motored engines by researchers such as Leppard (1985, 1987, 1989, 1990, 1992) and Green et al. (1987) has been invaluable to create better understanding of the impact of low and intermediate temperature chemistry on autoignition and knock.

2.4 Engine Model

In order to convert ignition delay data for a specific fuel molecule from either a RCM, a shock tube or any other experimental source to its octane numbers, it is essential to transform this data (which should have been measured over the same temperature and pressure ranges that are relevant in the CFR engine) by application of an appropriate thermodynamic engine model. The feasibility of such a predictive model of the CFR engine that captures the essence of the interaction between the fuel autoignition characteristics and the engine operating features, has been explored by Swarts in his PhD thesis (Swarts, 2006).

Although the specific details of the successful engine model of the CFR engine that was developed by Swarts fall outside the scope of this thesis, he described it as follows:

"To explore the basis for such a predictive model (of the CFR engine), a two-zone thermodynamic engine model was developed and utilised to predict the pressures and temperatures in the CFR engine under knocking and non-knocking combustion. The model considers the normal combustion heat release and calculates, in addition, the autoignition development for five autoignition elements in the endgas. Each of the elements was assumed to contain one fifth of the unreacted mass at any time during

the calculation and each underwent a unique temperature history due to different polytropic coefficients (due in turn to the application of the heat loss gradient). The autoignition development was monitored by applying the ignition delay model used throughout the study. When autoignition occurred in any one of the elements, there was an instantaneous reaction from the unburnt, end-gas state to the equilibrium burnt gas state. The reaction was however limited to the mass contained in the element reaching the point of autoignition. By the application of an overall energy and mass balance, compression heating of the remaining elements was achieved, leading to the acceleration of the reactions in the remaining autoignition elements." Swarts (2006), used with his permission.

There seems to be opposing views in literature regarding the necessity of transforming ignition delay data from measurements such as RCM data, before direct correlation with octane numbers are possible. Griffiths et al. (1997) found that there was little basis for the use of ignition delays obtained in the Leeds RCM, as a quantitative basis for the comparison of ON values. In contrast, Bradley and Head (2006), asserted that for RON and MON measurements, the underlying, principal combustion parameter is the ignition delay time for the mixture, described as a function of the temporal profile of temperature and pressure. An elaborate procedure is also described to transform the measured ignition delays into CFR engine relevant octane numbers (Bradley and Head, 2006).

A highly appropriate metaphor for octane measurements is offered by Bradley. He writes: *"The octane number measure of autoignition is a somewhat indirect one. It is as if the speed of a vehicle were to be measured by the weight carried by a standardized race horse and jockey that achieved a matching speed."* (Bradley and Head, 2006).

This metaphor serves to put the current study into context, and it goes some way in explaining why this research question is still relevant today.

Chapter 3 : Investigation of Autoignition by means of Chemical Kinetic Modelling

3.1 Introduction

Commercial gasoline fuels are complex mixtures of several hundreds of different types of fuel molecules, predominantly consisting of hydrocarbons in the C_4 to C_{13} range (Ghosh et al., 2006). The constituents of full boiling range gasoline, irrespective of whether it is from synthetic origin or petroleum derived from crude oil, consist of several different classes of molecules, including branched and straight-chain paraffins, alkenes (olefins), cyclic paraffins (naphthenes), aromatics and oxygenates.

The octane number of a fuel (regardless of whether it is represented by the RON or the MON), is an indication of its anti-knock quality, or stated differently, its resistance against the occurrence of knock when that fuel is used in an engine.

Knock is now universally accepted to be a consequence of autoignition in the unburnt end-gas ahead of the propagating spark-ignited flame front (Miller and Fisk, 1987, Heywood, 1988). This has the implication that the problem of octane prediction becomes dependent on one's ability to accurately predict the ignition delay of the unburnt end-gas, as one of the critical inputs, in conjunction with a physically and thermodynamically accurate engine model. Therefore the autoignition characteristics of each of the approximately seven to nine hundred types of molecules that are constituents of a typical automotive gasoline become required information, specifically their ignition characteristics in the temperature / pressure domain to which the end-gas in an engine is exposed. In this thesis the concepts of engine knock and autoignition are considered to be directly correlated.

In practice this data is only available for very few of the constituent molecules that are present in commercial gasoline blends. Furthermore, in order to predict the intricate blending interactions that occur in real gasolines among all the constituent

molecules, detailed information regarding the blending interaction of different molecules is required. In most instances, the necessary data is not available, except for binary blends of the Primary Reference Fuels, which define the octane scale.

3.2 Detailed chemical kinetic mechanisms

As mentioned earlier in Section 2.2.1.2, Westbrook's group at LLNL have performed extensive development and validation of detailed reaction mechanisms for the oxidation of PRF molecules over the last two decades (Curran et al., 1998; Curran et al., 2002). They have shown that the high temperature ignition can be adequately described by 9 elementary classes of reactions, e.g. unimolecular fuel decomposition, H atom abstraction to form an alkyl radical, alkyl radical decomposition, oxygen addition to the alkyl radical, radical isomerization, etc. The low and intermediate temperature mechanism is significantly more complex and a further 16 classes of elementary reactions are needed, starting with the addition of molecular oxygen to an alkyl radical: $R\bullet + O_2 \leftrightarrow RO_2\bullet$ followed by internal H atom abstraction, a second addition of O_2, another H atom abstraction and subsequent decomposition of the ketohydroperoxide species to yield 2 reactive hydroxyl radicals and a carbonyl radical. This sequence, producing 3 radicals from one fuel radical, is responsible for the low temperature chain-branching process (Westbrook, 2000).

Typical examples of the ignition delay information that is obtained from shock tube experiments (as those from Ciezki and Adomeit, 1993) are shown in Figure 3.1. These results indicate the principal features of the cool flame ignition delay region on the upper right, the intermediate region of negative temperature coefficient (NTC) behaviour and the high temperature ignition region in the lower left hand corner.

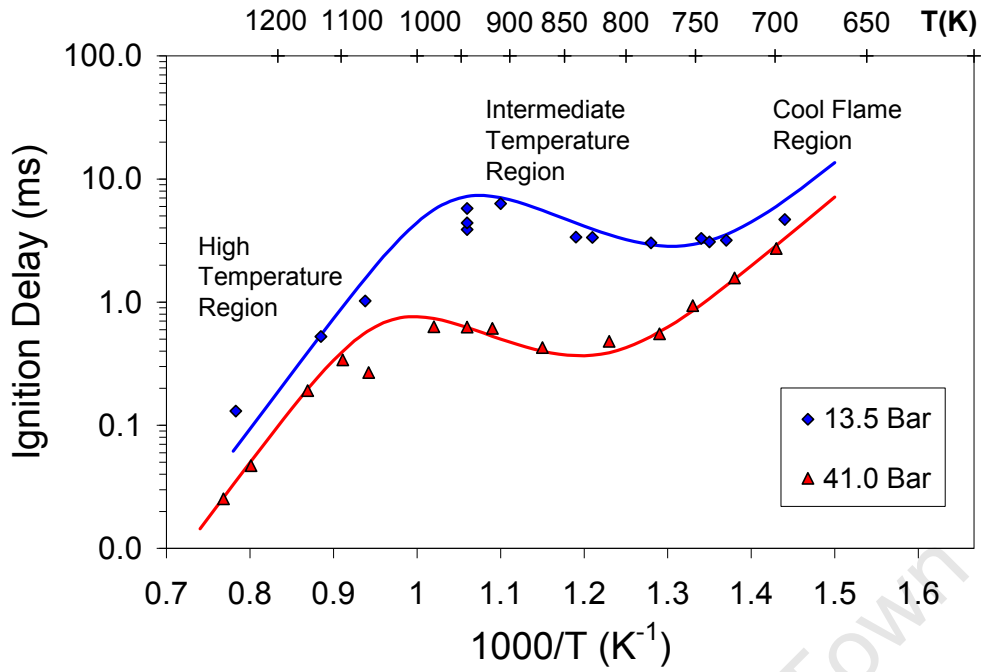

Figure 3.1: The typical ignition delay versus reciprocal temperature profiles of shock-tube data from Ciezki and Adomeit (1993) for n-heptane at Φ = 1

The NTC region for n-heptane at 13.5 bar, which is visible in Figure 3.1 from approximately 780 K to 900 K (shown on the top x-axis), is the temperature range where an increase in temperature (going from right to left) leads to an *increase* in ignition delay. This leads to the characteristic S-shaped curves in the Arrhenius plots for all hydrocarbon fuels that exhibit two-stage autoignition behaviour, as shown in Figure 3.1 for n-heptane. It is also clearly shown in this figure that the NTC region shifts to higher temperatures as the pressure increases from 13.5 bar to 41 bar, with the expected overall reduction in ignition delay (ID) across the whole ID curve at the higher pressure. The best-fit lines shown in Figure 3.1 were calculated by application of the so-called "Three-Arrhenius" ignition delay expression as developed by Yates et al. (2004):

$$\tau_{overall} = \left\{ \left(\tau_1 + \tau_2 \right)^{-1} + \left(\tau_3 \right)^{-1} \right\}^{-1} \qquad ..(3.1)$$

The least squares regression coefficients for n-heptane in this representation are given in Appendix B. From Figure 3.1 it is evident that the empirical three-Arrhenius description fits the experimental data adequately, however, the following sections

deal with the development of detailed kinetic models with which to describe the experimental data from Figure 3.1.

3.2.1 Selection of model fuel molecules

To model a commercial gasoline in terms of the mechanisms described above, it was necessary to select model fuel compounds, each representing the class of molecules to which it belongs. For example, the olefin 1-hexene would represent all olefins present in the gasoline, iso-octane would represent all iso-paraffins, toluene would represent all aromatics, and so forth. The following gasoline molecules were selected, based mainly on the availability of detailed chemical kinetic mechanisms for them, as these are prerequisites for the detailed chemical modelling of their ignition delays.

- n-Heptane (long chain n-paraffin)
- n-Butane (short chain n-paraffin)
- iso-Octane (iso-paraffin)
- 1-Hexene (olefin)
- Toluene (aromatic)
- Ethanol (alcohol)

Although many workers have developed various detailed kinetic mechanisms for the PRFs, perhaps the two leading groups of Westbrook and others at LLNL and Battin-Leclerc and co-workers at Nancy have expended the most effort in the validation of their oxidation mechanisms against experimental data from various sources. Although appropriate experimental data are generally still limited, Westbrook et al. (1996) have extensively validated their comprehensive mechanism for iso-octane against jet-stirred reactors, flow reactors, shock tubes and a motored engine (Curran et al., 2002). The mechanism was based on their low temperature mechanism previously developed for n-heptane (Curran et al., 1998). Therefore, for this study the complete PRF mechanism, containing 1034 species in 4238 reactions, was used unaltered from the form in which it had been supplied to us by William Pitz. He also kindly supplied a copy of LLNL's thermodynamic data file that contains data for all 1034 species included in the mechanism (Curran et al., 2002).

The detailed mechanism for 1-hexene had been developed in the group of Battin-Leclerc at Nancy by Sylvian Touchard. It consists of 1329 different species taking

part in 5471 reactions, and it is the largest mechanism that could still be practically used on a high end personal computer (with 4 Giga Byte RAM) during the course of this study. It was used unmodified from the version that was kindly supplied to us by Dr Battin-Leclerc (Touchard et al., 2004).

The detailed kinetic mechanism for toluene was used exactly as it was published by Djurisic, consisting of 93 species taking part in 617 reactions (Djurisic, 1999).

The comprehensive mechanism for ethanol was developed by Marinov, and consists of 57 different species in 383 reactions (Marinov, 1999).

Finally, the n-butane mechanism used in this study is from Battin-Leclerc's group (as generated by Warth through application of EXGAS, a code that automatically creates the detailed reaction mechanisms), consisting of 166 species in 797 reactions (Warth et al., 1998).

One of the complications of using different mechanisms from different origins, is the inconsistencies that were observed in the naming of species, for example. This meant that the same molecule or radical in the LLNL mechanism, for example, has a different name (or formula) in Nancy's mechanism, very often it also has significantly different thermodynamic data coefficients, leading to different rate coefficients for the same reaction in both mechanisms. This confounds the merging of different mechanisms into a single, internally consistent mechanism. An initial, unsuccessful attempt in this study to merge the toluene mechanism from Klotz (1998) with the Nancy PRF mechanism was abandoned.

3.2.2 Detailed chemical kinetic modelling methodology

The Chemkin Collection (Version 3.7) software, which has been used for all numerical simulations in this study, is a powerful software system for solving complex chemical kinetics problems. It was developed originally for gas phase combustion problems (Kee et al., 1989) and the Chemkin input data format has become the *de facto* standard in combustion modeling for describing all the chemical reactions, their rate parameters and the thermodynamic and transport properties of species (Simmie, 2003).

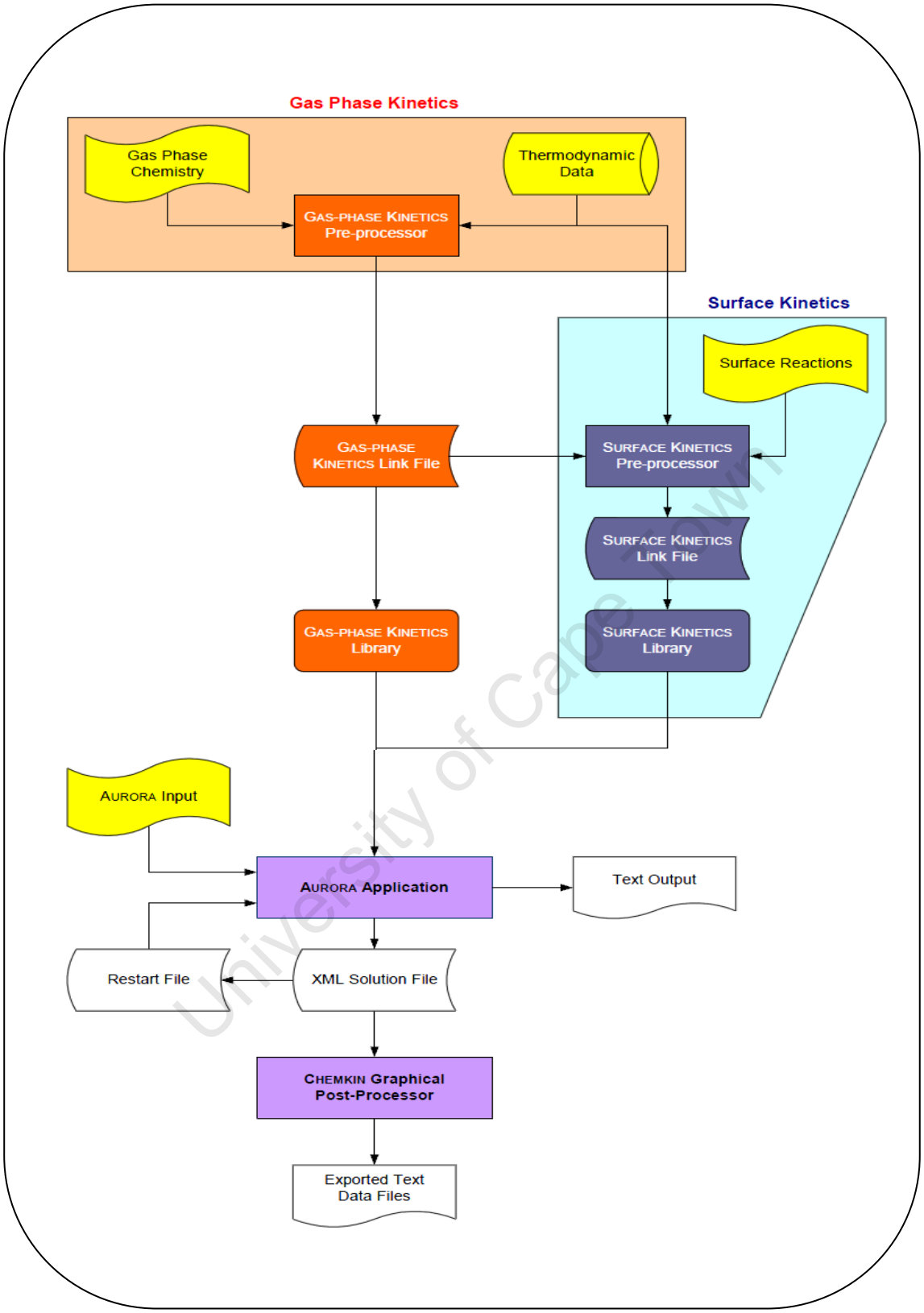

Figure 3.2: Schematic of the structure of Chemkin and its link to an application code, Aurora, adapted from Reaction Design, Chemkin Collection, Release 3.7, 2002

Chemkin is a highly structured package that requires the manipulation of a number of programs, FORTRAN subroutines, and data files. Figure 3.2 shows a schematic

diagram of the general structure of the Chemkin package for the Aurora module. It is composed of five main parts; the Interpreter, the Thermodynamic Database, the Linking File, the Gas-Phase Subroutine Library and the Physical Simulation model's application code. The well mixed reactor model (PSR – perfectly stirred reactor) in the Aurora application code was used for all the simulations carried out during this work. Even though Figure 3.2 shows that the Aurora module makes provision for surface reactions, this functionality was not used in this study, as all autoignition simulations were performed for gaseous systems that were assumed to be completely homogeneous (Kee et al. 2002).

3.2.2.1 Constant Volume Simulations

The physical model that was selected for the majority of simulations was that of a constant volume, closed adiabatic system, containing the fuel molecules and a stoichiometric amount of air in a perfectly mixed homogeneous system. This was considered to be a reasonable representation of a constant volume combustion bomb, shock tube or Rapid Compression Machine (RCM) for ignition delay calculations using detailed kinetic mechanisms (Maroteaux and Noel, 2006). Both the initial temperature (in Kelvin, K) and the starting pressure (in atmospheres, atm) of the system were specified. Thereafter the computer code solved the coupled conservation equations of energy, mass and those for each chemical species. The heat release due to the oxidation reactions leads to an increase in the temperature of the system, until the degenerate branching reactions and resultant exponential growth of the pool of free radicals causes the temperature runaway associated with autoignition. An example of a typical input file for a constant volume simulation is shown in Appendix A.

The time that had elapsed until a temperature threshold of 1400 K was reached, was reported as the ignition delay (in milliseconds). In all cases the temperature was shown to rise exponentially at this point, indicating the high temperature ignition event. Any threshold temperature between 1200 K and 1800 K could have been used, without significantly impacting the value of the ignition delay data that were generated by these calculations.

3.2.2.2 Simulations using CFR engine traces as input

Apart from the constant volume closed adiabatic model that was used in all the simulations thus far, a further set of simulations were performed on selected PRF blends that had been tested experimentally in a single-cylinder, instrumented CFR engine at their respective critical compression ratios. Full details of the experimental procedure are provided elsewhere by Swarts et al. (2005). The digitized pressure trace that was recorded in the CFR engine, was input to the Chemkin model and was used to constrain the model. Since the pressure-time profile is given as input to Chemkin as part of the model input file, the temperature of the adiabatic system is constrained. It consists of the heat of compression, the heat of combustion of the charge plus the heat release generated by the low - and intermediate temperature oxidation reactions taking place in the end-gas. It is implicitly assumed in the model, however, that the mass of the end-gas is so small compared to the total mass in the system that its increase in temperature does not lead to a further increase in the pressure of the macroscopic system.

The oxidation mechanism from LLNL, (Curran et al., 2002) was used for the PRF simulations, since earlier simulations using the Nancy PRF mechanism had shown that ignition delay times predicted by their mechanism were approximately 10% too slow (when compared to the LLNL mechanism in the same physical system).

3.2.3 Results

The ignition delays were computed for each of the model fuel molecules, for an initial system temperature ranging from 600 K to 1200 K, and at two pressures; 12 atm and 40 atm, respectively. These pressures were chosen as they span the typical pressures to which the end-gas may be exposed in a running CFR engine, regardless of whether it is determining RON or MON. Only in limited cases, further simulations at a middle pressure of 25 atm, were also performed.

3.2.3.1 Iso-octane

In Figure 3.3, the resultant ignition delay profiles for iso-octane at three pressures (including 25 atm) are shown. Unless stated otherwise, all the calculations were performed for a system of stoichiometric mass ratios between the fuel and air, such that the Equivalence Ratio (Φ) =1.

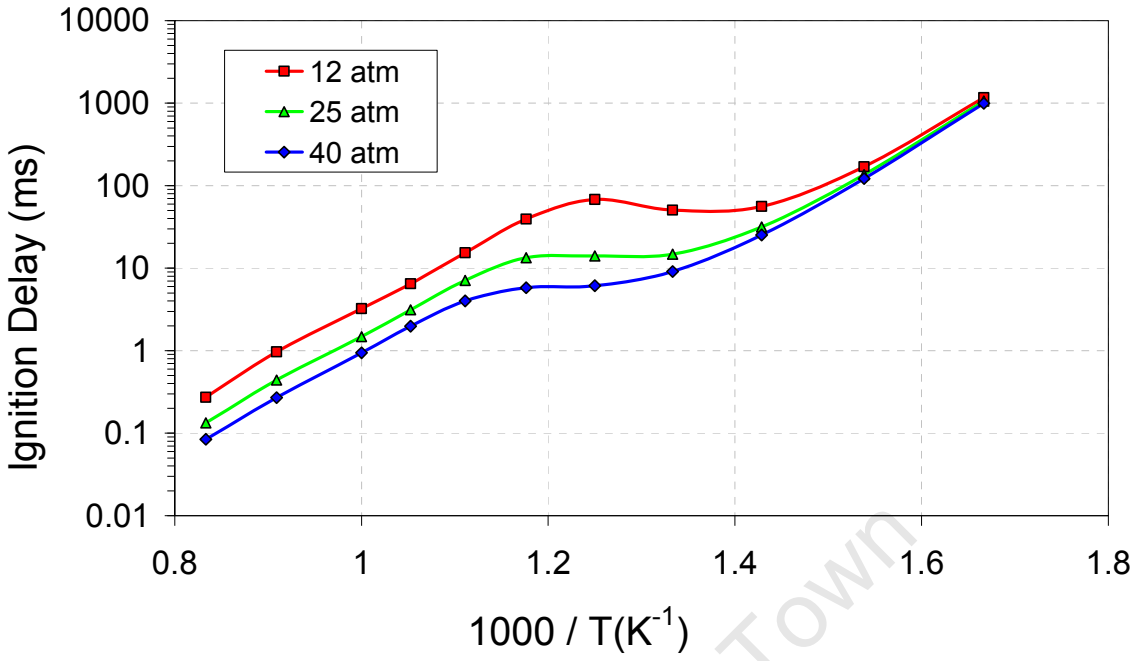

Figure 3.3: Ignition Delay versus reciprocal of initial temperature for iso-octane, as computed by Chemkin Aurora software at three pressures by means of the mechanism of Curran et al. (2002). Stoichiometric mass ratios were assumed for air and iso-octane (Φ=1)

The same ignition delay data for iso-octane, shown in Figure 3.3, when not plotted on a log scale and the temperature axis not in the familiar reciprocal Arrhenius format, is shown in Figure 3.4. Here the NTC behaviour is only clearly visible at the lowest pressure of 12 atmospheres, in the temperature range from about 730 K to 800 K. This type of representation is used by many researchers in the autoignition field, especially for experimental RCM data (Griffiths et al., 1997, Vanhove et al., 2006).

It is clear that the data format shown in Figure 3.4 does not present the data well, nor does it distinguish adequately between the different pressures on a linear time scale. Thus only the log(ID) vs. reciprocal T format (as in traditional Arrhenius-type plots) have been used to display ignition delay data in the rest of this thesis.

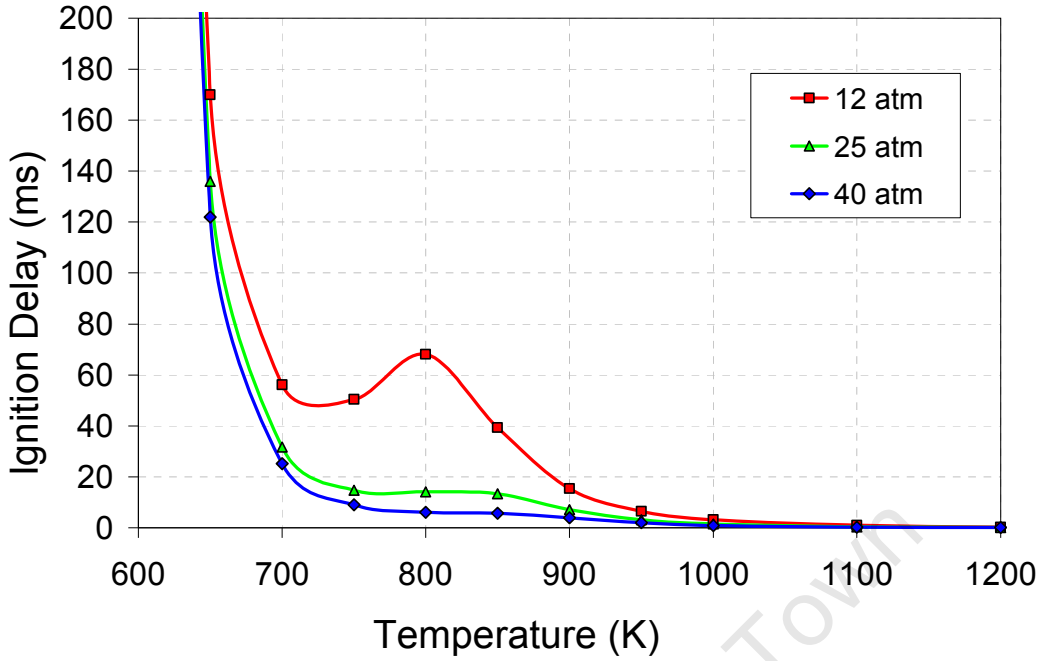

Figure 3.4: Ignition Delay (ms) versus initial temperature for iso-octane, as computed by Chemkin Aurora module at the three different simulation pressures

The predictions were compared to experimental data from the literature, and to data that was generated in an IQT™ device. The IQT™ is a constant volume combustion bomb that can be used for ignition delay determinations, specifically for diesel fuels, according to ASTM Method D6890. The experimental procedure and the limitations of this method have been discussed comprehensively in a previous paper by Yates et al. (2004). Comparisons of the ignition delays measured with the IQT™ for some of the gasoline molecules, versus the numerically predicted ignition delays, are shown in Figures 3.5, 3.8 and 3.10.

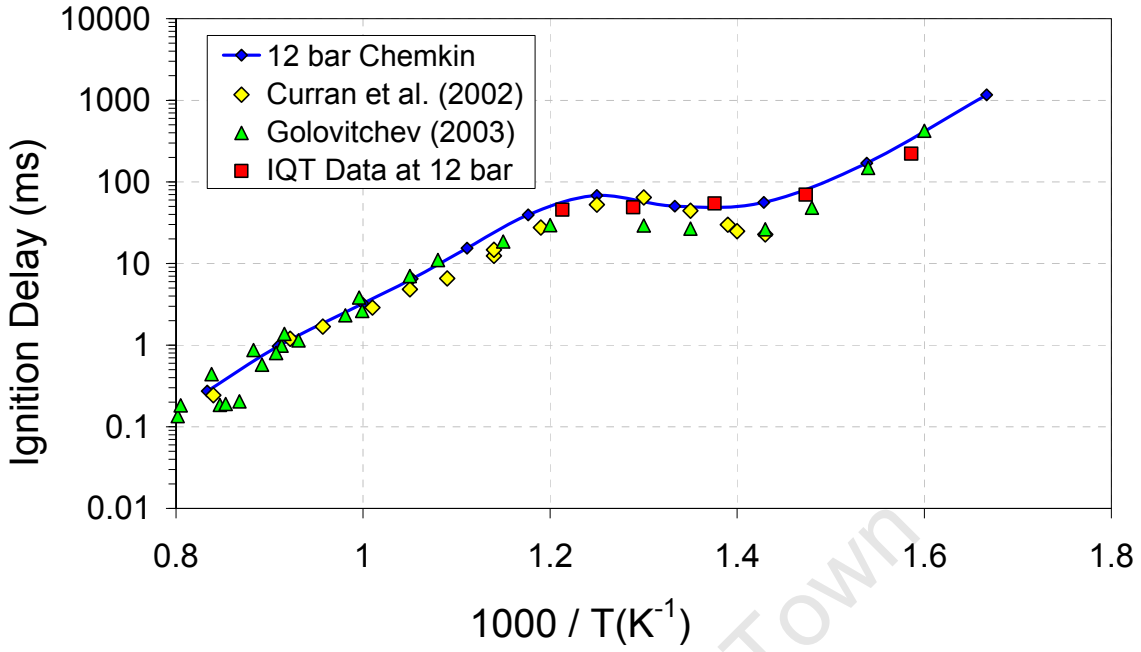

Figure 3.5: Comparison of the Chemkin prediction for ignition delay of iso-octane at 12 bar with literature data (Curran et al. (2002); Golovitchev and Ogink (2003)) (also transformed to 12 bar) and experimental data from this study obtained in the IQT™

3.2.3.2. n-Heptane

The paraffinic PRF molecules (which define the Octane Scale in practice) exhibit autoignition behaviour that are strongly pressure dependent, as indicated by the Chemkin simulations for iso-octane (Figure 3.3) and for n-heptane, shown in Figure 3.6. The effect of pressure is more pronounced for n-heptane, as well as the magnitude of the NTC behaviour, which forms a deeper trough as exemplified in Figure 3.6 when compared to Figure 3.3. The same comparison also shows the much shorter ignition delay for the NTC zone of n-heptane compared to that of iso-octane, both at stoichiometric conditions, indicating the greater reactivity that n-heptane display towards oxidation in comparison to iso-octane.

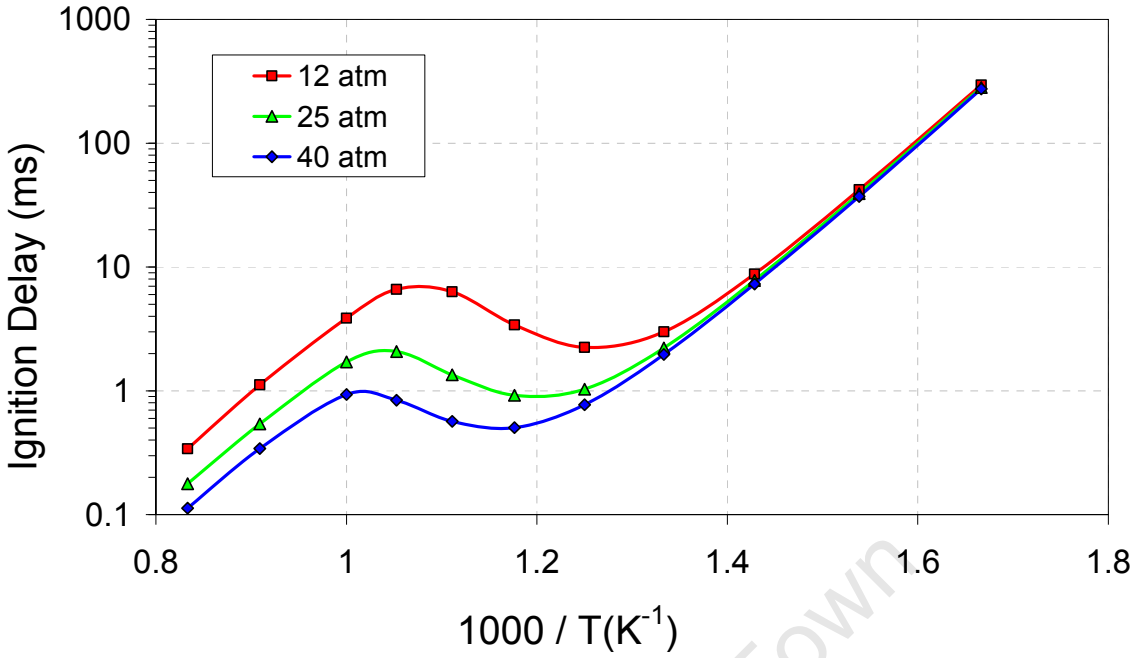

Figure 3.6: The Chemkin simulation of the ignition delay of n-heptane at three different pressures, using the PRF mechanism of Curran et al. (2002) for stoichiometric air/fuel mixtures

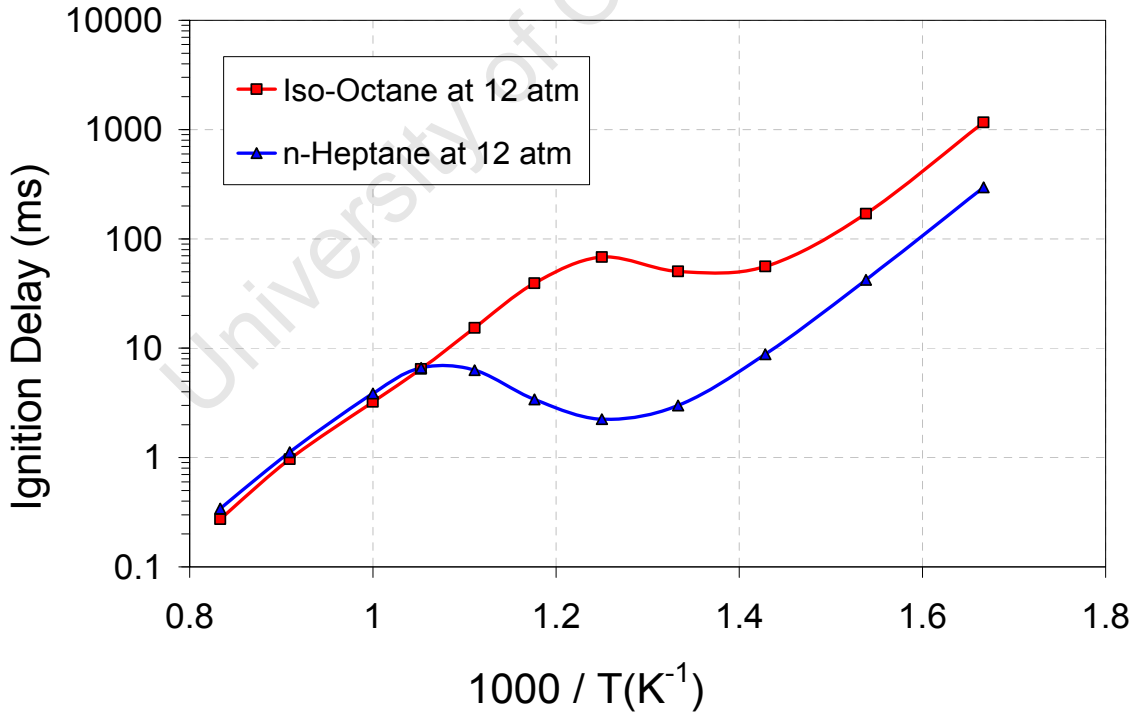

Figure 3.7: The Chemkin simulation of the ignition delay of n-heptane and iso-octane at 12 atm, using the PRF mechanism of Curran et al. (2002) for stoichiometric air/fuel mixtures

In Figure 3.7 a direct comparison of the predicted ignition delay curves at 12 atm of n-heptane and iso-octane are shown, clearly indicating the low temperature kinetics of n-heptane to be significantly more reactive than for iso-octane. At high temperatures, the kinetics of both molecules are similar, although the simulations indicate a crossover point at ~950 K. This has been observed before by previous studies in the pyrolytic regime (>1000 K), where for example Brezinsky and Dryer (1987) observed iso-octane to pyrolize at greater rates than either n-octane or n-heptane did. Similar conclusions were reached by Glaude et al. (2002), when they compared the oxidation pathways and rates of the two molecules at 1080 K.

In order to compare experimental ignition delay data obtained from literature sources with the values predicted by detailed kinetic models in the current work, it was necessary to normalise the data to a common pressure (12 bar, for example). This was done with due consideration of the pressure dependency of the original data, through a convenient technique as described by Yates et al. (2005). The basic concept of this transformation to a chosen pressure is indicated by the following relationship: $\tau_{p2}\big|_{Corrected} = \frac{\tau_{p2}}{\tau_{p1}}\Big|_{Calculated} \cdot \frac{\tau_{p1}}{1}\Big|_{Measured}$ (Swarts, 2006).

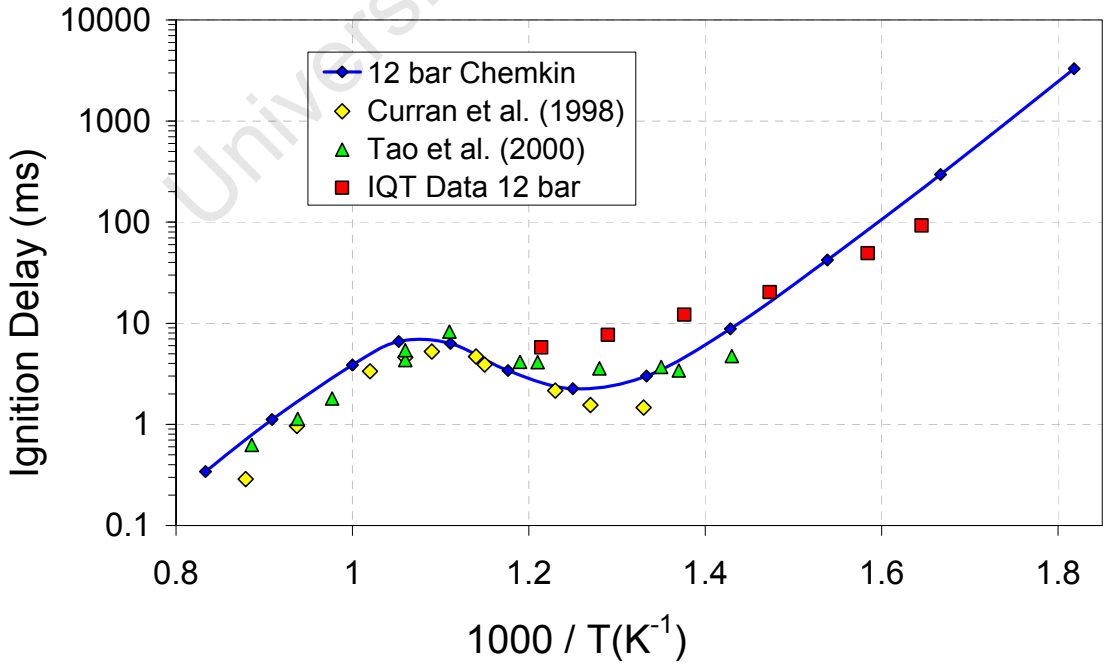

Figure 3.8: Comparison of the Chemkin prediction for ignition delay of n-heptane at 12 bar with literature data (Tao et al., 2000; Curran et al., 1998) (also transformed to 12 bar) and experimental data obtained in this study from the IQT™

The experimental IQT^{TM} data in Figure 3.8 shows that the heterogeneous nature of the IQT's charge has the effect of masking the NTC region. Furthermore, the non-stoichiometric conditions prevalent inside the combustion bomb would result in deviations from the assumptions of stoichiometry and perfectly mixed constant volume combustion that were intrinsic to the mathematical simulations. When Figure 3.5 (iso-octane) is compared with Figure 3.8 (n-heptane), however, it is interesting to note the relatively good fit which is obtained between ignition delays measured for iso-octane in the IQT^{TM} with the Chemkin predictions for iso-octane at 12 bar. These relatively long ignition delays would have allowed time for conditions in the IQT^{TM} to become more homogeneous (by complete evaporation of the fuel spray) and representative of constant volume, perfectly stirred reactor (PSR) combustion.

3.2.3.3 1-Hexene

The Chemkin predictions for the ignition delays of 1-hexene at two different pressures are shown in Figure 3.9. It is interesting to note that significant NTC character is indicated for 1-hexene, although less pronounced than that of n-heptane as shown in Figure 3.6. The position (on the temperature scale) of the ignition delays in the NTC region for 1-hexene are also more comparable to n-heptane than to iso-octane, probably due to the presence of a linear chain of secondary carbon atoms in 1-hexene, similar to those in the carbon chain structure of a n-paraffin. This similarity of 1-hexene to n-heptane is further substantiated by DFT calculations, shown in Chapter 4 (see Figure 4.10 and Table 4.1).

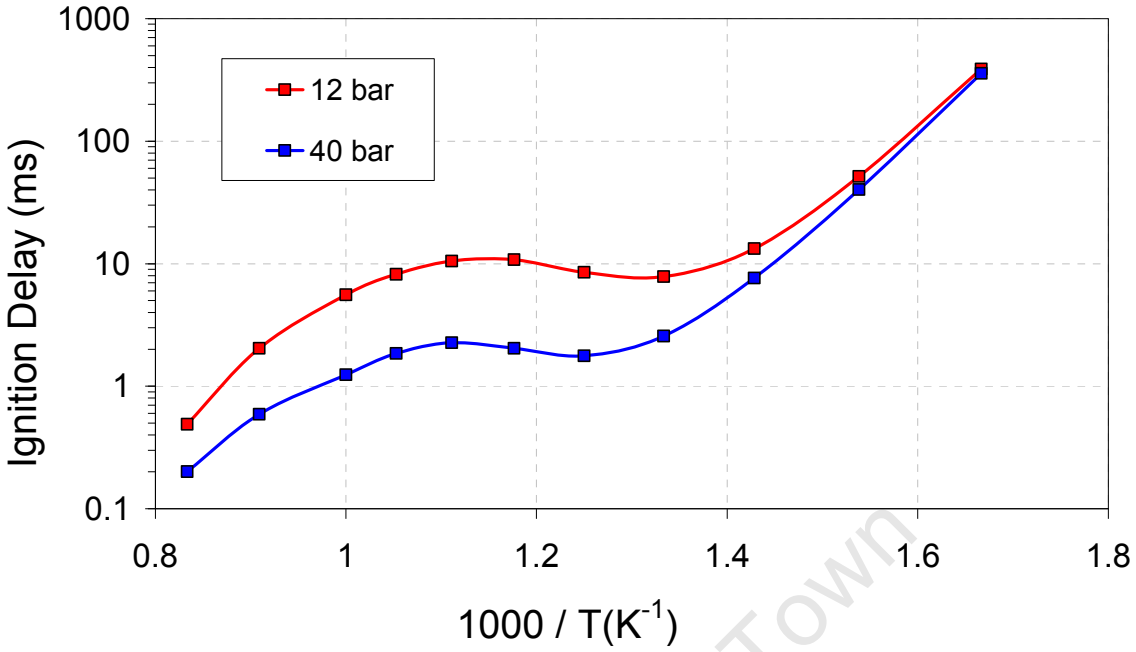

Figure 3.9: Predicted ignition delay diagram for 1-Hexene, based on the mechanism of Touchard et al. (2005), for Φ=1

Since no ignition delay data for 1-hexene, other than RCM data from Vanhove et al. (2005), was available in the literature, the Chemkin prediction at 12 bar was compared to IQT^{TM} data that was determined in this instrument as part of this study. These are shown in Figure 3.10, below. Since the RCM data was obtained at an initial temperature (at end of compression) of 725 K and 9.4 bar, the data shown was transformed to a pressure of 12 bar.

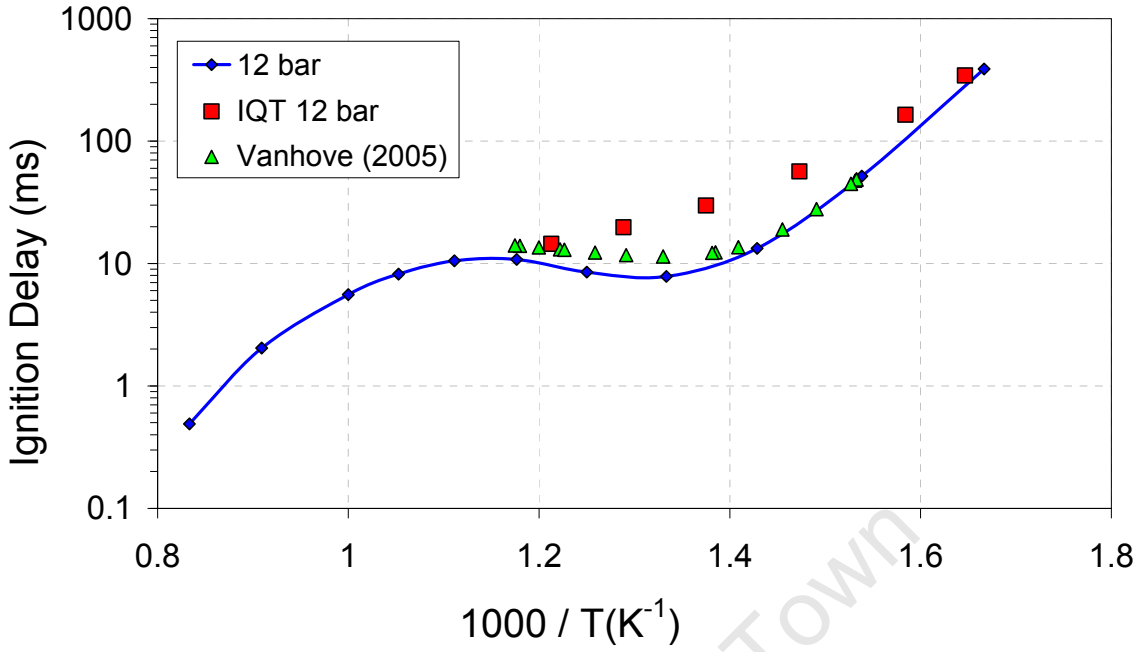

Figure 3.10: Comparison of experimental RCM data from Vanhove (2005) for 1-hexene, data from the IQT^{TM} determined at 12 bar during this study, and Chemkin predictions

As is the case with n-heptane (see Figure 3.8), the NTC behaviour of 1-hexene is masked to a large extent by the shortcomings caused by the IQT's deviation from stoichiometric homogeneity. With this instrument, no access is possible to the high temperature region, as the maximum operating temperature of the bomb that can be reached safely is approximately 595 °C. Thus the IQT^{TM} instrument cannot provide information regarding the curvature expected in the region of transition between the low-intermediate temperature and high temperature oxidation mechanisms. Although it has been shown by Yates et al. (2007) to be entirely possible to make corrections to the IQT^{TM} data in order to account for the effects of localized variation in equivalence ratio, Φ, the IQT^{TM} data shown in this thesis have not been corrected in this manner. The ignition delay data is represented here unmodified, exactly as measured by the IQT^{TM} instrument, even though it is acknowledged that these were not taken at strictly controlled stoichiometric air / fuel ratios. Thus the precise values of Φ at the loci of ignition centers in the combustion bomb are not known. Overall, the instrument measures under lean conditions (e.g. for pure n-heptane, the calculation based on the mass of fuel being injected per mass of air, indicates Φ = 0.653), as it had been designed for cetane number measurements of diesel fuels, but the points

where ignition occurs first are expected to be close to stoichiometric (Yates et al., 2007).

3.2.3.4 Toluene

In complete agreement with the literature, which often states that toluene did not autoignite under their experimental conditions (for example, Roubaud et al., 2000), the Chemkin predictions for the ignition delay of toluene according to the mechanism developed by Djurisic (1999) indicate the very high temperatures needed to effect autoignition. These simulations were done for stoichiometric conditions, Φ=1. Low- and intermediate temperature oxidation chemistry is absent, as can be seen in Figure 3.11. In contrast to paraffinic molecules, the single-stage ignition behaviour can be described perfectly by a single Arrhenius equation.

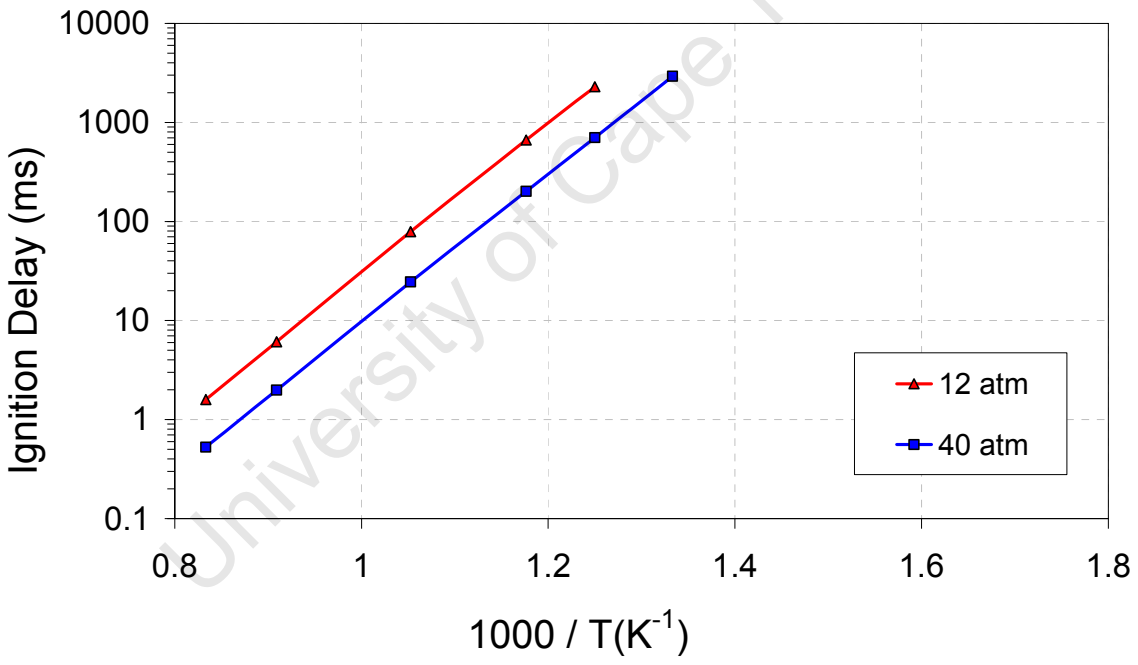

Figure 3.11: Toluene autoignition prediction by the Djurisic (1999) mechanism (at Φ=1), showing the absence of low temperature oxidation chemistry

The predicted ignition delay data for toluene at 12 bar was compared to experimental data taken from the literature (Golovitchev and Ogink, 2003), as is shown in Figure 3.12. Under these conditions of relatively low pressure (the standard operating pressure for the IQT^{TM} in conformance to ASTM D6890 is 21.4 bar), toluene did not ignite at all in the IQT^{TM}, due to its high intrinsic resistance towards autoignition. Unfortunately, safety considerations limit the maximum operating charge pressure in

the IQT™ to less than 22.0 bar. This explains the absence of own experimental data in Figure 3.12. The experimental data from Golovitchev and Ogink (2003) had to be transformed from 15 bar to 12 bar, using the pressure correction procedure mentioned earlier (Yates et al., 2005).

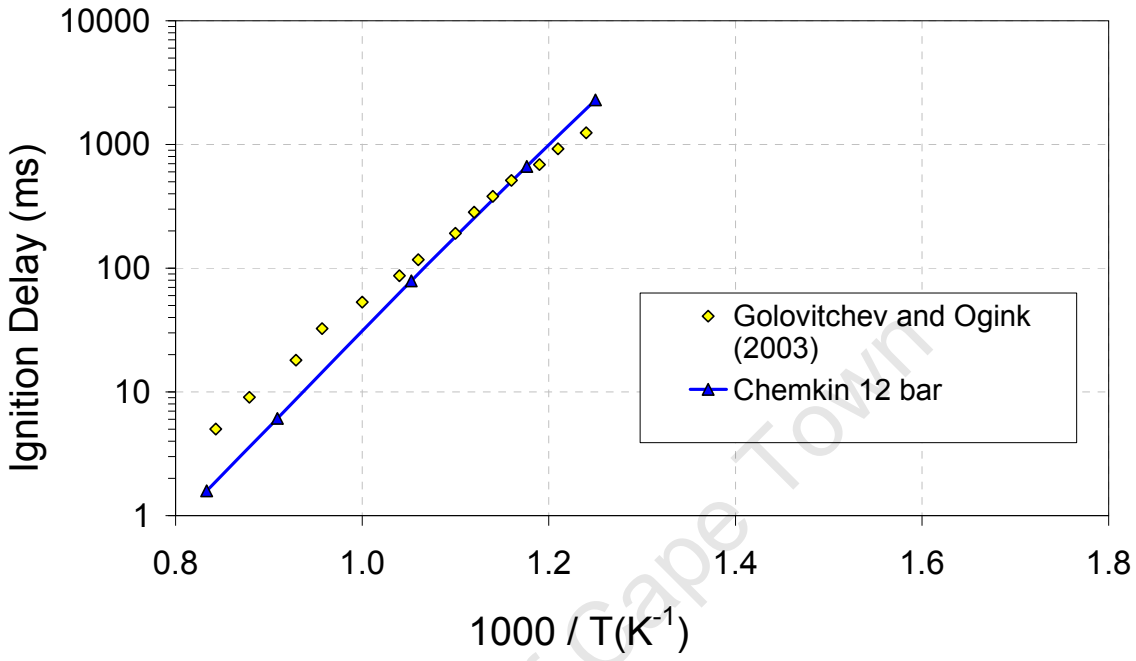

Figure 3.12: Modelled ignition delays for toluene compared to experimental data (adjusted to 12 bar) taken from Golovitchev and Ogink (2003)

3.2.3.5 Ethanol

Ethanol was selected as an example of an oxygenate molecule that is commonly found in gasoline compositions. It was selected as being representative of all alcohols occurring in commercial gasolines. This is probably an appropriate choice if actual concentrations of various alcohols in commercial fuels are considered. The ignition delay profiles at two different pressures, as predicted by means of the Marinov mechanism for ethanol (Marinov, 1999), are shown below in Figure 3.13.

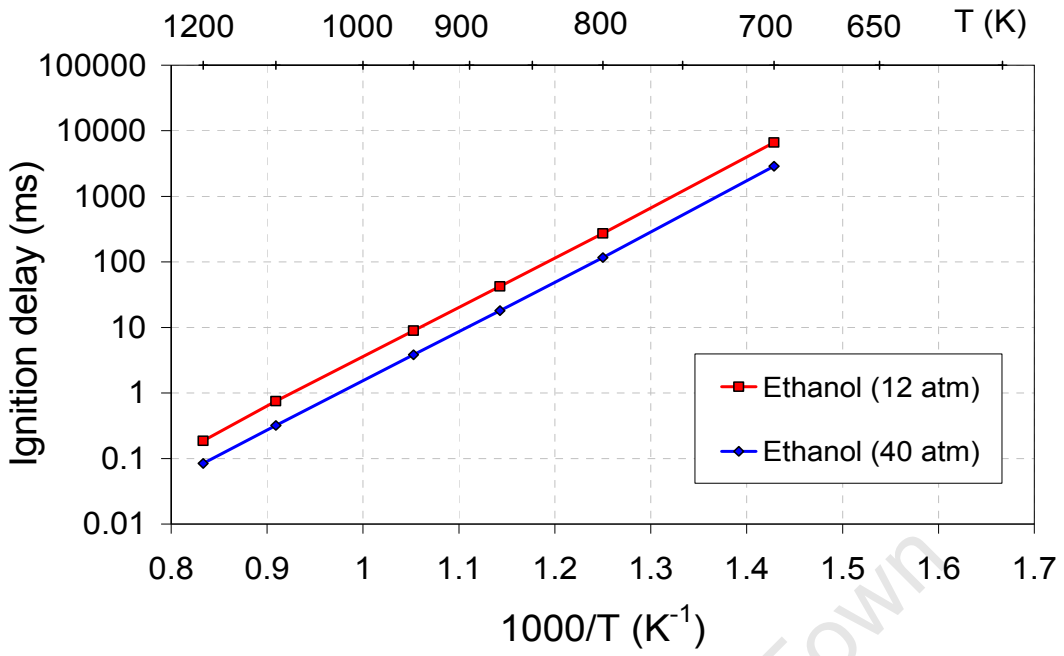

Figure 3.13: Ethanol exhibits only high temperature oxidation chemistry according to the Marinov (1999) mechanism

Similarly to toluene, ethanol exhibits only high temperature (single-stage) oxidation chemistry, shown by the linear ignition delay profiles in both Figures 3.13 and 3.14.

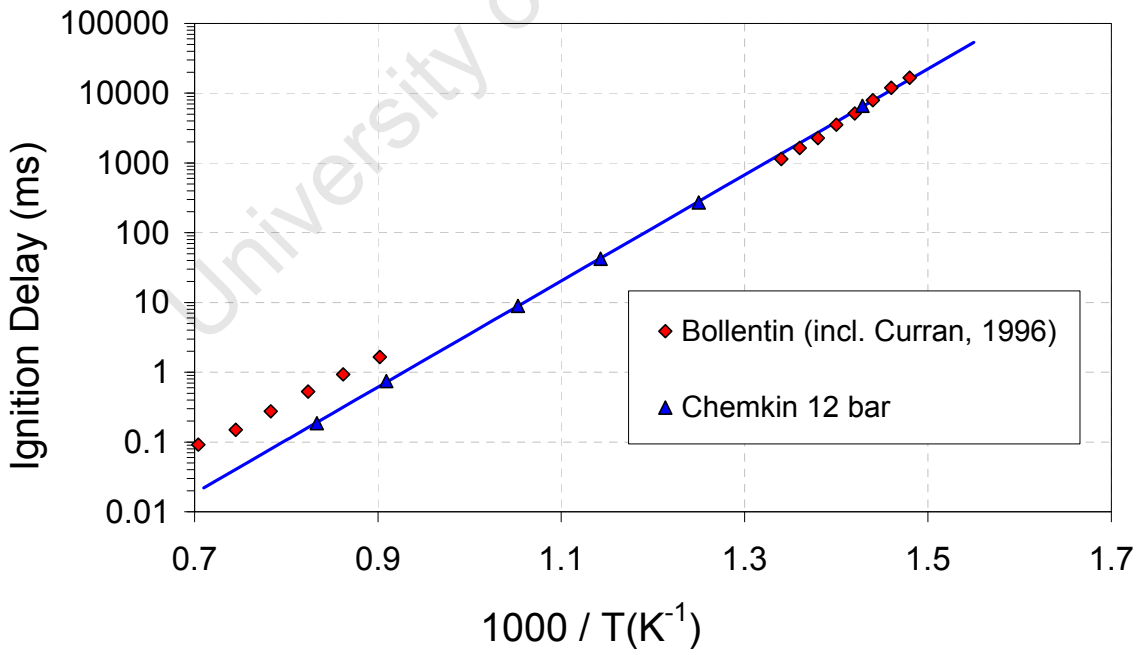

Figure 3.14: Ethanol compared to experimental ignition delay values from literature (after adjustment to 12 bar) (Bollentin, 1996)

A comparison of the ethanol autoignition profile, as generated with Chemkin according to the Marinov (1999) mechanism at 12 bar, with literature data from

Bollentin et al. (1996) is shown in Figure 3.14. Bollentin has included data from Curran et al. at higher temperatures, which is also shown in Figure 3.14 (the lower left experimental points). Although it is clear that the slopes of the different data sets are not absolutely the same, fair agreement is observed overall between predicted and measured ignition delays.

3.2.3.6 n-Butane

Finally, the autoignition profiles for n-butane are depicted in Figure 3.15. It is noteworthy that n-butane exhibits a pronounced NTC region according to the Nancy mechanism (Warth et al., 1998). This mechanism was generated semi-automatically by application of the EXGAS computer program that had been developed and validated at CNRS in the 1990's.

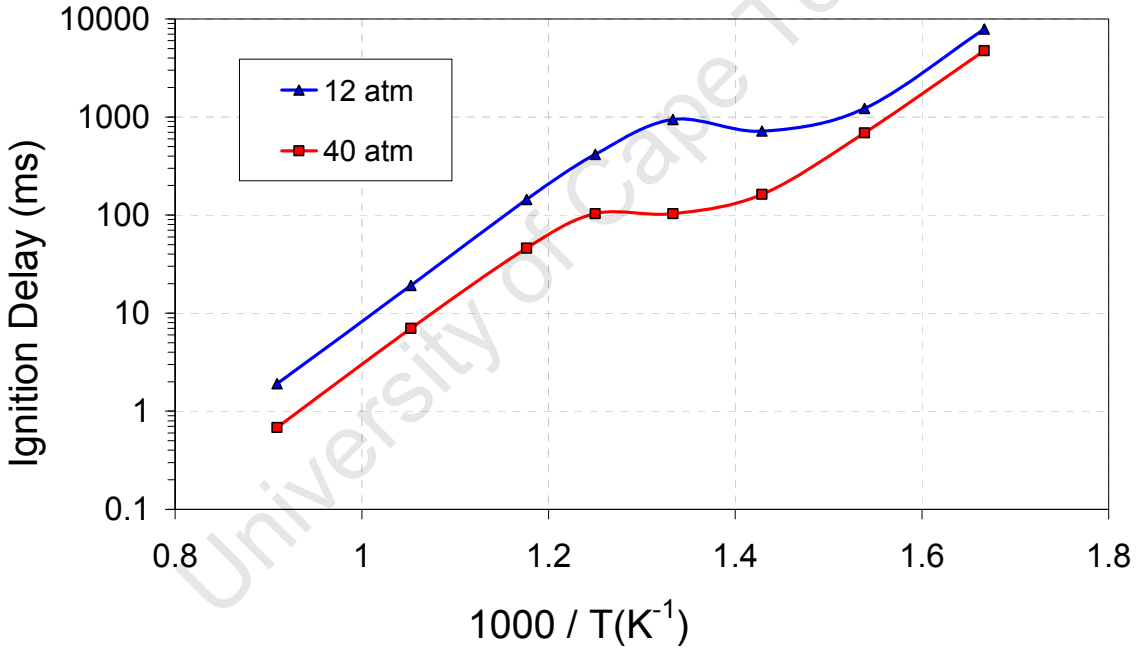

Figure 3.15: n-Butane ignition delays according to the computer-generated mechanism of Warth et al. (1998)

The transition from low temperature oxidation mechanism to high temperature chemistry occurs at a relatively low temperature (~750 K) compared to the other molecules that have been evaluated. This means that in the temperature and pressure domain of relevance to an engine, n-butane essentially exposes only its single stage (high temperature) ignition character. This is in accordance to deductions made by Yates et al. (2005), but contrary to earlier observations in motored engines made by Pitz et al.(1988), and Leppard (1987).

3.2.3.7 Modelling of PRF blends

The Chemkin simulations of PRF blends were also performed at pressures of 12 atm and 40 atm. The peak compression pressures occurring in a CFR octane engine fall between these limits for most octane determinations of commercial gasoline blends. The ignition delay profiles for the range of PRFs at 40 atm are shown in Figure 3.16.

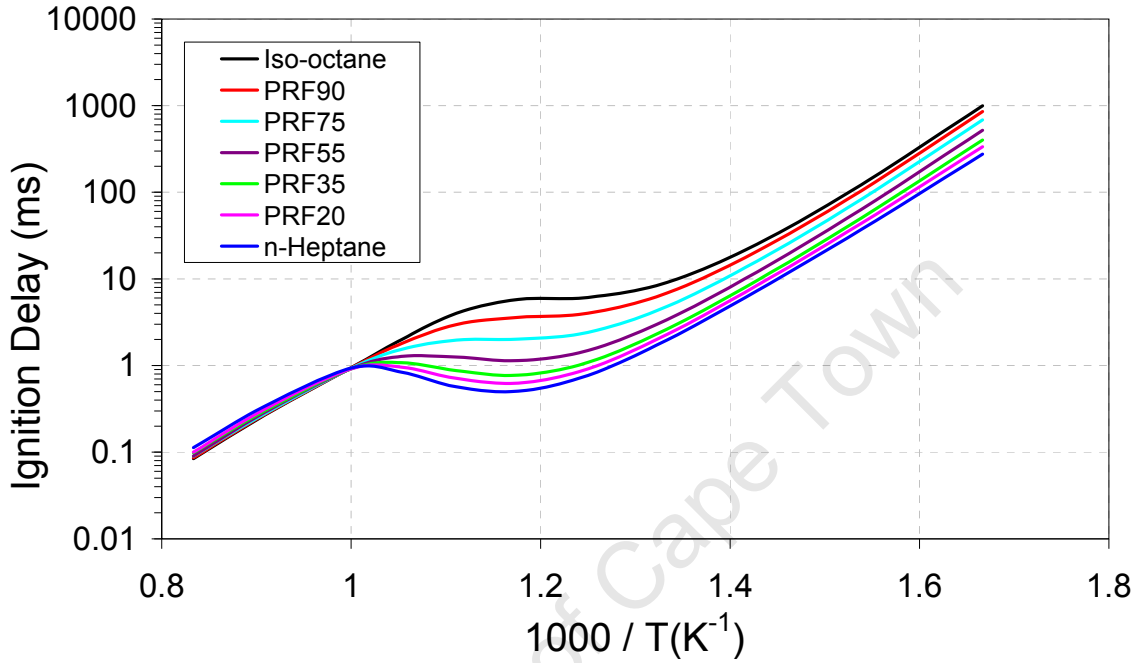

Figure 3.16: Chemkin simulation of ignition delay diagrams for a range of PRFs at 40 atm, indicating that the major difference between them is in their low temperature chemistry

Figure 3.16 indicates that the major difference between PRFs is in their low temperature oxidation chemistry, which is accentuated in the NTC region of the different blends shown on the graph. Ignition delays of the blends do not blend linearly with the blend ratio of their constituents. For example, the effect of the n-heptane in a blend is enhanced in terms of the reduction in ignition delay it contributes to the PRF blend, far more that the volumetric proportion of n-heptane in the blend. This aspect has been associated by Glaude et al. (2002) with the relative preference of n-heptane to form ethene and reactive ethyl radicals near the end of its oxidation sequence (i.e. at higher temperatures), compared to the less reactive methyl radicals and iso-butene formed by iso-octane. At the lower initial temperatures (e.g. ~650 K), the high reactivity of n-heptane compared to iso-octane is explained largely by the relative difference in the amounts and production rates of peroxide species (Glaude et al., 2002).

3.2.3.8 Pressure-constrained simulations of PRFs

For these simulations, the closed system was assumed to be homogeneous, with a fuel : air equivalence ratio of 1 (stoichiometric, see Equation 2.3), but the volume was left unconstrained. The initial temperature (440 K) of this system was chosen to be equal to the expected in-cylinder temperature at Inlet Valve Closure (IVC). The pressure profile recorded in the CFR engine, started at -146 Crank Angle Degrees (CAD), and this is also the point of IVC (Swarts, 2006). Therefore in all these RON engine simulations, -146 CAD corresponded to time zero, and Top Dead Centre (TDC) corresponded to a constant 40.556 ms. (The CFR engine runs at a constant 600 rpm during RON testing).

Thus this model represented the last unit mass element of end-gas, being pressurised by the moving piston and by the approaching flame front. When the exponential production of free radical species led to the autoignition event, the volume of this element (having a very small unit mass in comparison to the total mass of burnt gases behind the flame front) expands explosively into the oncoming flame front. An example of the Chemkin output obtained for a PRF 90 under knocking conditions, at standard knock intensity (SKI), is shown in Figure 3.17, below.

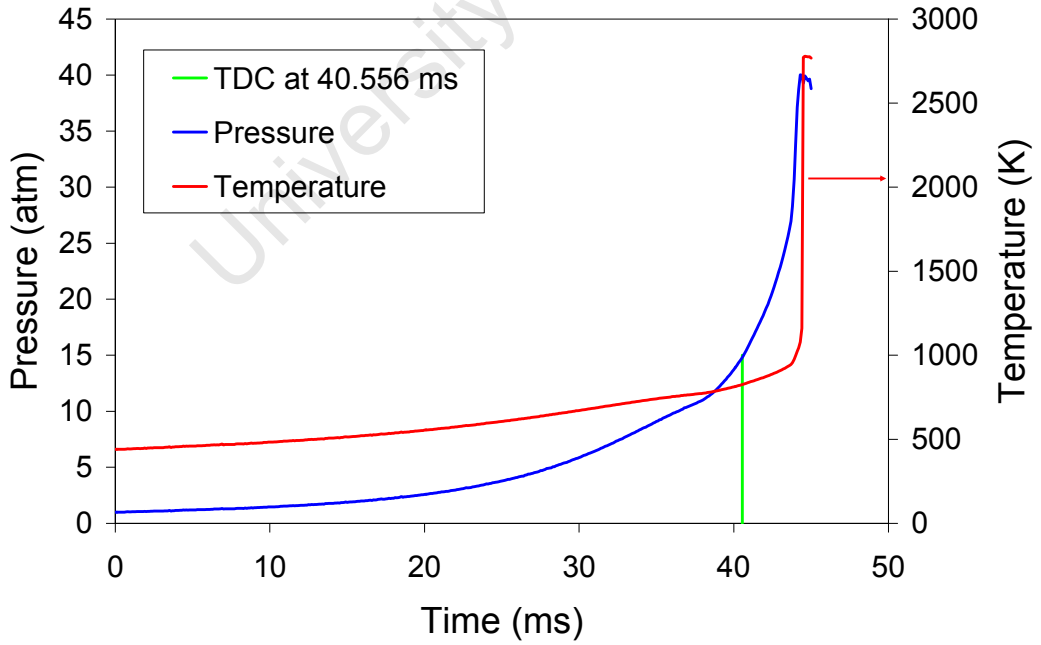

Figure 3.17: End-gas simulation of PRF 90 under knocking conditions, from an engine pressure trace recorded in a CFR engine at 600 rpm. TDC occurred at 40.556 ms and T_{init} was taken as 440 K. Time 0 is at -146 CAD (at IVC)

The equivalence ratio Φ, was taken as 1.0 in the simulation. The system was assumed to be homogeneous and adiabatic, with no heat loss taking place from the adiabatic end-gas core.

From the temperature trace shown in Figure 3.17, it is clear that the Chemkin simulation of the PRF 90 end-gas by means of detailed kinetics for PRFs is in good agreement with the engine experiment. The autoignition event is predicted to occur at essentially the same time step at which the peak pressure (40.03 atm) is reached when the initial temperature (440 K in the simulation) is aligned to the best estimate of the temperature in the engine cylinder at IVC. It is acknowledged, however, that the rapid increase in pressure at the knock point that is contained in the engine pressure profile, also serves to activate the simulated system into reaching a corresponding point of autoignition.

Considerable attention was given in all the different simulations to the predicted H_2O_2 concentration profiles, as it is believed that the final autoignition event in engines is always induced by the dissociation of the accumulated H_2O_2 species. As Westbrook (2000) states: *"The key is that H_2O_2 decomposes rapidly at temperatures of 900 – 1000K, so this temperature can be considered as a critical value in systems where the temperature approaches this value from lower temperatures. H_2O_2 is produced at lower temperatures by low and intermediate temperature kinetic pathways, until the decomposition temperature is reached, when the system suddenly produces large numbers of ·OH radicals and rapidly ignites. The most important variable is the time at which they reach this critical temperature. Anything that will accelerate reaching this critical temperature advances its ignition, while delaying it inhibits ignition."*

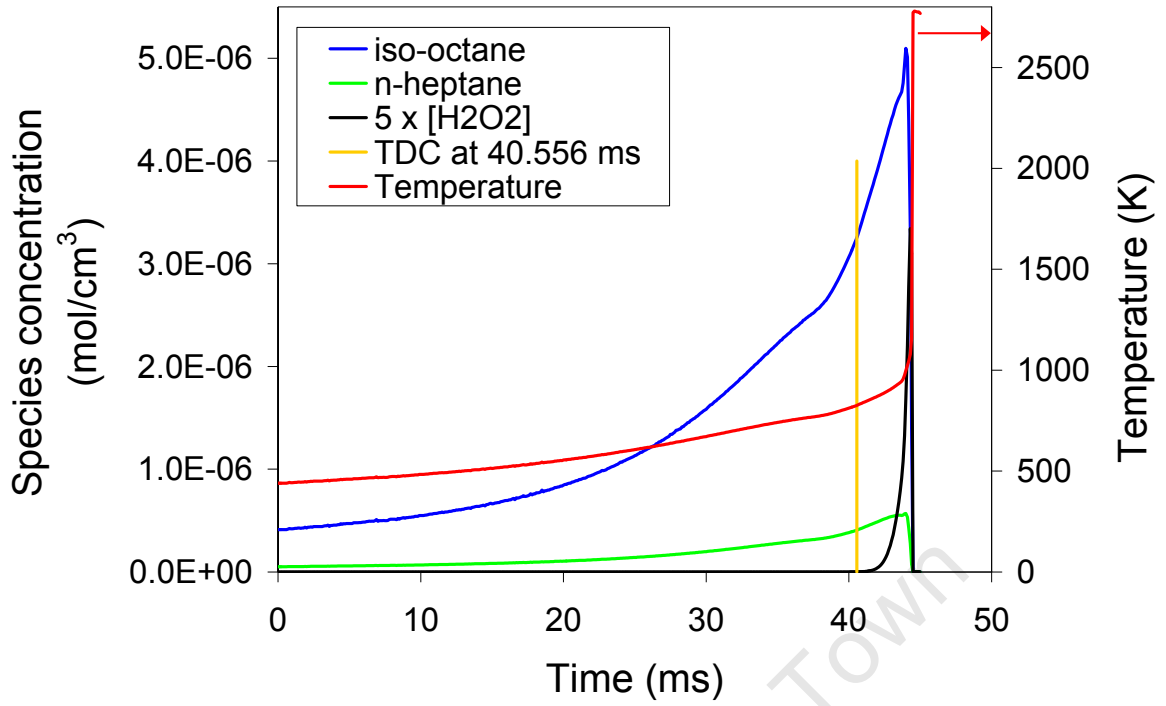

Figure 3.18: Fuel conversion for PRF 90 at knocking conditions (SKI) and Φ=1, showing the H_2O_2 dissociation at knock point (at the point of autoignition)

In Figure 3.18, which shows the H_2O_2 profile in the engine simulation (as already indicated by Figure 3.17), the small build-up of H_2O_2 is visible about 3 ms before the autoignition point, at which time the hydrogen peroxide dissociates to form •OH radicals which react rapidly with all the remaining fuel molecules at the point of ignition. This happens at 44.44 ms, at which point the temperature in the simulation is already at 1160 K, and at the next time step, 44.50 ms, the temperature had rapidly increased to 2772 K. Since the H_2O_2 concentration is much smaller than the fuel concentration, it has been scaled by a factor of 5 to make it more visible in Figure 3.18. The concentration profiles of the fuel molecules show that, since the volume of the end-gas in the model is being reduced by compression, the fuel concentrations prior to the autoignition event is increasing. This is a counter-intuitive result and is an implication of the choice of a pressure-constrained model. Since the mathematical system is thereby forced to follow the pressure profile recorded during one representative engine cycle in the CFR engine, the volume is left unconstrained in the Chemkin simulations, while the temperature is calculated by solving the energy and mass conservation equations at every time step.

Considering that the rates of chemical reactions are not only a function of temperature, but also of the concentration of the reactants, this 'amplification' of the reaction rates by the increase in species concentrations, due to the compression of the end-gas, adds considerable complexity to the problem of linking autoignition delay times to octane numbers in a CFR engine. The implication of this aspect could be that constant volume simulations (such as models of the IQT or a RCM (after completion of the compression stroke)) may not be absolutely appropriate in simulating the end-gas in an engine.

For further clarification, the more familiar way of representing the reactants and intermediates in terms of their mass fractions (or mole fractions, which are identical to the normalized mass fraction speciation), for the same PRF 90 system (at Φ=1), is shown in Figure 3.19.

The speciation traces shown in Figure 3.19 as mass fractions, do display the fuel conversion in a more familiar format, as the fuel and oxygen molecules have essentially constant mass fractions for the first 40 ms of the simulation. The first substantial conversion of fuel only starts after 41 ms, with about 20% of the fuel consumed by the cool flame reactions, very quickly leading to the hot ignition and total conversion of the fuel at approximately 44.5 ms. The volume trace shown in this graph is indicative of the increasing compression of the end-gas, up to the point where there is an almost instantaneous expansion caused by the hot ignition event.

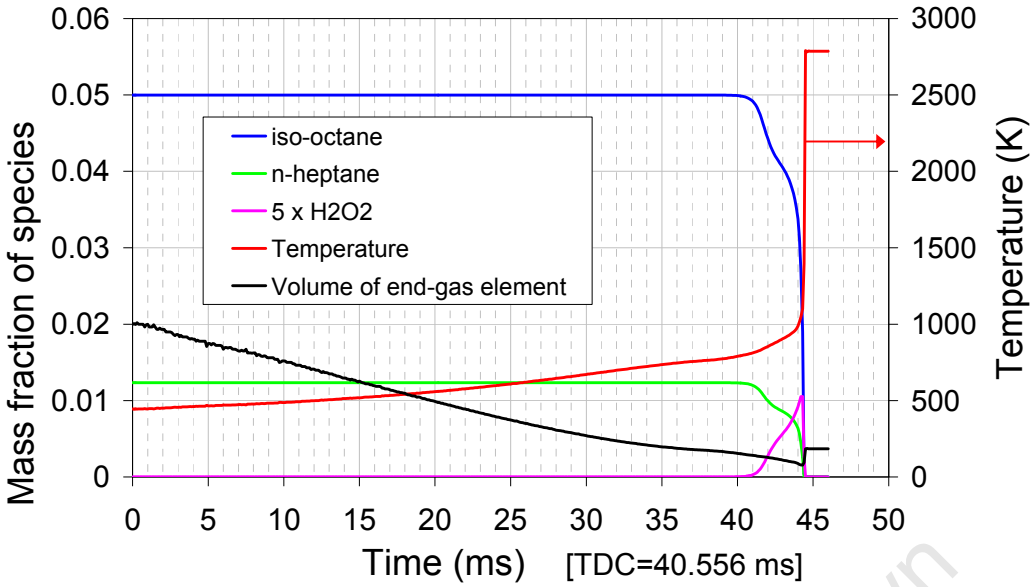

Figure 3.19: Fuel conversion for PRF 90 at knocking conditions (SKI) and Φ=1, showing the mass fractions of fuel and H_2O_2, including the reduction in the volume of the last end-gas mass element

The initial volume, V_{Total}, used in the simulation was arbitrarily set to 1.0 cm^3, so that the volume refers to the Y-axis (mole fraction) in Figure 3.19, where 0.02 is set equal to 1.0 cm^3. This has no significance other than allowing more data simultaneously on the same graph. Since the pressure trace that profiled this simulation was from the CFR engine at standard knock intensity (SKI), this is considered to be a realistic simulation of the mass element of end-gas to autoignite, thereby rapidly expanding into the approaching flame front.

In all of the preceding discussion about the PRF90 in a CFR engine (shown in Figures 3.17 - 3.19), the physical model used for the Chemkin simulation assumed a perfectly mixed system of air and fuel, in a completely homogeneous gas phase, and perfectly adiabatic (i.e. zero heat loss). Since engine traces are not normally available for all the molecules that were studied, the next step was to simulate the end-gas element as a homogeneous, well mixed, adiabatic gaseous system under constant volume conditions. These conditions were considered to be more relevant to the IQT™, and to RCM data that may become available from a new RCM that is being built in our laboratory. Thus the same PRF90 system was modelled in a constant volume system as described above, but the initial temperature was varied to obtain the same ignition delay as before (i.e. the 44.44 ms that was shown in Figure

3.17 and 3.18). The initial pressure was set at 40 atm, which was the same pressure that the pressure constrained system had reached at peak pressure, as shown in Figure 3.17.

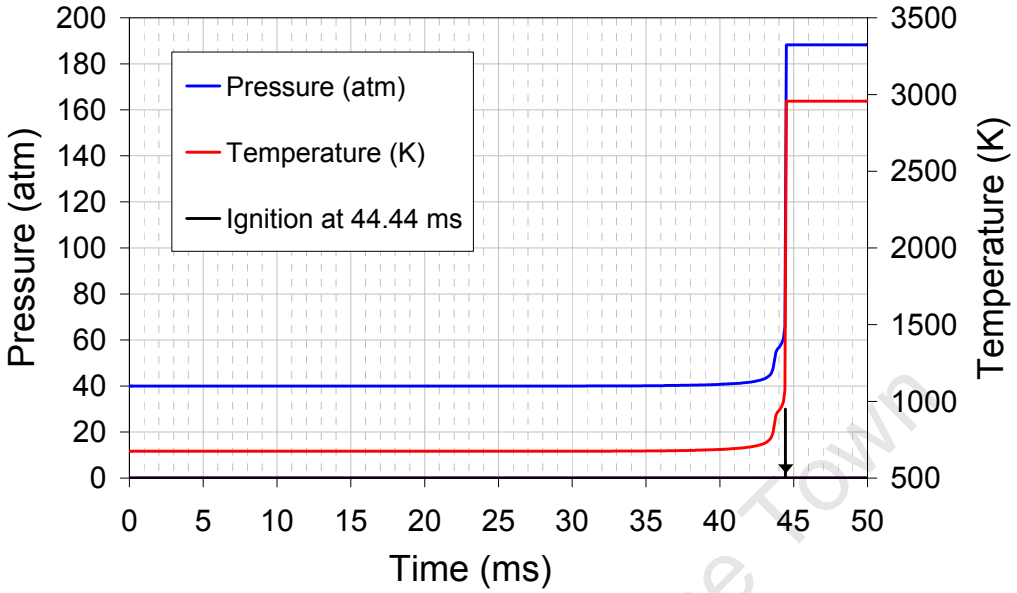

Figure 3.20: PRF 90 in Constant Volume simulation at Φ=1.0, P_{init} =40 atm and T_{init} = 674.5 K. These conditions were chosen to obtain ID at 44.44 ms, the same as in Figures 3.17-3.19. Note the cool flame heat release shown at 43.70 ms, 0.74 ms before the arrow indicating autoignition

The difference in the initial temperature of the constant volume system (T_{init} of 674.5 K) and that of the CFR pressure constrained system shown earlier in Figure 3.17 (T_{init} of 440 K), is an indication of the promoting effect of the heat of compression on the earlier system, coupled to the acceleration in kinetic rates due to the amplification in species concentrations (shown in Figure 3.18). In the constant volume system, thermal feedback is coming only from the chemical heat release, and these rates are almost negligible throughout the first ~40 ms of the system's lifetime. This can be seen by the flat temperature trace shown in Figure 3.20. At the same time, the fuel species concentrations are almost constant (similar to the mole fraction / mass fraction traces shown earlier in Figure 3.19). This is shown by the fuel concentration traces in Figure 3.21, below, which is another representation of the constant volume system described above.

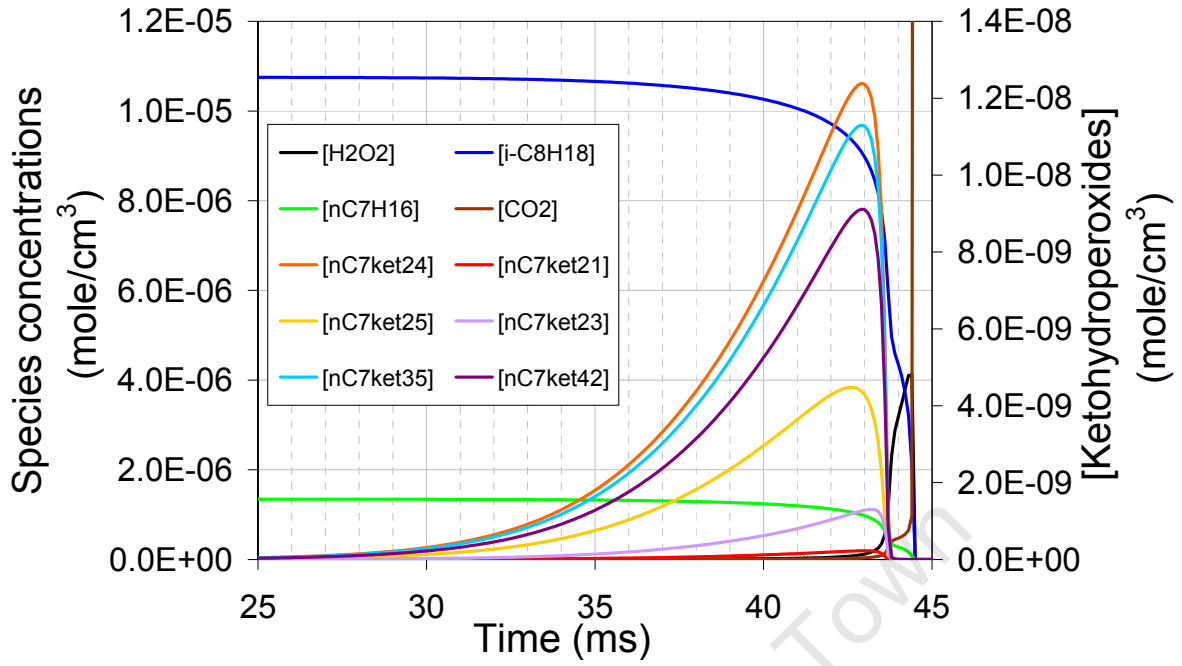

Figure 3.21: Simulation of Constant Volume system, containing PRF 90 at Φ=1, that had the T_{init} adjusted to 674.5 K in order to get ID at 44.44 ms. The initial pressure was set at 40 atm for the homogeneous, adiabatic system

In Figure 3.21, the cool flame heat release (and associated conversion of some iso-octane and n-heptane molecules) can be seen at 43.7 ms, with the hot ignition occurring less than 0.75 ms later at 44.44 ms, also indicated by the rapid increase in CO_2. As pointed out before, the concentration of hydrogen peroxide, $[H_2O_2]$ only becomes significant after the cool flame, and H_2O_2 has a short life time which ends at the point of hot ignition, when it dissociates almost instantaneously.

What is of major significance in Figure 3.21, are the concentration traces of some of the major ketohydroperoxides that form part of the low temperature oxidation sequence of n-heptane, which are depicted on the graph. Although these are about three orders of magnitude lower in concentration than the fuel molecules, it is obvious that they start accumulating about 10 ms before the cool flame ignition, and then rapidly decompose at the point of cool flame heat release. Here they act as branching agents and their dissociation products consist of ketones, aldehydes and at least two •OH radicals. Also of great significance, is the relative importance of the nC7Ket24 ketohydroperoxide versus the nC7Ket21 species. The latter species has been adopted by most researchers in the domain of skeletal or reduced kinetic

mechanisms, as the main ketohydroperoxide that can be used to represent all 16 possible isomers, even though the nC7Ket24 ketohydroperoxide is in reality (see further discussion in Chapter 4) a far better example to use. These two choices are evaluated and compared further by DFT calculations, later in this thesis (in Chapter 4; see Section 4.3.1.4: Critical evaluation and comparison of two postulated oxidation mechanisms for n-heptane).

3.2.3.9 Comparison of hydrogen peroxide profiles in PRFs

All the Chemkin constant volume simulations using the detailed kinetics for PRFs from Curran et al. (2002), were evaluated at one initial pressure (12 atm) in order to investigate the relative behaviour of hydrogen peroxide in these systems.

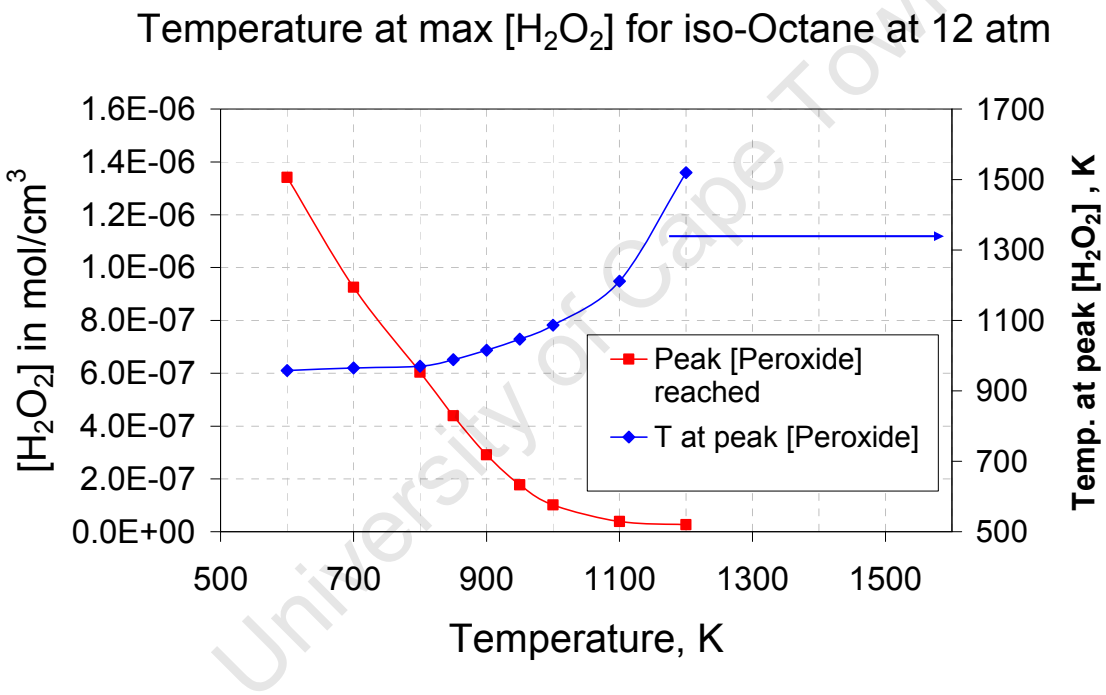

Figure 3.22: Investigation of hydrogen peroxide concentration profiles for all the constant volume simulations for iso-octane at initial pressure of 12 atm

The underlying data used to construct these curves are shown in Appendix C. The red curve in Figure 3.22 shows the maximum concentration of hydrogen peroxide that was reached, leading to the autoignition event. It is clear that this increases with decreasing initial temperature, which also causes a longer time for the accumulation of hydrogen peroxide in the system. The blue curve is an indication of the temperature at which the maximum peak in the concentration of hydrogen peroxide was obtained. These are obtained from the second column of graphs shown in Appendix C, plots of $[H_2O_2]$ vs. temperature.

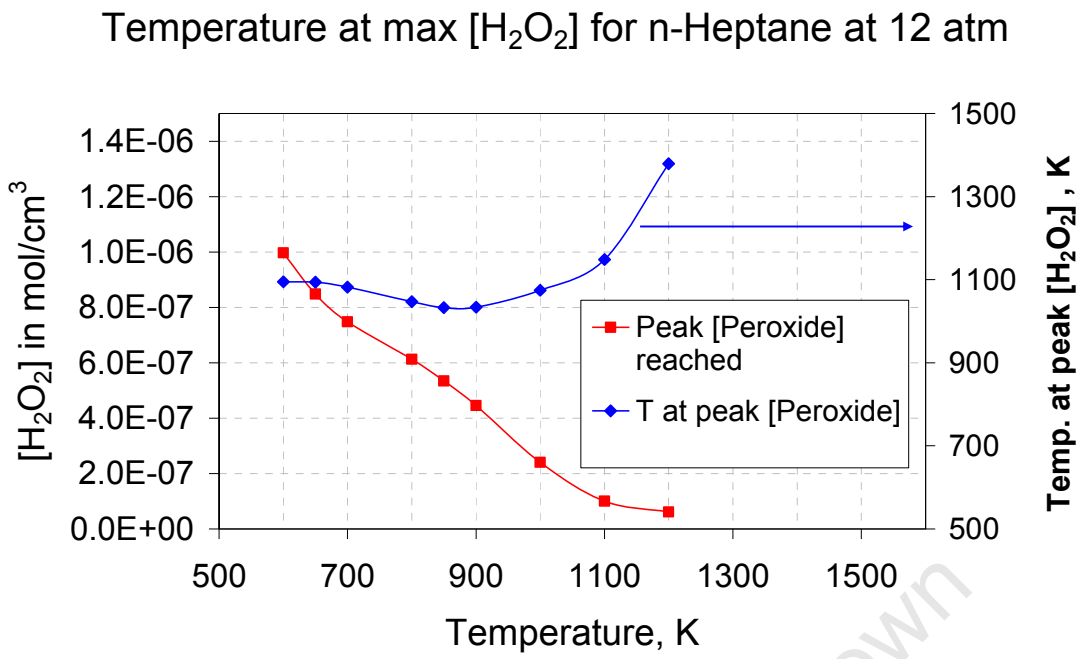

Figure 3.23: Investigation of hydrogen peroxide concentration profiles for all the constant volume simulations for n-heptane at P_{init} of 12 atm

The curves shown in Figures 3.22 and 3.23 were extracted from the Chemkin constant volume simulations using the detailed kinetics for PRFs from Curran et al. (2002). The results show that both the absolute concentration of hydrogen peroxide and the temperature of this species in the specific system are important factors determining the autoignition event. The stronger NTC behaviour of n-heptane is also visible in Figure 3.23, when compared to iso-octane. In general, these profiles seem to give credence to Westbrook's assertion that the dominant factor determining autoignition is the dissociation of H_2O_2 in that system (Westbrook, 2000). However, it is not a "critical temperature", but "temperature change" that is the key, because thermal feedback leading to a dramatic temperature rise is the cause of the escalation of •OH concentration, through chain branching, as a result of the accelerating rate of dissociation of H_2O_2. A comparison between the temperature curves (shown in blue) in the two preceding graphs is informative, as it clearly indicates the lower temperature at which hydrogen peroxide start disappearing from the iso-octane system, versus the same temperature in the n-heptane system, where the peak concentrations of $[H_2O_2]$ occurred at significantly higher temperatures than with iso-octane. Generally, the peak concentrations of $[H_2O_2]$ reached is similar for both iso-octane and n-heptane, only at the higher initial temperatures are larger concentrations prevalent for n-heptane. This would lead to the stronger knocking

expected for n-heptane, or to its enhanced reactivity with respect to autoignition, when compared to iso-octane.

Although it is commonly acknowledged that autoignition in practical systems are always associated with the dissociation of H_2O_2, e.g. by Westbrook (2000) and Griffiths et al. (2005), it is possible that the preceding discussion is not taking due consideration of the reactions preceding and leading up to the formation of H_2O_2. An investigation of the ceiling temperatures for the generic reaction:

$R\bullet + O_2 \leftrightarrow RO_2\bullet$ (Reaction 2 in Figure 2.1)

which may be taking place in either the iso-octane system or in the n-heptane system, has been conducted. The ceiling temperature is defined as the temperature when the ratio of $[RO_2\bullet]/[R\bullet]$ is equal to unity (Cavaliere and De Joannon, 2004). This analysis of the four different radicals for iso-octane and the four different isomers of R• for n-heptane (using the rate coefficients from the Curran et al. (2002) PRF mechanism), also indicated lower ceiling temperatures for iso-octane (in general) than for the n-heptane isomers. This is thought to be due to the steric factors that play a bigger part in the relative instability of the oxygen-added iso-octane radical adducts, compared to the comparable n-heptane radical adducts. Therefore the $RO_2\bullet$ species for iso-octane dissociates at lower temperatures, also consistent with the temperature trends shown in Figures 3.22 and 3.23.

3.2.4 Discussion of the limitations of detailed kinetics

Significant progress has been made over the last 25 years with the development of detailed chemical kinetic mechanisms for autoignition modeling used in various branches of combustion research. The large research emphasis over recent years on HCCI combustion in both gasoline and diesel engine/fuel systems, has contributed to the considerable improvement in the description of the low-to-intermediate temperature oxidation mechanisms that has taken place. The rapid development of cheaper computing power over the same time period, has also enabled accelerated progress in this field, by a large number of research groups around the globe.

Unfortunately, the development of a mechanism that could realistically describe the oxidation of commercial full boiling range gasoline, is still only a futuristic vision.

Various surrogate gasoline mechanisms are in continuous development, but the complexity and size of a “comprehensive” mechanism, severely limit the number of molecules that can be merged into one mechanism. The size of the mechanism (the combination of the number of species and the number of reactions considered in the mechanism) precludes the use of personal computers in cases where more than approximately 3000 species in 7000 reactions are included. This size of mechanism places high demands on computing resources, and results in excessively long run times. Thus the integration of detailed kinetics schemes, comprehensively describing autoignition, with CFD codes modelling real combustion systems, is not yet practically viable.

These types of research applications (especially when the aim is to predict the combustion chemistry in every grid cell, almost in real time) invariably lead to the replacement of the detailed kinetics mechanism with a reduced (or skeletal) kinetic mechanism. The rationale for this has been shown in Figure 2.2 in the preceding chapter (Aceves et al., 2005).

Experimental data is critical for the development of detailed mechanisms, as the mechanisms have to be validated against all available experimental data. These could include speciation studies in jet-stirred reactors, laminar flame speed measurements, shock tube measurements, RCM ignition delays etc., but the benefit is that the validated detailed mechanism should then be applicable to any physical system.

It is important to note, however, that even these well-validated detailed mechanisms are not always accurate when used in a range of pressures or temperatures that falls outside the ranges for which they were validated. An example of this behaviour was encountered when the IQT was recently modified to run at ambient pressures. The experimental results for n-heptane and iso-octane did not match up well with the ignition delays predicted by the Curran et al. (2002) mechanism in Chemkin simulations at constant volume, stoichiometric conditions at 1 bar (Savage, 2009). It may be due to the fact that this mechanism was not validated against any experimental data at pressures of less than 5 bar. On the other hand, the Djurisic mechanism for toluene and the Marinov mechanism for ethanol, both yielded ignition

delay predictions at ambient pressure that were in good agreement with the experimentally measured data for these fuels. This is shown in Figure 3.24, taken from Savage (2009).

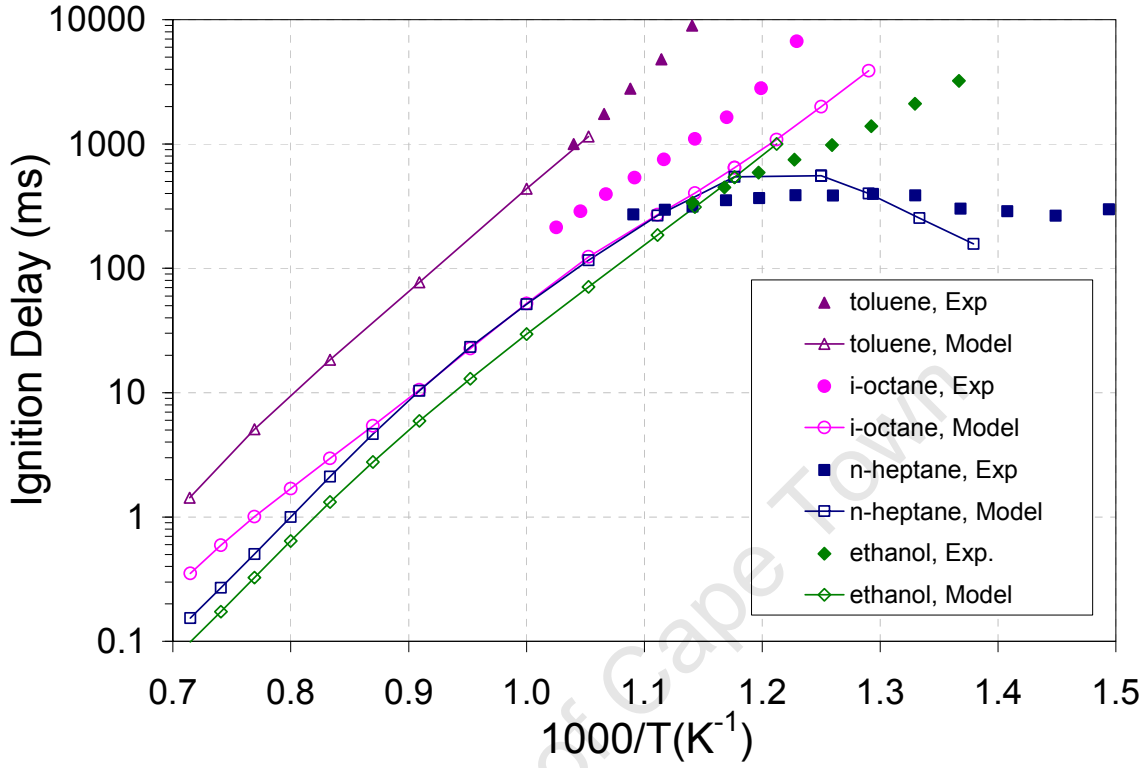

Figure 3.24: Constant volume experimental bomb measurements for the four reference fuels superimposed on the kinetic model simulation results (Savage, 2009)

It was speculated that the absence of NTC behaviour in the n-heptane experimental data could be due to heat loss effects from the cool flame to the vessel walls, but no definitive explanation could be given for the temperature off-set in the iso-octane data. Since the model simulations are assuming adiabatic conditions, it is not surprising that the two fuels with NTC character are impacted more by the actual heat loss and temperature gradient in the physical combustion bomb.

The availability of appropriate experimental data (also for blends of the relevant molecules) is one of the biggest obstacles to the development of accurate detailed kinetic mechanisms. In addition, detailed kinetic mechanisms are dependent on the availability of accurate rate coefficients for each elementary reaction, the pressure dependency of each reaction, as well as the appropriate thermodynamical data for every species that is contained in the mechanism (Dean, 2001). Although much

progress has been made, all this information is not readily available for complex systems that can start approximating commercial fuel mixtures.

3.3 Reduced (or Skeletal) Chemical Kinetics

A second modelling approach with which to describe hydrocarbon combustion, is a reduced (or simplified) kinetic model. The reason for consideration of this approach is firstly that it is far less expensive in terms of computational requirements and opens up the possibility of integrating kinetics calculations “on the fly” inside CFD codes. Furthermore it offers the possibility of the pragmatic deduction of blending rules among different molecules or classes of compounds. It has been shown in literature by Griffiths, (1986; 1993; 1995), Wang et al. (1985), Warnatz (1996), and Griffiths et al. (1992), that autoignition and the NTC region require a kinetic model meeting certain minimum criteria. Thus, in order to have a successful kinetic model, it must possess elements such as:

(i) chemical feedback,
(ii) temperature and concentration dependent, reversible “oxygen addition steps”,
(iii) thermal feedback and correct thermal heat release, and
(iv) conservation of mass.

With these ideas in mind it is possible to develop a kinetic model with the minimum number of reaction steps that will be able to predict the autoignition behaviour of a molecule over a wide range of temperatures and pressures. The “elementary” steps in the model can be linked to the chemical nature of the combustion species, although these are often lumped kinetic species. Such a model aims to retain generic links to the basic chemical steps and thus should be able to better represent the variations in chemical species and mixture rules can be related to chemical differences (Griffiths, 1993; 1995).

3.3.1 The Griffiths Model

Griffiths and co-workers (Schreiber et al., 1994) has developed an excellent simplified chemical kinetic scheme that meets the abovementioned criteria, and thus provides a good starting point for development of reduced kinetic models for single components and multi-components systems. The chemical equations for iso-octane (and n-heptane in brackets) are shown below:

$$
\begin{aligned}
R_1 &\quad F \rightarrow X \\
R_2 &\quad X + 12.5(11)O_2 \rightarrow P \\
R_{3+} &\quad F + 2O_2 \rightarrow I \\
R_{3-} &\quad I \rightarrow F + 2O_2 \\
R_4 &\quad I \rightarrow 2Y \\
R_5 &\quad Y + 0.5F + 11.5(10)O_2 \rightarrow P
\end{aligned}
\qquad ..(3.2)
$$

Where, for iso-octane oxidation:

F represents the feed (i-C_8H_{18})

X represents the intermediates ($3C_2H_4$ + $^{\bullet}CH_2$ + $^{\bullet}CH_3$ + $H^{\bullet}$)

P represents the products ($8CO_2$ + $9H_2O$)

I represents the oxygenated radicals ($O^{\bullet}C_8H_{15}O_2H$ + H_2O)

Y represents the chain-propagation species.

Reactions R_1 and R_2 represent the thermal high temperature ignition while the remainder of the reactions are responsible for the low temperature combustion. Reactions R_{3+}, R_{3-} and R_4 represent the hydroxyperoxide reactions and reactions R_{3+} and R_{3-} represent both the first and second O_2 addition equilibrium, while reaction R_4 is associated with the chain branching. Most of the heat is released in reactions R_1 and R_5 so that adiabatic reaction temperature is reached no matter if ignition occurs from the low or high temperature combustion pathway of the fuel.

The reaction rates as described by Schreiber et al. (1994) are shown below:

$$R_1 = k_1[F]\left(\frac{p}{p_0}\right)^a \qquad ..(3.3)$$

$$R_2 = k_2[X][O_2][M] \qquad ..(3.4)$$

$$R_{3+} = k_{3+}[F][O_2][M]\left(\frac{p}{p_0}\right)^b C_{3+} \qquad ..(3.5)$$

$$R_{3-} = k_{3-}[I]\left(\frac{p}{p_0}\right)^c \qquad ..(3.6)$$

$$R_4 = k_4[I]C_4 \qquad ..(3.7)$$

$$R_5 = k_5[O_2][Y] \qquad ..(3.8)$$

where:

k_i are the kinetic rate constants defined by $k_i = A_i e^{-Ei/RT}$

$[M] = \frac{p}{RT}$ represents the total concentration of all the species.

C_{3+} and C_4 are the adjustment parameters depending on the fuel characteristics, namely the octane number.

(p/p_0) represents the variation of reaction rates with pressure (a = 0.5, b = -2.2 and c = -3.5 for both iso-octane and n-heptane).

The reaction rates are non-elementary but they bear a close resemblance to the underlying chemical equations. The temperature and pressure-sensitive equilibrium reaction R_3 is responsible for controlling the branching reaction R_4.

The abovementioned reaction rates were used to determine ignition delay profiles for iso-octane and n-heptane. A sensitivity analysis was done to determine which model parameters affect the ignition delay diagrams. The most sensitive parameters were the activation energies of the reactions (E_i/R), especially for the reactions R_{3+} and R_3. This is to be expected as the R_3 reactions are temperature sensitive and these reactions determine whether low or high temperature combustion occurs. These model parameters were modified so that the ignition delay profiles obtained from the Griffiths model fitted the ignition delay profiles from the more detailed kinetic model. The ignition delay diagrams of iso-octane and n-heptane are shown in Figure 3.25 and it is clearly illustrated that the Griffiths model (Schreiber et al., 1994) adequately represents the autoignition and the NTC regions for both iso-octane and n-heptane.

Blends of iso-octane and n-heptane were also modelled based on the Griffiths model (Schreiber et al., 1994). Here the kinetic constants were scaled according to the octane number (ON) of the blend i.e.

C_{3+}= [(110-ON)/10] in reaction R_{3+} and

$C_4 = [(110\text{-}ON)/10]^{0.5}$ in reaction R_4 (Schreiber et al., 1994).

In addition, the E_1/R, E_{3+}/R, E_{3-}/R and E_4/R parameters were also scaled depending on the octane number (ON) of the fuel as shown below:

$$
\begin{aligned}
E_1/R &= (E_1/R)_{i-octane} + 4.874*(100 - ON) \\
E_{3+}/R &= (E_{3+}/R)_{i-octane} + 4.0*(100 - ON) \\
E_{3-}/R &= (E_{3-}/R)_{i-octane} + 9.75*(100 - ON) \\
E_4/R &= (E_4/R)_{i-octane} - 1.002*(100 - ON)
\end{aligned}
\qquad ..(3.9)
$$

In Figure 3.25, ignition delay diagrams of the PRF blends are shown. The curves were found to be in good agreement with the data from the detailed kinetic model generated by Chemkin using the mechanism of Curran et al. (2002). The table shown in Appendix D gives the parameters for the different blends of iso-octane and n-heptane based on their octane number.

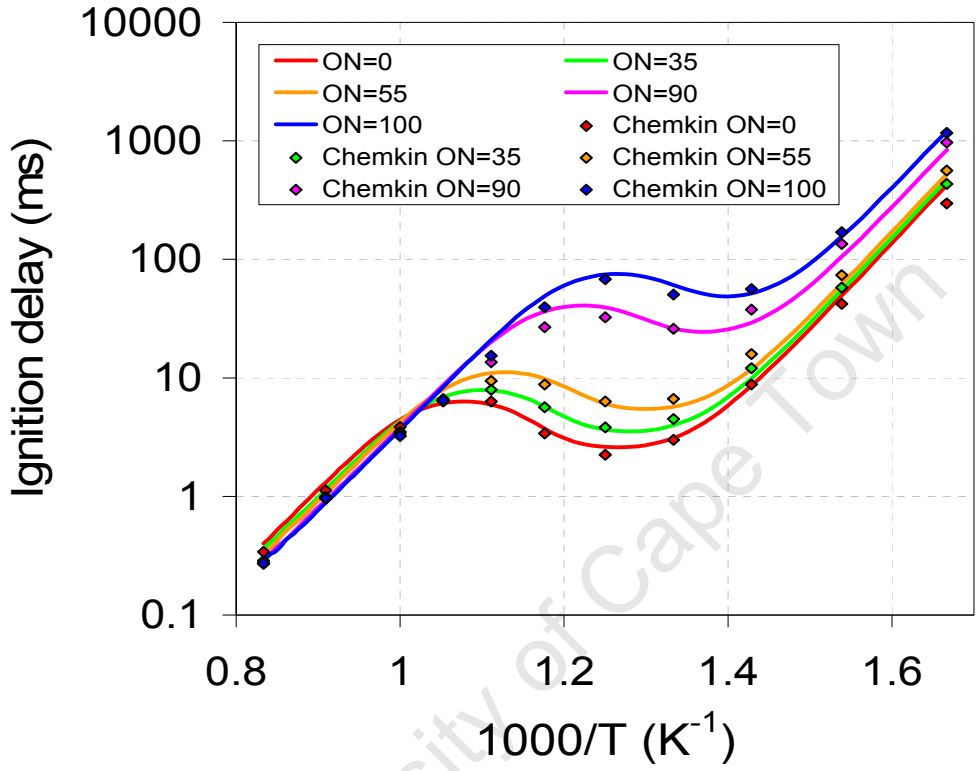

Figure 3.25: Ignition delay curves for blends of iso-octane and n-heptane using the Griffiths model (ON = octane number of the blend, shown by solid lines) and from using Chemkin for the detailed kinetic model (shown by points) at 12 bar

It is concluded that the reduced Griffiths model is sufficiently elaborate in its mechanisms to allow it to emulate the detailed chemical kinetic models over a wide range of temperatures and pressures with considerable precision. However, it is important to note that the model parameters cannot be predicted from first principles and therefore any reduced model is inevitably dependent on empirical data for its calibration. In the absence of such data (especially regarding blending behaviour amongst various molecules) the reduced kinetics approach is of limited value in the sense of octane prediction.

One further point of criticism that should be mentioned regarding the Griffiths model (and probably most other reduced models) is their inability to model the pre-cool

flame heat release accurately. In detailed kinetic simulations, the temperature is essentially constant in the period leading up to the cool flame temperature rise, whereas the reduced models predict a gradual temperature rise right from the start of the constant volume adiabatic system. This aspect can be seen clearly in a comparison that was made between the Griffiths model prediction of temperature for iso-octane in a constant volume simulation of iso-octane, at 780 K and stoichiometric conditions. The temperature profile shown in Figure 2(b) in Schreiber et al. (1994), for the constant volume oxidation of a stoichiometric iso-octane-air mixture at P_0=10 bar, has been reproduced in Figure 3.26. The same physical system was modelled by means of the detailed kinetics mechanism of Curran et al. (2002), but it was found that the initial pressure had to be increased to 15 bar in order to get a matching ignition delay of approximately 38 ms (with 10 bar the ignition delay was 99.8 ms).

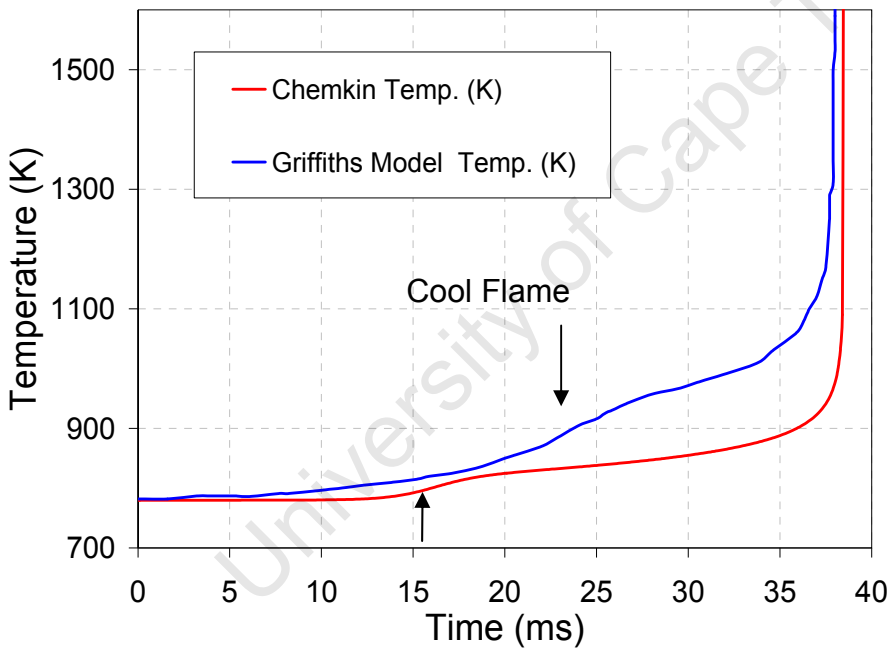

Figure 3.26: Comparison of detailed kinetics simulation of temperature in an adiabatic constant volume system with the Griffiths model simulation of temperature, Fig. 2(b) in Schreiber et al. (1994)

Although it is evident from Figure 3.26 that the cool flame ignition delays (shown by the arrows) did not correspond as well as the final ignitions did, the bigger concern is the relative difference in the rate of temperature increase versus time between the two simulations. The detailed kinetics simulation of temperature is almost flat before the occurrence of the cool flame, and relatively flat between the cool flame and the final ignition. In stark contrast, the simplified Griffiths model is not able to utilize the reaction enthalpies of only six reactions to obtain a realistic heat release over the

total induction period. Thus there is a gradual temperature increase, starting from the beginning of the simulation and increasing at a larger rate after the cool flame.

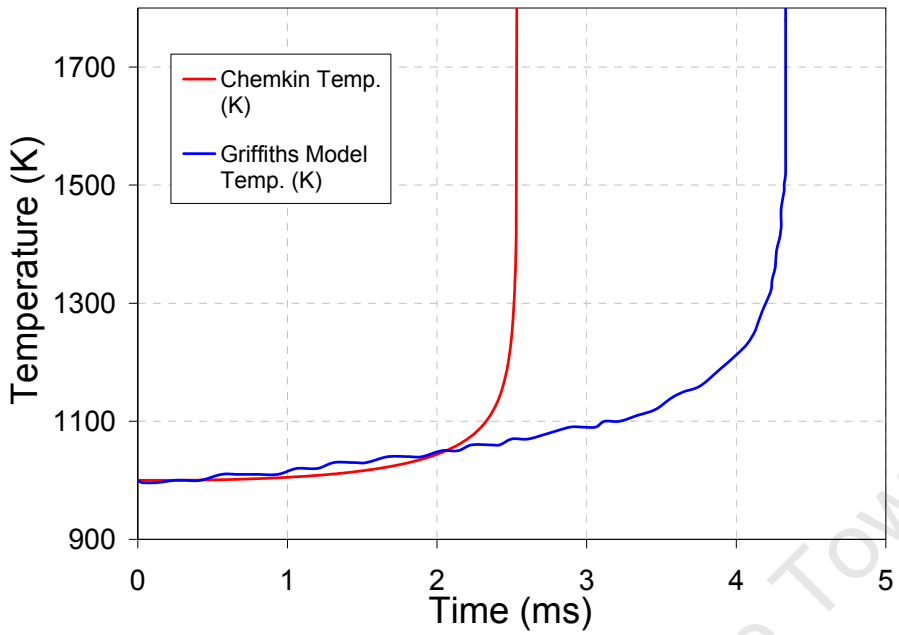

Figure 3.27: Comparison of detailed kinetics simulation of temperature in an adiabatic constant volume system with the Griffiths model simulation of temperature, for iso-octane at 10 bar and 1000 K as in Fig. 2(c) from Schreiber et al. (1994)

As shown in Figure 3.27, the ignition delays predicted by the two models were comparable only when the Curran et al. (2002) mechanism was applied to a system of stoichiometric iso-octane and air at 1000 K and with the initial pressure at 15 bar, not the 10 bar as reported by Schreiber et al. (1994). Again it can be observed that the Griffiths model leads to an incorrect rate of heat release across the induction period, whereas the detailed kinetic model reflects the essentially flat behaviour that is observed in reality.

3.3.2 History and new advances

In the past, kinetic modelling was categorized only in two broad classes; detailed kinetics reflecting comprehensive mechanisms, and reduced kinetics where the mechanisms consisted of a minimized subset of the detailed mechanism. Several different methodologies by which detailed mechanisms could be reduced in a systematic manner have been developed. Some of these approached it from a chemistry (sensitivity analyses) point of view (Ogink and Golovitchev, 2001, Saylam et al., 2007) while others approached the reduction from a mathematical (e.g. Computational Single Perturbation (CSP) analysis, as by Kazakov et al. (2006), or by

the Intrinsic Low Dimensional Manifold (ILDM) methods, e.g. Maas and Pope (1992), to name only one example. Other approaches lie even more into the domain of computer science than in combustion chemistry, e.g. Blurock (1995), Pepiot-Desjardins and Pitsch (2008) and Bhattacharjee et al. (2003).

Over the last 5 years or so, the attractive idea of coupling multidimensional CFD models with reduced chemical kinetic mechanisms (as these calculations are feasible on current computers), has been pursued by many workers, especially in targeting HCCI combustion modelling. Noteworthy is the attempts of Maroteaux and Noel (2006), Zheng et al. (2002), Huang et al. (2008) and Machrafi et al. (2009). It is interesting to note that most of them based their reduction of PRF (n-heptane and iso-octane mechanisms) on the reduced scheme of Golovitchev et al. (1999) that became widely known as the Chalmers mechanism.

3.4 Discussion of Detailed vs. Skeletal Kinetics in application to engine autoignition modelling

In the work conducted during this study, the elucidation of possible blending rules between components having single-stage ignition and ones with the more prevalent two-stage ignitions, have remained a key focus area. Analysis of the simulation results from detailed kinetic mechanisms (e.g. the PRF mechanism of Curran et al. (2002)) has been wrought by difficulties, mainly due to their size and complexity. Tools available in Chemkin Collection 3.7, such as reaction sensitivity analysis and rates of production (ROP) analysis, could not be used on these big mechanisms within the computing infrastructure available for this study.

For this reason the skeletal mechanisms, especially the one that included PRF molecules and toluene (Machrafi et al., 2009), was studied in detail as it was hoped that the underlying chemistry was being reflected realistically, while it is still small enough to explore and pin-point the species that are intimately associated with the occurrence (timing) and magnitude of the cool flame heat release. Thus the Machrafi skeletal mechanism for toluene, n-heptane and iso-octane, consisting of 49 species in a total of 62 reactions, was coded in Chemkin format and evaluated against the detailed mechanisms.

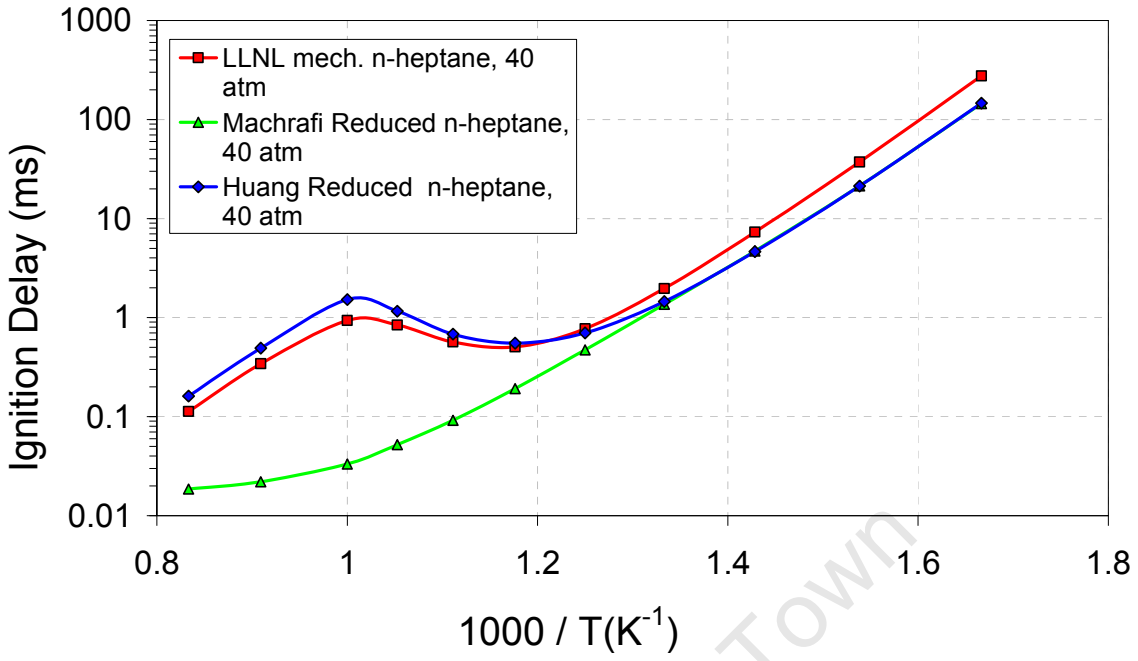

Figure 3.28: Skeletal mechanism of Machrafi et al. (2009), for pure n-heptane (Φ=1.0), showing its failure to represent NTC

It was clear that the NTC character of the n-heptane in the reduced mechanism was not reflected at all well, even though the Machrafi paper showed it to be successful for n-heptane alone. This is shown by the green curve in Figure 3.28. No plausible explanation could be found and communication with the author was not helpful, as he no longer has access to the Chemkin files (including the Thermodynamics data file) that were used (Machrafi, 2008). An evaluation of a PRF 60 using the same mechanism does show some NTC behaviour, but the error in the underlying heptane mechanism, leading to the relative absence of NTC, is still evident. This is shown in Figure 3.29.

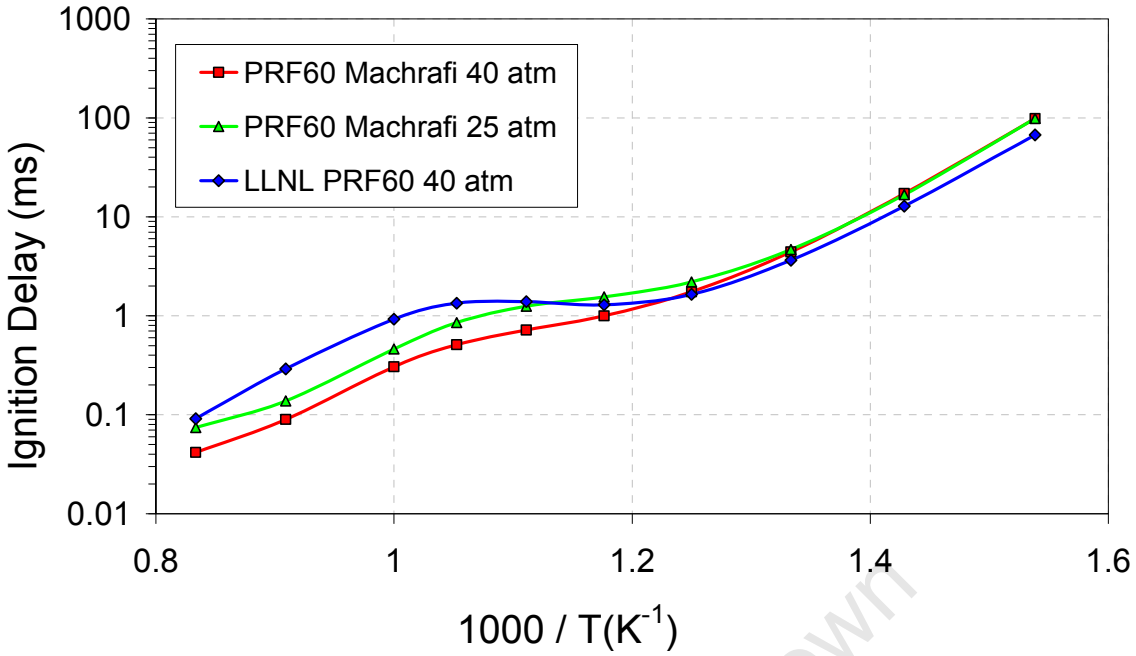

Figure 3.29: Skeletal mechanism of Machrafi et al. (2009), for a PRF 60 blend (60% iso-octane / 40% n-heptane) at Φ=1.0, showing reduced NTC character

The Machrafi et al. (2009) mechanism was therefore discarded in favour of another PRF skeletal mechanism that was recently published by Huang et al. (2008). This was coded into Chemkin format and it was established that this mechanism (using only n-heptane as fuel) reflected the NTC character of this molecule accurately in constant volume combustion simulations. An example is shown in Figure 3.30, where the detailed mechanism of LLNL (by Curran et al., 2002) is also shown for comparison.

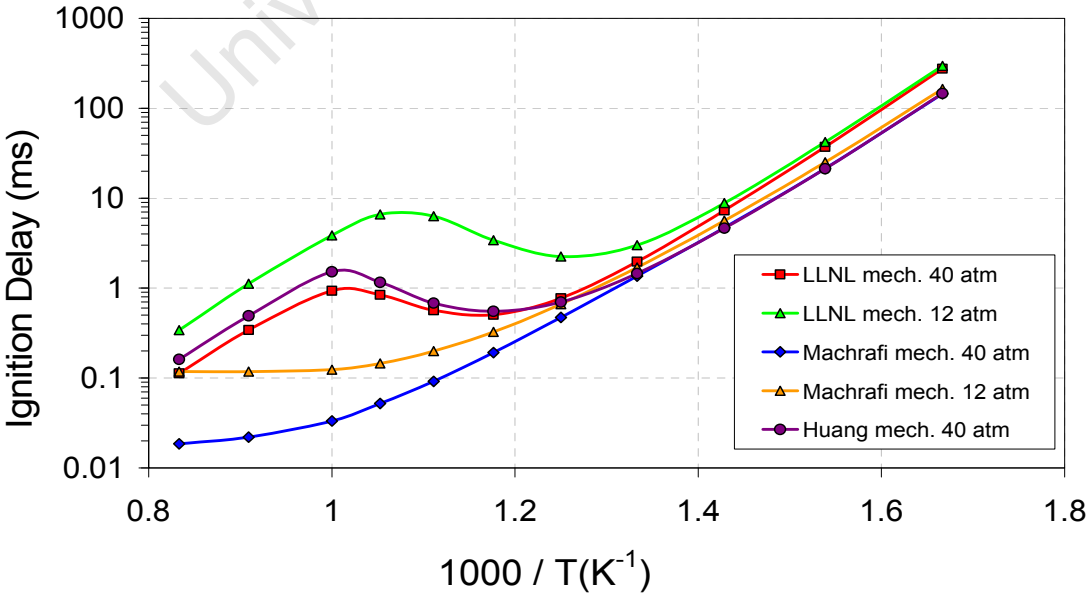

Figure 3.30: Skeletal mechanism of Huang and Machrafi, for pure n-heptane (Φ=1.0) compared to the LLNL mechanism of Curran et al. (2002)

The same approach of Machrafi et al. (2009) was subsequently followed and their reduced Toluene mechanism, based on the comprehensive one from Djurisic (1998), was merged with the PRF mechanism from Huang et al. (2008). This proved to be very successful, as the combined mechanism reflected the NTC in n-heptane very well, including the single–stage character of toluene, as is evident in Figure 3.31, below. The full mechanism, in Chemkin 3.7 format, is shown in Appendix E.

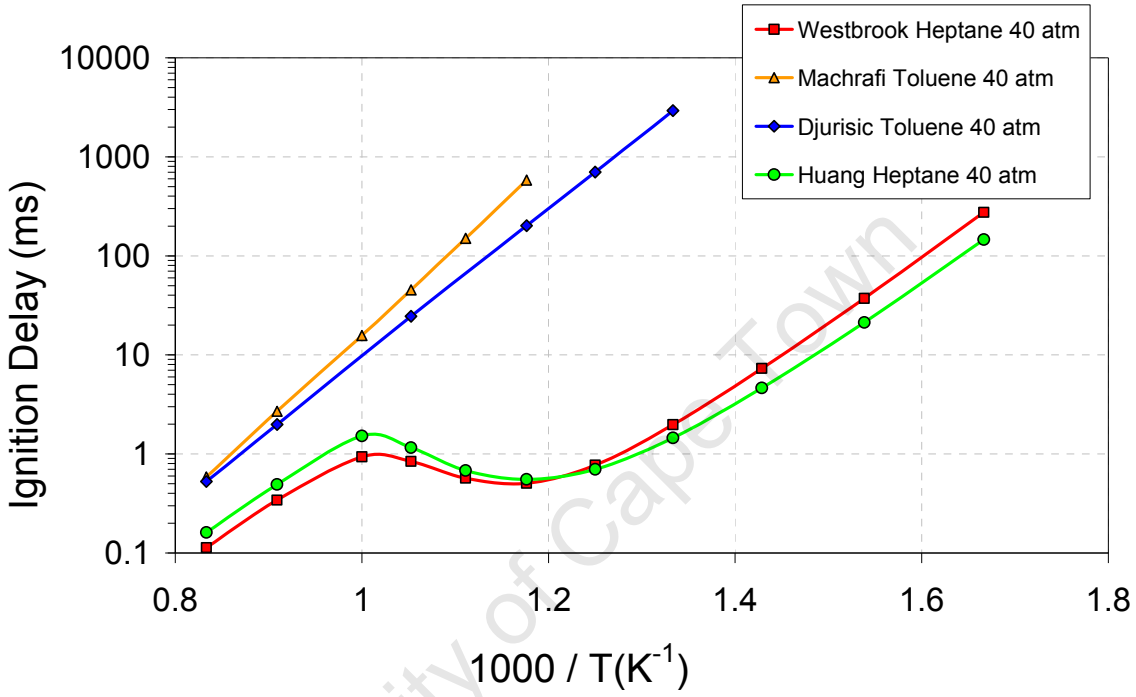

Figure 3.31: Skeletal mechanism of Huang with toluene incorporated, for pure n-heptane (Φ=1.0) and toluene, compared to detailed mechanisms

In Figure 3.31 the original detailed toluene and detailed n-heptane simulations are also shown for comparison, indicating that the reduced mechanism, now consisting of 48 species in 59 reactions, is representing the detailed mechanisms adequately. The next step was to evaluate blends of toluene and n-heptane, using the consolidated mechanism. This was performed by varying the blend ratios between toluene and n-heptane across the spectrum from 100% n-heptane to 100% toluene. A representation of these simulation results is shown in Figure 3.32.

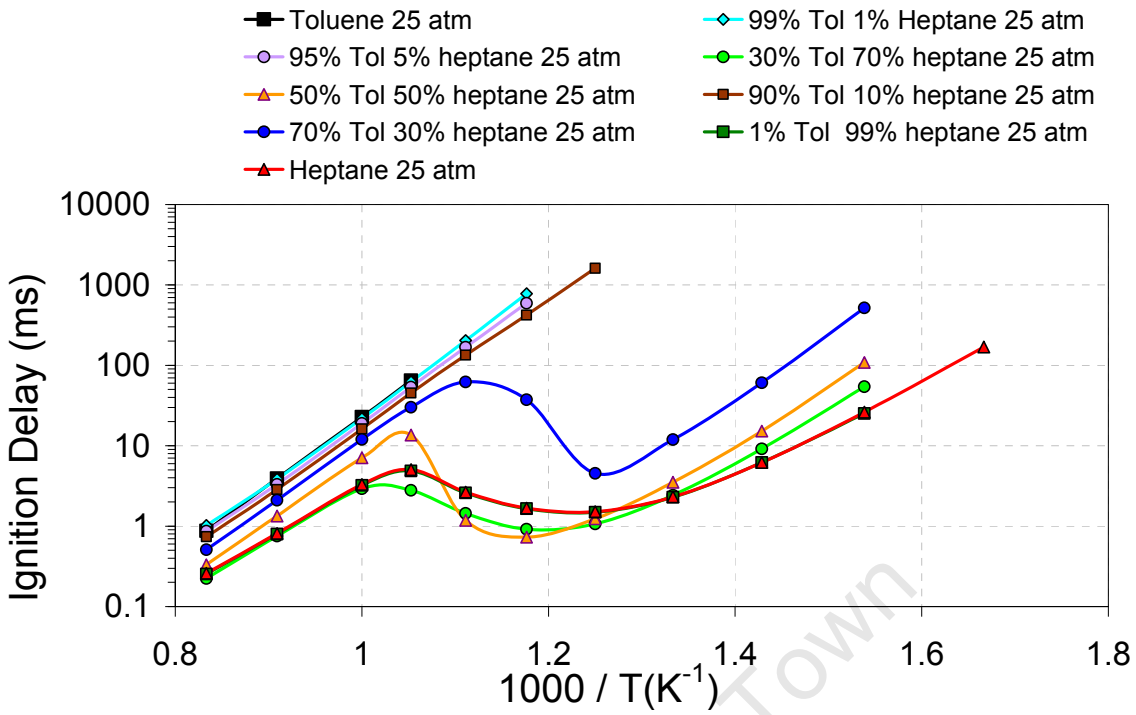

Figure 3.32: Skeletal mechanism of Huang et al. (2008) with toluene incorporated, for pure n-heptane (Φ=1.0) and toluene, and various blends in between, all at 25 atm

It is clear from the simulated ignition delay curves shown in Figure 3.32, that certain blends (e.g. 50% Toluene/ 50% heptane and 30% Toluene/ 70% heptane) are not handled well, especially in the NTC region where the presence of toluene seems to make the fuel mixture more reactive. This leads to an unexpected increase in reactivity in the temperature range from 750 °C to 900 °C, where the ignition delays for the blend are predicted to be shorter than for the most reactive molecule, n-heptane. This is of course in contradiction with experimental data and other modelling results from the literature (Andrae et al., 2007 and Andrae et al., 2008), thus it is attributed to be an artefact of the skeletal nature of the mechanism. The many reactions in which the less reactive benzylic radicals capture and annihilate the various radicals formed at lower temperatures from n-heptane, are not contained in the skeletal mechanism, thus the only interaction between the two different fuel molecules are contained in the common pool of small labile radicals (e.g. $\cdot C_2H_5$, $\cdot CH_3$ etc.) formed at a much later stage of the oxidation sequence. Since it is also possible that such a simple mechanism may handle the introduction of an extra molecule (toluene) by leaning out the mixture strength for n-heptane, thereby causing the exaggerated “dip” in the NTC region (visible in Figure 3.32), a few simulations at different equivalence ratio’s were performed. These are shown in Figure 3.33.

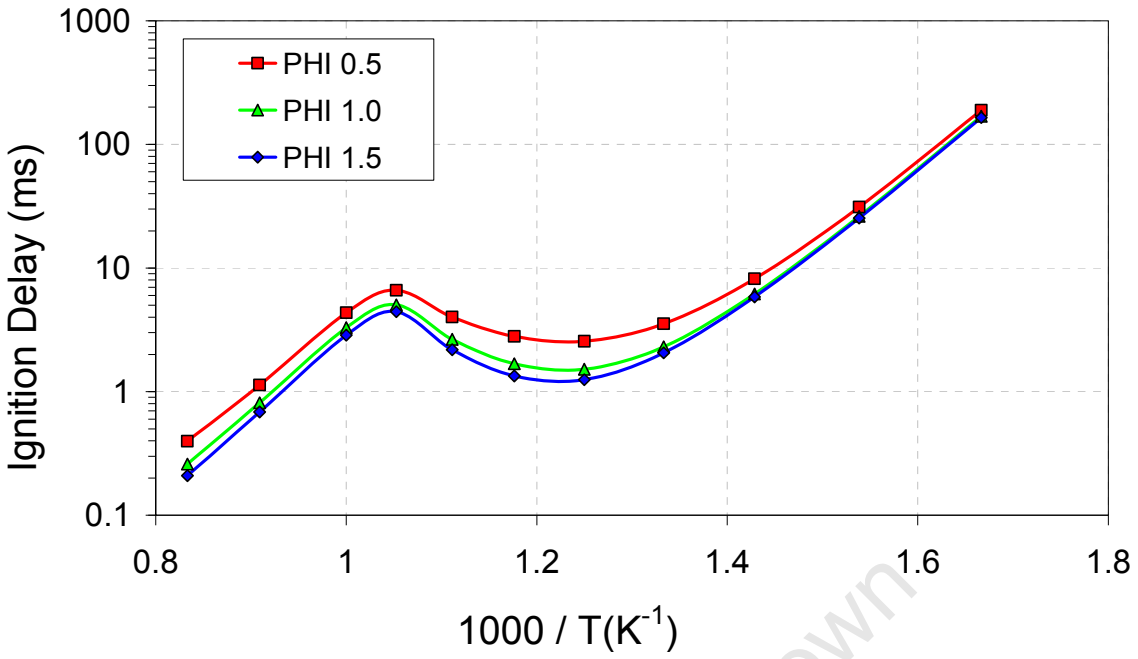

Figure 3.33: Skeletal mechanism of Huang with added toluene, showing pure n-heptane at P=25 atm, at different Φ values

The curves in Figure 3.33 are as expected, with leaning out causing the NTC trough to be shallower and ignition delays to shift to higher values, similar to behaviour that was previously observed in simulations using the detailed Curran et al. (2002) mechanism.

It thus seems that this inability of a highly reduced skeletal mechanism (such as the one that was tested here) to reflect real-world behaviour at crucial stages of the autoignition process (e.g. during the NTC regime) will always hinder their application in CFD codes simulating IC engine combustion processes. On the other hand, skeletal mechanisms, when tuned properly, may be used quite successfully at the appropriate T and P regimes for which they were fitted.

In contrast to the unsatisfactory blending behaviour between toluene and n-heptane that was demonstrated for the skeletal mechanism, shown earlier in Figure 3.32, a detailed kinetic mechanism has the ability to accurately simulate the blending interaction between a single stage molecule and one with NTC character. This has been demonstrated by Yates and Viljoen (2008), for blends of methanol and a PRF 80, where all three constituent molecules were contained in the Curran et al. (2002) PRF mechanism. In the current work, the blending behaviour between ethanol

(abbreviated as EtOH) and n-heptane was simulated, using the same PRF mechanism. Since ethanol is a single stage molecule that is already contained in the PRF mechanism, it can be blended (in a theoretical manner) easily with n-heptane by specifying initial starting mole fractions of both molecules, together with the appropriate mole fractions of oxygen and nitrogen that will provide a stoichiometric system (Φ = 1). The volumetric blend of 50% EtOH with 50% n-heptane will be taken as an example, for which the constant volume simulation at 40 atm, starting at different initial temperatures, is shown by the orange line in the middle of Figure 3.34. The reacting system was specified in mole fractions as follows:

Ethanol	: 0.02730194
n-Heptane	: 0.01087344
O_2	: 0.20151364
N_2	: 0.76031098

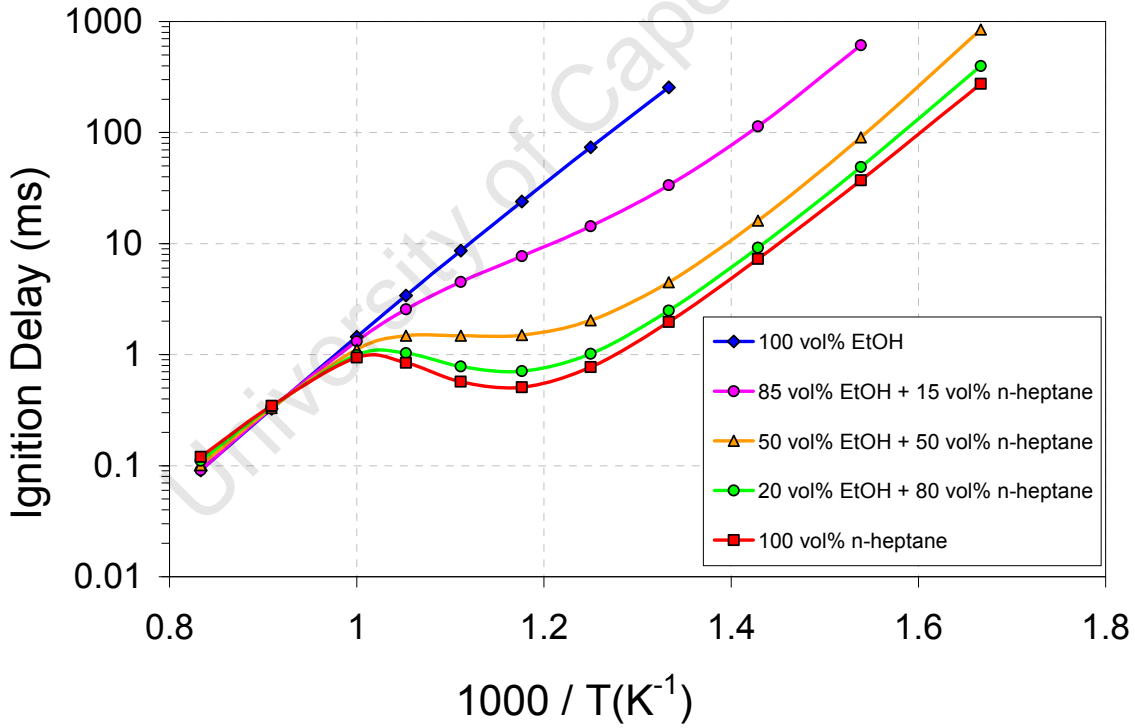

Figure 3.34: Realistic blend simulations of ethanol and n-heptane at various volumetric ratios, as calculated within the Curran et al. (2002) PRF mechanism for 40 atm under stoichiometric conditions

It was verified that the straight line obtained for ethanol in Figure 3.34 can be superimposed with the single stage line generated by the Marinov mechanism (Figure 3.13), although some divergence at the longer ignition delays (>100 ms) was

observed. It is important to note, however, that blends with high ratios of n-heptane (containing small amounts of ethanol) were less reactive than pure n-heptane, as expected. Thus all the binary blends would have ignition delays falling inside the envelope of ignition delays determined for the two pure substances, as shown in Figure 3.34, and in stark contrast to the unrealistic behaviour shown in Figure 3.32.

3.5 Conclusions

During this study, a comprehensive evaluation was carried out of all the fuel molecules for which detailed kinetic mechanisms could be obtained. These mechanisms were compared with one another in a relatively simple constant volume simulation system, as it had been postulated that the last mass element of end-gas to be consumed by the approaching flame front, would have had the longest life time in which it could reach the point of autoignition, in an essentially constant volume, adiabatic system. The results have pointed to the large differences between molecules that have single-stage ignition, and those that have two-stage ignition behaviour, implying the presence of significant NTC character in the latter group.

Although much has been learnt by studying the detailed kinetic simulations for a relatively small number of gasoline molecules, also in systems that simulated the CFR engine itself under RON measurement conditions, it became clear that there is not a simplistic link to be made between the simulated ignition delay in a constant volume system and the octane number of that specific molecule. The actual pressure trace obtained for the specific molecule in the CFR engine under knocking conditions (at SKI), would be needed in order to make an unequivocal link. Although there may be alternative approaches (e.g. by making multiple ignition delay measurements in a RCM to fully characterise the fuel), the biggest challenge is still the limited availability of detailed kinetic mechanisms. In addition, the size of merged mechanisms in which the blends of a number of different gasoline molecules can be considered simultaneously, quickly leads to these simulations becoming untenable on conventional computer hardware.

Skeletal mechanisms have been developed to address the need to integrate kinetics into CFD codes, and some of these have been shown to be relatively accurate, for example the Griffiths reduced model in simulation of PRF blends. However, their

main limitations are the need to tune them to experimental data, and the lack of transportability of such a mechanism to other physical applications. It has also been shown in this work that skeletal mechanisms are often omitting important reaction pathways, which may lead to nonsensical results in cases where more than one fuel molecule is blended together in the simulated system. A good example of this erroneous blending behaviour was shown in Figure 3.32, where the presence of toluene *increased* the reactivity of the system towards oxidation even beyond the reactivity of pure n-heptane.

This cast some doubts on the usefulness of skeletal mechanisms in the development of surrogate gasoline mechanisms that should contain at least one “representative” member of all the classes of gasoline constituents.

Overall, one of the main conclusions reached on the basis of the kinetic simulations conducted in this study, was that a practically implementable octane prediction capability will for the foreseeable future, still have to contain a large component of empiricism.

Chapter 4 : Investigating NTC by application of Molecular Modelling through DFT

4.1 Introduction

Since quantum mechanics explicitly represents all the electrons in a molecule in the calculation, it is possible to derive properties that depend upon the electronic distribution and to investigate chemical reactions in which bonds are broken and formed (Leach, 2001). As the presence or absence of NTC was previously associated with the internal hydrogen abstraction by a ROO· radical, through the formation of a transient cyclic (5 to 8 membered-ring) structure as the rate-determining step, it was evident that molecular modelling should be ideally suited to provide more information about the NTC character of specific molecules. The initial premise was that the energy barrier for this reaction (the activation energy of the transition state that must form during the exchange of the hydrogen atom) would discriminate between molecules that have single-stage ignition characteristics and those having pronounced NTC or two-stage ignition character.

This potential differentiating aspect of quantum mechanical calculations was investigated by focusing on different molecules as case studies, these are described in subsequent sections. It was also hypothesized that the molecular modelling results could yield some quantitative description or measure of the NTC character. This became a prime motivator for application of Density Functional Theory (DFT) techniques to this study, as it became apparent that the quantification of NTC character, or “NTC-icity” (see Chapter 5) would be a significant challenge. Finally, DFT calculations were applied very successfully in a comparison of two skeletal mechanisms with each other (as described in Chapter 3), showing that from a chemistry perspective the wrong skeletal mechanism is probably being used by many workers in the field.

4.2 Theory of Molecular Modelling based on DFT

Computational quantum mechanics in general rely on solving the Schrödinger equation for the system of atoms and electrons that represents the molecule or radical of interest. If the molecule has N electrons, then Hartree-Fock theory has to calculate the full N-electron wave function, something which does not have to be performed in a Density Functional Theory (DFT) calculation. The central idea which underpins DFT is that there is a direct relationship between the total electronic energy of a molecule and the overall electronic density. This is often expressed by stating that the energy, *E*, is a unique functional of $\rho(r)$. A simple example of a functional is the area under a curve, which takes a function *f*(r) defining the curve between two points and returns a single number (the area, in this case) (Leach, 2001).

4.2.1 The Schrödinger equation:

The Schrödinger equation in three dimensions has the following form (Barrow, 1966; Atkins, 1978; Leach, 2001):

$$-\frac{h^2}{8\pi \cdot m}\left(\frac{\partial^2\Psi_i}{\partial x^2}+\frac{\partial^2\Psi_i}{\partial y^2}+\frac{\partial^2\Psi_i}{\partial z^2}\right)+V(x,y,z)\cdot\Psi_i = E_i\cdot\Psi_i(r) \qquad ..(4.1)$$

This can be simplified to:

$$\left(-\frac{\hbar^2}{2m}\nabla^2+V\right)\cdot\Psi(r)=E\cdot\Psi(r) \qquad ..(4.2)$$

where $\nabla^2=\frac{\partial^2}{\partial x^2}+\frac{\partial^2}{\partial y^2}+\frac{\partial^2}{\partial z^2}$ ..(4.3)

It is usual to abbreviate the left hand side of equation (4.2) by introduction of the Hamiltonian operator, H, so that the Schrödinger equation reduces to:

$$H\cdot\Psi(r)=E\cdot\Psi(r) \qquad ..(4.4)$$

The first term in equation (4.1) is the kinetic energy and the second term is the potential energy. In equations 4.1 to 4.4, *h* is Planck's constant, $\hbar$ is Planck's

constant divided by 2π, *m* the mass, Ψ is the wave function, E the energy of the particle (or the system if Ψ is the total wave function), ∇^2 (del squared), is the second derivative operator with respect to x, y, and z, and *H* is the Hamiltonian operator.

It is acknowledged that equation (4.2) is a gross simplification of the Schrödinger equation, and that it would be more appropriate to write out the N-particle Schrödinger equation suitable for a molecule containing P nuclei and N - P electrons to lowest order (ignoring spin-angular momentum coupling), for it is an approximate solution to this equation that the DFT method is attempting to find. Thus equation (4.2) becomes:

$$i\hbar\frac{\partial\Psi(\vec{R}_1,\vec{R}_2,...,\vec{R}_P,\vec{r}_1,\vec{r}_2,....\vec{r}_{N-P},t)}{\partial t} = -\frac{\hbar^2}{2M_1}\nabla_1^2\Psi - \frac{\hbar^2}{2M_2}\nabla_2^2\Psi - ...\frac{\hbar^2}{2M_P}\nabla_P^2\Psi - \frac{\hbar^2}{2m_1}\nabla_{e_1}^2\Psi$$
$$-\frac{\hbar^2}{2m_2}\nabla_{e_2}^2\Psi - ...\frac{\hbar^2}{2m_{N-P}}\nabla_{e_{N-P}}^2\Psi - \sum_{i=1}^{P}\sum_{j=1}^{(N-P)}{}_{electrons}\frac{Z_i e^2}{4\pi\varepsilon_0\left|\vec{R}_i-\vec{r}_j\right|}\Psi + \frac{1}{2}\sum_{i=1}^{P}\sum_{j=1}^{P}\frac{Z_i Z_j e^2}{4\pi\varepsilon_0\left|R_i-R_j\right|}\Psi$$
$$+\frac{1}{2}\sum_{i=1}^{(N-P)}\sum_{j=1}^{(N-P)}\frac{e^2}{4\pi\varepsilon_0\left|\vec{r}_i-\vec{r}_j\right|}\Psi$$

..(4.5)

where $\vec{R}_i$, and $\vec{r}_i$ represent the position co-ordinates of the *i* 'th nucleus and electron respectively, M_i and m_i represent the masses of the *i* 'th nucleus and electron respectively, ∇_i^2 and $\nabla_{e_i}^2$ represent the div grad operator on the *i* 'th nucleus and electron respectively, and Z_i represents the atomic number and integral charge of the *i* 'th nucleus.

The lowest order, stationary ground state eigenfunction solution of the system then obeys the equation:

$$-\frac{\hbar^2}{2M_1}\nabla_1^2\Psi_g - \frac{\hbar^2}{2M_2}\nabla_2^2\Psi_g - ...\frac{\hbar^2}{2M_P}\nabla_P^2\Psi_g - \frac{\hbar^2}{2m_1}\nabla_{e_1}^2\Psi_g$$
$$-\frac{\hbar^2}{2m_2}\nabla_{e_2}^2\Psi_g - ...\frac{\hbar^2}{2m_{N-P}}\nabla_{e_{N-P}}^2\Psi_g - \sum_{i=1}^{P}\sum_{j=1}^{(N-P)}{}_{electrons}\frac{Z_i e^2}{4\pi\varepsilon_0\left|\vec{R}_i-\vec{r}_j\right|}\Psi_g \qquad ..(4.6)$$
$$+\frac{1}{2}\sum_{i=1}^{P}\sum_{j=1}^{P}\frac{Z_i Z_j e^2}{4\pi\varepsilon_0\left|R_i-R_j\right|}\Psi_g + \frac{1}{2}\sum_{i=1}^{(N-P)}\sum_{j=1}^{(N-P)}\frac{e^2}{4\pi\varepsilon_0\left|\vec{r}_i-\vec{r}_j\right|}\Psi_g = E_g\Psi_g$$

If the wave functions are known the energy of the system can be obtained by integrating on both sides (Leach, 2001).

$$E = \frac{\int \psi^* \cdot H \cdot \psi \cdot d\tau}{\int \psi^* \cdot \psi \cdot d\tau} \qquad ..(4.7)$$

The probability of finding a particle at a point is given by the wave function at the point, r, multiplied by its complex conjugate ψ^* (according to the Born interpretation of the wave function). The square of the wave function thus gives the electron density at any given point (Leach, 2001).

$$\rho(r) = \int |\Psi|^2 \cdot d\tau \qquad ..(4.8)$$

Integration over the whole space gives the probability of finding the particle anywhere in this space. The result must be unity as the particle must exist somewhere (see equation 4.9) (Leach, 2001; Atkins, 1978).

$$\int \Psi^* \cdot \Psi \cdot d\tau = 1 \qquad ..(4.9)$$

4.2.2 The Born-Oppenheimer approximation

The hydrogen molecule–ion (taken here as an example) consists of three particles: two protons and one electron. The protons repel each other but attract the electron. The balance between the kinetic energy and these repulsions and attractions must account for the stability of the species. The exact Schrödinger equation must deal with three particles simultaneously, but the nature of the species suggests a simplification, which is known as the Born-Oppenheimer approximation. The Born-Oppenheimer approximation uses the fact that protons are much more massive than the single electron (by a factor of nearly 2000). The nuclei therefore move much slower than the electron and may be regarded as fixed while the electron moves through the whole volume of the molecule. The Born-Oppenheimer approximation therefore implies that the motion of the nuclei may be neglected. It is sufficient to

consider the motion and distribution of the electrons for static nuclear positions (Atkins, 1978; Leach, 2001).

4.2.3 Linear Combination of Atomic Orbitals (LCAO) methods:

The molecular orbital may be expressed by a linear combination of atomic orbitals (LCAO) (Leach, 2001):

$$\varphi_i = \sum_{\mu=1}^{K} c_{\mu i} \cdot \phi_\mu \qquad ..(4.10)$$

In equation (4.10), φ_i is the molecular orbital, ϕ_μ is one of K atomic orbitals and $c_{\mu i}$ is a coefficient.

Gaussian type functions, which are called basis functions, may be used to describe the one-electron orbital. The atomic orbital is then represented by a linear combination of Gaussian functions (Leach, 2001).

$$\phi_\mu = \sum_{i=1}^{L} d_{i\mu i} \cdot \phi_i(\alpha_{i\mu}) \qquad ..(4.11)$$

In equation (4.11), ϕ_μ is the atomic orbital, $d_{i\mu i}$ is the coefficient of the primitive Gaussian function, ϕ_i, which has an exponent, $\alpha_{i\mu}$, and L is the number of functions in the expansion.

Normally, the more Gaussian functions are used, the better (more accurately) the orbital is described. Basis set functions used are centered on atomic nuclei and can give erroneous results for strongly anisotopic charge distributions (Leach, 2001). The charge around an atom in a molecule is usually perturbed in comparison with an isolated atom. The distortion can be considered to correspond to mixing p-type character into the 2s orbital of an isolated atom to give a form of sp hybrid (for elements in the second period). In a similar manner the unoccupied d orbitals introduce asymmetry into p orbitals. This problem is solved by introducing

polarisation functions into the basis sets. The polarisation functions have a higher angular quantum number and so correspond to p orbitals for hydrogen and d orbitals for the first and second row elements.

In this study a numerical (values on an atomic centered spherical-polar mesh) basis set rather than Gaussiun functions (analytical functions) were used. The Double Numerical basis set plus d-functions for all non-hydrogen atoms (abbreviated as DND) were used in this study (Accelrys (Inc.), 2002).

4.2.4 Density Functional Theory (DFT)

The basic idea in DFT is that the ground state total energy of a system depends on its electronic density, ρ. The constituents of the total energy can be written (Accelrys (Inc.), 2002; Viljoen, 2006):

$$E[\rho] = T[\rho] + U[\rho] + E_{ex}[\rho] \quad ..(4.12)$$

With $T[\rho]$ as the kinetic energy, $U[\rho]$ is the classical electrostatic energy due to Coulombic interaction and E_{ex} is the exchange correlation energy. The exchange correlation energy is all the other interactions that are required to reproduce the total energy exactly. This exchange correlation is not known and can be approximated with various functions as proposed by different researchers. The various functions give similar but not identical results. These proposed functions can be divided into two groups, (1) Local Density Approximation (LDA) and (2) Generalised Gradient Approximations (GGA). The functions of the first group, LDA functions, usually underestimate the exchange correlation in the low electron density regions. The LDA functions may also overestimate the bond energies (Accelrys (Inc.), 2002). Functions of the second group, GGA, are thus preferred. In this study a preferred functional (Becke exchange functional (B88)) was used in conjunction with the Lee-Yang-Parr correlation functional (BLYP)) from the GGA group. The BLYP functional was selected, since it gave the smallest error in a test reaction that was done for 2 $\cdot CH_3$ -> C_2H_6 (ΔH for the reaction). It was also in agreement with a more comprehensive

evaluation of 8 different functionals performed by Viljoen (2006), which found BLYP to be the most accurate.

The derivative of the exchange-correlation energy with respect to the electron density gives the exchange-correlation potential, μ_{ex}. (Accelrys (Inc.), 2002; Viljoen, 2006):

$$\mu_{ex} = \frac{\partial E_{ex}[\rho]}{\partial \rho} \qquad ..(4.13)$$

which can be added into the Hamiltonian operator in the Schrödinger equation.

$$\left(-\frac{\hbar}{m}\nabla^2 + V + \mu_{ex}(r) \right) \cdot \Psi(r) = E \cdot \Psi(r) \qquad ..(4.14)$$

The Schrödinger equation can be solved for the one-electron orbitals, from which the electron density, ρ, at any given point, r, can be calculated by

$$\rho(r) = \sum_{i=1}^{N} |\Psi_i(r)|^2 \qquad ..(4.15)$$

Solving the DFT equations is an iterative procedure starting from 'guessed' wave functions (Viljoen, 2006). The self-consistent field (SCF) procedure in DFT consists essentially of the following iterative steps:

1) Choosing an initial set of coefficients to expand the basis set,
2) Construction of a set of molecular orbitals (wave functions),
3) Using the trial set to construct the electron density according to Equation (4.15),
4) Using the density to calculate the Coulombic and the exchange-correlation potentials, a new set of molecular orbitals and the optimised electron density.

This procedure is repeated until the input and the output densities agree to within the specified tolerance value. This density is then used to evaluate the total energy (by application of Equation 4.12). In this study DMol^3, a density functional theory quantum mechanical software package from Accelrys Inc., was used to perform the calculations.

4.2.5 Vibrational frequencies (Infra-red spectroscopy)

DMol^3 can also calculate the vibrational frequencies, by using a matrix of Cartesian second derivatives (Hessian matrix). A minimum in energy (see Figure 4.1) is identified at the locus on the surface where the first derivative is zero and the second derivative is positive. For a saddle point (see Figure 4.1) the second derivative is negative (Frisch, 2004). For a first-order saddle point (where the transition state is expected to be found) the gradient vector is also zero, but the Hessian must have only one negative eigenvalue. The corresponding eigenvector will then point along the reaction coordinate. The implication of this is that after geometry optimization has been performed on the molecular system, it is necessary to check for negative frequencies (also known as imaginary frequencies). If all the calculated frequencies are positive, it is still possible that a local minimum has been obtained. The starting geometry should be changed and optimisation should be repeated to validate that a local minimum had not been obtained inadvertently, but a true global minimum.

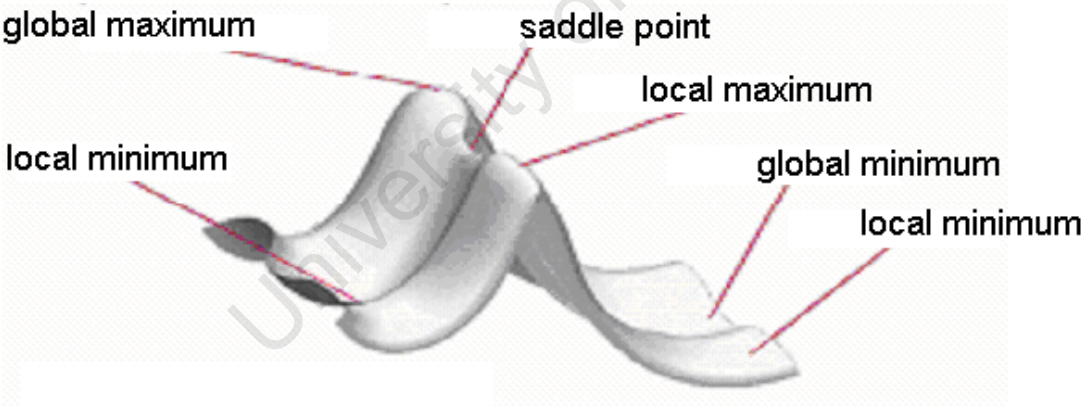

Figure 4.1: Illustration of maxima and minima in geometry optimisations (Frisch, 2004)

A nonlinear N-atomic molecule has 3N-6 vibrational degrees of freedom (since 3 rotational and 3 translational vibrations are not observed). The vibration frequencies calculated by DMol^3 are not identical to the infra-red frequencies measured typically through experiments. Calculated vibrational frequencies are typically larger than the frequencies observed experimentally (Scott and Radom, 1996). Scaling factors are used, which are dependent on the choice of exchange functional and correlation functional (Scott and Radom, 1996). The vibrational frequencies calculated are for

gas molecules and will be different from experimental infra-red frequencies of solids since the relaxation of molecules in the gas phase occurs more rapidly through inter-molecular collision. This leads to sharper absorption lines in the IR-spectra for gas phase molecules, whereas IR-spectra of solids or liquids show broad absorption bands.

4.2.6 Transition State searching

After both the reactant and the product molecules (radicals in this study) had been optimized geometrically (i.e. the structures were allowed to adopt the configuration of minimum electronic energy), the Transition State (TS) search functionality in DMol^3 was used to find the energy of the TS. When the TS had been found, it was verified that the single imaginary frequency was in the reaction coordinate, before the TS Optimization routine was performed subsequently. The difference in absolute energy value obtained for the optimized Transition State (after correcting for the zero-point energy) from the corrected absolute energy of the reactant radical, was calculated as the activation energy barrier, E_a in units of kJ/mol. Similarly, the difference between the corrected absolute energy of the Product radical and that of the Reactant radical was taken as the reaction enthalpy, also in units of kJ/mol.

4.3 Quantification of the Activation Energy of the Rate Determining Step

There is no doubt that molecular structure is of paramount importance in determining the oxidation reaction pathways of hydrocarbon molecules. After the first bimolecular initiations with oxygen (O_2) molecules or •OH radicals, alkyl radicals (denoted by R•) and HO_2• (perhaps represented more accurately as HOO•) radicals are produced. The low and intermediate temperature reactions of the alkyl radicals with oxygen involve the classical sequence of oxygen addition, isomerization by internal hydrogen abstraction, second oxygen addition, second isomerization, and β-scission to lead to the formation of hydroperoxides, which are degenerate branching agents and decompose to yield •OH radicals and smaller molecules and radicals. The reactivity of the molecule towards oxidation is related to the type and number of C-H bonds, the ability of the stabilized radicals to react, and the cyclic strain of the transition state formed during the isomerization reactions (Vanhove et al., 2005).

Tanaka et al. (2003) have postulated that the distinction between molecules with pronounced NTC autoignition behaviour and those exhibiting notionally single-stage ignition could be attributed to the availability of a chain of at least 3 adjacent, secondary or tertiary carbons within the structure of the molecule. In this study, quantum mechanical molecular modelling techniques were employed to quantify the activation energy barrier of the first internal hydrogen abstraction, as it was postulated that the formation of this first cyclic transition state would most probably be the rate-determining step in the whole sequence of low-temperature oxidation reactions that are associated with two-stage ignition (NTC behaviour). The aim was also to correlate the energy barrier of the transition state to the NTC index of the molecule, as it was suspected that there could be a direct link. If this correlation could be established, then quantum mechanically based molecular modelling could in principle be used to illuminate the NTC character of molecules for which no measured octane data exists. A survey of the literature also indicated that very few previous studies exist where molecular modelling techniques were applied to the study of autoignition or octane numbers of gasoline fuel molecules (no studies specific to octane numbers could actually be found). The only previous DFT studies on autoignition that could be found in the literature, were focused exclusively on correlating cetane numbers with molecular structure (El Marrouni et al., 2004; Abou-Rachid et al., 2003 and Yonei et al., 2003).

4.3.1 Molecular modelling results

As has become customary in gasoline research, the first fuel molecule that was studied was iso-octane, as it is the PRF with a defined RON (and MON) of 100.

4.3.1.1 Case study #1: iso-octane

The paper by Leppard and co-workers (Roberts et al., 1996) was used as a guide with respect to the nomenclature by which the 4 distinguishable alkyl radicals of iso-octane are named. Thus the first oxygen addition can take place on Sites a, b, c or d. These sites are indicated in the following graphical representation, taken from Roberts et al. (1996).

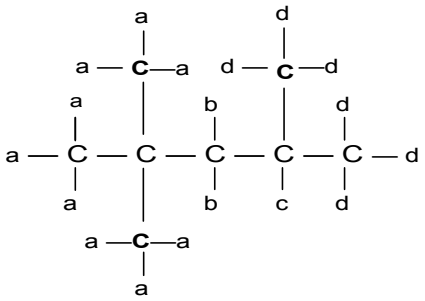

Figure 4.2: Distinguishable H atom sites in iso-octane molecule (Roberts et al., 1996)

It is implicitly assumed that each of the 9 hydrogen atoms that are designated to be attached at "a" sites, are absolutely equivalent to one another. Since it is also assumed that each of the methyl groups can rotate freely on its C-C bond axis, the first assumption may be valid, but from a quantum mechanical point of view it is understood to be a simplification only.

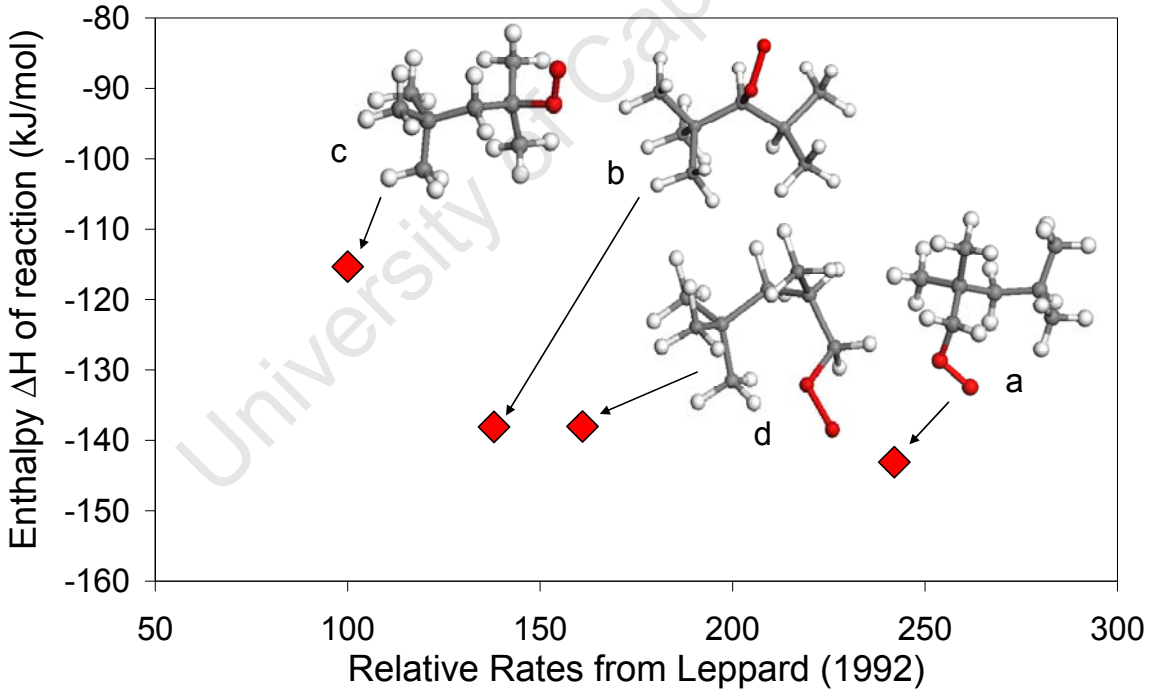

Figure 4.3: DMol3 calculated enthalpy of reaction for oxygen addition reactions to the 4 different free radicals from iso-octane, compared to their relative rates at 850 K (Leppard, 1992, and Roberts et al., 1996)

The enthalpy of reaction (for the generalized reaction $\cdot R + O_2 \leftrightarrows RO_2\cdot$), as calculated by the DMol[3] software at conditions of 0 K in a vacuum, is indicated in Figure 4.3. Logically, (based on the Evans-Polanyi relationship, as described by Dean, (2001))

the reaction with the largest (negative) enthalpy ΔH (implying the most exothermic) corresponded with the one to which Leppard (1992) had assigned the largest relative rate, whereas the reaction with the smallest negative ΔH exhibited the slowest rate. Note that these are relative rates, as calculated by Leppard at 850 K, and are dimensionless since the slowest rate (O_2 addition to site ***c***) is defined as 100 (Roberts et al., 1996). Relative to that, the fastest reaction (O_2 addition to site ***a***) is more than twice as fast at a relative rate of 242 (Roberts et al., 1996).

As the iso-octane free radical ***a***, having lost the H atom at any of the equivalent sites indicated as ***a*** in Figure 4.2, is being formed at the largest relative rate (242) according to Leppard (1992), the peroxy species with the oxygen at site ***a*** has been evaluated in the subsequent transitions state searches. The internal hydrogen abstraction by the alkylperoxy species of H atoms from each of the 4 different sites was evaluated. The energy of the optimized transition state was calculated in each case to obtain the activation energy of the internal hydrogen abstraction, as are shown in Figures 4.4 to 4.7.

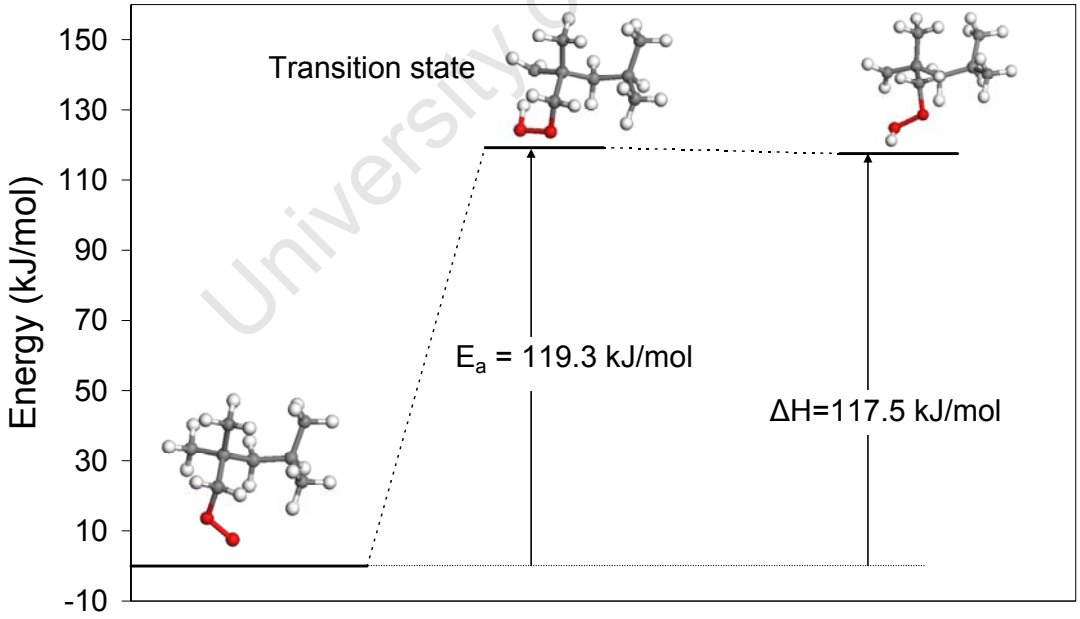

Figure 4.4: Activation energy barrier and Enthalpy of reaction for iso-octane radical "a" with Site a

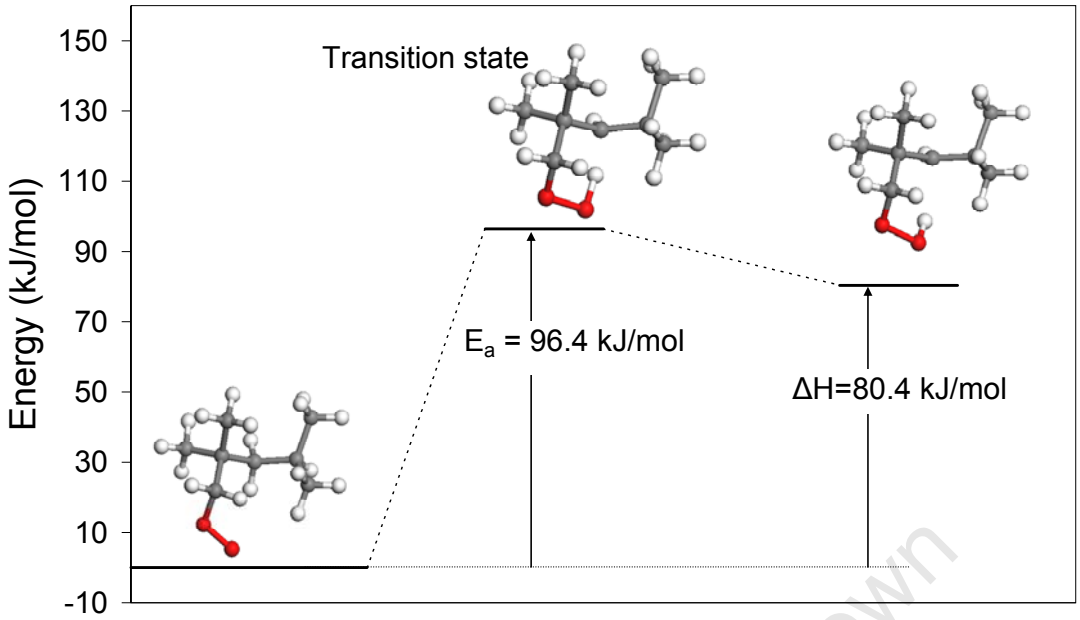

Figure 4.5: Activation energy barrier and Enthalpy of reaction for iso-octane radical "a" with Site b

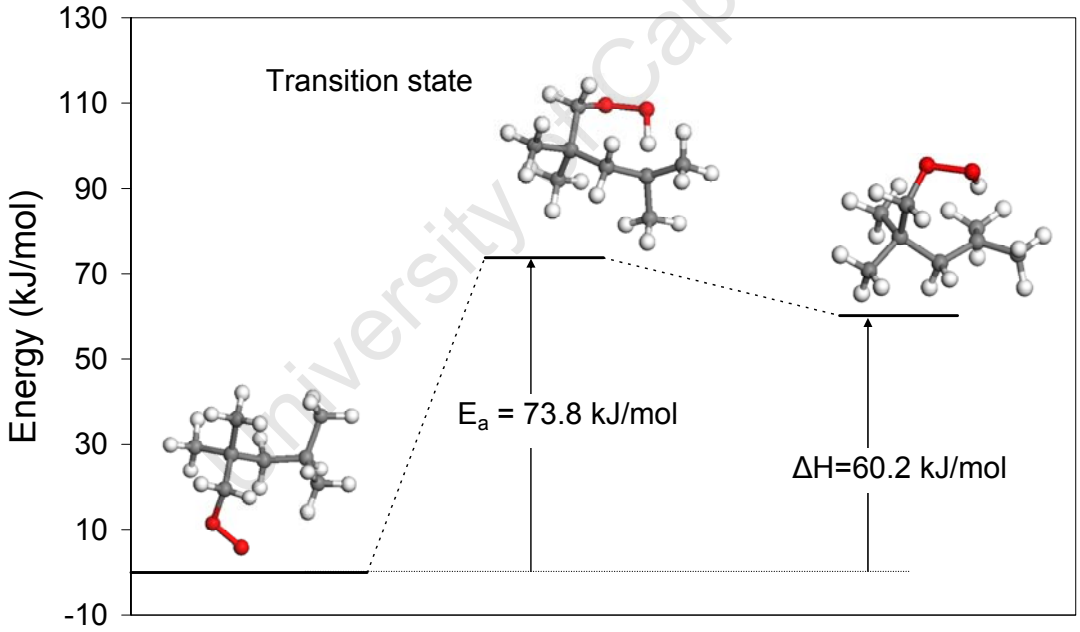

Figure 4.6: Activation energy barrier and Enthalpy of reaction for iso-octane radical "a" with Site c

In Figure 4.6 the activation energy of the transition state is shown as 73.8 kJ/mol, which was the lowest of the four scenarios. This would suggest that this pathway is kinetically more favoured than any of the other three. It is consistent with the relative rate which Leppard (1992) have attributed to this reaction, being the largest at a relative value of 202. These are relative rates for the internal hydrogen abstractions

that can be effected by the peroxy radical which was formed upon oxygen addition to site ***a***.

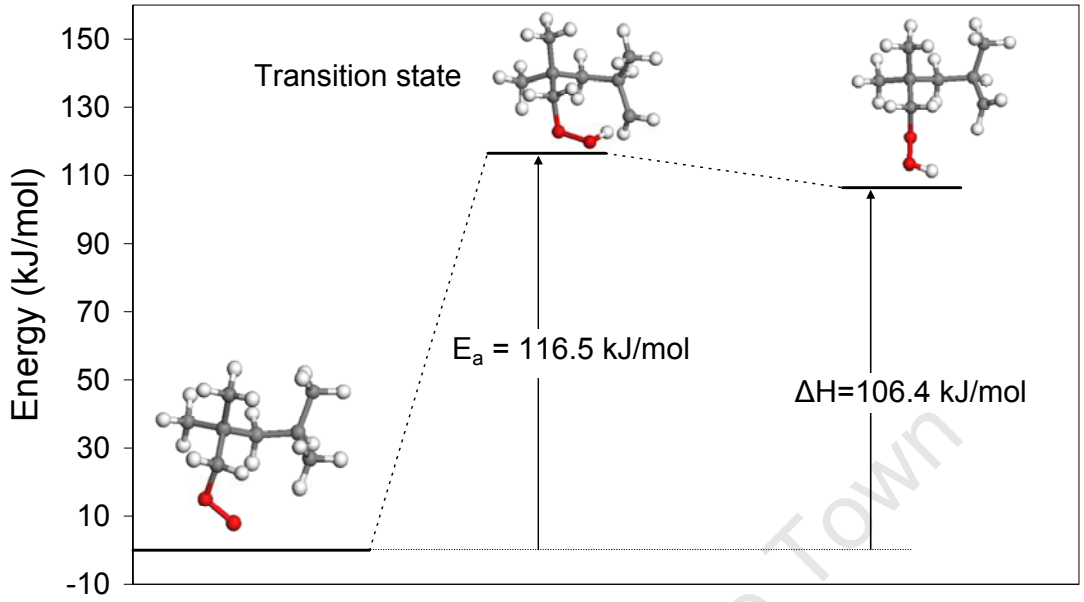

Figure 4.7: Activation energy barrier and Enthalpy of reaction for iso-octane radical "a" with Site d.

As indicated by Roberts et al. (1996) in their Figure 6, the relative rates calculated by Leppard (1992) varied from the slowest (abstraction from site ***d*** at taken as 1.0), from site ***a*** at relative rate of 2.2, site ***b*** at 9.4 and site ***c*** the fastest at a relative rate of 202.

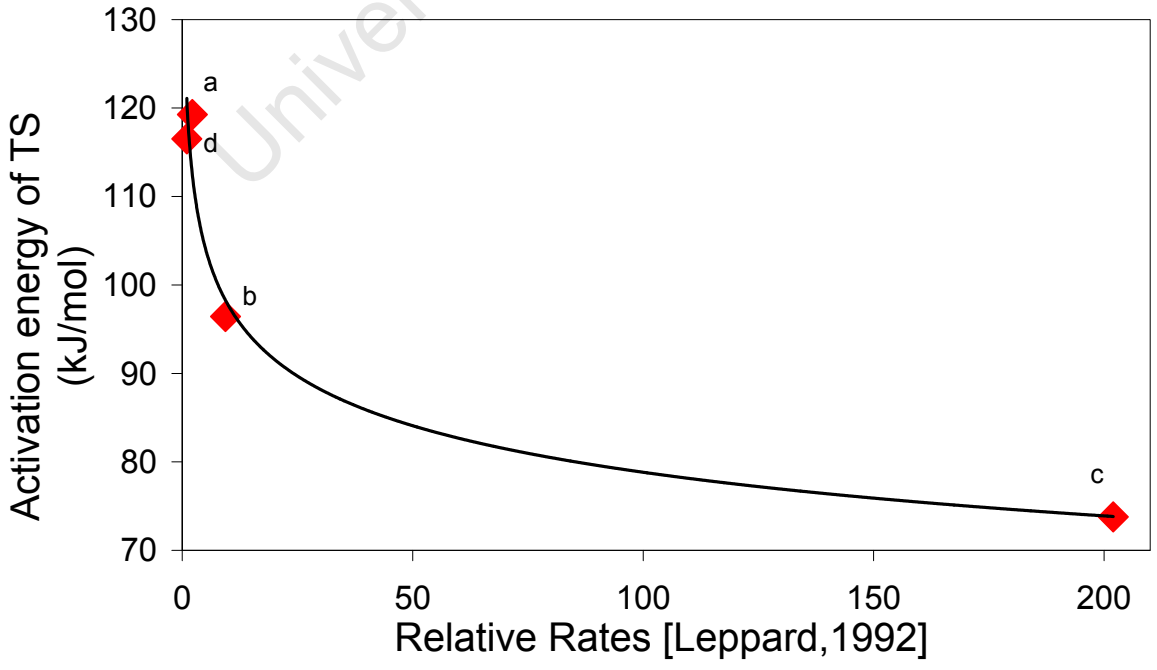

Figure 4.8: Correlation between Activation Energy (Ea) barrier of the TS calculated by DFT and relative rates from Leppard (1992) as reported in Roberts et al. (1996)

It has been shown in Figures 4.4 to 4.7 above that the internal hydrogen abstraction from all four sites is an endothermic process, and each pathway has an individual activation energy barrier to overcome, as would be expected from a rate determining step. The comparison shown in Figure 4.8 reveals the self-consistency between the activation energy barriers calculated by quantum mechanical means in this work, compared to relative rate constants that were obtained by the application of empirical thermochemical kinetics methods as those proposed by Benson (1976). The latter were based on group additive rules. The slow rates, associated with high activation energies, and the larger rates associated with smaller activation energies, are clearly exposed in the comparison shown in Figure 4.8.

4.3.1.2 Case study #2: Hexene Isomers

The second case study was a molecular modelling evaluation of the three different hexane isomers; 1-hexene, trans-2-hexene, and trans-3-hexene. These were compared in terms of their relative activation energy barriers upon formation of the 6-membered cyclic transition state during internal hydrogen abstraction.

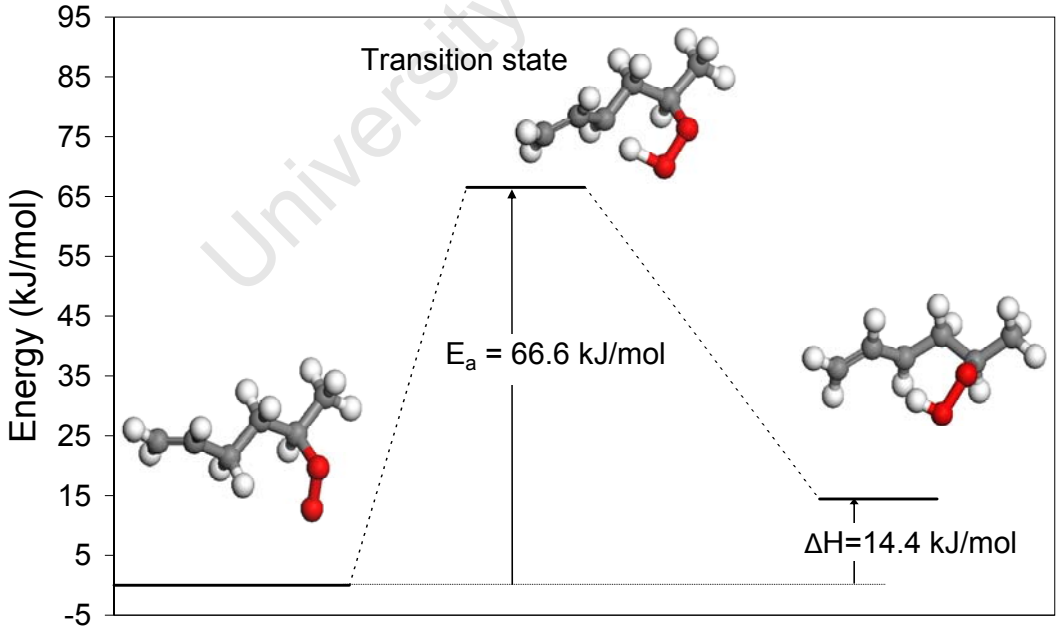

Figure 4.9: Activation energy barrier and Enthalpy of reaction for 1-Hexene, TS forming 6-membered ring

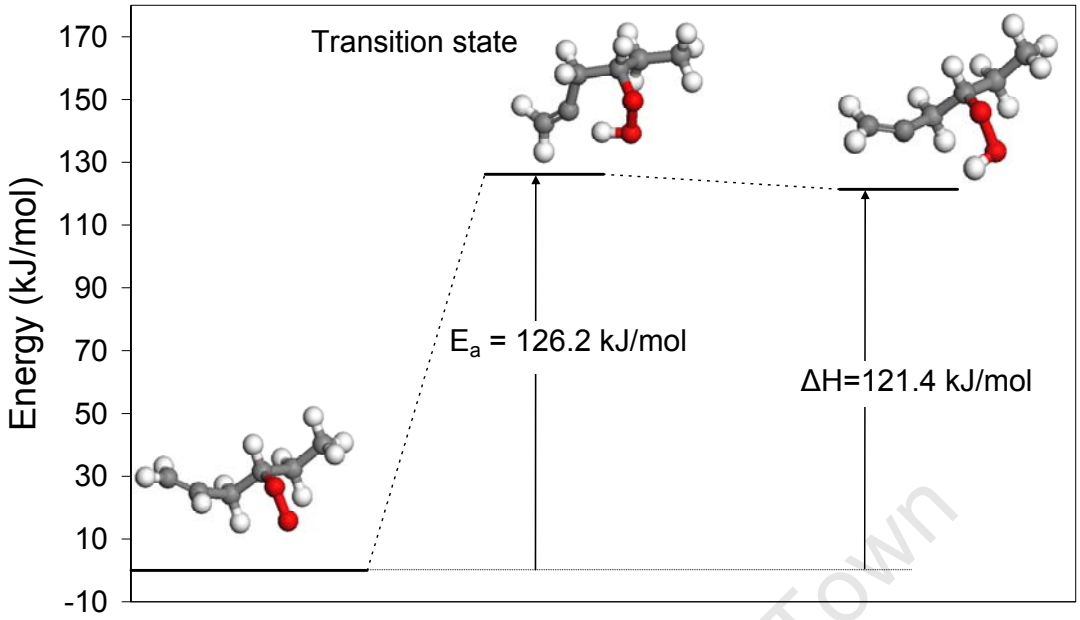

Figure 4.10: Activation energy barrier and Enthalpy of reaction for 1-Hexene when H is to be abstracted from the double bond

A comparison of Figures 4.9 and 4.10 indicates that the activation energy barrier is almost twice as high when the hydrogen is being abstracted from a carbon attached to the double bond itself, indicating that the pathway depicted in Figure 4.10 is not feasible at low-to-intermediate temperatures.

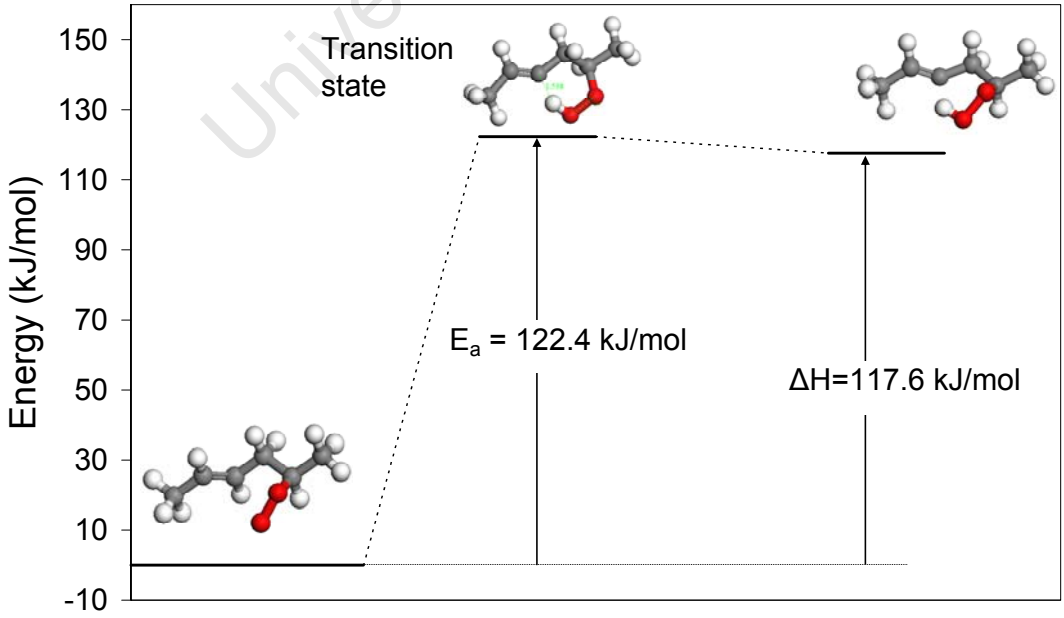

Figure 4.11: Activation energy barrier and Enthalpy of reaction for 2-Hexene when H is to be abstracted from the double bond

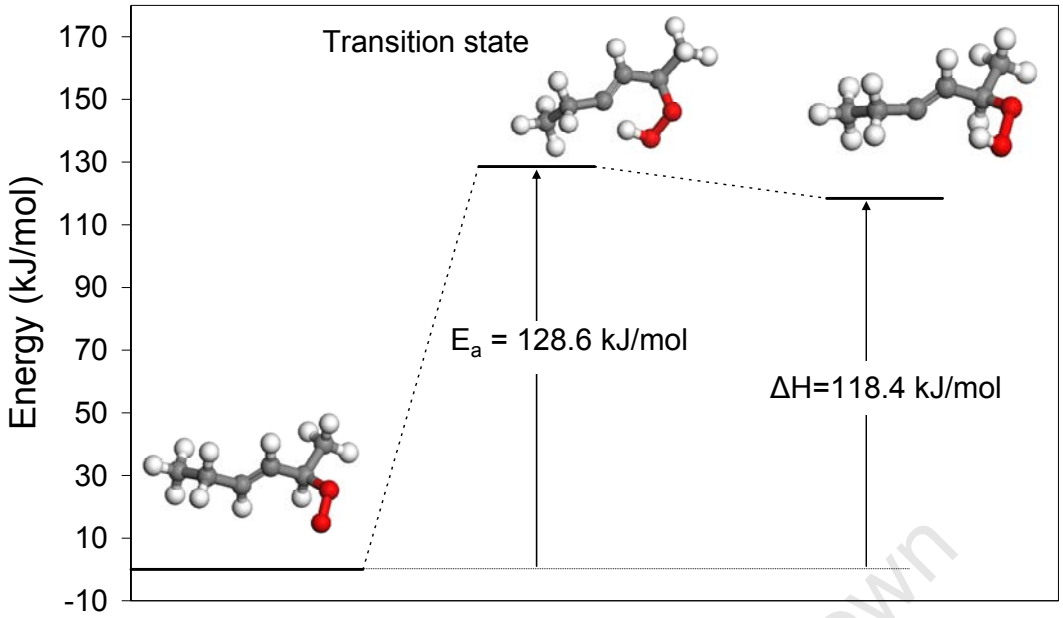

Figure 4.12: Activation energy barrier and Enthalpy of reaction for 3-Hexene when H is to be abstracted from the double bond

Figures 4.11 and 4.12 also indicate that the formation of 6-membered transition state rings are not feasible at low-to-intermediate temperatures, which is in agreement with the classification in Vanhove et al. (2005) of these two olefins as having less NTC character than 1-hexene (Viljoen et al., 2007).

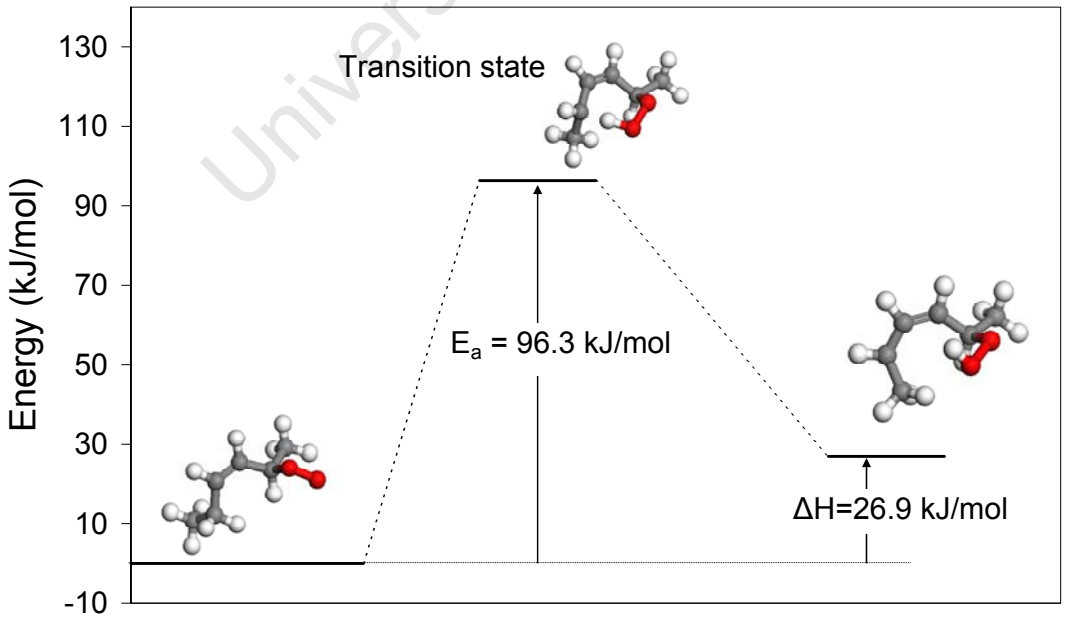

Figure 4.13: Activation energy barrier and Enthalpy of reaction for 3-Hexene when TS is forming a 8-membered ring across the double bond

The formation of a 8-membered TS ring structure across the double bond in 3-hexene was also considered, and the resultant activation energy barrier is reduced, as shown in Figure 4.13. However, the added strain of having a double bond as part of the ring structure causes the barrier to be such that it is not a kinetically feasible pathway at lower temperatures.

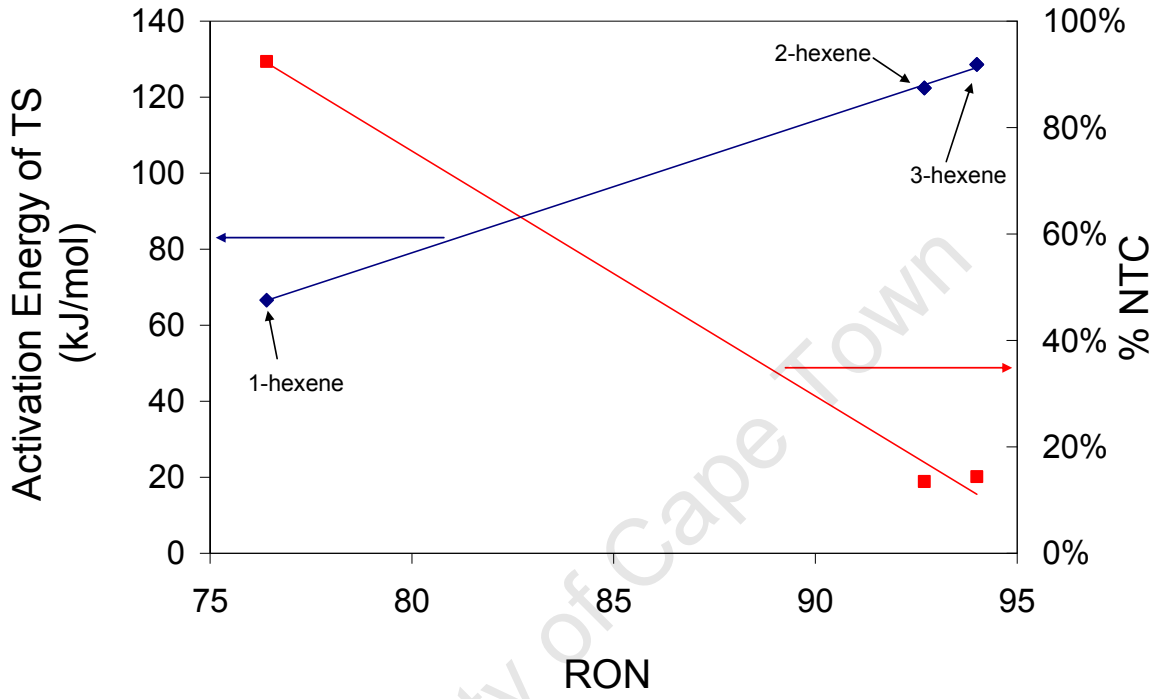

Figure 4.14: Correlation between activation energy barrier for hexene isomers and RON (literature values only available for the trans-isomers)

When the smallest activation energies of the three different olefins were plotted against their RON values, then an apparent linear trend emerged, as is shown in Figure 4.14. The slope of the line, going diagonally from the lower left to upper right, also conformed to the expected behaviour. The expectation would be that a low activation energy barrier would make low temperature oxidation pathways more feasible, leading to a low RON value, whereas a high activation energy barrier would be associated with resistance against oxidation and thus with a higher RON value. The % NTC, also shown in Figure 4.14, seemed to follow the same general trend, which is consistent with the previous discussion. A high % NTC value indicates easy two-stage ignition and many prevalent low temperature oxidation pathways, leading to low RON, and vice versa (Viljoen et al., 2007). The quantification of the % NTC values shown here are discussed in more detail in Chapter 5.

4.3.1.3 Case study #3: Toluene and ortho-xylene

The interesting comparison between these two aromatic molecules was discussed in an earlier paper (Viljoen et al., 2005), which noted that ortho-xylene exhibits significant NTC character, in contrast to toluene which possesses only high-temperature ignition chemistry.

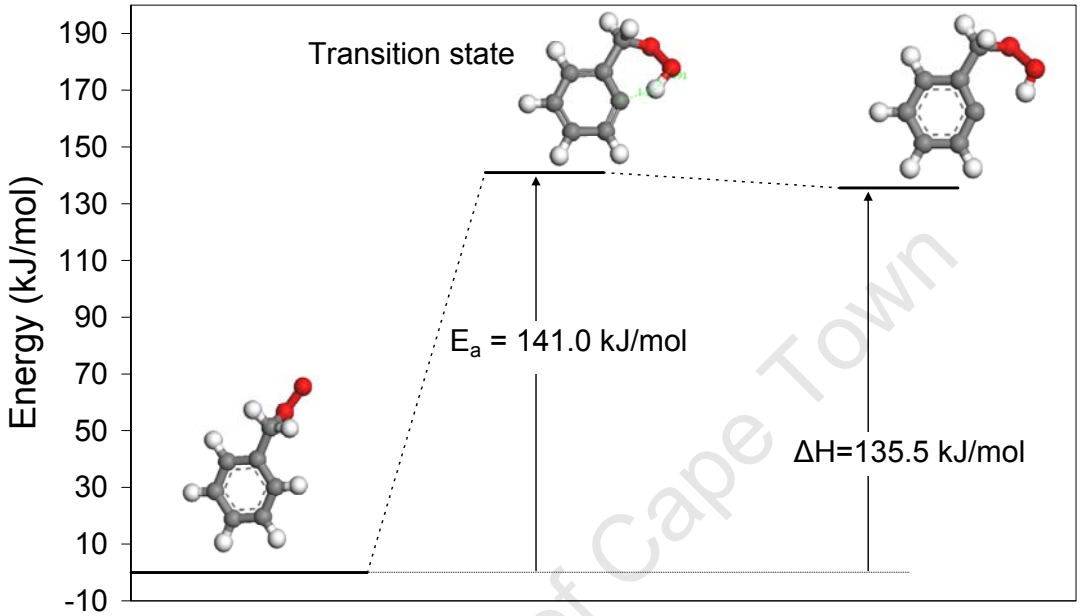

Figure 4.15: Activation energy barrier and Enthalpy of reaction for toluene

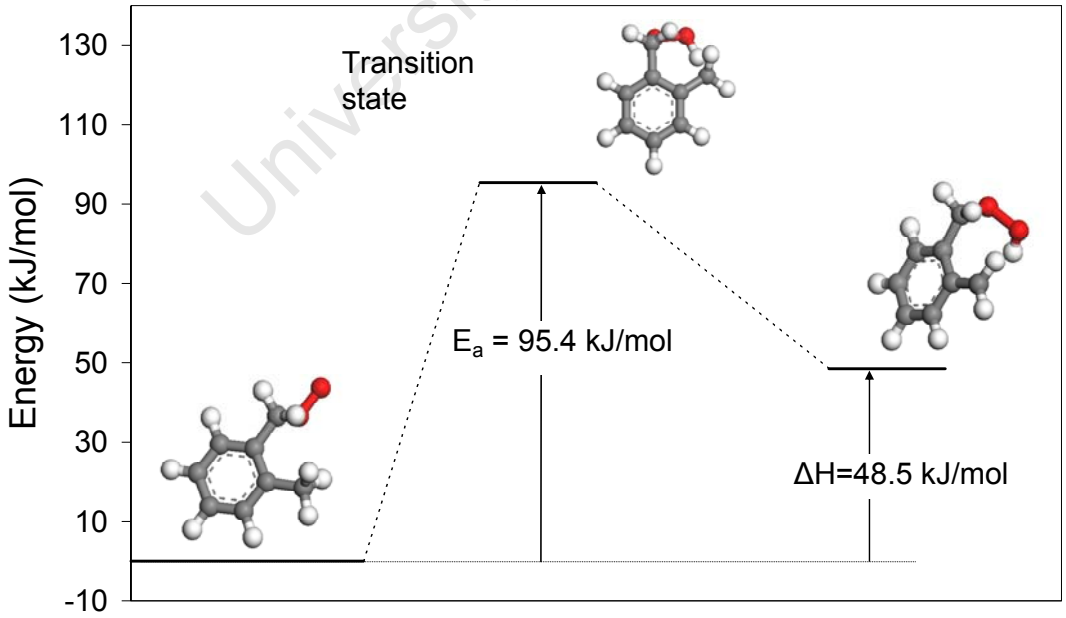

Figure 4.16: Activation energy barrier and Enthalpy of reaction for ortho-xylene, showing the feasibility of low-temperature chemistry, leading to its NTC characteristics

The quantum mechanically–derived activation energy barriers for the two molecules, evaluating only the cyclic transition state formed during the first internal hydrogen abstraction, are shown in Figures 4.15 and 4.16. The significant difference in the magnitude of the activation energies, corroborates the conclusion of Roubaud et al. (2000) regarding the accessible low temperature oxidation pathways which are available for ortho-xylene, but not for toluene. It is also noteworthy that the high RON value for toluene, accepted as 120.3 (from API Project 45 data), seems to correspond to the fact that it has higher activation energy for this reaction than any of the other molecules that were evaluated in this work.

4.3.1.4 Case study #4: Critical evaluation and comparison of two postulated oxidation mechanisms for n-heptane

During the course of this study, it was expected initially that DFT results should show the lowest energy barrier (for the first internal hydrogen abstraction reaction, also called internal isomerization) for the PRF having the lowest octane number, n-heptane (0). It soon became clear, however, that the notion that the lowest octane molecule should also have the lowest activation energy barrier was not supported by the results. The magnitude of the activation energy is determined more by the variation in C-H bond strengths between the various hydrogen atoms bound to primary, secondary and tertiary carbon atoms in the molecule, respectively. These are similar across different molecules, regardless of their octane values, as was borne out by the fact that E_a values in the range from 80-140 kJ/mol were obtained for the various n-heptane oxidation reaction pathways that were considered. Additional DFT calculations for a range of molecules from n-butane to n-hexane (not shown here), have confirmed that the activation energy for the abstraction of a secondary hydrogen through the formation of a 6-membered TS is largely independent of the carbon number of the specific paraffin. Values in the range of 75.7 kJ/mol (for the 2-4 abstraction in n-hexane) to 87.0 kJ/mol (for the 2-4 abstraction in n-pentane) were obtained. Interestingly, for n-butane the 1-3 abstraction gave a corresponding activation energy of 79.0 kJ/mol. These are all in good agreement with the more empirical group additivity-derived value of 88 kJ/mol for a similar transition state, as shown by Glaude et al. (2002).

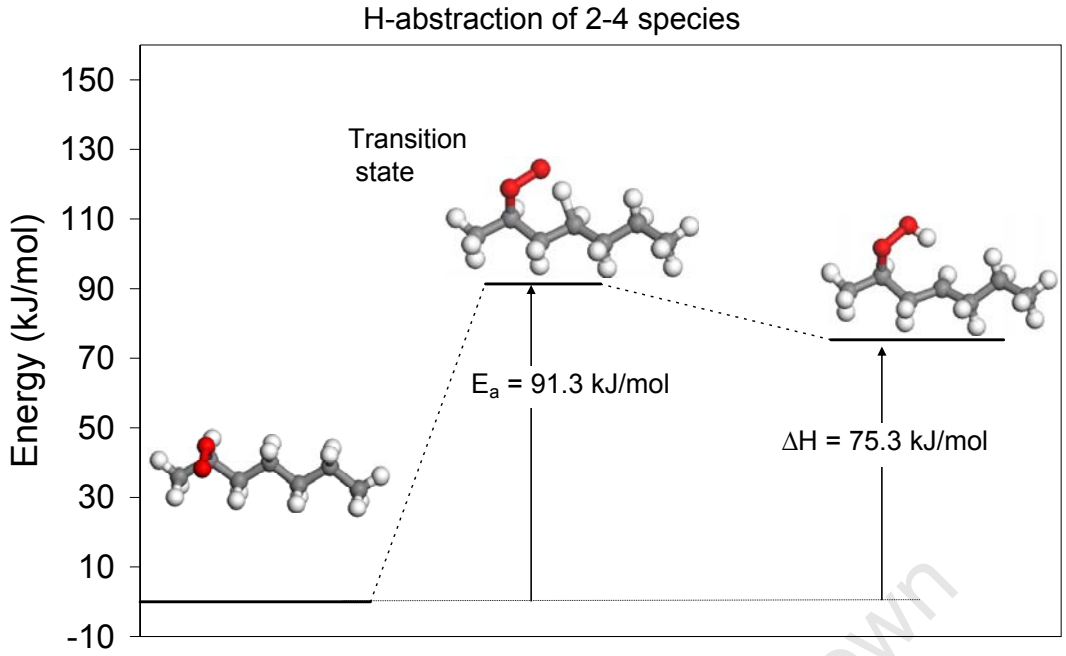

Figure 4.17: Activation energy barrier and Enthalpy of reaction for n-heptane, using the 2-4 abstraction pathway

Two examples are shown in Figure 4.17, above and Figure 4.18, below. These two are on the extremes of the range of activation energies that were determined for n-heptane. A large number of activation energies for some of the other possible pathways for n-heptane have also been calculated. These, having different ring sizes for the cyclic structure that must form during the internal hydrogen abstraction, are shown in Table 4.1.

Table 4.1: Various internal isomerization pathways for n-heptane that were modelled in this DFT study

n-Heptane oxidation species	Transition state (picture of optimised TS)	Ring size	E_a (kJ/mol)	ΔH (kJ/mol) of internal abstraction reaction
2-1 abstraction	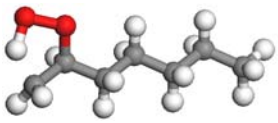	5 - membered	144.0	95.9
2-3 abstraction	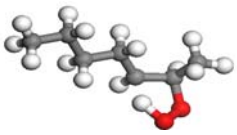	5 – membered	130.2	72.6
2-4 abstraction	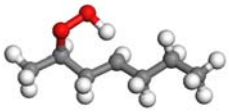	6 – membered	91.3	75.3
2-5 abstraction	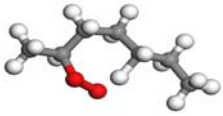	7 – membered	78.7	77.7
2-6 abstraction	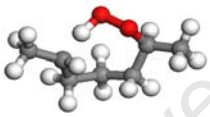	8 – membered	99.3	84.7

The abstraction of a hydrogen from a primary carbon is clearly more difficult than from a secondary carbon, as can be seen by a comparison of the 2-1 abstraction (shown in Fig. 4.18, below) to a 2-3 abstraction. Since both of these transition states are similarly strained 5-membered rings, the difference of 13.8 kJ/mol can be attributed to the difference in C-H bond strengths. This is in good agreement with the group additivity derived difference of 13 kJ/mol in the energy barrier that needs to be overcome in abstracting a secondary hydrogen vs. the abstraction of a primary hydrogen (71 kJ/mol vs. 84 kJ/mol, as tabulated by Glaude et al. (2002)).

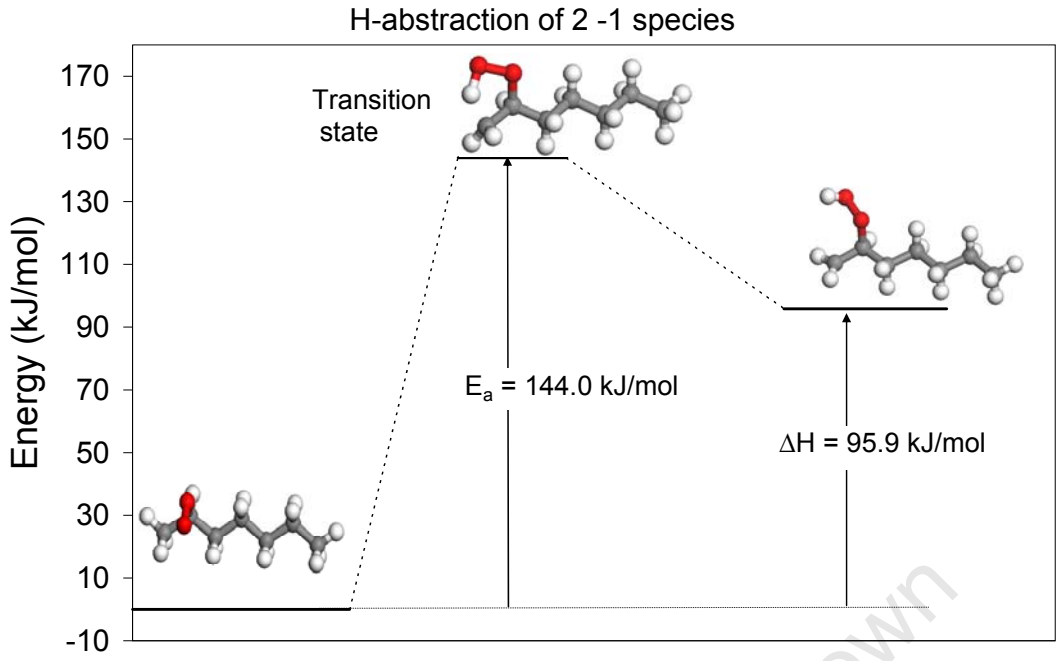

Figure 4.18: Activation energy barrier and Enthalpy of reaction for n-heptane, using the 2-1 abstraction pathway

The very high activation energy obtained during the 2-1 abstraction pathway can be understood if one considers that a primary hydrogen has to be abstracted from the terminal carbon atom in the chain. It is interesting that the magnitude of this energy barrier is comparable to the value obtained when abstracting an aromatic hydrogen from toluene (see Figure 4.15). This is surely an indication that the choice of the 2-1 species as being representative of all the possible intermediates for n-heptane in most of the skeletal mechanisms for surrogate gasolines, as made by Golovitchev and Ogink (2003), Machrafi et al. (2009), and Huang et al. (2008), is unfortunate. The choice of the heptane (2-4) abstraction pathway and oxidation mechanism would have been more appropriate and far more chemically defensible.

This becomes clear when the full low temperature oxidation pathway is considered and compared for the two mechanistic routes. These are shown in Figures 4.19 and 4.20, below.

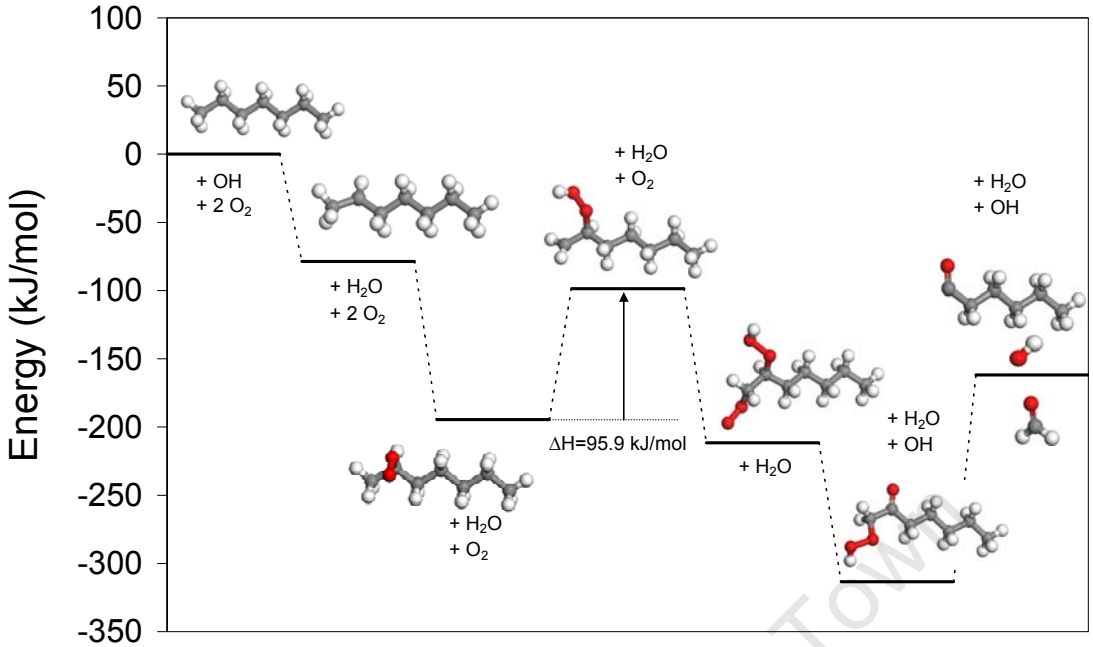

Figure 4.19: Energy diagram for the successive low temperature oxidation steps of n-heptane, leading to the dissociation of nC7ket21

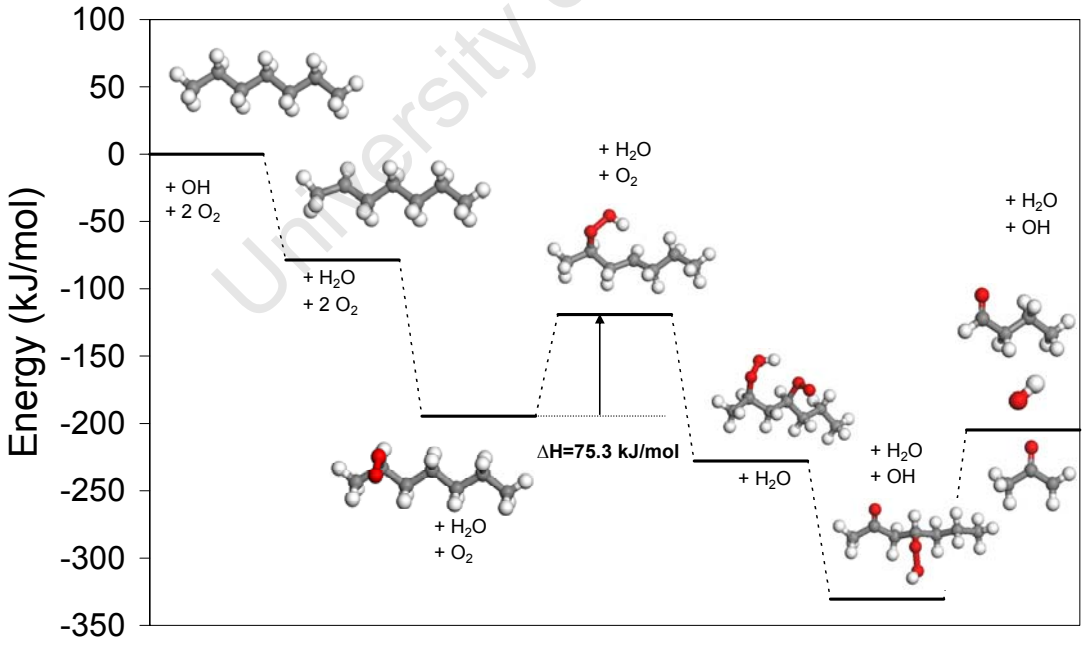

Figure 4.20: Energy diagram for the successive low temperature oxidation steps of n-heptane, leading to the dissociation of nC7ket24

In both Figures 4.19 and 4.20 only the stable intermediates are shown, according to the reaction steps as outlined in the skeletal mechanism postulated by Machrafi et al.

(2009). This means that the transition states identified earlier in Figures 4.17 and 4.18, respectively, are not shown explicitly between the 3rd and the 4th stable intermediates (or, stated differently, during the course of Step 3 in the mechanisms). In order to compare the two mechanisms more easily, these transition states were included in Figure 4.21, which is a combination of the previously mentioned four graphs. From Figure 4.21 it is clear that the 2-4 mechanism is favoured above the 2-1 mechanism for two obvious reasons. Not only is the energy barrier that has to be overcome in the formation of the TS significantly reduced in the case of the 2-4 internal hydrogen abstraction, the overall energy balance in going from the RO_2• species, through the dissociation of the respective ketohydroperoxides (nC7ket21 vs nC7ket24) to the •OH and aldehyde or ketone products, is slightly exothermic (-10.3 kJ/mol). In the case of the 2-1 mechanism, on the other hand, this step is endothermic (by + 32.7 kJ/mol) and therefore thermodynamically and kinetically less favoured. This provides further motivation for the deduction that the 2-4 mechanism would have been a more appropriate choice for the single representative skeletal mechanism than the 2-1 mechanism. The latter was originally chosen somewhat arbitrarily by Golovitchev (Ogink and Golovitchev, 2001) for the reduced n-heptane mechanism that has subsequently become known as the Chalmers mechanism.

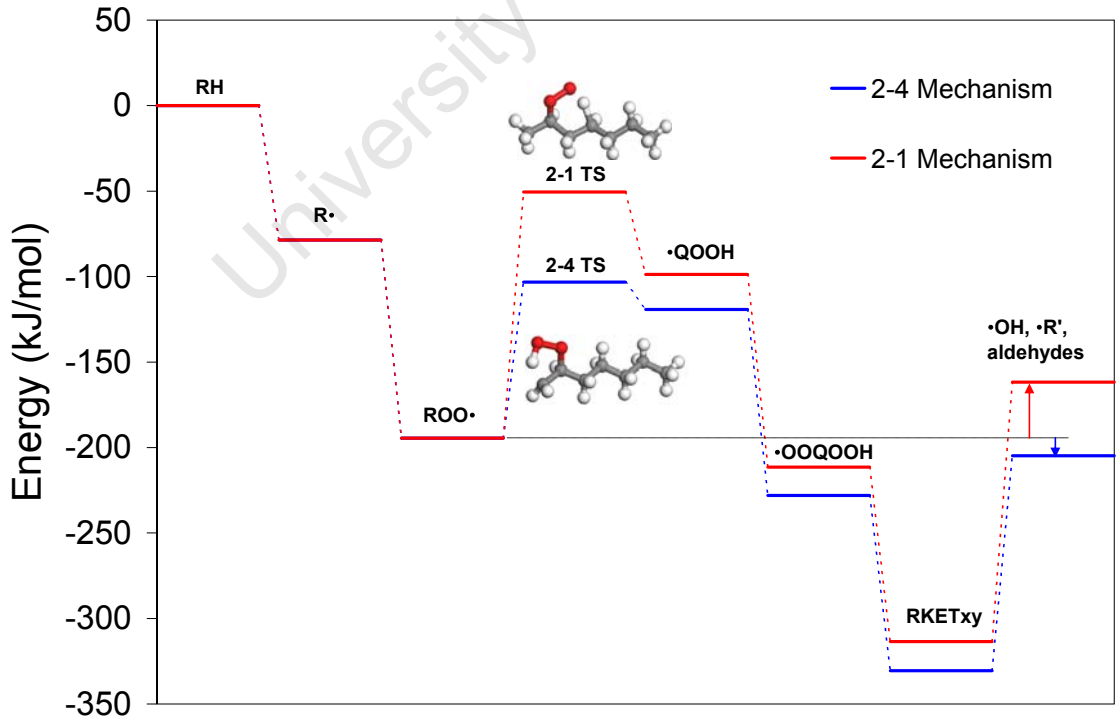

Figure 4.21: Energy diagram comparing the 2 skeletal mechanisms for n-heptane

It is interesting to note in the literature that many workers have chosen a preferred oxidation pathway in a reduced or skeletal mechanism, without providing any motivation or substantiating evidence for their choice. A recent example is the reduced mechanism for n-heptane by Zheng and Yao (2007), where only the 3-5 internal hydrogen abstraction is considered, leading to the eventual dissociation of nC7ket35 at the point of cool flame heat release. Another recent paper by Lu and Law (2008), dealing with mechanism reduction strategies by application of computational singular perturbation (CSP), identifies only three mechanistic pathways of importance for the low temperature oxidation of n-heptane. These are only the ones passing through 6-membered cyclic transition states leading to the following three ketohydroperoxides: nC7ket24, nC7ket35, and nC7ket42. It can probably be expected that in reality, each of the 6-membered transition states which involves the abstraction of a secondary hydrogen will occur to a comparable extent, making little difference whether it is the 2-4 or the 3-5 abstraction mechanism. It does matter, however, whether the 2-1 or the 2-4 mechanism is used as a skeletal mechanism that has to represent all the low temperature pathways for n-heptane, as there are significant differences in the total activation energy barrier, which can be taken as the sum of the activation energy for the H-abstraction (E_{abs}) and the strain energy of the cyclic TS (E_{cycle}) (Glaude et al., 2002).

4.4 Discussion of Results

It is important to note that DFT has been used successfully (as described in the preceding section) to quantify the difference between the kinetically unfavourable (2-1) mechanism: E_a =144.0 kJ/mol (from Figure 4.18) and the more energetically favourable (2-4) mechanism: E_a = 91.3 kJ/mol (from Figure 4.17). Since the accuracy of DFT calculations are estimated to be in the order of ±10 kJ/mol (Delley (2000), reported an average absolute deviation of 6.6 kJ/mol for a dataset of 148 test molecules), this observed difference is considered to be significant and an indication that the (2-4) pathway is the more chemically defensible one.

These DFT-derived values compare favourably with the empirically derived numbers (based on group additivity rules by Benson (1976)), as published by Glaude et al. (2002), according to which:

$E_a = E_{abs} + E_{cycle}$ for the (2-1) mechanism will be:

E_a = (84 + 65) kJ/mol = 149 kJ/mol.

Similarly, for the (2-4) mechanism;

E_a = (71 + 35) kJ/mol = 106 kJ/mol.

Interestingly, the values shown by Glaude et al. (2002) indicate that the ring strain for the TS that contains 7 atoms, is lower at 21 kJ/mol than for the 6-membered ring (E_{cycle} = 35 kJ/mol), with the 8-membered ring the lowest at only 17 kJ/mol. Thus it should not be unexpected that the DFT result for the 7-membered ring (see the 2-5 mechanism in Table 4.1) showed a lower activation energy than that obtained for the 2-4 mechanism. In Figure 4.22 a parity plot is shown which relates DFT results for n-heptane to similar calculations based on the group and bond additivity methods proposed by Benson (1976), as tabulated by Glaude et al. (2002).

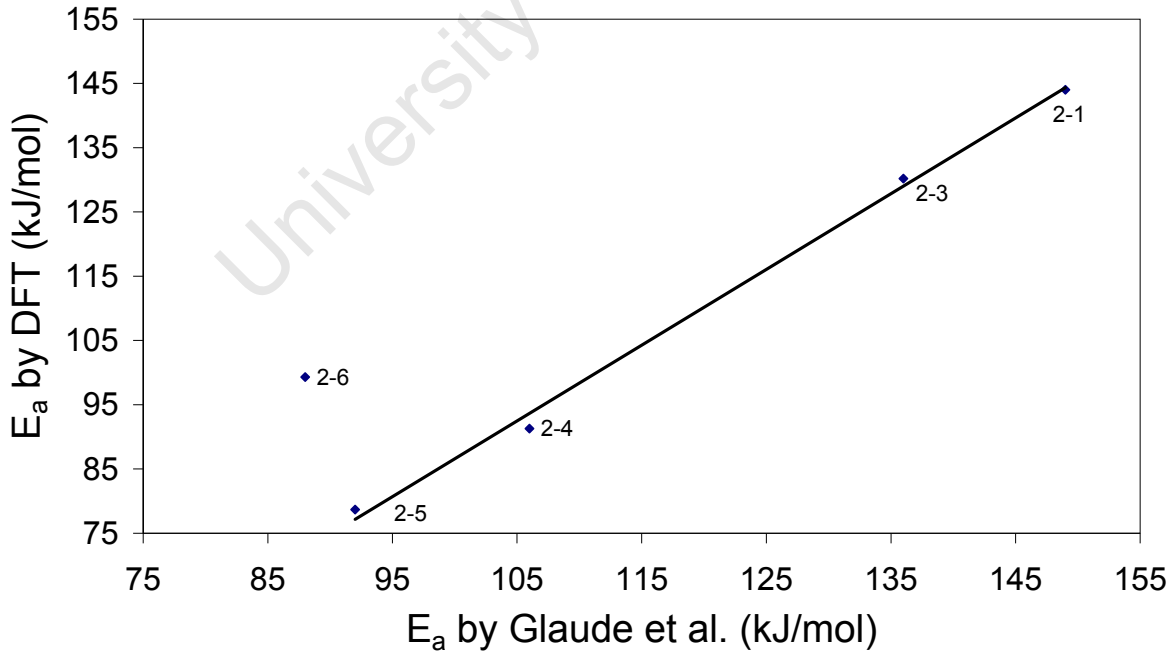

Figure 4.22: Comparison of E_a for various abstraction pathways for n-heptane, calculated by DFT and by Benson's additivity methods

It is clear that the DFT value calculated for the (2-6) mechanism is too high, thus it is shown as an outlier in Figure 4.22. After several attempts, starting from different geometries, this was the lowest value that could be obtained. Apart from this, there is satisfactory correlation between the two methodologies, especially if it is borne in mind that the DFT numbers were calculated under conditions of 0 K in an absolute vacuum. Even under these somewhat unrealistic conditions, DFT calculations have been shown to be able to differentiate successfully between comparable mechanistic pathways. A good example of this discrimination is shown by Figure 4.21, where the lower energy pathway is presented by the 2-4 mechanism.

A further important deduction based on Figure 4.21, is that DFT provides support for the common assumption that the rate determining step in the sequence of oxidation reactions that occurs during the low-to-intermediate-temperature regime in hydrocarbon fuels, is the internal hydrogen abstraction by ROO• to form the hydroperoxide radical, •QOOH, and not any of the subsequent reaction steps. This is in agreement with Glaude et al. (2002), who stated that at low temperatures, the reactivity of a PRF mixture is directly related to the amount of peroxides formed from the two reactants, and that the primary initiations (i.e. the formation of the •R radicals) have no kinetic effect. This is in direct contrast to El Marrouni et al. (2004), who found a correlation between the activation energy for the reaction between O_2 and small alkanes, to produce the initial alkyl radical, with the cetane number of those molecules. Since cetane numbers of -60 (ethane), -20 (propane) and 10 (butane) are not experimentally measurable, their conclusions must be treated with caution.

The most important energy barrier, representing the rate determining step, is clearly visible in the middle of Figure 4.21, following the essentially barrierless addition of O_2 to •R in the preceding step. This provides further support to the original postulate made in this study, where the NTC character of a specific molecule was associated with its propensity to undergo the internal hydrogen abstraction in an accessible, low-energy pathway.

The approach of relating the activation energy of the first internal hydrogen abstraction to octane number was considered in this work only for pure molecules. Its extension to blends (such as in PRFs) remains challenging, as the minimum

activation energy barrier would remain the same for all systems that contain n-heptane, but as the ratio of n-heptane to iso-octane decreases, RON increases. Thus the pre-exponential factor, A (incorporating the collision frequency or reaction path degeneracy) has to be included in any such discussion, but unfortunately DFT calculations do not provide access to quantitative information about A. It is known, however, that the PRFs only interact with one another via the pool of small labile free radical species (Leppard, 1992) that form much later in the sequence of oxidation reactions, not in the early reaction step considered here (Curran et al., 1998).

On the other hand, for molecules of similar sizes, such as the different isomers of hexene, it can be assumed that A will be relatively constant among the group, and thus NTC can be associated with the activation energy of the rate determining step. This may be the reason why a rudimentary correlation between E_a and octane could be seen in Figure 4.14. Unfortunately, no simple correlation between the E_a of the rate determining step of the low temperature oxidation sequence, for different molecules (e.g. n-heptane and iso-octane), and their octane numbers, could be found. This makes the application of DFT calculations to find a link between NTC character and octane prediction, rather dubious.

4.5 Conclusions

The conclusions that were reached by application of Density Functional Theory to the investigation of NTC character of selected fuel molecules can be summarised as follows:

- Although quantum mechanics - based molecular modelling techniques, such as Density Functional Theory, provided a new tool to gain fundamental insight into the autoignition properties of fuel molecules, the direct application thereof to octane prediction is not feasible.

- The DFT results are directionally consistent with empirically-based reaction rates that are commonly used in autoignition research. In particular, very good agreement was obtained between the DFT results and the group and bond additivity methodology of Benson (1976).

- In general, the activation energies for the first internal hydrogen abstraction, have confirmed this to be the appropriate rate-determining step, as this step was shown to be the determining step between single stage molecules and those having NTC character (e.g. toluene vs. ortho-xylene).

- Further work is necessary to address the realization that the magnitude of energy barriers (which can be quantified relatively easily by means of DFT) do not contain enough information to correlate with the NTC character of the molecule or their octane numbers.

- The preferred application of DFT, based on the outcome of this study, would be in the comparison of alternative reaction mechanisms with each other to find the lowest energy pathways. This was shown in the comparison of the 2-4 mechanism of n-heptane with its “equivalent” 2-1 mechanism. This ability of DFT can be put to very good use in the construction of reduced or skeletal mechanisms, to ensure that these remain chemically meaningful.

Chapter 5 : Empirical Modelling with Fundamental Insights applied to Octane Prediction

5.1 Introduction

It has been stated earlier that commercial gasoline fuels are complex mixtures of several hundreds of different types of fuel molecules. The actual octane numbers of gasoline mixtures (or blends of different gasoline component streams) is of great economic importance to fuel refineries, very often determining whether the refinery is making a profit or not. Thus there has always been great interest in the development of empirical equations with which gasoline blends' octane numbers could be predicted to a high degree of accuracy.

In practice, this means the prediction can only be as accurate as the repeatability of the test methods. The repeatability, *r*, is defined as: *"The difference between two test results, obtained on identical test samples under repeatability conditions (the same operator using the same instrument to analyse the same sample) would, in the long run, in the normal and correct operation of the test method, exceed r only in one case in twenty."* (ASTM D2699, 2007). For RON (Research Octane Number) measurements according to ASTM D2699, the repeatability is 0.2 RON (in the range of 90 - 100 RON), whereas for MON (Motor Octane Number) determinations in conformance to ASTM D2700, the repeatability is also 0.2 MON (in the equivalent range of 80 - 90 MON).

The reproducibility of both methods is much larger; it is defined (for the RON method, in the range from 90 -100 RON) as: *"The difference between two single and independent results obtained on identical test samples under reproducibility conditions would, in the long run, in the normal and correct operation of the test method, exceed 0.7 ON only in one case in twenty."* (ASTM D2699, 2007). The equivalent value for MON (in the range of 80 - 90 MON), is 0.9 ON (ASTM D2700, 2007).

Blending studies always involve more than one sample, and often more than one operator running the CFR engines. Therefore the standard deviation of the reproducibility is a more appropriate precision target for the accuracy of the blend prediction equations (Leonpacher, 1981). For RON values lying between 90 and 100 Research ON, the reproducibility standard deviation is 0.25, unaffected by octane level (ASTM D2699, 2007). This is indicated by Figure 5.1, below.

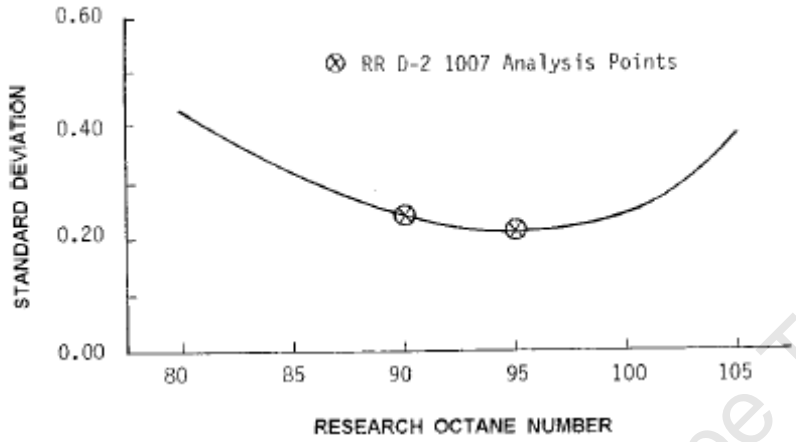

Figure 5.1: Variation of Reproducibility Standard Deviation with Research Octane Number, as displayed in ASTM D2699 (2007)

For the prediction of MON, the reproducibility standard deviation is considered to be the practical limit of precision that can be reached by the blending equation. ASTM Method D2700 (2007) states: *"Between 80 and 90 Motor ON, the reproducibility standard deviation is 0.34 unaffected by octane level."* This is also shown by Figure 5.2, taken from ASTM D2700 (2007).

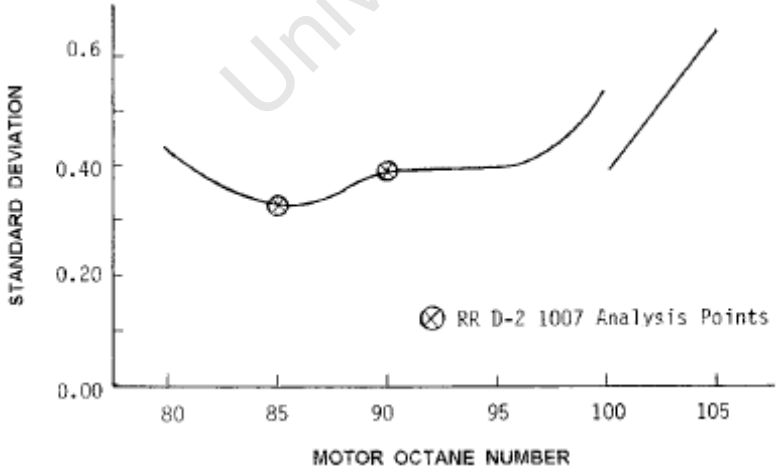

Figure 5.2 : Variation of Reproducibility Standard Deviation with Motor Octane Number, ASTM D2700 (2007)

The linear paraffin, n-heptane, has an equal RON and MON value, defined to be 0.0 on Edgar's scale, while the branched paraffin, iso-octane (2,2,4-trimethyl pentane) has a defined RON and MON value of 100.0. Also by definition, these two PRF molecules blend perfectly linear by volume. Thus a commercial FBR R95 gasoline is defined by the oil industry (based on Edgar's scale) to have an identical RON value to a PRF blend consisting of 95.0 vol.% iso-octane and 5.0 vol.% n-heptane. Similarly, the MON of the same FBR gasoline (being typically 10 numbers lower due to the increased severity of the MON test compared to the RON test) would be by definition equivalent to the MON of a PRF blend consisting of 85.0 vol.% iso-octane and 15.0 vol.% n-heptane. The sensitivity of the R95/M85 commercial gasoline, is defined as:

$$\text{Sensitivity} = \text{RON} - \text{MON} = 10 \qquad ...(5.1)$$

Its sensitivity does indicate, however, that this fuel cannot be equivalent to a PRF in all respects, as all possible PRF blends have a defined sensitivity of zero. This aspect also encapsulates the complexity of octane modelling, in the sense that real gasoline blends always have non-zero sensitivities, but they are being characterized by unrepresentative (insensitive) PRFs. Westbrook commented on this conundrum by describing octane measurements as being made by comparison to a skewed measuring stick. He explained it as follows: *"By defining octane numbers in terms of alkane fuel oxidation, non-linear and complex reaction paths are built into the rating scale, and non-alkane fuels with inherently simpler oxidation mechanisms appear, erroneously, to be unusual in their ignition properties"* (Westbrook et al., 1998).

5.2 History of Octane Modelling

It would be fair to say that the history of octane modelling is closely linked to the quest for finding higher octane fuels that was brought about by the higher compression ratio spark ignition (SI) aircraft engines used in fighter planes during the Second World War. The need for aviation gasoline (Avgas) of much higher octane (or anti-knock quality) than what was commonly available in the 1940's also led to the rapid development of new refinery processes during this time, all of which produced higher octane component streams than the straight run gasoline that was commonly used in land vehicles before the war (Ogston, 1981). Examples are the alkylation processes (commercialized in 1940) that produced more branched paraffins to

increase the octane of the gasoline pool, and the catalytic platinum-based reforming process, known as “Platforming”. The latter process was developed by UOP in 1949 (producing aromatic molecules from n-paraffins) and became the major octane-producing process in most refineries around the world. The integration of these ‘new’ refinery streams necessitated enhanced methods by which the final octane of an optimized blend could be predicted.

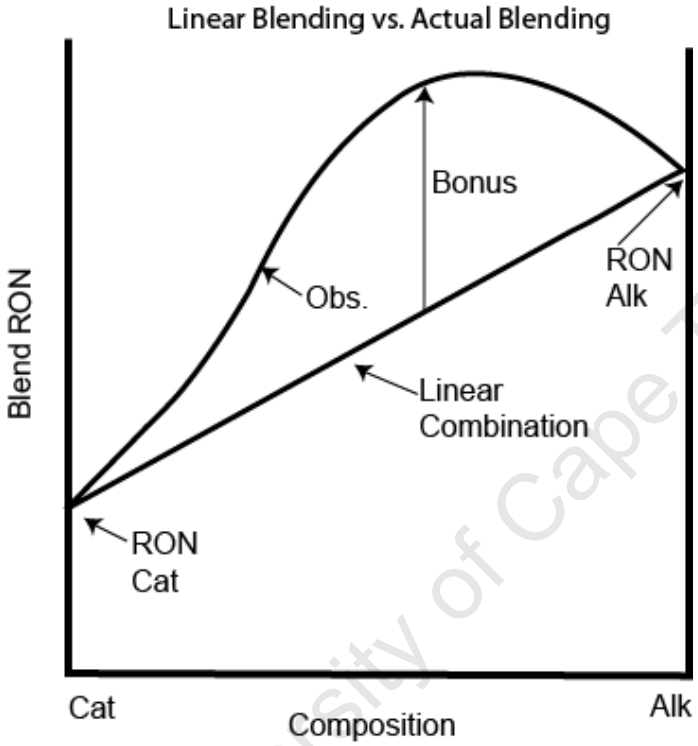

Figure 5.3: An early example of the non-linear blending behaviour of real gasoline streams, adapted from Leonpacher (1981). Cat is catalytically cracked petrol, and Alk is alkylate

Especially the advent of catalytically cracked petroleum streams in the mid 1930’s, made the industry realize that more accurate blending equations were needed. This is shown in Figure 5.3, which indicates the octane “bonus” effect that these olefin-rich streams had in blends with more paraffinic (being resembled better by PRFs) streams, such as Alkylate in this example.

5.2.1 Stewart’s Model

The non-linearity of the blending behaviour of typical gasoline streams, with specific reference to their octane numbers, has been described in a number of research investigations with varying success. A good example is the model proposed by Stewart, (1959), who developed an empirical correlation that was based only on the

measured octane numbers of the separate component streams and on their volumetric olefin contents. The correlation is expressed by the following equation:

$$ON_{Mix} = \frac{\sum_i V_i D_i (R_i + CP_i)}{\sum_i V_i D_i} \quad \ldots (5.2)$$

Where V_i = Volume of component *i* added to the blend, P_i = Olefin difference, $P_i = U_i - U_{mix}$, in volume%, with U_{mix} the linearly calculated (LBV) olefin content of the blend and U_i the olefin content of component *i*, D_i is a weighting factor, given by:

$$D_i = \frac{AP_i}{1 - e^{(-AP_i)}} \quad \ldots(5.3)$$

Where R_i = octane rating measured for component *i* by the given test method, RON or MON. Both *A* and *C* are regression constants, as obtained by Stewart through fitting the correlation to data consisting of a large set of different refinery blends. It is interesting to note that this correlation has been used in exactly this form for many years at Sasol Fuels Research. It seems to be quite accurate for olefinic fuels such as those produced from synthetic petrol as is being manufactured at the CTL complex in Secunda. Since it classifies aromatics together with paraffins (as non-olefins), even though the former group has high sensitivities and paraffins are known to be insensitive, it is clear that Stewart's correlation cannot be equally adequate under all circumstances (e.g. with blends having high concentrations of aromatics).

When Stewart's model was applied to the API Project 45 dataset (described later in Section 5.3.1), an average Standard Error (SE) of 4.14 RON units was obtained across the set of 154 ternary blends contained in the data. The SE in the MON predictions across the same dataset was only slightly better at 3.84 MON. Both predictions made use of the standard regression coefficients as published by Stewart (1959). When the regression coefficients were subsequently optimised by least squares regression, the RON Standard Error improved slightly to 3.91, while the SE in MON was reduced to 3.21 MON units. This level of accuracy is not considered to be adequate for use in practical blending scenarios.

5.2.2 Morris' and Healy's Models

Morris et al. (1975) developed an empirical octane blending methodology, which became known as the binary interaction coefficient model. The equation that they proposed to describe the nonlinear gasoline blending behaviour is as follows:

$$ON = x_1a_1 + x_2a_2 + b_{12}x_1x_2 \quad \ldots(5.4)$$

where a_i and x_i are the octane number and the volume fraction of component i, respectively and b_{12} is the binary interaction coefficient for components 1 and 2. This equation has been shown to be effective in correlating the octane numbers of gasoline blends, as it represents a simple excess octane number function, similar to other thermodynamic properties (e.g. excess molar volume). The disadvantages are that b_{12} is an empirical constant, depending on the characteristics of Components 1 and 2, as well as on their octane levels individually and the magnitude of the octane difference between them. The interaction coefficients are empirical constants that have to be determined experimentally. If a number of n components are to be blended, then a total of $\frac{n(n-1)}{2}$ interaction parameters are required, leading to a very expensive blending study. The binary interaction parameters, determined in such an experimental blending study, will remain valid only as long as there are no changes in stream compositions and provided no new streams are introduced to the pool of components (Twu and Coon, 1996).

The Stewart approach has been extended by other workers (e.g. Healy et al., 1959) to describe the non-linearity of blending not only in terms of the olefinicity, but also in terms of aromaticity, incorporating the squares of these entities in the equation as well. The sensitivity, or the difference between RON and MON, is also used extensively in the Healy et al. equations to account for the non-linear nature of refinery component stream blending (Healy et al., 1959).

The Healy equation for RON (also called the Ethyl RT-70 equation) is the following:

$$RON_{Blend} = \sum_{i=1}^{n} (P_i \times RBV_i) \quad \ldots(5.5)$$

With $RBV_i = R_i + a_1(R_i - \underline{R})(J_i - \underline{J}) + a_2(O_i - \underline{O})^2 + a_3(A_i - \underline{A})^2$ …(5.6)

In these two equations, the terms are defined as follows:

RBV_i is the RON blending value of Component *i*

P_i is the volume fraction of Component *i*

R_i is the RON_{clear} of component *i*

$\underline{R}$ is the volume averaged blend RON (in this thesis called the LBV value)

J_i is the sensitivity (RON – MON) of component *i*

$\underline{J}$ is the volume averaged sensitivity of the blend (of *n* components)

O_i is the olefin content in volume % of component *i*

$\underline{O}$ is the volume averaged olefin content of the blend (of *n* components)

A_i is the aromatics content in volume % of component *i*

$\underline{A}$ is the volume averaged aromatics content of the blend (of *n* components)

a_1, a_2 and a_3 are regression coefficients, with a_1= 0.03324, a_2 = 0.00085 and a_3 = 0 for unleaded fuels.

Similar equations were developed by Ethyl Corporation (Healy et al., 1959) for MON, using the same set of data of 135 blends:

$$MON_{Blend} = \sum_{i=1}^{n} (P_i \times MBV_i) \quad \text{…(5.7)}$$

Where MBV_i is the MON blending value of component *i* , given by the following equation (5.8):

$$MBV_i = M_i + b_1(M_i - \underline{M})(J_i - \underline{J}) + b_2(O_i - \underline{O})^2 + b_3\left[\frac{A_i - \underline{A}}{100}\right]^2 \quad \text{…(5.8)}$$

P_i is again the volume fraction of Component *i,* and the other parameters are as defined before, except for:

M_i which is the MON_{clear} of component *i* ,

$\underline{M}$ which is the volume averaged blend MON (the linear-by-volume value), and the regression coefficients b_1, b_2 and b_3 . For unleaded fuels, these are: b_1 = 0.04285, b_2 = 0.00066 and b_3 = -0.00632.

It is debateable whether these extensions and the increased complexity of the resultant equations did add significant benefit in increased accuracy when compared to the original Stewart equation. A brief comparison between the Stewart and Ethyl

methods on real FBR fuel blends made in our laboratory, indicated a slight advantage (~0.3 RON) in accuracy of the Ethyl equation with respect to RON, but the same magnitude of error from both methods for MON (~1.2 MON).

When the Ethyl method was implemented on the API dataset (shown in Appendix F), the SE for RON (using the regression coefficients as shown above, published by Healy et al. (1959)), was 4.36 RON. The SE for MON was a relatively poor 6.56 for the set of 154 ternary blends. When the Ethyl regression coefficients were optimised by least squares regression, the Standard Error for RON improved to 3.30 and for MON the SE improved to 2.43. This relatively poor accuracy is an indication that the Ethyl methodology is probably not suited for application to blends of pure compounds such as these, as it was originally developed for blends of FBR (and compositionally complex) refinery streams.

5.2.3 Twu and Coon's Model

In order to improve on the prediction accuracy of the Stewart (1959) model, Twu and Coon (1996) proposed a different binary interaction coefficient model, incorporating some of the concepts initially proposed by Morris (1975). This model utilized binary interaction coefficients between all the descriptors in the blend, i.e. between olefins, aromatics and saturates, for example, and was non-linear in the coefficients. In their original paper Twu and Coon assumed that the octane number of the descriptors in a blend had the same octane number as the blend itself. Twu and Coon (1997) improved this approach by adjusting the octane prediction such that the descriptors in the blend can have a different octane number than the blend itself. The modified binary interaction coefficient model, as proposed by Twu and Coon (1997) is discussed in the subsequent section.

The octane number, *a*, of a fuel is predicted by an equation with the general form:

$$a = \sum_i \sum_j x_i x_j a_{ij} \qquad ...(5.9)$$

where $a_{ij} = \frac{1}{2}(a_i + a_j)(1 - k_{ij})$ ...(5.10)

A binary interaction parameter, k_{ij} , is included in the blending correlation to correct the assumed mathematical average mean rule for the a_{ij} parameter in equation (5.9).

This binary interaction parameter represents the interaction between two descriptors within the same gasoline cut or blend. It is assumed that the binary interaction parameters, $k_{ij} = k_{ji}$, [so that they are perfectly symmetrical] and that equation (5.9) for the prediction of octane number is also symmetrical. Although Twu and Coon (1996) provided the expression for asymmetrical binary interaction coefficients as well, the symmetrical octane prediction was found to be sufficient for commercial fuel blends (Twu and Coon, 1997).

Laboratory analysis of gasoline blends, in general, usually includes results for RON, MON and olefins, aromatics and saturates, and some other physical properties of the fuel. In the Twu and Coon approach, olefins, aromatics and saturates were considered as "descriptors" and the fuel or fuel component stream was a mixture of these descriptors. Although the same name was given to the descriptors contained in different fuels, they were really different components because fuels are complicated mixtures, containing various types of aromatics, for example. An illustration of the significant distinction between two aromatic molecules, toluene and ortho-xylene, has been discussed in Chapter 4, in Section 4.3.1.3. Therefore, when two fuels containing olefins, aromatics and saturates, are blended together the number of different descriptors in this blend is considered to be six, not three. However, there is no information available on the octane numbers of the various descriptors in a fuel. Twu and Coon (1997), instead of assigning the same octane number of the fuel to its descriptors as they did in their first paper (Twu and Coon, 2006), could estimate the octane number of the descriptor within the fuel. Assume that a fuel *A* with an octane number a_A is a mixture of three descriptors x_1, x_2 and x_3, for example, aromatics, olefins and saturates. From the standard laboratory analysis of the fuel, the only constraint available on fuel *A* is that its octane number must be recovered after blending these three descriptors together (Coetzer, 2006). With only one constraint, only one unknown can be solved for. Therefore, it is assumed that the descriptors in the same fuel have the same octane number, but not necessarily the same value as the octane number of the fuel. Let a_x represent the octane number of the descriptors in fuel *A*, then equation (5.9) can be used to solve for a_x:

$$a_x = \frac{a_A}{\sum_i \sum_j x_i x_j (1 - k_{ij})} \qquad ...(5.11)$$

where the k_{ij} are the binary interaction coefficients between descriptors in fuel A. This results in obtaining interaction coefficients for descriptors within as well as between fuels. Note that if the k_{ij} are assumed to be zero between descriptors inside the same fuel then a_x reduces to a_A, which is the assumption made in Twu and Coon (1996). Furthermore, if i and j are two hydrocarbon types (e.g. aromatics and olefins), the binary interaction parameter between them, k_{ij} , is the same for all fuels. Therefore, the advantage of these assumptions is that the number of interaction coefficients to be estimated from blending two three-descriptor fuels together is only six; i.e. three for within-fuel interactions plus three for between-fuel interactions (Coetzer, 2006).

The binary interaction parameters between the descriptors are derived from fitting the octane number prediction model to fuel blending data through least squares minimisation. These binary interaction parameters are then used to calculate global binary interaction parameters between fuels. The binary interaction parameter between the two fuels X and Y, K_{XY}, is calculated from the binary interaction coefficients between descriptors by:

$$K_{XY} = 1 - \frac{\sum_{i}^{m}\sum_{j}^{m} x_i y_j \left(\frac{1}{2}(a_i + a_j)\right)(1 - k_{ij})}{\sum_{i}^{m}\sum_{j}^{m} (x_i x_j + y_i y_j)\left(\frac{1}{2}(a_i + a_j)\right)(1 - k_{ij})} \qquad ...(5.12)$$

where k_{ij} is the binary interaction coefficients between descriptor i and j, and a_i and a_j are the octane numbers of descriptors i and j, respectively, estimated from equation (5.11). After calculating the interaction parameters between fuels, the octane number for the fuel blend, which is a mixture of *n* fuels, can be predicted by the equation:

$$a = \sum_{i}^{n}\sum_{j}^{n} z_i z_j a_{ij} \qquad ...(5.13)$$

$$a_{ij} = \frac{1}{2}(a_i + a_j)(1 - K_{ij}) \qquad ...(5.14)$$

where z_i and a_i are the volume fraction and the octane number, respectively, of fuel i. The binary interaction coefficients between the descriptors, k_{ij}, for within fuels and between fuels, need to be optimized in an iterative procedure for predicting the octane number of the blend with maximum precision. Equations (5.11), (5.12) and (5.13) are used in the optimisation of the binary coefficients. Twu and Coon (1996) used data from 11 blends, containing 6 different refinery streams, to obtain their optimized binary interaction coefficients. They obtained average absolute deviation

percentages (AAD%) of 0.45% for RON and 0.49% for MON, using their own methodology inside this very limited data set (Twu and Coon, 1996). However, when the Twu and Coon model (with their universal set of binary interaction coefficients as published in Twu and Coon (1997)) was applied to the API Project 45 dataset (shown in Appendix F), the accuracy of prediction was disappointingly poor. The Standard Error for RON was 9.93, with the SE for MON being determined as 8.24. Upon optimization of the universal interaction coefficients by a least squares regression technique, the accuracy of prediction across the set of 154 of ternary blends improved considerably. The SE for RON was then determined as 4.49, with the SE for MON improving to only 4.62, while the accuracy of the model failed to even approach the published levels of accuracy that had been reached upon application to refinery streams.

The reason why Twu and Coon's approach has not found general acceptance in refineries around the world, is probably the cost and complexity of the blending study that is first needed to determine and optimize all the interaction coefficients. Since fuel specifications are continuously changing (due to ever more stringent environmental legislation being implemented), the gasoline pool at any refinery is not at all constant in terms of stream compositions and the blending ratios between them. As soon as stream compositions change (e.g. by more severe hydrogenation to achieve better desulphurization) or their destinations inside the refinery are changed, then a new set of interaction coefficients needs to be determined.

5.3 Empirical model containing the % NTC concept

As it had emerged from earlier parts of this study (e.g. Chapter 4) that certain classes of molecules (e.g. olefins, or aromatics, amongst others) could exhibit either NTC ignition behaviour, or in some instances a total absence of NTC character, resulting in pure single-stage ignition behaviour, it became self-evident that the application of the NTC concept to empirical models needed to be investigated. It was believed that this concept represented the core, most fundamental level of what actually determines the autoignition character of fuel molecules. Thus it should lead to more accurate semi-empirical descriptions of the practically relevant autoignition behaviour if the NTC concept could be successfully incorporated in these descriptions. The

application to molecular octane data, as contained in the API Project 45 data set, is discussed in the next section.

5.3.1 Analysis of the API Project 45 octane data using a NTC classification based on molecular structure

The API data represents one of the best sources of octane data that exists. It was generated during the landmark API Project 45, over a period of 19 years between 1938 and 1957 (American Petroleum Institute, 1957; Boyd, 1950; ASTM, 1959). It describes individual molecular characterisations and it comprises the RON and MON measurement of some 154 pure hydrocarbon compounds plus their RON and MON octane values when blended at a 20 vol.% ratio with 80 vol.% of a 60 PRF base fuel. It is to be expected that any proposed octane blending model should be bench-tested against this database to establish credibility and to evaluate the octane predictive capability.

5.3.2 Adaptations of the Twu and Coon model

The Twu and Coon (1997) model was adapted to the API data by regarding each ternary blend as comprising three “streams” which were, in this case, the single compounds: n-heptane (abbreviated as n-C7), iso-octane (i-C8) and one of the API test hydrocarbon molecules. To these components were assigned the a_i and k_{ij} descriptors shown previously in equation (5.12). In each instance, the blend ratio was identical: 32% n-C7, 48% i-C8 and 20% of the API test compound. Each compound was regarded as having a degree of NTC/single-stage character which formed the “component” descriptor, a_x in equation (5.11). n-C7 and i-C8 were defined initially as having 100% NTC attributes in order to ensure linear PRF blending with no possible PRF interaction.

By virtue of this assumed structure, deviations from linear blending were possible only via the interaction between the NTC and the single-stage behaviour and the analysis was therefore constrained to the determination of a single NTC/single-stage interaction coefficient for RON and one for MON. The statistical regression problem was thus reduced to finding the apparent NTC/single-stage proportion for each component in the API data base that would yield the best RON and MON prediction, whilst simultaneously finding the overall RON and MON interaction coefficients.

Initial trials based on this approach revealed a flaw in the basic assumption that n-C7 and i-C8 represented the upper limit of NTC character. To accommodate this discovery, the NTC character of the n-C7 and i-C8 molecules was kept fixed at 100%, but the NTC value of the API molecules was allowed to exceed 100%. Such cases would represent molecules with a stronger NTC character than the PRF molecules. Retaining the 100% NTC definition for the PRF molecules preserved the linear, non-interaction requirement of the defined octane scale.

Thus the original Twu and Coon formulation was retained, but their three interaction coefficients, between Aromatics and Saturates, Olefins and Aromatics, and Olefins and Saturates, were replaced with a single NTC – Single Stage (SS) interaction. This meant one NTC-SS interaction coefficient was optimised for the RON data, while another NTC-SS interaction coefficient could be fitted to the MON data. The best fit RON NTC-SS interaction coefficient was found to be -0.7474, while the one for MON was -0.7846. The overall standard error of the octane prediction was 0.98 ON. See Appendix F for a complete listing of the API Project 45 data, as well as the correlated % NTC values that were obtained.

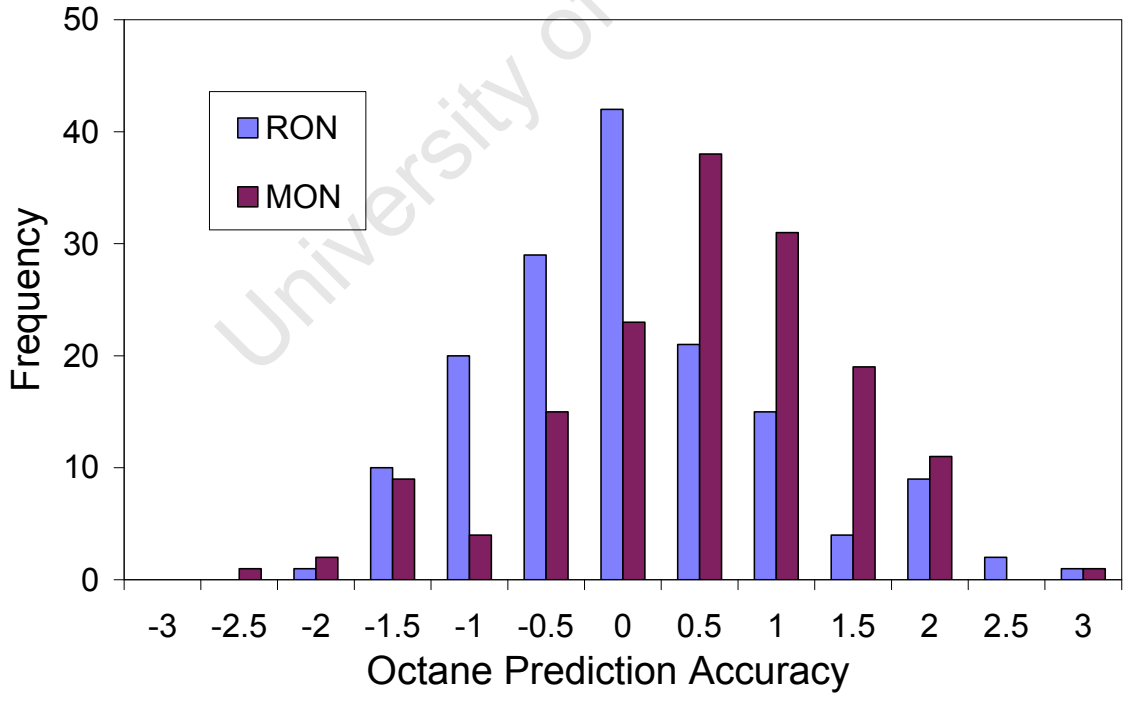

Figure 5.4: Histogram showing the frequency of standard errors for RON and MON across the API Project 45 data set, using Twu and Coon methodology applied to a single NTC-SS interaction coefficient

A frequency histogram of the octane prediction accuracy, shown in Figure 5.4, revealed that the mean values of the RON and MON predictions were clearly not aligned, despite the freedom of having a unique interaction coefficient for each method. This bi-modal error distribution is clearly visible in Figure 5.4, when RON values are compared to the MON values.

A further concern was noted inasmuch that the octane value of the NTC/single-stage interaction, as defined by the Twu and Coon interaction coefficient, represented a multiple of the mean octane-clear values of any two stream components. It was considered that a more judicious approach would be that the interaction should perhaps be expressed in absolute terms rather than a relative scaling factor. The Twu and Coon model was therefore modified by altering the $\left(\frac{\boldsymbol{a}_i + \boldsymbol{a}_j}{2}\right).\left(1 - \boldsymbol{k}_{i,j}\right)$ term to $\left(\frac{\boldsymbol{a}_i + \boldsymbol{a}_j}{2} - \boldsymbol{k}'_{i,j}\right)$ where $k'_{i,j}$ has units of octane number.

The misalignment of the RON and MON mean predictions was addressed by recognising that the MON test takes the fuel to a significantly higher temperature regime where the intrinsic NTC influence is less pronounced. The NTC values ascribed to the MON evaluation were therefore scaled down across the entire API database by a single factor (= 0.985) which was determined by the regression analysis.

The result of these adaptations is shown in the error frequency plot (shown in Figure 5.5) and produced a useful 8% improvement in the standard error of the octane prediction, bringing it to 0.90 ON. Considering the intrinsic imprecision of the octane measurement, this achievement was considered to be an adequate starting-point for the next stage of the analysis.

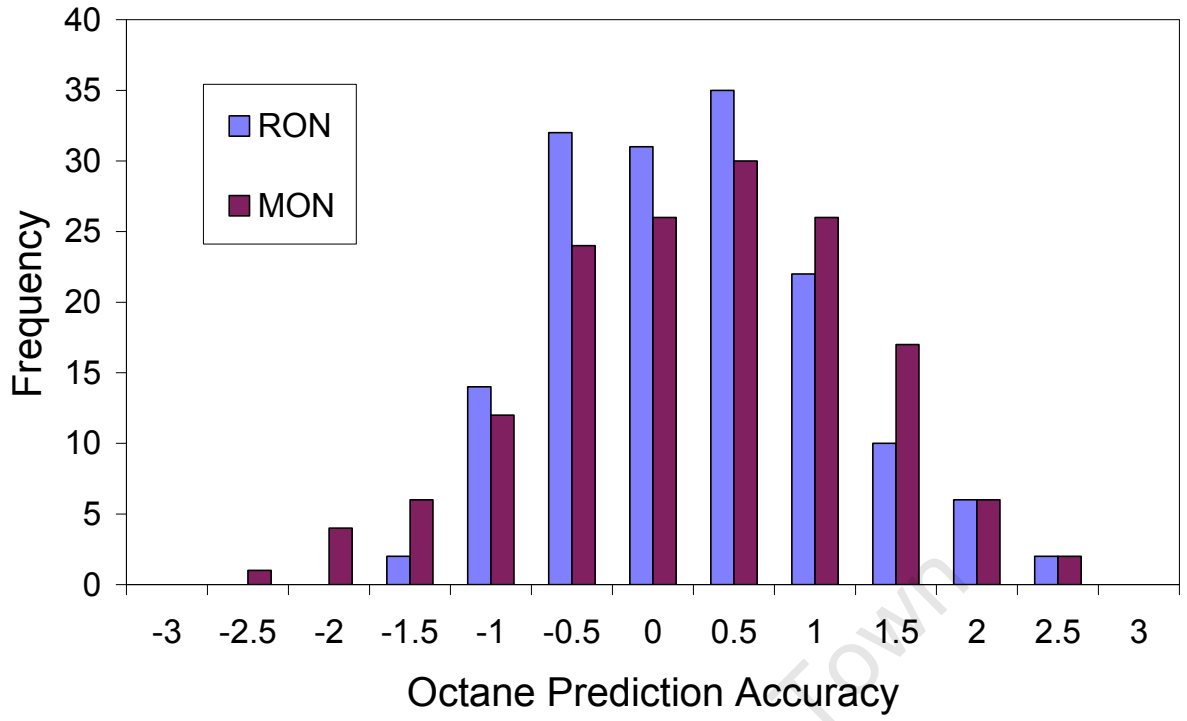

Figure 5.5: Frequency histogram obtained with the modified Twu and Coon method and scaled MON as described in the text, showing disappearance of bi-modal error distributions that were present in Figure 5.4

It is clear that the overall standard error of 0.90 ON that was obtained with these modifications to the Twu and Coon, is significantly better than the standard errors determined for the Stewart, Healy et al., and original Twu and Coon methods that were shown in the preceding sections. Since all these standard errors were determined on the same set of API data, it is considered to be a true reflection of the relative accuracy of the different methods.

5.3.3 Molecular model basis

The API database was grouped according to molecular class (cyclo-paraffins, aliphatic paraffins, olefins and aromatics) and the groups were ranked according to the computed NTC/single-stage proportion. The complete resulting table is appended in Appendix F.

At a cursory inspection, it was clear that there was an emergent pattern between the deduced NTC ranking and the molecular structure. This is not surprising, as the general links between molecular structure and octane ratings had been well established at the time of API Project 45 data's generation (Boyd, 1950; Livingston,

1951; Taylor, 1985). The following discussion represents an overview of an attempt to construct a simple linear model that would compute the NTC proportion directly from the molecular structure, i.e.,

$$\boldsymbol{NTC} = \boldsymbol{A}_0 + \boldsymbol{A}_1(\boldsymbol{Parameter}\,1) + \boldsymbol{A}_2(\boldsymbol{Parameter}\,2) + \ldots\ldots \quad \ldots(5.15)$$

The data for each sub-group were analysed in a spreadsheet, from which the molecular model coefficients and the interaction coefficients could be combined and optimised to give the best overall prediction accuracy. The standard error of this initial optimization was 1.1 ON, although six molecules were disregarded as "outliers" (see discussion below).

5.4 Discussion of Results

5.4.1 Aliphatic Paraffins

The following observations were made upon evaluation of the data (See Appendix F for a tabulation of the % NTC assignments that resulted from this analysis):

- There was a basic correlation between the NTC proportion and the skeletal carbon number. This is in agreement with the premise of Tanaka et al. (2003), that at least 3 adjacent carbons has to be present in a chain, before the molecule could express NTC ignition behaviour.
- The modelled NTC proportion was adjusted by the presence of a single methyl group, dimethyl groups, trimethyl groups or tetramethyl substitution. With the exception of the dimethyl substitution which was essentially benign, the others had a negative influence on the NTC proportion.
- A further (negative) adjustment was inferred by the presence of an ethyl (or longer) side chain.
- A strong positive influence (increased NTC proportion) was caused by the combined presence of methyl groups plus ethyl (or higher) side chains.
- A single methyl group that was not located in position 2 (on the β-carbon) warranted a unique correction.

A further improvement in the overall correlation was achieved by allowing for a linear adjustment that was based on the total carbon count, provided the carbon number was capped at a maximum value which was determined by the regression (= 5.4)

5.4.2 Cyclo-Paraffins

- As with the aliphatic paraffins, there was a basic correlation between NTC proportion and the skeletal carbon number.
- The modelled NTC proportion was similarly adjusted by the presence of a single methyl group, a dimethyl group, etc. In this case, however, the methyl groups all had a strong positive influence on the NTC character.
- A further (positive) adjustment was inferred by the presence of an ethyl (or longer) side chain.
- As before, a positive total-carbon influence was observed up to a capped value of 5.8.

It was noted that the predicted octane numbers of ethyl-cyclobutane and cycloheptane were statistical outliers and they were omitted. It was postulated that the ring may have opened, especially for the cyclo-butane, which would result in a linear paraffin being formed. This would fit with the observation that the predicted octane value was too high.

5.4.3 Aliphatic Olefins

The olefins proved to be substantially more challenging. Even with the proposed model, the octane values of four of the molecules were poorly predicted and they were therefore omitted.

- Initial attempts to find a reasonable starting correlation failed until it was recognised that the aliphatic chain-length was more important than the skeletal length.
- The NTC proportion showed only a weak dependency on the presence of a methyl group, a dimethyl group, an ethyl group etc.
- A much more dominant influence was shown where the methyl group was attached to one of the double-bond carbons. In such cases, the NTC influence was diminished. This aspect was also confirmed by the DFT modelling results, reported in Chapter 4 (see Figures 4.10 to 4.12).

- A further correlation was found where a methyl group is attached to a carbon that was the immediate neighbour to one of the double-bond carbons (positive NTC effect).
- The capped total carbon correlation showed little improvement. However, a correlation improvement was obtained by including the capped skeletal length.

5.4.4 Cyclic Olefins

There were only six cyclo-olefin molecules in the API data and a good correlation was obtained on the basis of skeletal length, the presence of methyl and ethyl groups, and whether the methyl/ethyl group was attached to the double-bond carbon.

5.4.5 Aromatics

- Since the skeletal group was always a benzene ring (C6), a basic correlation with total carbons (capped at 9.1) was used as the starting point.
- The NTC proportion was enhanced by the presence of dimethyl or trimethyl substituents. Single methyl groups and tetramethyl substituents had little effect.
- The presence of ethyl (or longer) chains increased the NTC character.
- A propenyl group and indene were lumped together as having a similar effect, which was to decrease the NTC character.
- An interesting and important feature was indicated by two methyl/ethyl groups being non-neighbours on the benzene ring. The presence of this situation lowered the overall NTC character. This is in accordance with previous observations of the NTC character of ortho-xylene in comparison to para-xylene or meta-xylene, or of the two-stage ignition of 1,2,3-trimethylbenzene versus the single stage ignition of 1,3,5-trimethylbenzene (Roubaud et al., 2000).

5.5 Conclusions

The use of a NTC/single-stage characterisation in conjunction with the Twu and Coon model yielded a very reasonable octane prediction for the entire API data set.

With slight adaptations, the prediction accuracy was able to approach the intrinsic octane measurement precision.

The resulting NTC/single-stage characterisation was not constrained to a single value for all molecules within a sub-group such as the paraffins, olefins or aromatics. This aspect allowed the NTC/single-stage characterisation to produce a better octane prediction than other empirical models, such as the Stewart model or the Healy et al. model. It is also more consistent with the mounting body of experimental and modelling evidence that one class cannot adequately represent all members, e.g. xylenes (Roubaud et al., 2000). Similarly, as was shown in Chapter 4, all hexene isomers are not equivalent, as was also proven experimentally by Tanaka et al. (2003 b) in their RCM evaluation of 3 heptene isomers.

The magnitude of the NTC/single-stage proportion could, to a first approximation, be determined by a relatively simple molecular characterisation which was aligned with the current understanding of the NTC/single-stage phenomenon. This demonstrated that the NTC principle had potential for further development. It is entirely possible that a more rigorous chemical basis and understanding would produce a better alignment. It became clear that the treatment of the olefin group, in particular, had scope for improvement.

The concept can be readily transferred to refinery stream applications and it is likely to retain an intrinsic robust predictive capability. Since it is based on a known, intrinsic chemical phenomenon that has a direct relation to octane rating, it is to be expected that the technique will also accommodate other types of hydrocarbon molecules such as oxygenates (e.g. ethers and alcohols), and possibly also octane boosting additives.

The concept was subsequently applied to refinery blends, which were made up specifically for this study from synthetic components from Sasol's CTL plant in Secunda (Coetzer, 2006). The results of solving all the available sets of octane data simultaneously, using a single set of NTC/SS interaction coefficients, are shown in Table 5.1. It was noted that the average SE for the API data had deteriorated very slightly from 0.90 ON to 1.11 ON. However, this accuracy was still significantly better

than the standard errors obtained by any of the other methods that were evaluated in this study.

Table 5.1 Final prediction errors for all data sets solved simultaneously, using NTC/SS interaction coefficients

Data set	RON error	MON error	Average error	No. of blends
API data	1.109	1.111	1.110	152
Twu and Coon (1996)	0.436	0.560	0.498	11
Synfuels 2 blends	0.010	0.095	0.052	2
Synfuels binary blends	1.000	1.133	1.067	36
PRF blends	0.000	0.000	0.000	9
Average SE	0.511	0.580		
Weighted SE	0.997	1.028		
Overall average SE	0.546			
Overall weighted SE	1.013			

It is evident from the Average Standard Error (SE), that very satisfactory prediction accuracies have been obtained for both RON and for MON predictions, across all the different data sets. It is an indication that the concept of using NTC as a more fundamental descriptor of the autoignition behaviour of either FBR refinery streams, or single molecules, is indeed superior to the alternative descriptions of chemical classes. The reason for the improved accuracy is most probably the fact that the NTC character is quantified exactly as it is exhibited under the RON and MON measurement conditions of temperature and pressure versus time, thus it follows that it should also be very accurate as the descriptor with which RON and MON values are to be predicted.

Chapter 6 : Assessment of different approaches to octane number prediction

6.1 Introduction

During the course of this study, an assessment of various seemingly disparate methodologies for, and approaches to, the prediction of octane numbers for a blend of different components were made. This was the result of a multi-facetted research project that has been pursued in the Sasol Advanced Fuels Laboratory over several years, and of which this thesis forms an integral part. The high-level outline of the bigger research project can be succinctly represented by a diagram, as shown in Figure 6.1. The initial aim was to develop the competency to be able to predict the octane number of a gasoline blend, based on quantitative knowledge of the blend composition at a molecular level. This characterization of gasoline samples is commonly performed by a GC/MS analytical procedure. Since commercial gasoline blends are extremely complex mixtures of several hundreds of different molecules (Ghosh et al., 2006), the analytical procedure has to separate and quantify all the constituent species above a certain threshold value. If the threshold is chosen as >0.5 mass %, then approximately 200 to 300 components still need to be quantified. Modern gas chromatographic (GC) techniques allow this level of detail, which is sufficient for most refinery purposes, to be obtained during the routine operation of the equipment.

Of the different aspects shown in Figure 6.1, the investigation of autoignition chemistry by means of chemical kinetic modeling has fallen squarely within the ambit of this thesis, while the Engine Model development and understanding the peculiarities of octane measurements in CFR engines formed part of a previous PhD study (Swarts, 2006).

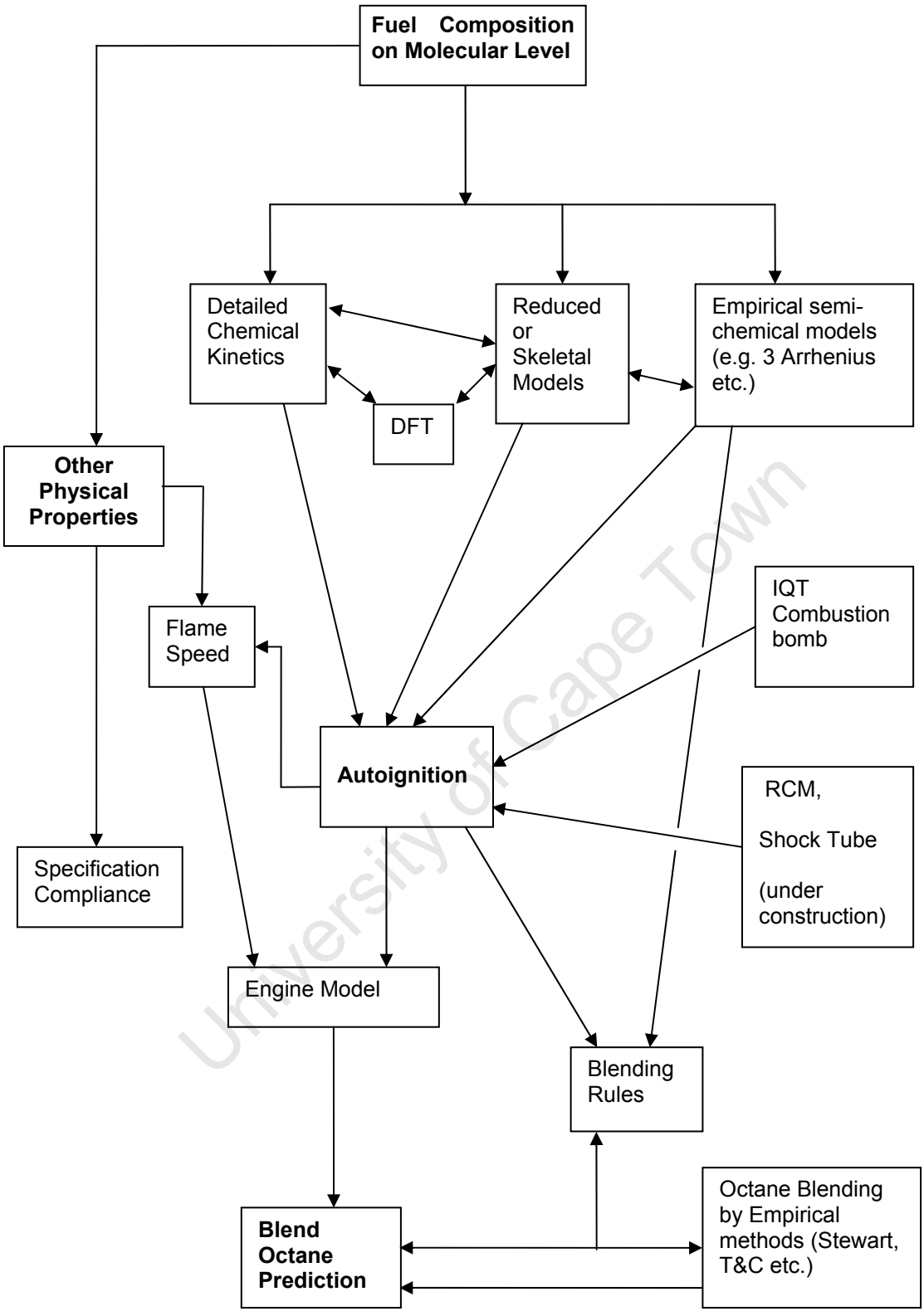

Figure 6.1: A simplified diagram depicting the scope and outline of the initial Octane Modelling project

It is also clearly shown in Figure 6.1 that the original outline of the project contained the implicit assumption that it should be possible to use some kind of autoignition model (i.e., a calculated ignition delay for the blend) to obtain a predicted octane number. As was indicated earlier in Chapter 1 (Figure 1.3), it was realized very early on that this transformation of ignition delay to octane number necessitated a thermodynamic engine model that accurately represented the CFR engine. As shown in Figure 6.1, the IQT was the only device available for experimental ignition delay measurements for this project. Two other research projects (development of a RCM and a shock tube) have subsequently been initiated at the Sasol Advanced Fuels Laboratory, but these were not available for the present study.

The emphasis of this study was on assessing both detailed chemical kinetics and skeletal (reduced) kinetics, as presented in Chapter 3. This led to the appreciation that the magnitude of the NTC character of a molecule was at the heart of its autoignition behaviour in an engine environment. This was something that could be explored by the application of DFT techniques, as was subsequently described in Chapter 4. Since no simple correlations could be found between the E_a of different molecules and their respective octane numbers, the prediction of octane based on molecular composition was taken back into the realm of empirical modeling, using measured octane numbers as necessary input. This empirical approach, incorporating the slightly more fundamental concept of NTC, as an additional descriptor for the molecule or stream that is being blended, was discussed in Chapter 5. The scheme that originally illustrated the outline of the thesis (see Chapter 1, Figure 1.4) can now be populated with the findings from this study (see Figure 6.2).

6.2 Assessment and comparison

In Figure 6.2 the different approaches to the prediction of octane numbers that were evaluated in this study, are juxtaposed and compared to each other. The criteria that were used, are the following:

1. Accuracy of prediction
2. Ease of application (e.g. does it depend entirely on the availability of experimental data)
3. Ability to predict ON for a new stream that did not form part of the calibration set, based on physical properties and/or structure

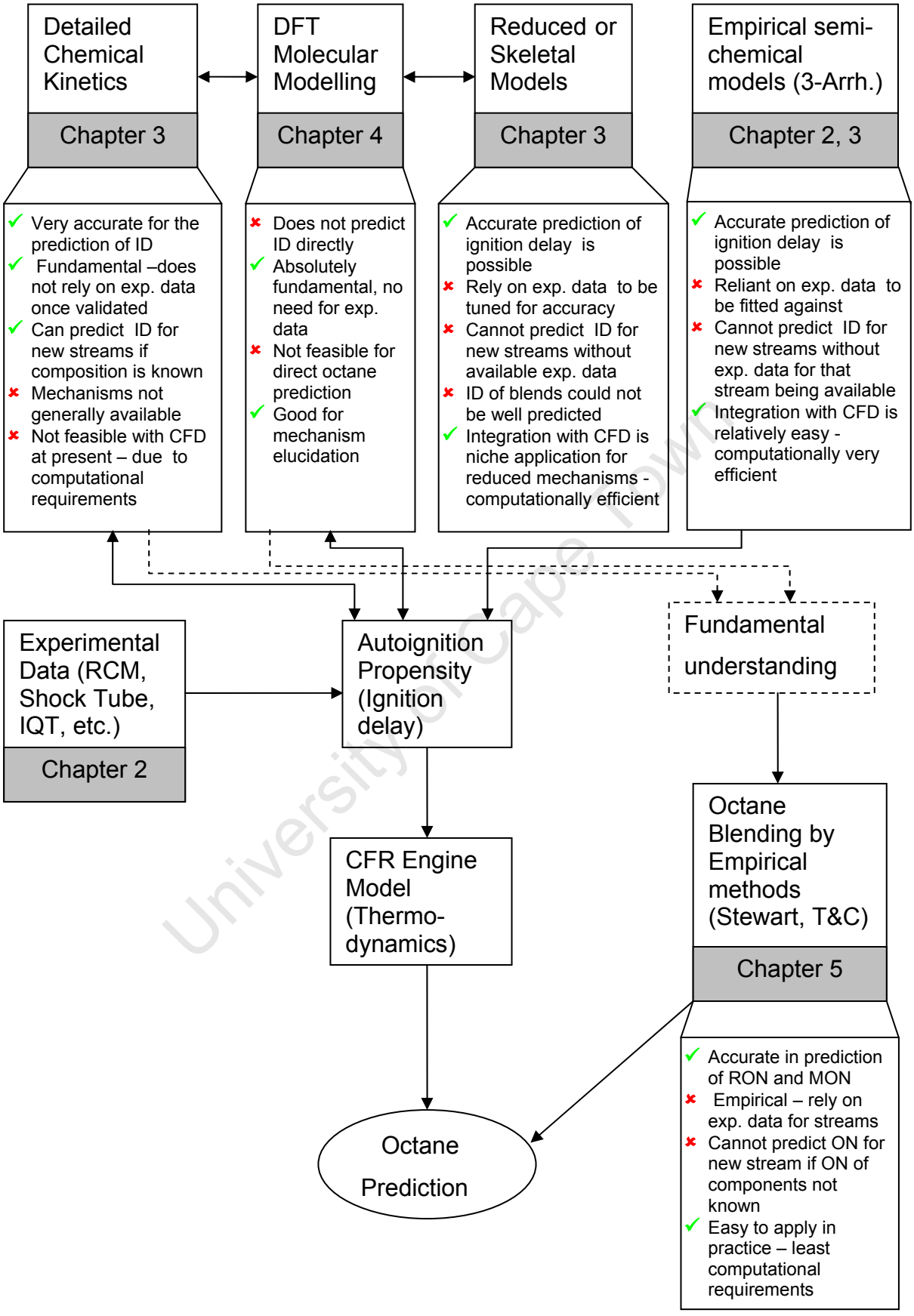

Figure 6.2: An overview of the aspects of Octane Modelling, as assessed in this thesis

4. Suitability of application to CFD simulations (e.g. its computational requirements)

6.2.1 Accuracy of prediction

The prediction accuracy cannot be assessed easily, as neither kinetic simulations nor the semi-chemical ignition delay models can be used to predict octane numbers directly. These predictions of ignition delay have to be transformed to octane numbers by the application of an engine model. This requirement is substantiated by convincing evidence reported by Griffiths et al. (1997). Their RCM ignition delay measurements (see Figure 1 in their paper) for various fuel molecules and PRF blends showed a remarkable poor correlation to RON, especially in the range for RON >60.

However, assuming that the autoignition characterizations for the PRFs are known accurately and that the ignition delay data for an unknown fuel is available for a range of CFR engine-relevant temperatures and pressures, then it would be possible to predict the octane number for the fuel to a level of precision as good as the underlying ignition delay data. Therefore the focus area has been reduced (at least for the purposes of this study) to the prediction of an ignition delay. Thus the assessment was made qualitatively, based on the perceived accuracy of ignition delay simulations compared to experimental data from shock tubes and RCM, such as those shown previously in Figures 2.3 and 2.4.

From these, it is clear that the accuracy of ID predictions from detailed kinetics is relatively good, but that reduced kinetic mechanisms are almost equally successful when limited to pure components. In certain cases, the empirical semi-chemical ignition delay models can be just as accurate, especially when they had been fitted to their substantiating experimental data.

DFT does not directly provide predictions of ID or octane numbers. The empirical octane models, however, do provide direct calculation of octane numbers, and average standard errors (SE) of <0.5 ON are easily obtained. This is considered to be accurate compared to the experimental variation in octane measurements (RON reproducibility of 0.7 ON, repeatability 0.2 ON; and MON reproducibility of 0.9 ON,

repeatability of 0.2 ON). This is shown in the right-hand data block in Figure 6.2, named “Octane Blending by Empirical methods”.

6.2.2 Ease of application

In principle, a detailed kinetic mechanism of oxidation provides a fundamental treatment of the chemical system in a specific physical environment, thus there is no requirement for experimental measurements or data (once the mechanism has been developed and validated). In reality, however, the application of detailed kinetic mechanisms to the simulation of ignition delays are hindered by the general unavailability of these mechanisms, a paucity of data relating to their underlying rate coefficients and thermodynamic data for all the relevant species. Also due to the complexity, special software packages like Chemkin and others are required to solve these systems of differential equations in order to obtain a predicted ignition delay.

The reduced or skeletal kinetic mechanisms as well as the semi-chemical ignition delay models, on the other hand, are absolutely dependent on the availability of macroscopic performance experimental data for the system under study, as they need to be calibrated against the measured data. Once this is done, their application is relatively easy, with the last group obviously requiring less complex calculations than the reduced models may require. The big drawback of both classes is that they can only be applied accurately inside the envelope of physical parameters or conditions spanned by the experimental data to which these models were fitted. Extrapolation to points outside of the calibration set may lead to significant errors.

Quantum mechanical molecular modelling by DFT is also absolutely fundamental in nature, although it does not necessarily provide a pathway to octane numbers. It therefore has no requirement for ignition delay data, but it also requires specialised software packages in order to be applied to any problem.

Lastly, the empirical octane blending methods such as those of Twu and Coon, Stewart, Morris, etc. require measured octane data for the streams that are to be blended. Without this measured data, they cannot be usefully applied to predict the octane number for the blend.

6.2.3 Ability to be applied to an unknown stream

The ease with which detailed kinetic simulations can be applied to new streams (provided that the composition is known and that the mechanism contains all the molecules present in the stream), may be their biggest benefit. Since detailed kinetics is a fundamental consideration of the interaction between molecules on an atomic level, new molecules (or streams) can be accommodated, as long as these are fully defined. In contrast, reduced kinetic schemes cannot predict the ignition delay for a stream that did not form part of the calibration set, neither can the semi-chemical ignition delay models (See “Empirical semi-chemical models“ in the top right data block in Figure 6.2).

Again, since DFT is a fundamental quantum mechanical approach to electrons and atoms, new molecules are easily considered, but not in an octane or ID predictive sense. The empirical octane models are similarly incapable of predicting the octane number of a new stream without prior knowledge of the octane numbers of all of its components.

6.2.4 Suitability of application to CFD simulations

As was evident in Figure 2.2, (taken from Aceves et al., 2005), when detailed chemical kinetic mechanisms are integrated with CFD simulations of combustion systems, computational times in the order of months or years may result. These cannot realistically be run for useful research work on currently available computer hardware. This has been the key motivating factor for the ongoing development of skeletal and reduced mechanisms. These small mechanisms can be integrated into CFD codes that are computationally efficient, while retaining vestiges of their chemical integrity. The same integration can also be done very effectively with the semi-chemical ignition delay models (for example the 3-Arrhenius model). The price to be paid for significantly enhanced computational efficiency, is an increase in the chemical empiricism.

Lastly, although the empirical octane models are not relevant to the discussion of CFD integration, it must be obvious that these are easily applied in practice, having quite modest computational requirements.

Summarizing the preceding assessment, it may be concluded that at the present moment, only empirical methods are capable of directly predicting octane numbers, due to limitations of the alternative chemical kinetics-based procedures currently available. The investigation of this alternative, fundamental procedures are still very valuable since new insights, as those gained in this study, can be used to refine existing empirical models for more accurate octane predictions.

Chapter 7 : Conclusions and Recommendations

7.1 Introduction

This chapter concludes the thesis and provides a summary of the conclusions that were reached and recommendations for further work to be done.

7.2 Conclusions

From the assessment of detailed chemical kinetics and reduced kinetics that were carried out and described in Chapter 3, the following conclusions were made:

- Despite all the early promise that was shown at the beginning of the 1990's, there are still only a limited number of detailed kinetic mechanisms available for a small number of molecules, and there is consensus that a practically useful mechanism for a FBR commercial fuel is not yet feasible.
- When these mechanisms were compared with one another in a relatively simple constant volume adiabatic simulation system, the results replicated the large differences between molecules that have single-stage ignition, and those that have two-stage ignition behaviour, implying the presence of significant NTC character in the latter group. It was concluded that these simulations are useful in exploring the behaviour of the end-gas in CFR engine traces.
- The Chemkin simulations were relatively successful in predicting the available experimental data for certain systems, e.g. n-heptane, iso-octane, 1-hexene, toluene and ethanol, thus providing confidence that the mechanisms at least encapsulate the real-world behaviour correctly.
- The important role of H_2O_2 in initiating the hot ignition event (independently from the specific fuel molecule(s), was underlined, whilst its formation after the cool flame heat release in the two-stage fuels was observed in all fuels having NTC behaviour.
- During simulations of the CFR engine under RON measurement conditions, it became clear that there is not a simplistic link to be made between the simulated ignition delay in a constant volume system and the octane number of that specific molecule. The actual pressure trace obtained for the specific

molecule in the CFR engine under knocking conditions (at SKI), is required information in order to make an unequivocal link. This integrated pressure / temperature history is required to transform the ignition delay to an octane number.

- It was shown that the Griffiths reduced model, when tuned to the appropriate experimental data, can be an efficient tool to predict the ignition delay of PRF blends. It was concluded that Griffiths-type models may be useful in cases where sufficient experimental data exists across the relevant temperature, time, and ignition delay space.
- An investigation of other highly reduced (skeletal) mechanisms has indicated that blends of molecules inside the skeletal mechanism could not be predicted well, most probably due to the omission of critical reaction pathways in the skeletal scheme.
- Finally, one of the main conclusions reached on the basis of the kinetic simulations conducted in this study, was that a practically implementable octane prediction capability will for the foreseeable future, still have to contain a large component of empiricism.

The conclusions that were reached by application of Density Functional Theory to the investigation of NTC character of selected fuel molecules can be summarised as follows:

- The DFT results are directionally consistent with empirically-based reaction rates that are commonly used in autoignition research. In particular, very good agreement was obtained between the DFT results and the group and bond additivity methodology of Benson (1976).

- In general, the activation energies for the first internal hydrogen abstraction, have confirmed this to be the appropriate rate-determining step, as this step was shown to be the determining step between single stage molecules and those having NTC character (e.g. toluene vs. ortho-xylene).

- It was concluded that, although DFT provides relatively easy access to information about the relative activation energy barriers in a sequence of reactions (or for the same reaction for different molecules), it does not provide

enough information in order to quantify either the NTC character or the octane of the molecule under study.

- The preferred application of DFT, based on the outcome of this study, would be in the comparison of alternative reaction mechanisms with each other to find the lowest energy pathways. This was shown in the comparison of the 2-4 mechanism of n-heptane with its “equivalent” 2-1 mechanism. This ability of DFT can be put to very good use in the construction of reduced or skeletal mechanisms, to ensure that these remain chemically meaningful.

Based on the assessment of empirical octane prediction methods, and the incorporation of the NTC concept into the Twu and Coon (1997) methodology, the following conclusions were reached:

- The use of a NTC/single-stage characterisation in conjunction with the Twu and Coon model yielded a very reasonable octane prediction for the entire API data set. With slight adaptations, the prediction accuracy was able to approach the intrinsic octane measurement precision.
- The resulting NTC/single-stage characterisation was not constrained to a single value for all molecules within a sub-group such as the paraffins, olefins or aromatics. This aspect allowed the NTC/single-stage characterisation to produce a better octane prediction that other empirical models, such as the Stewart model.
- The magnitude of the NTC/single-stage proportion could, to a first approximation, be determined by a relatively simple molecular characterisation which was aligned with the current understanding of the NTC/single-stage phenomenon. This demonstrated that the NTC principle has potential for further development.
- The concept can be readily transferred to refinery stream applications and it is likely to retain an intrinsic robust predictive capability. Since it is based on a known, intrinsic chemical phenomenon that has a direct relation to octane rating, it is to be expected that the technique will also accommodate other types of hydrocarbon molecules such as oxygenates like ethers and alcohols.

7.3 Recommendations for further work

Based on the observations made in this study, and the conclusions reached in the preceding section, the following recommendations can be made:

- The continued study of detailed chemical kinetic models remains very important. This is particularly relevant to the understanding and quantification of blending interactions between different types of molecules, where it is believed that skeletal mechanisms will never be accurate enough.
- Specifically, it is recommended that detailed kinetic modelling of surrogate jet fuel systems in combustors and in laminar flames should be studied next, as synthetic jet fuel is a new focus area of the international aviation fuels community.
- Reduced or skeletal mechanisms may be appropriate under more limited ranges of temperature and pressure, e.g. in simulating either a shock tube experiment or a RCM experiment, but not both at the same time. These small mechanisms may have a niche in interfaces with CFD simulations of real combustion systems, therefore this area demands further investigation.
- There is still an unmet need for reliable autoignition data from relevant experimental systems (e.g. RCM and shock tubes, and laminar flame speed measurements). Only if the experimental data is available, can reduced models such as the Griffiths'-type be fitted, or detailed mechanisms be developed for "new" fuel molecules that may be of specific interest to a synthetic fuel producer.
- Further work is necessary in order to understand (and predict) the blending interactions of different fuel molecules, e.g. the interaction of a strong NTC fuel molecule (having two-stage ignition) with a single-stage fuel molecule. This could build on the initial blends of ethanol with n-heptane (with both molecules contained in the same mechanism) that were made in this study, but the single-stage component should preferable be an aromatic molecule.

References

Abou-Rachid, H., El Marrouni, K., and Kaliaguine, S. (2003), "DFT studies of the hydrogen abstraction from primary alcohols by O_2 in relation with cetane number data", *Journal of Molecular Structure (Theochem),* 631, 241–250

Accelrys (Inc.) 2002, Materials Studio DMol^3 version 2.2, User Manual, Accelrys (Inc.)

Aceves, S.M., Flowers, D.L., Martinez-Frias, J., Espinosa-Loza, F., Christensen, M., Johansson, B., and Hessel, R.P. (2005) "Analysis of the Effect of Geometry Generated Turbulence on HCCI Combustion by Multi-Zone Modeling", SAE Paper 2005-01-2134

American Petroleum Institute (1957), 19th Annual Report on API Project 45: *"Synthesis, Purification, and Properties of Hydrocarbons of Low Molecular Weight"*, API

Andrae, J.C.G. (2008), "Development of a detailed kinetic model for gasoline surrogate fuels", *Fuel*, 87, 2013–2022

Andrae, J.C.G., Björnbom, P., Cracknell, R.F., and Kalghatgi, G.T. (2007), "Autoignition of toluene reference fuels at high pressures modeled with detailed chemical kinetics", *Combustion & Flame*, 149, 2–24

Andrae, J.C.G., Brinck T., and Kalghatgi, G.T., (2008), "HCCI experiments with toluene reference fuels modelled by a semi-detailed chemical kinetic model", *Combustion & Flame*, 155, 696–712

ASTM (1959), ASTM Special Technical Publication No.225 "Knocking Characteristics of Pure Hydrocarbons", Philadelphia, American Society for Testing Materials

ASTM Method D 2699 (2007), "Standard Test Method for Research Octane Number of a Spark-Ignition Engine", ASTM International

ASTM Method D 2700 (2007), "Standard Test Method for Motor Octane Number of a Spark-Ignition Engine", ASTM International

Atkins, P.W. (1978), *Physical Chemistry*, 2nd edition, London, Oxford University Press

Barrow, G.M. (1966), *Physical Chemistry*, 2nd edition, McGraw Hill Company

References

Battin-Leclerc, F., Glaude, P.A., Warth, V., Fournet, R., Scacchi, G., Côme, G.M., (2000), "Computer tools for modelling the chemical phenomena related to combustion", *Chemical Engineering Science*, 55, 2883-2893

Benson, S.W. (1976), *Thermochemical Kinetics* 2nd Ed., New York, John Wiley

Bhatttacharjee, B., Baron, P.I., Schwer, D.A., and Green, W.H. (2003), "Optimally Reduced Kinetic Models: Reaction Elimination in Large-Scale Kinetic Mechanisms", *Combustion & Flame*, 135,191-208.

Biet, J., Hakka, M.H., Warth, V., Glaude, P., and Battin-Leclerc, F. (2008), "Experimental and Modeling Study of the Low-Temperature Oxidation of Large Alkanes", *Energy & Fuels*, 22, 2258–2269

Blurock, E.S., (1995), "REACTION: System for Modeling Chemical Reactions", *J. Chem. Inf. Comput. Sci*. 35, 607-616

Bollentin, Joseph W.; Wilk, Richard D. (1996), "Autoignition Characteristics of Ethanol", SAE Paper 961175

Bood, J., Bengtsson, P.E., Mauss, F., Burgdorf, K., and Denbratt, I. (1997), "Knock in S.I. Engines: End-gas temperature measurements using Rotational CARS and detailed kinetic calculations of the autoignition process", SAE Paper 971669

Boyd, T.A. (1950), "Pathfinding in fuels and engines", *SAE Transactions*, Vol.4, No.2, 182-195

Bradley, D. and Head, R.A. (2006), "Engine autoignition: The relationship between octane numbers and autoignition delay times", *Combustion & Flame,* 147, 171-184

Brezinsky, K. and Dryer, F.L. (1987), "Molecular Structure and Component Blending Effects on Knock Related Chemistry", SAE Paper 872109

By, A., Kempinski, B. and Rife, J.M. (1981), "Knock in spark ignition engines", SAE Paper 810147

Cavaliere, A., and De Joannon, M., (2004), "Mild Combustion", *Progress in Energy and Combustion Science*, 30, 329–366

Ciezki, H.K., and Adomeit, G. (1993), "Shock-tube investigation of self-ignition of n-heptane-air mixtures under engine relevant conditions", *Combustion & Flame*, 93, 421-433

Coetzer, R.L.J. (2006), “The Development of a Semi-Fundamental Octane Number Prediction Model”, Sasol Technology R&D, Bulletin PDR/06/0040/RTIS

Coetzer, R.L.J., Rossouw, R., Swarts, A and Viljoen, C.L. (2006), “The estimation of knockpoints of fuels by a weighted mean square error criterion”, *Fuel*, 85, 1880–1893

Cowart, J.S., Keck, J.C., Heywood, J.B., Westbrook, C.K., and Pitz, W.J. (1990), “Engine knock predictions using a fully-detailed and a reduced chemical kinetic mechanism”, *Twenty-third Symposium (Int.) on Combustion*, The Combustion Institute, 1055-1062

Cox, R.A., and Cole, J.A. (1985), “Chemical aspects of the autoignition of hydrocarbon-air mixtures”, *Combustion & Flame*, 60, 109-123

Cracknell, R.F., Andrae, J.C.G, McAllister, L.J., Norton, M. and Walmsley, H.L., (2009), “The chemical origin of octane sensitivity in gasoline fuels containing nitroalkanes”, *Combustion & Flame,* 156, 1046-1052

Curran, H.J., Gaffuri, P., Pitz, W.J., Westbrook,C.K. (1998), “A Comprehensive Modeling Study of n-Heptane Oxidation”, *Combustion & Flame*, 114, 149-177

Curran, H.J., Gaffuri, P., Pitz, W.J., Westbrook,C.K. (2002), “A Comprehensive Modeling Study of iso-Octane Oxidation”, *Combustion & Flame*, 129, 253-280

Dagaut, P., Cathonnet, M., Rouan, J.P., Foulatier, R., Quilgars, A., Boettner, J.C., Gaillard, F., and James, H. (1986), “ A jet-stirred reactor for kinetic studies of homogeneous gas-phase reactions at pressures up to ten atmospheres (~1MPa)”, *J. Phys. E: Sci. Instrum.*,19, 207-209

Dean, A.M., (2001), “Development and Application of Detailed Kinetic Mechanisms for Free Radical Systems”, *International conference on the foundations of molecular modeling and simulations (FOMMS), AIChE Symposium Series*, 97, 85-95

Delley, B. (2000), “DMol^3 DFT studies: from molecules and molecular environments to surfaces and solids”, *Computational Materials Science*, 17, 122-126

Dimpelfield, P.M. and Foster, D.E. (1986), “Predictions of autoignition in a spark-ignition engine using chemical kinetics”, SAE Paper 860322

Djurisic, Zoran M., (1999), "Detailed kinetic modeling of benzene and toluene oxidation at high temperatures", MS Thesis, University of Delaware

References

Douaud, A.M., and Eyzat, P. (1978), “Four-octane-number method for predicting the anti-knock behaviour of fuels and engines”, SAE Paper 780080

Downs, D., and Wheeler, R.W. (1952), “Recent developments in ‘Knock’ research”, *Proc. Inst. of Mech. Engineers*, 89-99

Edwards, C.F., Siebers, D.L., and Hoskin, D.H. (1992), “A Study of the Autoignition Process of a Diesel Spray via High Speed Visualization”, SAE Paper 920108

El Marrouni, K., Abou-Rachid, H., and Kaliaguine, S., (2004), “Density functional theory kinetic assessment of hydrogen abstraction from hydrocarbons by O_2”, *Journal of Molecular Structure (Theochem),* 681, 89–98

Elliott, L., Ingham, D.B., Kyne, A.G., Merab, N.S., Pourkashanian, M., and Whittaker, S., (2006), “Reaction mechanism reduction and optimisation for modelling aviation fuel oxidation using standard and hybrid genetic algorithms”, *Computers and Chemical Engineering*, 30, 889–900

Faravelli, T., Gaffuri, P., Ranzi, E. and Griffiths, J.F. (1998), “Detailed thermokinetic modelling of alkane autoignition as a tool for the optimization of performance of internal combustion engines”, *Fuel,* 77, 3, 147-155

Fikri, M., Herzler, J., Starke, R., Schulz, C., Rotha, P., and Kalghatgi, G.T. (2008), “Autoignition of gasoline surrogates mixtures at intermediate temperatures and high pressures”, *Combustion & Flame*, 152, 276–281

Fish, A., Read, A., Affleck, W.S., and Haskell, W.W. (1969), “The controlling role of cool flames in two-stage ignition”, *Combustion & Flame*, 13, 39-49

Flowers, D., Aceves, S., Smith, R., Torres, J., Girard, J. and Dibble, R. (2000), “HCCI in a CFR engine: Experiments and detailed kinetic modeling”, SAE Paper 2000-01-0328

Frisch, A., ChemNews.Com11.2, http://chemnews.cambridgesoft.com/art.cfm?S=155, Site last accessed 14/7/2004

Gaffuri, P., Faravelli, T., Ranzi, E., Cernansky, N.P., Miller, D., D’Anna, A., and Ciajolo, A. (1997), “Comprehensive Kinetic Model for the Low-Temperature Oxidation of Hydrocarbons”, *Am. Inst. Chem. Eng. J.* 43, 1278–1286.

Gauthier, B.M., Davidson, D.F., and Hanson, R.K., (2004), “Shock tube determination of ignition delay times in full-blend and surrogate fuel mixtures”, *Combustion & Flame*, 139, 300–311

Ghosh, P, Hickey, K.J. and Jaffe, S.B., (2006), “Development of a Detailed Gasoline Composition-Based Octane Model”, *Ind. Eng. Chem. Res.*, 45, 337-345

Glassman, I. (1996), *“Combustion”*, 3rd edition, San Diego, Academic Press

Glaude P.A., Conraud, V., Fournet, R., Battin-Leclerc, F., Côme, G.M., Scacchi, G., Dagaut, P., and Cathonnet, M. (2002), “Modeling the Oxidation of Mixtures of Primary Reference Automobile Fuels”, *Energy & Fuels*, 16 (5), 1186–1195.

Gluckstein, M.E. and Walcutt, C. (1961), “End-gas temperature-pressure histories and their relation to knock”, *SAE Transactions*, 69, 529-553

Golovitchev, V. and Ogink, R. (2003), “Numerical Evaluation of Main Features of Chemical Models for Motor Fuel Surrogates” [paper presented at ISCHIA 2003 Joint meeting of the Scandinavian-Nordic and Italian sections of the Combustion Institute]

Golovitchev, V.I., Tao, F., and Chomiak, J., (1999), “Numerical Evaluation of Soot Formation Control at Diesel-Like Conditions by Reducing Fuel Injection Timing”, SAE Paper 1999-01-3552

Green, R. M., Cernansky, N.P., Pitz, W.J., and Westbrook, C.K. (1987), “The role of low temperature chemistry in the autoignition of n-butane”, SAE Paper 872108

Griffiths, J.F, Jiao, Q., Schreiber, M., Meyer, J., Knoche, K.F. (1992), "Development of thermokinetic models for autoignition in a CFD code: experimental validation and application of the results to rapid compression studies", *Proceedings of the Twenty-fourth Symposium (International) on Combustion*, The Combustion Institute, Pittsburgh, USA, 1809-1815

Griffiths, J.F. (1986), "The fundamentals of spontaneous ignition of gaseous hydrocarbons and related organic compounds", *Adv. Chem. Phys.*, 64, 203-303

Griffiths, J.F. (1993), "Kinetic fundamentals of alkane autoignition at low temperatures", *Combustion & Flame*, 93, 202-206

References

Griffiths, J.F. (1995), "Reduced kinetic models and their application to practical combustion systems.", *Prog. Energy Combust. Sci.*, 21, 25-107

Griffiths, J.F., Halford-Maw, P.A. and Mohamed, C. (1997)," Spontaneous Ignition Delays as a Diagnostic of the Propensity of Alkanes to Cause Engine Knock", *Combustion & Flame*, 111, 327-337

Griffiths, J.F., Hughes, K.J. and Porter, R. (2005), "The role and rate of hydrogen peroxide decomposition during hydrocarbon two-stage autoignition", *Proceedings of the Combustion Institute*, 30, 1083–1091

Griffiths, J.F., Hughes, K.J., Schreiber, M. and Poppe, C. (1994), "A Unified Approach to the Reduced Kinetic Modeling of Alkane Combustion", *Combustion & Flame*, 99, 533-540

Griffiths, J.F., MacNamara, J.P., Mohammed, C., Whitaker, B.J., Pan, J., and Sheppard, C.G.W. (2001), "Temperature fields during the development of autoignition in a rapid compression machine", *Faraday Discuss.*, 119, 287-303

Griffiths, J.F., MacNamara, J.P., Sheppard, C.G.W., Turton, D.A. and Whitaker, B.J. (2002), "The relationship of knock during controlled autoignition to temperature inhomogeneities and fuel reactivity", *Fuel*, 81, 2219-2225

Griffiths, J.F., Rose, D.J., Schreiber, M., Meyer, J., and Knoche, K.F. (1992), "Novel features of end-gas autoignition revealed by Computational Fluid Dynamics". *Combustion & Flame*, 91:209-212

Halstead, M. P., Kirsch, L. J., and Quinn, C. P. (1977), "The Autoignition of Hydrocarbon Fuels at High Temperatures and Pressures -Fitting of a Mathematical Model", *Combustion & Flame*, 30, 45-60

Halstead, M. P., Kirsch, L. J., Prothero, A., and Quinn, C. P. (1975), "A mathematical model for hydrocarbon autoignition at high pressures", *Proc. Roy. Soc. London*, A346, 515-538

Healy, W.C., Maassen, C.W., and Peterson, R.T. (1959), "A New Approach to Blending Octanes", *Proceedings of the 24th Midyear Meeting of the American Petroleum Institute's Division of Refining*, 39 (3), 132-192

Heywood, J.B. (1988), *Internal Combustion Engine Fundamentals*, New York, McGraw-Hill Book Company

Hu, H. and Keck, J.C. (1987), "Autoignition of adiabatically compressed combustible gas mixtures", SAE Paper 872110

Huang, C., Lu, X., and Huang, Z. (2008), "New Reduced Chemical Mechanism for Homogeneous Charge Combustion Ignition Combustion Investigation of Primary Reference Fuels", *Energy & Fuels*, 22, 935-944

Kalghatgi, G.T., (2005), "Auto-ignition quality of practical fuels and implication for fuel requirements of future SI and HCCI engines", SAE Paper 2005-01-0239

Kazakov, A., Chaos, M., Zhao, Z. and Dryer, F.L. (2006), "Computational Singular Perturbation Analysis of Two-Stage Ignition of Large Hydrocarbons", *J. Phys. Chem. A* 110 (21), 7003-7009

Kee, R.J., F. M. Rupley, J. A. Miller, M. E. Coltrin, J. F. Grcar, E. Meeks, H. K. Moffat, A. E. Lutz, G. Dixon-Lewis, M. D. Smooke, J. Warnatz, G. H. Evans, R. S. Larson, R. E. Mitchell, L. R. Petzold, W. C. Reynolds, M. Caracotsios, W. E. Stewart, P. Glarborg, C. Wang, O. Adigun, W. G. Houf, C. P. Chou, and S. F. Miller, (2002), *Chemkin Collection*, Release 3.7, Reaction Design, Inc., San Diego, CA (2002)

Kee, R.J., Rupley, F.M., and Miller, J.A. (1989), "CHEMKIN-II: A Fortran Chemical Kinetics Package for the Analysis of Gas Phase Chemical Kinetics"; Sandia Report no. SAND 89-8009B; Sandia National Laboratories

Kirsch, L. J., and Quinn, C. P. (1976), "A fundamentally based model of knock in the gasoline engine", *Proceedings of the Sixteenth Symposium (Int.) on Combustion*, The Combustion Institute, 233-244

Klotz, S.D., (1998) , "Interactive Oxidation Chemistry of Aromatic and C4 Hydrocarbon Fuel Components", Ph.D. thesis, Princeton University

Leach, A.R. (1998), *Molecular Modelling, Principles and Applications*, Singapore, Addison Wesley Longman

Leach, A.R. (2001), *Molecular Modelling, Principles and Applications*, 2nd Edition", Harlow, Pearson Education

Lenhert, D.B., Khan, A.R., Cernansky, N.P., Miller, D.L., and Owens, (2003), "The Oxidation of an ISF Surrogate and its Components in the Negative Temperature Coefficient

Region “, *Proceedings of the Third Joint Meeting of the U.S. Sections of The Combustion Institute*, March 17th, 2003

Leonpacher , R.M. (1981), "The Ethyl Technique of Octane Prediction", Report No. RTM - 400A, Ethyl Corporation, October 1981

Leppard, W. R. (1990), “The Chemical Origin of Fuel Octane Sensitivity”, SAE Paper 902137

Leppard, W.R. (1985), “A Detailed Chemistry Kinetics Simulation of Engine Knock”, *Combustion Science and Technology*, 43, 1-20.

Leppard, W.R. (1987), “The Autoignition Chemistry of n-Butane: An Experimental Study”, SAE Paper 872150

Leppard, W.R. (1989), “A Combustion of Olefin and Paraffin Autoignition Chemistries: A Motored-Engine Study”, SAE Paper 892081

Leppard, W.R. (1992), “The Autoignition Chemistries of Primary Reference Fuels, Other Mixture and Blending Octane Numbers”, SAE Paper 922325

Lewis B., von Elbe G. (1961), *Combustion, Flames and Explosions of Gases*, 2nd ed, Academic Press

Li, H., Miller, D. L., and Cernansky, N. P. (1996), “Development of Reduced Kinetic Model for Prediction of Preignition Reactivity and Autoignition of Primary Reference Fuels,” SAE Paper 960498

Litzinger, T.A., (1990), “A Review of Experimental Studies of Knock Chemistry in Engines”, *Prog. Energy Combust.Sci.*, 16, 155-167

Livengood, J. C. and Wu, P. C. (1955), “Correlation Of Autoignition Phenomena In Internal Combustion Engines And Rapid Compression Machines”, *Proceedings of the 5th Symposium (International) on Combustion*, The Combustion Institute, 347-356

Livingston, H.K., (1951), “Knock resistance of pure hydrocarbons – correlation with chemical structure”, *Ind. and Eng. Chem.*, 43, 12, 2834-2840

Logan, S.R., (1996), *Fundamentals of Chemical Kinetics*, London, Longman

Lu, T. and Law, C.K. (2008), “Strategies for mechanism reduction for large hydrocarbons: n-heptane”, *Combustion & Flame*, 154, 153–163

Maas, U., and Pope, S.B. (1992), “Simplifying chemical kinetics: intrinsic low-dimensional manifolds in composition space”, *Combustion & Flame*, 88, 239–264

Machrafi, H. (2008), personal communication by e-mail, 12 December 2008

Machrafi, H., Cavadias, S., and Amouroux, J. (2009), “The development and experimental validation of a reduced ternary kinetic mechanism for the auto-ignition at HCCI conditions, proposing a global reaction path for ternary gasoline surrogates”, *Fuel Process. Tech.*, 90 (2), 247-263

Marinov, N.M. (1999), "A Detailed Chemical Kinetic Model for High Temperature Ethanol Oxidation", *Int J. Chem Kinet.*, 31,183–220

Marinov, N.M., Pitz, W.J., Westbrook, C.K., Vincitore, A.M., Castaldi, M.J., Senkan, S.M., and Melius, C.F. (1998), "Aromatic and polycyclic aromatic hydrocarbon formation in a laminar premixed n-butane flame", *Combustion & Flame*, 114, 192-213

Maroteaux, F., and Noel, L. (2006), “ Development of a reduced n-heptane oxidation mechanism for HCCI combustion modeling”, *Combustion & Flame*, 146, 246–267

Mehl, M., Faravelli, T., Giavazzi, F., Ranzi, E., Scorletti, P., Tardani, A., and Terna, D. (2006), “Detailed Chemistry Promotes Understanding of Octane Numbers and Gasoline Sensitivity”, *Energy & Fuels* , 20, 2391-2398

Miller, J.A., and Fisk, G.A. (1987), “Special report: Combustion Chemistry.”, *Chem. & Eng*., August 31, 22-46

Millo, F., Ferraro, C.V., Barbera, E. and Magaria, G. (1995), “Octane Rating Methods at High Revolution Speed”, SAE Paper 952520

Minetti, R., Carlier, Ribaucour, M., Therssen, E., L Sochet, L.R., (1995), “A rapid compression machine investigation of oxidation and auto-ignition of n-Heptane: Measurements and modeling”, *Combustion & Flame* 102, 298–309

Mittal, V., and Heywood, J.B., (2008), “The Relevance of Fuel RON and MON to Knock Onset in Modern SI Engines”, SAE Paper 2008-01-2414

Moran, D.P. and Taylor, A.B. (1995), “An evaporative and engine-cycle model for fuel octane sensitivity prediction”, SAE Paper 952524

References

Morris, W.E. (1975), "The interaction approach to gasoline blending", NPRA Paper AM-75-30, NPRA 73rd Annual Meeting, March 1975

Nates, R.J. and Yates, A.D.B. (1994), "Knock damage mechanisms in spark-ignition engines", SAE Paper 942064

Ogink R, and Golovitchev V., (2001), "Gasoline HCCI modeling: computer program combining detailed chemistry and gas exchange processes", SAE Paper 2001-01-3614

Ogink, R.,and Golovitchev,V.I. (2003), "Reaction Mechanisms For Natural Gas and Gasoline in Homogeneous Charge Compression Ignition (HCCI) Engine Modelling", ICE 2003, 6th Int. Conf. on Engines for Automobile, SAE_NA 2003-01-42, Capri, Italy

Ogston, A.R. (1981), "A short history of aviation gasoline development, 1903 – 1980", SAE Paper 810848.

Pepiot-Desjardins, P., and Pitsch, H. (2008), "An efficient error-propagation-based reduction method for large chemical kinetic mechanisms", *Combustion & Flame*, 154, 67–81

Peters, N.; Paczko, G.; Seiser, R.; Seshadri, K. (2002), "Temperature Cross-Over and Non-Thermal Runaway at Two-Stage Ignition of n-Heptane", *Combustion & Flame*, 128, 38.

Pitz, W.J., Westbrook, C.K., and Leppard, W.R. (1988), "Autoignition Chemistry of n-Butane in a Motored Engine: A Comparison of Experimental and Modeling Results", SAE Paper 881605

Rifkin, E.B. and Walcutt, C. (1957), "A basis for understanding antiknock action", *SAE Transactions*, 65, 552-565

Roberts, C.E., Matthews, R.D., and Leppard, W.R. (1996), "Development of a Semi-Detailed Kinetics Mechanism for the Autoignition of Iso-Octane", SAE Paper 962107

Roubaud, A., Minetti, R., and Sochet, L.R. (2000), "Oxidation and Combustion of Low Alkylbenzenes at High Pressure: Comparative Reactivity and Auto-Ignition", *Combustion & Flame*, 121, 535-541

Savage, N. (2009), "The Use of a Modified IQT^{TM} Apparatus and Detailed Kinetic Model to Investigate the Atmospheric Autoignition Characteristics of Model Fuels", M.Sc. thesis, University of Cape Town

Saylam, A., Ribaucour, M., Pitz, W.J., and Minetti, R., (2007), “Reduction of Large Detailed Chemical Kinetic Mechanisms for Autoignition Using Joint Analyses of Reaction Rates and Sensitivities“, *International Journal of Chemical Kinetics*, 39 (4), 181–196

Sazhin, S.S., Sazhina, E.M., Heikal, M.R., and Marooney, C. (1999), “The Shell Autoignition Model: A New Mathematical Formulation”, *Combustion & Flame*, 117, 529-540

Sazhina, E.M., Sazhin, S.S., Heikal, M.R., and Marooney, C.J. (1999), “The Shell Autoignition Model: Applications to Gasoline and Diesel Fuels”, *Fuel*, 78, 389-401

Schreiber, M., Sadat Sakak, A., Lingens, A, and Griffiths, J.F. (1994), “A reduced thermokinetic model for the autoignition of fuels with variable octane ratings”, *Proceedings of the Twenty-Fifth Symposium (Int.) on Combustion*, The Combustion Institute, 933-940

Scott, A. Radom, L. (1996), “Harmonic Vibrational Frequencies: An evaluation of Hartree-Fock, Moller-Plesset, quadratic configuration interaction, density functional theory and semiempirical scale factors”, *Journal of Physical Chemistry*, 100, 16502-16513

Seiser, R.; Pitsch, H.; Seshhadri, K.; Pitz, W. J.; Curran, H. J., (2000), "Extinction and Autoignition of n-Heptane in Counterflow Configuration", *Proceedings of the Combustion Institute*, 28, 2029-2037

Simmie, J.M. (2003), "Detailed chemical kinetic models for the combustion of hydrocarbon fuels", *Progress in Energy and Combustion Science*, 29(6), 599-634

Sivaramakrishnan, R., Tranter, R.S., and Brezinsky, K. (2004), “High-pressure, high-temperature oxidation of toluene”, *Combustion & Flame*, 139, 340–350

Stewart, W.E. (1959), “Predict octanes for gasoline blends”, *Petroleum Refiner*, 38 (12), 135-139

Sutton, D.L. (1984), “Knock protection – future fuels and engines”, SAE Paper 841289

Swarts, A. (2006), “Insights relating to octane rating and the underlying role of autoignition”, Ph.D. thesis, University of Cape Town

Swarts, A., Viljoen, C.L. and Coetzer, R. (2003), “The analysis of observed burn rates in a spark-ignition engine and the relation to fuel properties”, SAE Paper 2003-01-3125

Swarts, A., Yates, A., Viljoen, C. and Coetzer, R. (2004), ”Standard knock intensity revisited: atypical burn rate characteristics identified in the CFR octane rating engine”, SAE Paper 2004-01-1850

Swarts, A., Yates, A., Viljoen, C. and Coetzer, R. (2005), “A further study of inconsistencies between autoignition and knock intensity in the CFR octane rating engine”, SAE Paper 2005-01-2081

Tanaka, S, Ayala, F., Keck, J.C. (2003), “A reduced chemical kinetic model for HCCI combustion of primary reference fuels in a rapid compression machine”, *Combustion & Flame*, 133, 467–481

Tanaka, S, Ayala, F., Keck, J.C., Heywood, J.B. (2003 b), "Two-stage ignition in HCCI combustion and HCCI control by fuels and additives", *Combustion & Flame*, 132, 219–239

Tao, F., and Chomiak, J. (2002), “Numerical Investigation of Reaction Zone Structure and Flame Liftoff of DI Diesel Sprays with Complex Chemistry “, SAE Paper 2002-01-1114

Tao, F., Golovitchev V. I., Chomiak J. (2000), “Self-Ignition and Early Combustion Process of n-Heptane Sprays Under Diluted Air Conditions: Numerical Studies Based on Detailed Chemistry”, SAE Paper 2000-01-2931

Taylor, C. F. (1985), *The Internal Combustion Engine In Theory And Practice - Volume 2: Combustion, Fuels, Materials, Design*, Revised Edition 1985, Cambridge, The MIT Press

Touchard, S., Fournet, R., Glaude, P.A., Warth, V., Battin-Leclerc, F., Vanhove, G., Ribaucour, M., and Minetti , R. (2004), “Modelling of the oxidation of large alkenes at low temperature” , *Proceedings of the Combustion Institute*, 30(1), 1073-1081

Twu, C.H., and Coon, J.E. (1996), “Predict octane numbers using a generalized interaction method.”, *Hydrocarbon Processing*, February 1996, 51-56

Twu, C.H., and Coon, J.E. (1997), “Estimate octane numbers using an enhanced method”, *Hydrocarbon Processing*, 75, March 1997, 65-68

Van Gulick, H. (1975), “Refineries and engines as a technical system”, *The Journal of Automotive Engineering*, April 1975, 11-16

Vanhove, G., Minetti, R., Touchard, S., Fournet, R., Glaude. P.A., and Battin-Leclerc, F., (2006), ”Experimental and modeling study of the autoignition of 1-hexene/isooctane mixtures at low temperatures”, *Combustion & Flame*, 145, 272–281

Vanhove, G., Ribaucour, M, and Minetti, R., (2005), “On the influence of the position of the double bond on the low-temperature chemistry of hexenes”, *Proceedings of the Combustion Institute*, 30, 1065-1072

Vasu, S.S., Davidson, D.F., and Hanson, R.K., (2008), “Jet fuel ignition delay times: Shock tube experiments over wide conditions and surrogate model predictions”, *Combustion & Flame*, 152,125–143

Vermeersch, M. L., Held, T. J., Stein, Y. and Dryer, F.L. (1991), “Autoignition chemistry studies of n-butane in a variable pressure flow reactor”, SAE Paper 912326

Viljoen, C.L., Yates, A.D.B., and Coetzer, R.L.J. (2007), “A Molecular Modelling Investigation of Selected Gasoline Molecules to Relate Oxidation Pathways to their Autoignition Behaviour”, SAE Paper 2007-01-0005

Viljoen, C.L., Yates, A.D.B., Swarts, A., Balfour, G. and Möller, K. (2005), “Investigation of the ignition delay character of different fuel components and assessment of various autoignition modelling approaches”, SAE Paper 2005-01-2084

Viljoen, E.L. (2006), “The influence of molybdenum and vanadium on the activity and selectivity of a cobalt Fischer-Tropsch catalyst”, Ph.D. thesis, University of Cape Town.

Wang, S., Miller, D.L., Cernansky, N.P., Curran, H.J., Pitz, W.J., Westbrook,C.K., (1999), “A Flow Reactor Study of Neopentane Oxidation at 8 Atmospheres: Experiments and Modeling”, *Combustion & Flame*, 118, 415–430

Wang, X.-J., Mou, C.Y. (1985), "A thermokinetic model of complex oscillations in gaseous hydrocarbons oxidation", *J. Chem. Phys.,* 83 (9), 4554

Warnatz, J. (1996), "Experimental and computational study of ignition and flame propagation in internal combustion engines", *Endeavour* 20 (1), 31-36

Warnatz, J. (2000), “Hydrocarbon oxidation high-temperature chemistry”, *Pure Appl. Chem.*, 72 (11), 2101-2110

Warnatz, J., Maas, U., and Dibble, R.W. (1996), *Combustion: Physical and Chemical Fundamentals, Modeling and Simulation, Experiments, Pollutants Formation*, 3rd Edition, Berlin, Springer-Verlag

Warth, V., Stef, N., Glaude, P. A., Battin-Leclerc, F., Scacchi, G.,and Come, G. M., (1998), "Computer-Aided Derivation of Gas-Phase Oxidation Mechanisms: Application to the Modelling of the Oxidation of normal-butane", *Combustion & Flame*, 114: 81-102.

Warth, V., Stef, N., Glaude, P. A., Battin-Leclerc, F., Scacchi, G., and Come, G. M. (1998), "Computer-Aided Derivation of Gas-Phase Oxidation Mechanisms: Application to the Modelling of the Oxidation of normal-Butane", *Combustion & Flame*, 114, 81-102

Waukesha Motor Company (ca. 1946), “A brief history of fuel testing”, Wisconsin, Waukesha Motor Company

Westbrook, C.K. (1992), “The chemistry behind engine knock”, *Chem. & Ind.*, 3 August 1992, 562-566

Westbrook, C.K. and Pitz, W.J. (1984), “Modelling chemical kinetic aspects of engine knock”, Lawrence Livermore National Laboratory, Publication UCRL-90577

Westbrook, C.K. and Pitz, W.J. (1987), “Detailed Kinetic Modeling of Autoignition Chemistry” SAE Paper 872107

Westbrook, C.K. and Pitz, W.J. (1989), ”Computer modelling of autoignition chemistry.”, Lawrence Livermore National Laboratory, Publication UCRL-99324

Westbrook, C.K., Curran, H.J., Pitz, W.J., Griffiths, J.F., Mohamed, C. and Wo, S.K., (1998) “The Effects of Pressure, Temperature, and Concentration on the Reactivity of Alkanes: Experiments and Modeling in a Rapid Compression Machine”, *Proceedings of the Twenty-seventh symposium (International) on Combustion*, The Combustion Institute, 371-378

Westbrook, C.K., Curran, H.J., Pitz, W.J., Griffiths, J.F., Mohamed, C., (1996), “Kinetic Modeling of Hydrocarbon Autoignition at Low and Intermediate Temperatures in a Rapid Compression Machine”, *Proceedings of 3rd Workshop on Modeling of Chemical Reaction Systems*, University of Heidelberg, 1996

Westbrook, C.K., Pitz, W.J., Herbinet, O., Curran, H.J., Silke, E.J., (2009), “A comprehensive detailed chemical kinetic reaction mechanism for combustion of n-

alkane hydrocarbons from n-octane to n-hexadecane", *Combustion & Flame*, 156, 181–199

Westbrook, C.K., Warnatz, J., and Pitz, W.J. (1988), "A detailed chemical kinetic reaction mechanism for the oxidation of iso-octane and n-heptane over an extended temperature range and its application to analysis of engine knock", *Proceedings of the Twenty-second Symposium (Int.) on Combustion*, The Combustion Institute, 893-901

Westbrook, Charles K., (2000), "Chemical kinetics of hydrocarbon ignition in practical combustion systems", *Proceedings of the Combustion Institute*, 28(2), 1563-1577

Wilk, R.D., Koert, D.N., and Cernansky, N.P. (1989), "Low-temperature carbon monoxide formation as a means of assessing the autoignition tendency of hydrocarbons and hydrocarbon blends", *Energy & Fuels*, 3 (3), 292-298

Yates, A.D.B (1988), "Abnormal combustion methanol versus gasoline" Ph.D. thesis, University of Cape Town.

Yates, A.D.B, Swarts, A, and Viljoen, C.L., (2005), "Correlating Auto-Ignition Delays And Knock-Limited Spark-Advance Data For Different Types Of Fuel", SAE Paper 2005-01-2083.

Yates, A.D.B., Swarts, A. and Viljoen, C.L. (2003), "An Investigation of Anomalies Identified Within the ASTM Research and Motor Octane Scales", SAE Paper 2003-01-1772

Yates, A.D.B., Swarts, A. and Viljoen, C.L. (2004), "Understanding the Relation Between Cetane Number and Combustion Bomb Ignition Delay Measurements", SAE Paper 2004-01-2017

Yates, A.D.B., Swarts, A. and Viljoen, C.L. (2005), "Correlating auto-ignition delays and knock limited spark-advance for different types of fuel", SAE Paper 2005-01-2083

Yates, A.D.B., Viljoen, C.L., and Metcalf, O. (2007), "An Accurate Determination of the Cetane Number Value of GTL Diesel", SAE Paper 2007-01-0026

Yates, A.D.B. and Viljoen, C.L. (2008), "An Improved Empirical Model for Describing Auto-ignition", SAE Paper 2008-01-1629

Yonei, T., Hashimoto,K., Arai, M., and Tamura, M. (2003) , "Quantum Chemical Study of Cetane Improvers", *Energy & Fuels*, 17, 725-730

Zahed, A.H., Mullah, S.A and Bashir, M.D. (1993), "Predict octane number for gasoline blends", *Hydrocarbon Processing*, May 1993, 85-87

Zheng, J., Yang, W., Miller, D.L. and Cernansky, N.P. (2001), "Prediction of Preignition Reactivity and Ignition Delay for Using a Reduced Chemical Kinetic Model", SAE Paper 2001-01-1025

Zheng, J., Yang, W., Miller, D.L. and Cernansky, N.P. (2002), "A Skeletal Chemical Kinetic Model for the HCCI Combustion Process", SAE Paper 2002-01-0423

Zheng, Z and Yao, M. (2007), "Numerical Simulation of the Effects of Charge Stratification on Combustion and Emissions", *Energy & Fuels*, 21, 2018-2026

APPENDIX A : Example of a Chemkin Aurora input file for simulation of the IQT™, using a PRF 90 and the mechanism of Curran et al. (2002)

```
! Aurora Input File for IQT simulation - C.L. Viljoen, August 2009
!*************************************************************
! This is a transient, closed-system combustion simulation
! which involves gas-phase kinetics only.
! In this case the pressure is held constant by default
! and the system is adiabatic.  The system is assumed to
! be closed since no flow rate is specified.
!
!           Transient simulation
TRAN
!
!           Solve the energy equation
ENRG
!           Adiabatic system
QLOS 0.0
!           Zero heat loss assumed
!
!           Fix the equivalence ratio of the fuel to oxidant
!
EQUI   1.0
!
TLIM 1400  !Report the time when system reaches 1400K – used as ID in this work
!
!          Composition of the fuel blend (mole ratio)
!
FUEL   nc7h16  0.1112449          ! n-heptane in PRF90
FUEL   ic8h18   0.8887551         ! iso-octane in PRF90
!          Composition of the oxidizer air
OXID o2  0.2095                   ! in accordance with Heywood (1988)
OXID n2  0.7905                   ! in accordance with Heywood (1988)
!
!        Identify equilibrium products to help determine the initial guesses of the
!        species fractions
PROD h2o
PROD n2
PROD co2
!        Volume profile must fix volume as constant
VPRO 0.0        213        !Volume of the IQT bomb in cm3
VPRO 6.0E-03  213
!        Initial Pressure in atmospheres (no longer assumed constant
!        due to [VPRO] that was added)
!
PRES  22.21263            !atm, including fuel contribution
!         Initial Temperature in system
TEMP  840                 !Kelvin
```

```
!
!         Initial gas moles in system
!         Note: input will be normalized to mole fractions
! REAC o2  0.20601216          ! This is the alternative to FUEL / OXID specification,
! REAC n2  0.77728388          ! giving identical  results as specification above
! REAC nc7h16 0.00185823   ! equivalent to PRF90 at stoichiometric conditions
! REAC ic8h18  0.01484573
!
!         End time for the simulation
TIME  12.0E-3
!         Time-step for printing to diagnostic output file
DELT 1.E-3
!         Time-step for writing to binary solution file
DTSV 1.E-5
!         End of input keywords
END
```

APPENDIX B : Least squares regression coefficients for Three-Arrhenius ID correlation fitted to Chemkin simulation data

The least squares regression coefficients for PRF90 in the simulation shown in Figure 2.5 (p.2-29) are given in Table B-1:

Table B-1: Three-Arrhenius optimized coefficients for PRF90

Fuel	$Ln(A_1)$	n_1	B_1	$Ln(A_2)$	n_2	B_2	$Ln(A_3)$	n_3	B_3
PRF 90 (Chemkin Best fit)	-19.68	-0.048	16024	16.48	-2.185	-5757	-9.98	-0.953	13544

Since simulations were carried out only at stoichiometric air-fuel ratios in this work, the effect of the fuel-air equivalence ratio, Φ , on the ID has been omitted. The Φ correction can be added as a power law correction according to (Yates et al., 2005):

$$\tau = \tau_{(\Phi=1)} \cdot \Phi^{m} \quad \text{.. (B-1)}$$

The correction can be accounted for, when appropriate, by adding a 10^{th} parameter (m) to the tables shown here (see for example, Swarts (2006)).

Table B-2: Three-Arrhenius optimized coefficients for n-Heptane

Fuel	$Ln(A_1)$	n_1	B_1	$Ln(A_2)$	n_2	B_2	$Ln(A_3)$	n_3	B_3
n-Heptane (Chemkin Best Fit)	-18.69	-0.078	14721	18.52	-2.082	-10263	-12.48	-0.927	16441

In Table B-2 the optimized regression coefficients for n-heptane, as used to construct Figure 3.1 on page 3-3, are shown.

APPENDIX C : Chemkin simulation data for comparison of PRFs

Data from the constant volume simulations using the PRF mechanism from Curran et al. (2002), for n-heptane at stoichiometric conditions, at 12 bar. Since the ignition delays lengthened considerably at lower initial temperatures, the time was normalized with respect to the overall ignition delay. This data was used to construct Figure 3.23 in the text.

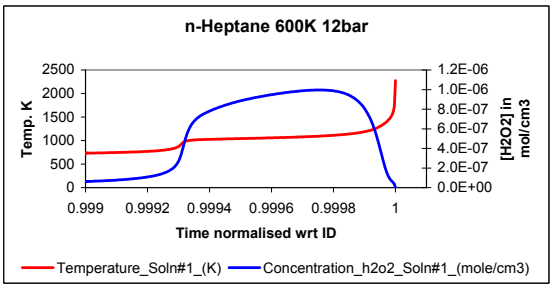

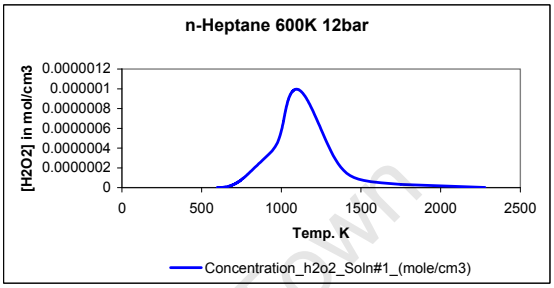

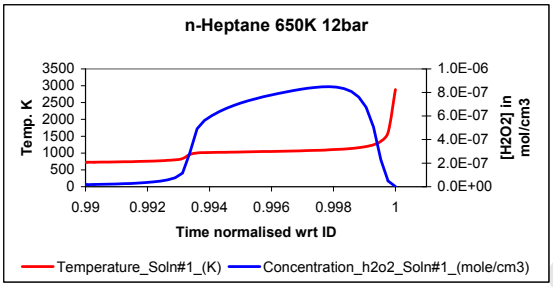

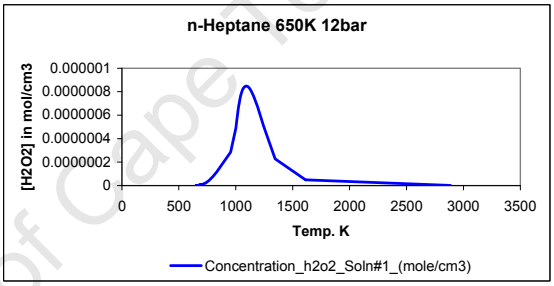

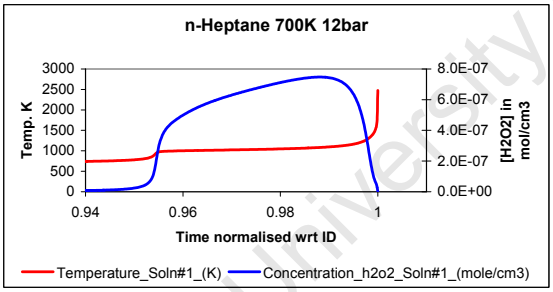

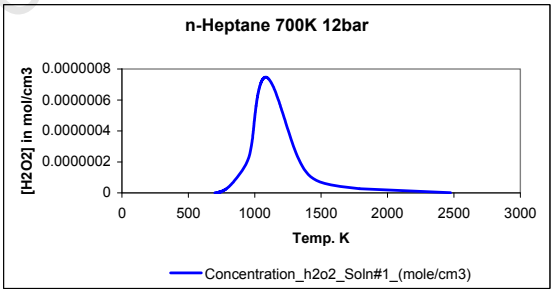

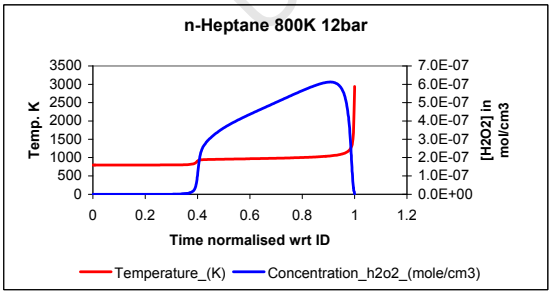

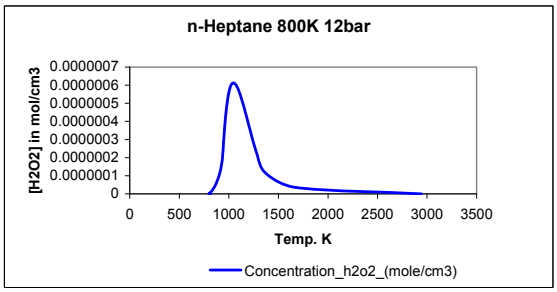

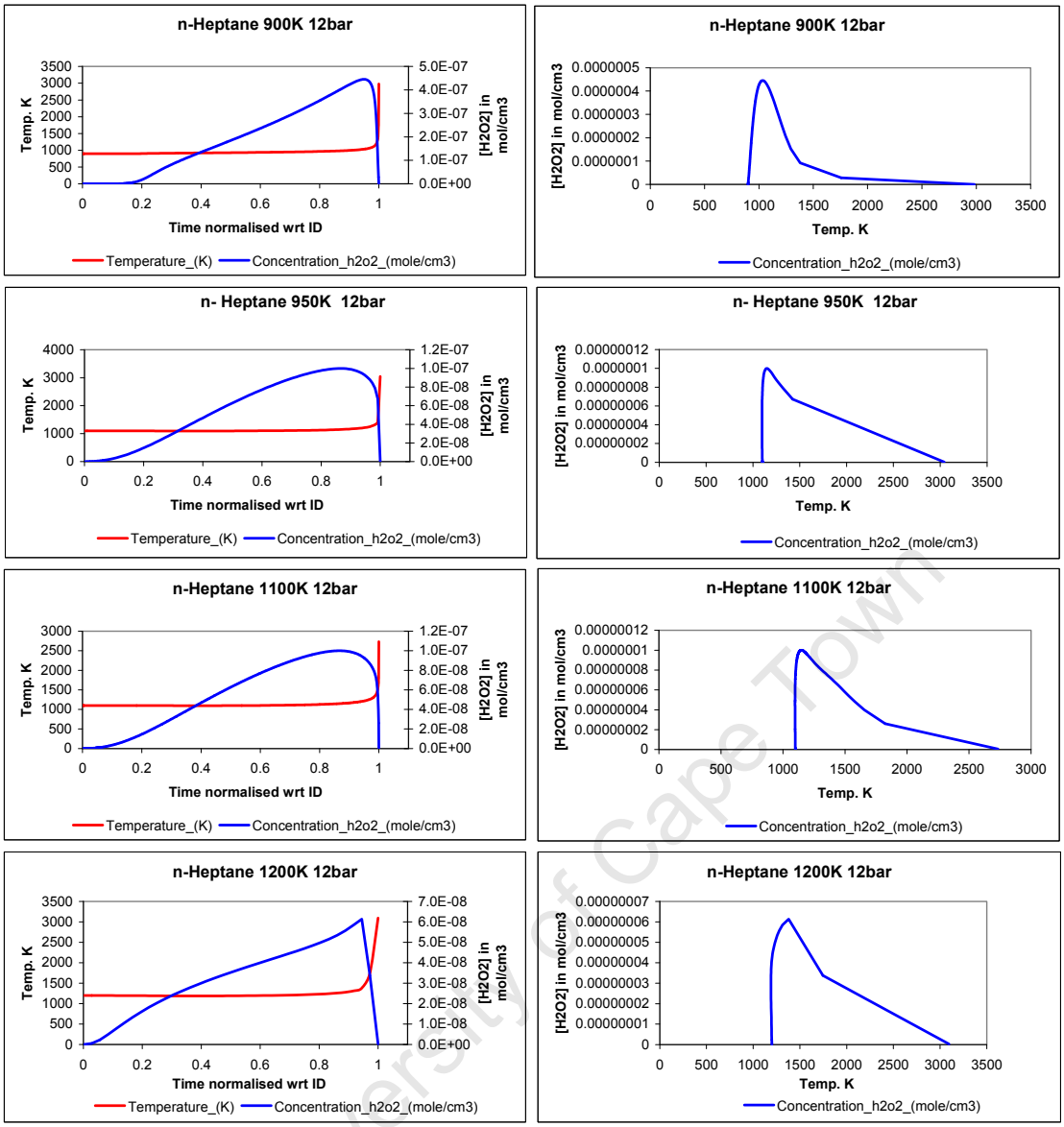

Continuation of the data for n-heptane, 12 bar, as plotted in Figure 3.23.

Data from the constant volume simulations using the PRF mechanism from Curran et al. (2002), for Iso-Octane at stoichiometric conditions, at 12 bar. Since the ignition delays lengthened considerably at lower initial temperatures, the time was normalized with respect to the overall ignition delay. This data was used to construct Figure 3.22 in the text.

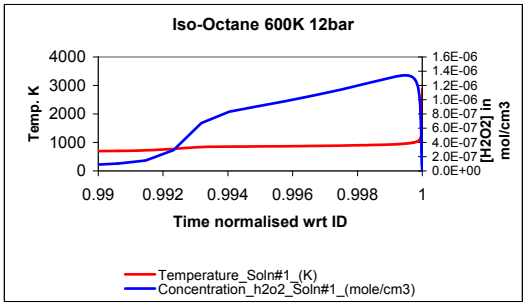

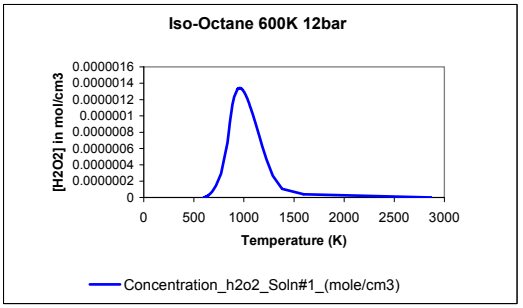

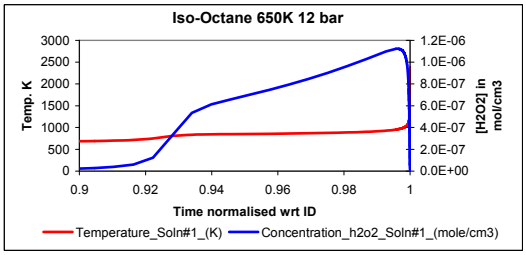

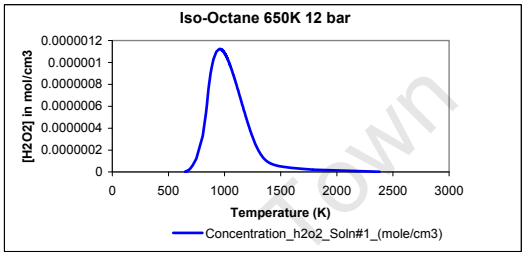

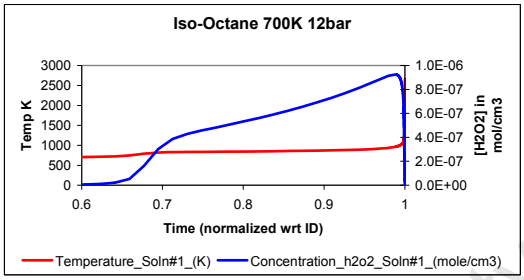

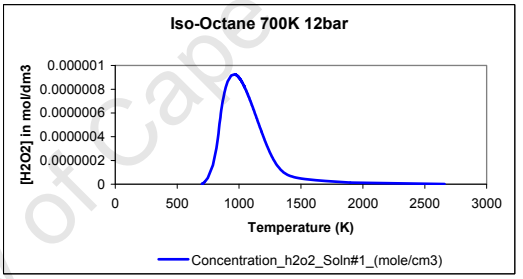

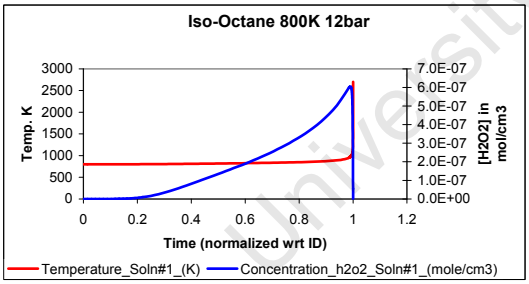

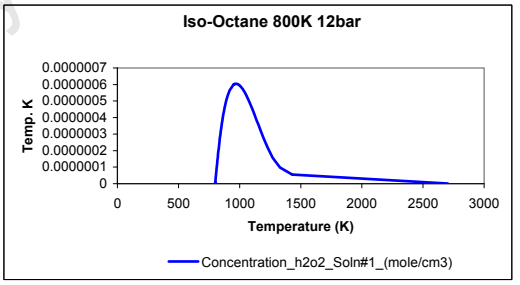

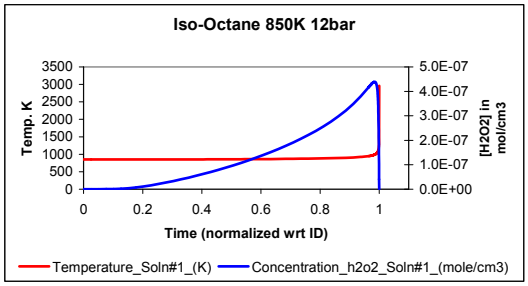

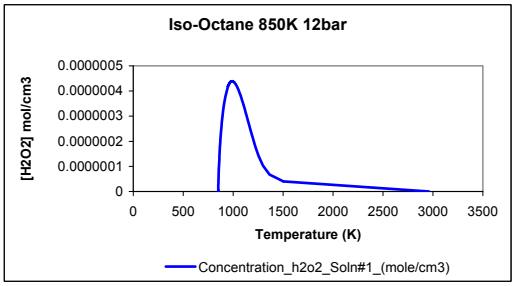

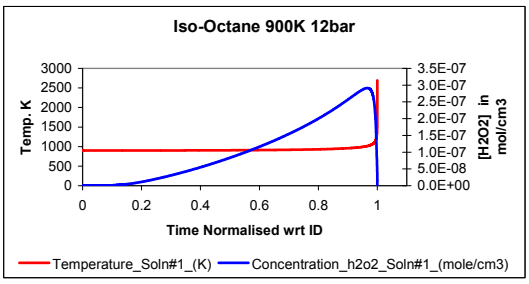

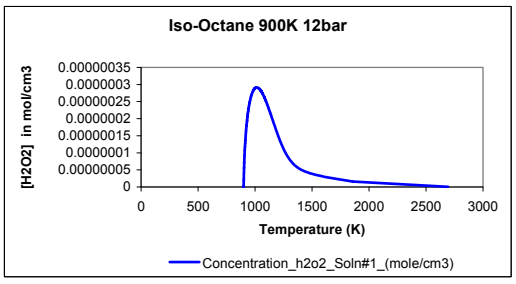

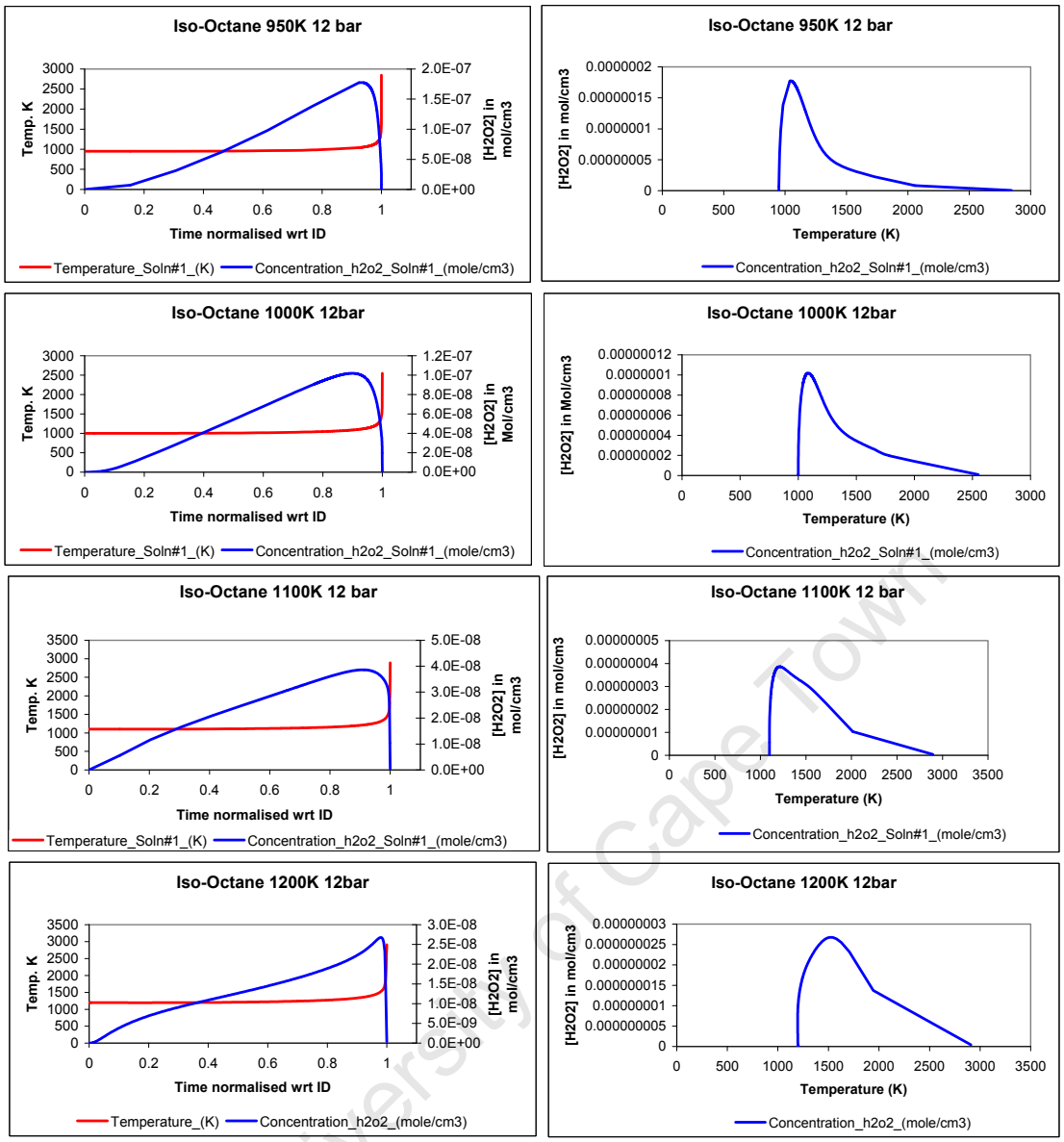

Continuation of the data for Iso-Octane, at P_{init} 12 bar, as plotted in Figure 3.22.

APPENDIX D : Model parameters used in the Griffiths model
(Section 3.3.1, page 3-33)

The model parameters (A_i [mol m^3 s], E_i/R [K] and ΔH_i [kJ/mol]) for the blends of iso-octane and n-heptane shown in Figure 3.25 (on page 3-36).
(ON = octane number, temperature range 600 - 1400K, pressure range 12 - 40 bar).

	ON = 0	**ON = 35**	**ON = 55**	**ON = 90**	**ON =100**
$\mathbf{A_1}$	5.00E8	5.00E8	5.00E8	5.00E8	5.00E8
$\mathbf{A_2}$	7.00E6	7.00E6	7.00E6	7.00E6	7.00E6
$\mathbf{A_{3+}}$	3.50E9	3.50E9	3.50E9	3.50E9	3.50E9
$\mathbf{A_{3-}}$	6.00E27	6.00E27	6.00E27	6.00E27	6.00E27
$\mathbf{A_4}$	6.00E7	6.00E7	6.00E7	6.00E7	6.00E7
$\mathbf{A_5}$	1.00E9	1.00E9	1.00E9	1.00E9	1.00E9
$\mathbf{E_1/R}$	18.55E3	18.37E3	18.27E3	18.10E3	18.05E3
$\mathbf{E_2/R}$	7.20E3	7.20E3	7.20E3	7.20E3	7.20E3
$\mathbf{E_{3+}/R}$	20.50E3	20.26E3	20.18E3	20.04E3	20.00E3
$\mathbf{E_{3-}/R}$	38.70E3	38.50E3	38.13E3	37.94E3	37.50E3
$\mathbf{E_4/R}$	5.00E3	5.35E3	5.55E3	5.90E3	6.00E3
$\mathbf{E_5/R}$	16.50E3	16.50E3	16.50E3	16.50E3	16.50E3
$\Delta\mathbf{H_1}$	709.9	709.9	709.9	709.9	709.9
$\Delta\mathbf{H_2}$	-4709.9	-4709.9	-4709.9	-4709.9	-4709.9
$\Delta\mathbf{H_{3+}}$	-53.9	-53.9	-53.9	-53.9	-53.9
$\Delta\mathbf{H_{3-}}$	53.9	53.9	53.9	53.9	53.9
$\Delta\mathbf{H_4}$	-60.0	-60.0	-60.0	-60.0	-60.0
$\Delta\mathbf{H_5}$	-3913.1	-3913.1	-3913.1	-3913.1	-3913.1

.

APPENDIX E : Skeletal mechanism for PRFs and Toluene as constructed during this study

Shown here is the Chemkin chemistry output file containing the skeletal mechanism for PRFs and toluene that was constructed in this study. It was done by merging the Huang et al. (2008) PRF mechanism with the toluene mechanism from Djurisic as it is contained in the mechanism of Machrafi et al. (2009). Note that only the C7KET21 ketohydroperoxide species is considered in this mechanism, as used in the simulations shown in Figure 3.31 to Figure 3.33 on pages 3-42 to 3-44.

PRF + Toluene Mechanism, based on Huang et al.(2008)PRF
plus Machrafi et al. (2009) Toluene, CLV January 2009

```
*************************************************************
*               CHEMKIN Collection Release 3.7              *
*                     CHEM Application                      *
*              GAS-PHASE MECHANISM INTERPRETER               *
* Copyright 1997-2002 Reaction Design.  All Rights Reserved. *
*************************************************************
```

ELEMENTS CONSIDERED	ATOMIC WEIGHT
1. H	1.00797
2. O	15.9994
3. C	12.0112
4. N	14.0067
5. AR	39.9480

SPECIES CONSIDERED	PHASE	CHARG	MOLECULAR WEIGHT	TEMPERATURE LOW	TEMPERATURE HIGH	ELEMENT COUNT H	O	C	N	AR
1. H	G	0	1.00797	300	5000	1	0	0	0	0
2. H2	G	0	2.01594	300	5000	2	0	0	0	0
3. H2O	G	0	18.01534	300	5000	2	1	0	0	0
4. H2O2	G	0	34.01474	300	5000	2	2	0	0	0
5. HO2	G	0	33.00677	300	5000	1	2	0	0	0
6. HCO	G	0	29.01852	300	5000	1	1	1	0	0
7. O	G	0	15.99940	300	5000	0	1	0	0	0
8. O2	G	0	31.99880	300	5000	0	2	0	0	0
9. OH	G	0	17.00737	300	5000	1	1	0	0	0
10. CO	G	0	28.01055	300	5000	0	1	1	0	0
11. CO2	G	0	44.00995	300	5000	0	2	1	0	0
12. CH2O	G	0	30.02649	300	5000	2	1	1	0	0

13. CH3	G	0	15.03506	300	5000	3	0	1	0	0
14. CH3O	G	0	31.03446	300	3000	3	1	1	0	0
15. CH3CHO	G	0	44.05358	200	6000	4	1	2	0	0
16. CH4	G	0	16.04303	300	5000	4	0	1	0	0
17. C2H5	G	0	29.06215	300	5000	5	0	2	0	0
18. C2H4	G	0	28.05418	300	5000	4	0	2	0	0
19. C2H3	G	0	27.04621	200	6000	3	0	2	0	0
20. C3H6	G	0	42.08127	300	5000	6	0	3	0	0
21. C3H5	G	0	41.07330	200	6000	5	0	3	0	0
22. C3H4	G	0	40.06533	200	6000	4	0	3	0	0
23. C4H8	G	0	56.10836	300	5000	8	0	4	0	0
24. C7H16	G	0	100.20557	300	5000	16	0	7	0	0
25. C7H15-2	G	0	99.19760	300	5000	15	0	7	0	0
26. C7H15O2	G	0	131.19640	300	5000	15	2	7	0	0
27. C7H14O2H	G	0	131.19640	300	5000	15	2	7	0	0
28. C7H14O2HO2	G	0	163.19520	300	5000	15	4	7	0	0
29. C7KET21	G	0	146.18783	300	5000	14	3	7	0	0
30. C5H11	G	0	71.14342	298	5000	11	0	5	0	0
31. C5H11CO	G	0	99.15397	300	5000	11	1	6	0	0
32. C8H18	G	0	114.23266	300	5000	18	0	8	0	0
33. C8H17	G	0	113.22469	300	5000	17	0	8	0	0
34. OOC8H16OOH	G	0	177.22229	300	5000	17	4	8	0	0
35. OC8H15O	G	0	143.20755	300	5000	15	2	8	0	0
36. C8H16	G	0	112.21672	300	5000	16	0	8	0	0
37. C8H17OO	G	0	145.22349	300	5000	17	2	8	0	0
38. C8H16OOH	G	0	145.22349	300	5000	17	2	8	0	0
39. OC8H15OOH	G	0	160.21492	300	5000	16	3	8	0	0
40. C6H5CH3	G	0	92.14181	200	5000	8	0	7	0	0
41. C6H5CH2	G	0	91.13384	200	5000	7	0	7	0	0
42. C5H5	G	0	65.09560	300	4000	5	0	5	0	0
43. C6H5O	G	0	93.10615	300	4000	5	1	6	0	0
44. C6H5CHO	G	0	106.12527	298	5000	6	1	7	0	0
45. C6H5CO	G	0	105.11730	300	2500	5	1	7	0	0
46. C6H5	G	0	77.10675	300	4000	5	0	6	0	0
47. C5H4O	G	0	80.08703	300	3000	4	1	5	0	0
48. N2	G	0	28.01340	300	5000	0	0	0	2	0

REACTIONS CONSIDERED	(k = A T**b exp(-E/RT)) A	b	E
1. C7H16+O2=C7H15-2+HO2	2.80E+14	0.0	47180.0
2. C7H16+OH=C7H15-2+H2O	4.80E+09	1.3	690.5
3. C7H15-2+O2=C7H15O2	2.00E+12	0.0	0.0
4. C7H15O2=C7H14O2H	6.00E+11	0.0	20380.0
5. C7H14O2HO2=C7KET21+OH	2.97E+13	0.0	26700.0
6. C7H14O2H+O2=C7H14O2HO2	9.00E+10	0.0	0.0
7. C7KET21=C5H11CO+CH2O+OH	1.00E+16	0.0	42400.0
8. C5H11CO=C5H11+CO	1.00E+11	0.0	9600.0
9. C5H11=C2H5+C3H6	3.20E+13	0.0	28300.0
10. C7H15-2=CH3+2C3H6	3.00E+13	0.0	29800.0
11. C7H15-2=C3H6+C2H5+C2H4	1.20E+13	0.0	29600.0
12. C8H18+O2=C8H17+HO2	5.00E+15	0.0	46000.0
Reverse Arrhenius coefficients:	1.00E+12	0.0	0.0
13. C8H17+O2=C8H17OO	1.00E+12	0.0	0.0
Reverse Arrhenius coefficients:	2.51E+13	0.0	27400.0
14. C8H17OO=C8H16OOH	1.14E+11	0.0	22400.0
Reverse Arrhenius coefficients:	1.00E+11	0.0	11000.0
15. C8H16OOH+O2=OOC8H16OOH	3.16E+11	0.0	0.0
Reverse Arrhenius coefficients:	2.51E+13	0.0	27400.0
16. OOC8H16OOH=OC8H15OOH+OH	8.91E+10	0.0	17000.0

```
 17. C8H18+OH=C8H17+H2O                          1.00E+13    0.0     3000.0
 18. C8H17+O2=C8H16+HO2                          3.16E+11    0.0     6000.0
     Reverse Arrhenius coefficients:             3.16E+11    0.0    19500.0
 19. OC8H15OOH=OC8H15O+OH                        3.98E+15    0.0    43000.0
 20. OC8H15O+O2=C2H3+2CH2O+C3H4+CH3+HO2          2.45E+13    0.0    32000.0
 21. C8H17=C4H8+C3H6+CH3                         1.28E+12    0.0    49000.0
 22. C8H16=C4H8+C3H5+CH3                         1.92E+12    0.0    48000.0
 23. C4H8+O2=C2H3+C2H4+HO2                       2.00E+14    0.0    35900.0
 24. HO2+HO2=H2O2+O2                             2.00E+12    0.0        0.0
 25. H2O2+M=OH+OH+M                              7.59E+16    0.0    46000.0
 26. O2+H=OH+O                                   2.63E+16   -0.7    17040.0
     Reverse Arrhenius coefficients:             1.45E+13    0.0      700.0
 27. OH+OH=HO2+H                                 3.72E+04    2.4    -2110.0
 28. H+O2+M=HO2+M                                2.82E+18   -0.9        0.0
 29. HO2+OH=H2O+O2                               3.01E+15    0.0    17330.0
 30. OH+H+M=H2O+M                                2.19E+22   -2.0        0.0
 31. O+O+M=O2+M                                  1.20E+17   -1.0        0.0
 32. CO+OH=CO2+H                                 4.79E+07    1.2       70.0
 33. CO+HO2=CO2+OH                               1.50E+14    0.0    23600.0
 34. CO+O+M=CO2+M                                1.82E+10    0.0     2385.0
 35. O2+CO=O+CO2                                 2.50E+12    0.0    47800.0
 36. HCO+O2=CO+HO2                               1.35E+13    0.0      400.0
 37. HCO+M=CO+H+M                                1.86E+17   -1.0    17000.0
 38. CH2O+OH=HCO+H2O                             2.43E+10    1.2     -447.0
 39. CH2O+HO2=H2O2+HCO                           3.00E+12    0.0     8000.0
 40. CH3+HO2=CH3O+OH                             4.30E+13    0.0        0.0
 41. CH3O+O2=CH2O+HO2                            7.59E+10    0.0     2700.0
 42. C2H3+O2=CH2O+HCO                            3.98E+12    0.0     -250.0
 43. C2H4+OH=C2H3+H2O                            3.63E+06    2.0     2500.0
 44. C2H4+O=CH3+HCO                              1.26E+07    1.8      220.0
 45. C2H5+O2=C2H4+HO2                            8.32E+11    0.0     3875.0
 46. C3H4+OH=CH2O+C2H3                           1.00E+12    0.0        0.0
 47. C3H5+O2=C3H4+HO2                            6.03E+11    0.0    10000.0
 48. C3H6+OH=C3H5+H2O                            3.09E+06    2.0     -300.0
 49. C3H6+O2=C3H5+HO2                            1.95E+12    0.0    39040.0
 50. C3H6+HO2=C3H5+H2O2                          3.16E+11    0.0    14900.0
 51. C6H5CH3+O2=C6H5CH2+HO2                      3.00E+14    0.0    42922.2
 52. C6H5CH3+OH=>C6H5CH2+H2O                     5.27E+13    0.0     2578.8
 53. C6H5CH2+HO2=>C6H5CHO+H+OH                   5.00E+12    0.0        0.0
 54. C6H5CHO+OH=>C6H5CO+H2O                      2.25E+10    1.2     -446.3
 55. C6H5CO=>C6H5+CO                             3.98E+14    0.0    29352.2
 56. C6H5+O2=>C6H5O+O                            2.60E+13    0.0     6110.1
 57. C6H5O=>CO+C5H5                              3.76E+54  -12.1    74179.3
 58. C5H5+O2=>C5H4O+OH                           1.80E+12    0.1    17970.8
 59. C5H4O+O+2O2=>3CO+2HCO+H2O                   3.60E+16    1.4     -856.6

 NOTE: A units mole-cm-sec-K, E units cal/mole


NO ERRORS FOUND ON INPUT:
ASCII Vers. 1.2 CHEMKIN linkfile chem.asc written.


WORKING SPACE REQUIREMENTS ARE
   INTEGER:     2140
   REAL:        1839
   CHARACTER:     53

Total CPUtime: Less than 1 second
```

APPENDIX F : API Project 45 Data (AMERICAN PETROLEUM INSTITUTE, 1957; ASTM, 1959)

Data from this compilation of octane numbers for pure components and blends of 20 vol% of the pure compound with 80 vol% of a PRF60 was used in this study, including the final optimized quantification of the %NTC associated with the compound, shown in the last column.

			Clear		RON	Predict	Diff	MON	Predict	Diff	NTC
No	**Blends**		**RON**	**MON**	**Blend**			**Blend**			
	n-Heptane		0	0							90.47%
	iso-Octane		100	100							50.25%
1	trans-1,4-dimethylcyclohexane	C8H16	68.3	62.2	60.7	60.3	0.4	59.8	60.3	-0.5	70.91%
2	n-propylcyclopentane	C8H16	31.2	28.1	53.3	53.1	0.2	53.4	53.6	-0.2	58.06%
3	1,c-2,t-4-trimethyl-cyclopentane	C8H16	89.2	79.5	64.0	64.9	-0.9	65.2	64.1	1.1	58.85%
4	ethylcyclohexane	C8H16	45.6	40.8	56.6	56.2	0.4	55.9	56.3	-0.4	56.06%
5	cis-1,4-dimethylcyclohexane	C8H16	67.2	68.2	61.6	60.9	0.7	61.2	62.1	-0.9	52.26%
6	trans-1,3-dimethylcyclohexane	C8H16	66.9	64.2	61.3	60.9	0.4	60.9	61.4	-0.5	51.16%
7	isopropylcyclohexane	C9H18	62.8	61.1	60.4	60.1	0.3	60.4	60.8	-0.4	50.58%
8	cycloheptane	C7H14	38.8	40.2	56.3	55.6	0.7	56.0	56.8	-0.8	72.55%
9	n-butylcyclopentane	C9H18	-3.0	-2.0	47.2	47.5	-0.3	49.0	48.6	0.4	50.38%
10	isopropylcyclopentane	C8H16	81.1	76.2	64.6	64.5	0.1	64.2	64.4	-0.2	43.93%
11	cis-1,2-dimethylcyclohexane	C8H16	80.9	78.6	64.9	64.5	0.4	64.4	64.9	-0.5	73.44%
12	isobutylcyclopentane	C9H18	33.4	28.2	54.8	55.1	-0.3	55.3	54.9	0.4	81.65%
13	trans-1,2-dimethylcyclohexane	C8H16	80.9	78.7	65.0	64.7	0.3	64.8	65.1	-0.3	76.94%
14	ethylcyclopentane	C7H14	67.2	61.2	62.9	62.0	0.9	60.6	61.7	-1.1	40.18%
15	trans-1,3-dimethylcyclopentane	C7H14	80.6	72.6	66.1	65.1	1.0	63.0	64.2	-1.2	78.40%
16	1,1-dimethylcyclohexane	C8H16	87.3	85.9	67.0	66.8	0.2	66.9	67.2	-0.3	34.57%
17	ethylcyclobutane	C6H12	41.1	63.9	53.9	53.9	0.0	60.3	60.3	0.0	56.80%
18	1,1,3-trimethylcyclopentane	C8H16	87.7	83.5	66.8	66.9	-0.1	66.9	66.8	0.1	33.93%
19	cyclooctane	C8H16	71.0	58.2	64.0	63.9	0.1	61.9	62.0	-0.1	29.83%
20	1,1-dimethylcyclopentane	C7H14	92.3	89.3	67.3	68.3	-1.0	69.6	68.4	1.2	35.80%
21	cis-1,3-dimethylcyclopentane	C7H14	79.2	73.1	67.7	65.9	1.8	63.1	65.3	-2.2	30.29%
22	methylcyclopentane	C6H12	91.3	80.0	69.4	69.5	-0.1	67.8	67.7	0.1	26.24%
23	ethylcyclopropane	C5H10	102.5	83.8	71.0	71.9	-0.9	69.6	68.5	1.1	26.38%
24	methylcyclohexane	C7H14	74.8	71.1	68.8	67.3	1.5	64.8	66.8	-2.0	90.74%
25	cyclohexane	C6H12	83.0	77.2	69.9	69.2	0.7	67.4	68.2	-0.8	90.64%
26	cis-1,2-dimethylcyclopropane	C5H10	104.4	84.3	72.4	73.7	-1.3	71.3	69.8	1.5	89.11%
27	cyclopentane	C5H10	101.3	84.9	76.2	78.0	-1.8	76.2	74.1	2.1	13.62%
28	2,4-dimethyl-3-ethylpentane	C9H20	105.3	96.6	65.5	66.1	-0.6	66.5	65.8	0.7	57.97%
29	2-methyl-3-ethylpentane	C8H18	87.3	88.1	63.2	63.4	-0.2	65.0	64.8	0.2	64.51%
30	2,4-dimethylpentane	C7H16	83.1	83.8	63.3	62.9	0.4	63.7	64.2	-0.5	67.13%
31	3.4-dimethylhexane	C8H18	76.3	81.7	61.4	61.5	-0.1	64.0	63.8	0.2	54.09%
32	3,3,5-trimethylheptane	C10H22	86.4	88.7	63.5	63.6	-0.1	65.4	65.3	0.1	59.12%
33	n-hexane	C6H14	24.8	26.0	51.8	51.4	0.4	52.4	52.9	-0.5	57.64%
34	2,2-dimethylpentane	C7H16	95.8	95.6	65.8	65.6	0.2	66.6	66.8	-0.2	61.80%
35	2-methylheptane	C8H18	20.6	23.0	50.5	50.8	-0.3	52.7	52.4	0.3	60.82%
36	2,2-dimethylhexane	C8H18	72.5	77.4	61.4	61.3	0.1	63.2	63.4	-0.2	60.84%
37	2-methylhexane	C7H16	42.4	46.4	56.1	55.4	0.7	56.4	57.3	-0.9	57.23%
38	3,3-dimethylhexane	C8H18	75.5	83.4	62.5	62.0	0.5	64.2	64.7	-0.5	59.73%
39	3,3-diethylpentane	C9H20	84.0	91.6	63.9	63.7	0.2	66.2	66.4	-0.2	59.22%

40	3-methyl-3-ethylpentane	C8H18	80.8	88.7	63.3	63.2	0.1	65.7	65.8	-0.1	54.50%
41	2,3-dimethylhexane	C8H18	71.3	78.9	62.1	61.4	0.7	63.2	64.0	-0.8	56.39%
42	2,3-dimethylpentane	C7H16	91.1	88.5	65.5	65.5	0.0	66.0	66.0	0.0	55.31%
43	3-methylheptane	C8H18	26.8	35.0	54.0	52.8	1.2	54.0	55.5	-1.5	64.78%
44	2,3,4-trimethylpentane	C8H18	102.5	95.9	67.4	68.0	-0.6	68.4	67.7	0.7	63.25%
45	n-heptane	C7H16	0.0	0.0	48.0	47.5	0.5	48.0	48.6	-0.6	90.47%
46	2,2,4-trimethylpentane	C8H18	100.0	100.0	68.0	67.5	0.5	68.0	68.6	-0.6	50.25%
47	2,2-dimethylbutane	C6H14	91.8	93.4	65.9	66.0	-0.1	67.4	67.3	0.1	48.73%
48	3-ethylpentane	C7H16	65.0	69.3	60.9	60.8	0.1	62.5	62.6	-0.1	48.01%
49	2,3,3-trimethylpentane	C8H18	106.0	99.4	68.0	69.0	-1.0	69.9	68.7	1.2	47.15%
50	2,3-dimethylbutane	C6H14	103.5	94.3	67.2	68.6	-1.4	69.3	67.7	1.6	44.43%
51	2,4-dimethylhexane	C8H18	65.2	69.9	60.9	60.9	0.0	62.8	62.8	0.0	52.14%
52	n-pentane	C5H12	61.7	62.6	60.3	60.2	0.1	61.3	61.4	-0.1	57.34%
53	3,3-dimethylpentane	C7H16	80.8	86.6	64.7	64.2	0.5	65.6	66.3	-0.7	42.43%
54	2,2,3-trimethylpentane	C8H18	109.6	99.9	68.9	70.0	-1.1	70.3	69.0	1.3	41.94%
55	3-methylhexane	C7H16	52.0	55.8	59.3	58.6	0.7	59.4	60.3	-0.9	42.18%
56	2,2-dimethyl-3-ethylpentane	C9H20	112.1	99.5	69.6	70.7	-1.1	70.3	69.0	1.3	41.93%
57	2,2,3-trimethylbutane	C7H16	112.1	101.3	70.5	71.1	-0.6	70.5	69.8	0.7	39.95%
58	4-methylheptane	C8H18	26.7	39.0	54.1	54.2	-0.1	57.5	57.4	0.1	88.80%
59	3-ethylhexane	C8H18	33.5	52.4	57.8	55.7	2.1	57.7	60.2	-2.5	39.52%
60	2-methylpentane	C6H14	73.4	73.5	64.5	63.8	0.7	63.7	64.6	-0.9	31.65%
61	3-methylpentane	C6H14	74.5	74.3	65.1	64.3	0.8	64.1	65.0	-0.9	32.64%
62	2-methylbutane	C5H12	92.3	90.3	67.9	68.1	-0.2	68.7	68.4	0.3	81.01%
63	2,2,3,3-tetramethylpentane	C9H20	116.8	95.0	72.5	73.3	-0.8	70.6	69.6	1.0	33.81%
64	2,2-dimethylpropane	C5H12	85.5	80.2	68.0	67.3	0.7	66.0	66.8	-0.8	29.87%
65	2,2,3,3-tetramethylhexane	C10H22	112.8	92.4	73.1	73.5	-0.4	70.3	69.9	0.4	29.77%
66	n-butane	C4H10	93.8	89.6	70.6	70.9	-0.3	70.7	70.3	0.4	24.13%
67	iso-butane	C4H10	101.3	97.6	72.4	72.5	-0.1	72.1	72.0	0.1	25.01%
68	1-heptene	C7H14	80.2	50.7	60.9	62.6	-1.7	60.0	57.9	2.1	77.22%
69	3-methyl-1-hexene	C7H14	82.2	71.5	63.4	64.4	-1.0	64.3	63.2	1.1	62.43%
70	1-octyne	C8H14	50.5	51.5	59.0	58.2	0.8	58.4	59.3	-0.9	40.12%
71	5-methyl-1-hexene	C7H14	75.5	64.0	63.6	63.8	-0.2	62.6	62.3	0.3	34.56%
72	trans-2-heptene	C7H14	89.5	68.8	66.9	67.7	-0.8	65.2	64.2	1.0	89.83%
73	cis-2-octene	C8H16	56.3	56.5	62.9	62.1	0.8	61.6	62.6	-1.0	22.40%
74	4-methyl-1-hexene	C7H14	86.4	74.0	69.0	68.7	0.3	66.3	66.6	-0.3	24.78%
75	3-ethyl-1-pentene	C7H14	95.6	81.6	70.1	70.7	-0.6	69.0	68.3	0.7	25.54%
76	trans-3-octene	C8H16	72.5	68.1	67.0	66.4	0.6	65.0	65.8	-0.8	90.28%
77	4-methyl-1-pentene	C6H12	95.7	80.9	70.4	71.3	-0.9	69.7	68.6	1.1	24.65%
78	3,3-dimethyl-1-pentene	C7H14	103.5	86.1	72.3	73.3	-1.0	71.3	70.0	1.3	23.39%
79	2,3-dimethyl-1-hexene	C8H16	96.3	83.6	71.5	71.8	-0.3	69.8	69.5	0.3	89.32%
80	1-hexene	C6H12	76.4	63.4	67.3	68.2	-0.9	66.7	65.7	1.0	92.43%
81	3-methyl-1-pentene	C6H12	96.0	81.2	70.7	72.1	-1.4	70.8	69.3	1.5	21.89%
82	trans-4-octene	C8H16	73.3	74.3	67.8	67.9	-0.1	68.2	68.1	0.1	92.70%
83	3,3-dimethyl-1-butene	C6H12	111.7	93.3	75.4	75.6	-0.2	72.2	72.0	0.2	23.38%
84	3,4-dimethyl-1-pentene	C7H14	98.9	80.9	73.4	73.1	0.3	69.2	69.6	-0.4	23.50%
85	2-methyl-1-hexene	C7H14	90.7	78.8	71.5	71.7	-0.2	69.5	69.3	0.2	19.88%
86	1-pentene	C5H10	90.9	77.1	71.7	72.1	-0.4	69.8	69.3	0.5	18.30%
87	trans-4-methyl-2-hexene	C7H14	96.8	83.0	73.0	73.8	-0.8	71.8	70.9	0.9	18.55%
88	4-methyl-cis-2-pentene	C6H12	99.7	84.5	73.8	74.4	-0.6	71.9	71.2	0.7	18.62%
89	trans-3-heptene	C7H14	98.2	79.3	72.8	74.1	-1.3	71.8	70.2	1.6	15.95%
90	2,3-dimethyl-1-pentene	C7H14	99.3	84.2	73.9	74.6	-0.7	72.2	71.4	0.8	18.29%
91	3-methyl-2-ethyl-1-butene	C7H14	97.0	82.0	73.6	74.3	-0.7	71.9	71.1	0.8	17.32%
92	trans-3-methyl-2-pentene	C6H12	97.2	81.0	74.0	74.5	-0.5	71.6	71.0	0.6	17.63%
93	2,4-dimethyl-2-pentene	C7H14	100.0	85.3	75.0	75.4	-0.4	72.6	72.2	0.4	17.08%
94	2,3,3-trimethyl-1-pentene	C8H16	106.0	85.7	75.5	76.7	-1.2	73.7	72.3	1.4	17.86%
95	trans-4-methyl-2-pentene	C6H12	98.0	82.6	74.7	75.3	-0.6	72.7	71.9	0.8	16.29%
96	t-4,4-dimethyl-2-pentene	C7H14	105.3	90.9	76.3	76.9	-0.6	74.3	73.6	0.7	17.14%
97	2-methyl-2-hexene	C7H14	91.6	79.2	73.8	74.1	-0.3	71.7	71.3	0.4	15.43%
98	2,3,3-trimethyl-1-butene	C7H14	105.3	90.5	76.9	77.0	-0.1	73.9	73.7	0.2	17.08%
99	1,5-hexadiene	C6H10	71.1	37.6	71.5	70.5	1.0	62.2	63.4	-1.2	8.76%
100	trans-3-hexene	C6H12	94.0	80.1	75.3	75.2	0.1	71.9	72.0	-0.1	14.41%

101	2,4-dimethyl-1-pentene	C7H14	99.2	84.6	76.4	76.3	0.1	72.8	72.9	-0.1	15.11%
102	trans-3-methyl-2-hexene	C7H14	91.5	79.6	74.4	74.9	-0.5	72.7	72.1	0.6	13.98%
103	cis-2,2-dimethyl-3-hexene	C8H16	106.7	88.0	76.9	78.1	-1.2	75.2	73.8	1.4	15.94%
104	cis-3,4-dimethyl-2-pentene	C7H14	96.0	82.2	76.0	76.2	-0.2	73.1	72.9	0.2	14.22%
105	trans-2-hexene	C6H12	92.7	80.8	74.8	75.7	-0.9	73.8	72.7	1.1	13.50%
106	trans-2-methyl-3-hexene	C7H14	97.9	82.0	76.0	76.8	-0.8	74.0	73.0	1.0	13.67%
107	4,4-dimethyl-1-pentene	C7H14	104.4	85.4	76.9	78.2	-1.3	75.3	73.8	1.5	14.64%
108	1-butene	C4H8	97.4	80.8	76.7	76.9	-0.2	73.2	73.0	0.2	13.69%
109	2-methyl-1-butene	C5H10	102.5	81.9	77.1	78.1	-1.0	74.5	73.3	1.2	14.01%
110	2,3-dimethyl-1-butene	C6H12	101.3	82.8	77.7	77.8	-0.1	73.7	73.5	0.2	13.68%
111	2-ethyl-1-butene	C6H12	98.3	79.4	76.5	77.3	-0.8	73.8	72.9	0.9	13.05%
112	trans-3-methyl-3-hexene	C7H14	96.4	81.4	76.5	77.0	-0.5	74.0	73.4	0.6	12.48%
113	cis-3-methyl-2-hexene	C7H14	92.4	80.0	75.8	76.3	-0.5	73.8	73.2	0.6	12.19%
114	cis-2-butene	C4H8	100.0	83.5	78.9	78.5	0.4	73.9	74.4	-0.5	12.42%
115	3-ethyl-2-pentene	C7H14	93.7	80.6	77.4	77.6	-0.2	74.4	74.1	0.3	11.13%
116	2,3-dimethyl-2-hexene	C8H16	93.1	79.3	76.9	77.6	-0.7	74.9	74.0	0.9	10.82%
117	2,4,4-trimethyl-1-pentene	C8H16	106.0	86.5	80.8	82.1	-1.3	78.6	77.0	1.6	10.47%
118	2-methyl-2-pentene	C6H12	97.8	83.0	79.8	80.7	-0.9	77.7	76.6	1.1	9.02%
119	2,3-dimethyl-2-pentene	C7H14	97.5	80.0	80.9	81.3	-0.4	77.0	76.5	0.5	7.90%
120	2-methyl-2-butene	C5H10	97.3	84.7	83.1	81.7	1.4	76.1	77.8	-1.7	7.97%
121	3-methyl-1,3-butadiene	C5H8	61.0	42.4	74.1	74.6	-0.5	70.0	69.4	0.6	0.48%
122	2,3-dimethyl-2-butene	C6H12	97.4	80.5	85.0	83.6	1.4	76.8	78.5	-1.7	6.18%
123	2-methyl-1,3-butadiene	C5H8	99.1	81.0	88.3	86.0	2.3	78.1	80.3	-2.2	4.71%
124	3-ethylcyclopentene	C7H12	90.8	71.4	73.0	73.6	-0.6	70.2	69.5	0.7	14.74%
125	cyclohexene	C6H10	83.9	63.0	75.4	74.4	1.0	68.4	69.6	-1.2	10.43%
126	1-ethylcyclohexene	C8H14	85.0	70.5	76.3	76.1	0.2	72.0	72.3	-0.3	9.52%
127	1-ethylcyclopentene	C7H12	90.3	72.0	80.8	80.2	0.6	74.4	75.2	-0.8	6.74%
128	cyclopentene	C5H8	93.3	69.7	82.2	80.9	1.3	73.2	74.8	-1.6	6.92%
129	1-methyl-cyclopentene	C6H10	93.6	72.9	84.9	84.2	0.7	77.3	78.1	-0.8	4.36%
130	toluene	C7H8	120.1	103.5	72.7	72.7	0.0	70.3	70.2	0.1	40.10%
131	1,2,3-trimethylbenzene	C9H12	105.3	100.7	71.5	70.4	1.1	68.9	70.2	-1.3	35.85%
132	ethylbenzene	C8H10	107.4	97.9	72.8	71.9	0.9	69.4	70.5	-1.1	31.46%
133	sec-butylbenzene	C10H14	106.7	95.7	71.2	72.0	-0.8	71.3	70.3	1.0	30.19%
134	iso-butylbenzene	C10H14	111.4	98.0	72.3	73.0	-0.7	71.6	70.8	0.8	30.21%
135	n-butylbenzene	C10H14	104.4	94.5	70.7	71.7	-1.0	71.3	70.2	1.1	29.62%
136	m-xylene	C8H10	117.5	115.0	76.9	75.1	1.8	72.8	74.9	-2.1	29.39%
137	2-ethyltoluene	C9H12	102.5	92.1	73.1	72.7	0.4	70.3	70.8	-0.5	25.12%
138	n-propylbenzene	C9H12	111.0	98.7	73.4	74.6	-1.2	73.8	72.4	1.4	25.15%
139	iso-propylbenzene	C9H12	113.1	99.3	74.4	75.1	-0.7	72.8	72.6	0.2	25.95%
140	p-xylene	C8H10	116.4	109.6	77.1	75.9	1.2	73.3	74.8	-1.5	25.68%
141	1,2,4-trimethylbenzene	C9H12	110.5	106.0	77.5	75.7	1.8	72.7	74.8	-2.1	22.69%
142	1,4-dimethyl-2-ethylbenzene	C10H14	106.0	96.0	76.0	75.3	0.7	72.5	73.3	-0.8	20.65%
143	1,2,3,4-tetramethylbenzene	C10H14	105.3	100.3	77.1	75.6	1.5	72.6	74.4	-1.8	20.41%
144	1,3-dimethyl-4-ethylbenzene	C10H14	106.0	95.9	76.9	75.8	1.1	72.3	73.6	-1.3	19.91%
145	1,2,3,4-tetrahydro-naphthalene	C10H12	96.4	81.9	74.6	73.9	0.7	70.0	70.8	-0.8	18.53%
146	1,3,5-trimethylbenzene	C9H12	120.5	106.0	82.1	80.5	1.6	75.3	77.2	-1.9	18.12%
147	indene	C9H8	113.7	106.7	80.7	79.5	1.2	76.2	77.6	-1.4	17.39%
148	1,3-diethylbenzene	C10H14	115.7	97.0	79.0	79.9	-0.9	76.8	75.7	1.1	16.89%
149	cis-1-propenyl benzene	C9H10	105.3	91.7	77.3	78.1	-0.8	75.8	74.8	1.0	15.24%
150	1,4-diethylbenzene	C10H14	106.0	95.2	78.2	78.3	-0.1	75.7	75.6	0.1	15.50%
151	3-ethyltoluene	C9H12	112.1	100.0	80.4	79.5	0.9	75.5	76.5	-1.0	16.15%
152	1,3-dimethyl-5-ethylbenzene	C10H14	114.8	102.5	80.4	80.1	0.3	76.8	77.1	-0.3	16.37%
153	trans-1-propenyl benzene	C9H10	104.4	92.1	78.3	78.3	0.0	75.2	75.2	0.0	14.76%
154	2-propenyl benzene	C9H10	113.1	101.3	83.9	82.7	1.2	77.9	79.3	-1.4	13.27%